

University of Southampton Research Repository ePrints Soton

Copyright © and Moral Rights for this thesis are retained by the author and/or other copyright owners. A copy can be downloaded for personal non-commercial research or study, without prior permission or charge. This thesis cannot be reproduced or quoted extensively from without first obtaining permission in writing from the copyright holder/s. The content must not be changed in any way or sold commercially in any format or medium without the formal permission of the copyright holders.

When referring to this work, full bibliographic details including the author, title, awarding institution and date of the thesis must be given e.g.

AUTHOR (year of submission) "Full thesis title", University of Southampton, name of the University School or Department, PhD Thesis, pagination

UNIVERSITY OF SOUTHAMPTON

FACULTY OF ENGINEERING AND THE ENVIRONMENT

Engineering Sciences

Thick-Film Underground Sensors

by

Marios Sophocleous



Thesis for the degree of Doctor of Philosophy

September 2015

UNIVERSITY OF SOUTHAMPTON

ABSTRACT

FACULTY OF ENGINEERING AND THE ENVIRONMENT

Environmental Condition Monitoring

Thesis for the degree of Doctor of Philosophy

THICK-FILM UNDERGROUND SENSORS

Marios Sophocleous

The aim of this study was to investigate the use of novel Thick-Film (TF) sensor technology suitable for in-situ real-time monitoring of important soil or water parameters. This technology should ideally be placed underground such that it can transmit data on soil parameters in a timely manner to help soil scientists to develop a more precise model for changes in soil quality. The study involved the development of low cost TF sensing arrays that can be used underground and, due to their lower cost, at much higher spatial densities than when using existing technologies, such that it is possible to obtain a more accurate spatial analysis. Thick-Film Technology was chosen because it offers low cost fabrication of robust sensors and the ability to incorporate multiple sensors on to a common supporting substrate that are compatible with simple electronic interface circuits. Further work was carried out to improve the performance of a previously developed TF water quality sensor array incorporating a pH sensor, a dissolved oxygen sensor and a platinum resistance thermometer. A novel TF printed conductivity sensor that can be incorporated onto the same substrate was also designed, fabricated and characterised.

A significant challenge of the project was the development of a solid state silver/silver chloride (Ag/AgCl) reference electrode having a sufficiently stable potential in different chloride concentrations and with a lifetime long enough to allow for soil deployments. The developed

reference electrode was subsequently and successfully employed in conjunction with an Ion-Selective-Electrode (ISE) based on ruthenium (II) oxide for the measurement of soil pH. Another major challenge of the project was the development of a suitable deployment technique for use in soil that enabled reliable readings of soil parameters to be obtained from the sensing array. Although the electrochemical sensors operated reliably in laboratory solutions, ensuring their reliable operation in soil proved to be a major issue. Additionally, the development of a screen printed conductivity sensor posed a major challenge in that printed, planar conductivity cells usually present problems due to electrical field fringing with increasing ac drive frequency as well as with increasing conductivity, resulting in non-linear cell constants. However with the novel sensor design described here it has been proven possible to obtain a constant conductivity sensor cell constant over the relatively wide range of conductivities encountered in soil sensing.

The pH sensor utilised in the TF sensor array was based on potentiometric measurement with the use of a TF ruthenium (II) oxide ISE and a TF Ag/AgCl reference electrode exhibiting typical chloride susceptibilities as low as $+2\text{mV/decade}[\text{Cl}^-]$ and a sensitivity of approximately 50mV/pH . The dissolved oxygen sensor was based on a TF printed Clark cell that was used to make amperometric measurements of approx. 1 micro amp/ppm of dissolved oxygen. The temperature sensor was based on a TF printed Platinum Resistance Thermometer exhibiting a sensitivity of approximately $40\text{mV}/^\circ\text{C}$ over a temperature range of 50°C . Conductivity measurements were based on a four electrodes arrangement using a specifically developed electronic circuit for the interface between the sensor and a data logger. The conductivity sensor was found to perform linearly over a range of approximately two decades of conductivity and fully characterised over the range of 0.1 to 4mS/cm .

An experimental setup was developed in the laboratory that could mimic real life field deployment of the sensors. Experiments were performed

using the experimental rig to understand the detailed in-situ behaviour of the sensing arrays. A deployment technique was also identified which provided an improved performance of the sensing arrays in the soil. A first attempt to evaluate the sensors' performances in a real life field deployment was also undertaken.

Although the developed sensing array has not yet fully met the specified requirements of the specific project, great progress has been achieved in that direction. TF sensing arrays have been shown to possess great potential for the areas of soil and water quality monitoring. It has also been demonstrated that these arrays can be used to replace many of the existing expensive and relatively fragile probes that are currently used for soil sensing. It has also been concluded that these sensors could be used in-situ to replace the timely and labour intensive procedures of soil sampling and testing that has traditionally been undertaken in specialised laboratories.

Table of Contents

ABSTRACT	i
Table of Contents	iii
List of Tables	vii
List of Figures	xi
DECLARATION OF AUTHORSHIP	xxi
List of Publications	xxiii
Acknowledgements	xxv
List of Abbriviations	xxvii
Chapter 1: Introduction	1
1.1 Soil Monitoring.....	3
1.2 Precision Agriculture.....	3
1.3 Impact of Climate Change on Soil Quality.....	4
1.4 Floodplain Underground Sensors (FUSE).....	5
1.5 Network Rail (NR).....	8
1.6 Aims & Objectives of Project.....	8
1.7 Chapters Organisation.....	13
Chapter 2: Literature Review	17
2.1 Current Monitoring Techniques.....	19
2.1.1 Soil Quality Indicators.....	19
2.1.2 Conventional Techniques.....	20
2.1.3 Limitations.....	24
2.2 Rationale of Thick-Film Technology.....	25
2.2.1 State of the art.....	25
2.2.2 Thick-Film Screen Printing Procedure.....	26
2.2.3 Lab-on-a-chip.....	28
2.3 Background Theory of Sensors.....	30
2.3.1 Electrochemical Cells.....	30
2.3.2 Reference Electrodes.....	32
2.3.3 Ion Selective Electrodes.....	38
2.3.4 pH Ion Selective Electrodes.....	40

2.3.5	Oxygen Sensors	41
2.3.6	Temperature Sensors	42
2.3.7	Conductivity Cells	43
2.3.8	Summary	57
2.4	User Requirements & Characteristics of Existing Commercial Technologies.....	59
2.5	Sensing Technologies at Research Level	62
2.5.1	Reference Electrodes.....	63
2.5.2	pH Ion-Selective-Electrodes.....	69
2.5.3	Dissolved Oxygen Sensors.....	71
2.5.4	Platinum Resistance Thermometers	76
2.5.5	Conductivity Cells	76
2.5.6	Interfaces between sensor & environment	79
2.5.7	Summary	80
Chapter 3:	Reference Electrodes	83
3.1	Instrumentation & Experimental Setup	85
3.2	Proposed Reference Electrode Structure	88
3.3	Experimental Work.....	91
3.3.1	The effect of Ag/AgCl paste on chloride susceptibility... 92	
3.3.2	Electrodes without the Ag/AgCl layer - Optimum KCl weight percentage	96
3.3.3	Electrodes without the Ag/AgCl layer - Hydration, Lifetime & Drift rate	101
3.3.4	Electrodes without the Ag/AgCl layer - Electrodes' performances in pH buffers.....	107
3.3.5	Polymer Ag/AgCl paste - Optimum KCl weight percentage	108
3.3.6	Glass PPCFB2 & PPCFC3 Ag/AgCl pastes - Optimum KCl weight percentage	112
3.3.7	Effect of Ag in KCl polymer matrix	116
3.3.8	Ag to AgCl & binder to powder ratios	122
3.3.9	Ag to AgCl & binder to powder ratios - Effect of adding KCl layer.....	134

Chapter 4: pH ISEs	143
4.1 Proposed pH Ion Selective Electrode Structure	144
4.2 Experimental Work	145
4.2.1 Investigation of the dielectric layer on electrode performance	146
4.2.2 Temperature effect on the pH ISEs' performance.....	148
Chapter 5: Relative Humidity & Temperature Sensor	157
5.1 SHT21	159
5.2 Experimental Work	160
5.2.1 Investigation of wire length on sensor accuracy	160
5.2.2 The effect of covering the sensor with PTFE membrane on sensor's performance	162
5.2.3 PTFE membrane as a waterproofing method.....	163
5.3 SHT21S.....	165
5.3.1 Investigation on sensors' performance consistency between sensors	166
5.3.2 The effect of PTFE membrane on SHT21S performance	167
5.3.3 Effect of PTFE on the exact same sensors	168
Chapter 6: Conductivity Cell.....	173
6.1 Instrumentation	175
6.2 Proposed Cell Geometry & Fabrication	176
6.3 Experimental Work.....	178
6.3.1 Solution Experiments - Investigation of frequency and current level effects.....	178
6.3.2 Solution Experiments - Investigating the effect of the distance between substrates.....	181
Chapter 7: Soil Rig.....	189
7.1 Soil Columns for Multi-sensor Arrays	191
7.1.1 1 st Soil Columns Design.....	192
7.2 Experimental Work.....	200
7.2.1 Investigation of sensor array performance in solutions	200
7.2.2 Investigation of sensor array in soil pipes	202

7.2.3	Investigation of sensor array performance in modified soil pipes	210
7.3	2 nd Soil Column Design	214
7.4	Soil Column for Conductivity Measurements	217
7.4.1	Instrumentation	217
7.4.2	Initial Soil Experiments with Conductivity Cell and Theta Probe	219
7.4.3	Investigation of water content versus conductivity curve in different soil types	221
Chapter 8:	Field Trials.....	231
8.1	Field Trials	233
8.1.1	Instrumentation	233
8.2	Experimental Work.....	235
8.2.1	Sensor array calibration in solutions	235
8.2.2	Investigation of sensor array performance in the field	237
Chapter 9:	Conclusions & Further Work	243
9.1	Reference Electrodes	245
9.1.1	Further work	248
9.2	pH Ion-Selective-Electrodes.....	249
9.2.1	Further work	250
9.3	Humidity & Temperature Sensor	251
9.4	Conductivity Sensor	252
9.4.1	Further work	253
9.5	Soil Experiments	254
9.5.1	Soil pipes Experiments	254
9.5.2	Soil Column for conductivity measurements.....	256
9.6	Field Trials	257
9.6.1	Further work	258
Appendix.....		259
PCB Circuit		259
List of References		261

List of Tables

Table 1-1: Chapter organisation and description of each chapter.	14
Table 2-1: Selecting the right conductivity cell (Radiometer, n.d.).....	50
Table 2-2: Indicative conductivity values of some commonly used samples.....	51
Table 2-3: Indicative temperature coefficients for several samples	55
Table 2-4: User requirements for each separate sensor.	59
Table 2-5: Characteristics of existing technologies for direct soil pH sensing. (Specifications obtained from official websites of manufacturers).....	60
Table 2-6: Characteristics of existing technologies for soil conductivity sensing. (Specifications obtained from official websites of manufacturers).....	61
Table 2-7: Experimental results for each type. (Cranny & Atkinson, 1998)	65
Table 2-8: Experimental results of each type. (Belford, et al., 1987)	70
Table 3-1: RE structure to investigate the effect of Ag/AgCl paste on RE's performance.....	93
Table 3-2: Electrode susceptibilities from different Ag/AgCl pastes and the tested KCl concentration ranges	94
Table 3-3: RE structure for electrodes without Ag/AgCl layer to find optimum KCl weight percentage in KCl polymer matrix on top.	97
Table 3-4: REs performance without Ag/AgCl paste (bare Ag) and adding the KCl polymer matrix on top	98
Table 3-5: RE structure for electrodes tested for hydration, lifetime and drift rate.....	102
Table 3-6: Lifetimes, drift rates and hydration times of the best performing electrodes.	103
Table 3-7: RE structure to find the optimum KCl weight percentage for Polymer Ag/AgCl paste.....	109
Table 3-8: Susceptibilities of electrodes with polymer based Ag/AgCl layer	110
Table 3-9: RE structure to find the optimum KCl weight percentage for Glass PPCFB2 Ag/AgCl paste.....	112

Table 3-10: RE structure to find the optimum KCl weight percentage for Glass PPCFC3 Ag/AgCl paste.	112
Table 3-11: Performances of electrodes with glass PPCFB2 Ag/AgCl paste..	113
Table 3-12: Performances of electrodes with PPCFC3 Ag/AgCl paste	115
Table 3-13: RE structure for investigating the effect of Ag in KCl polymer matrix.	116
Table 3-14: Ag/AgCl paste composition for investigating Ag to AgCl & binder to powder ratios.	122
Table 3-15: Averaged potentials for each electrode type in each solution.	133
Table 3-16: Ag/AgCl paste composition for investigating the effect of adding the KCl polymer matrix on electrodes' performance.	134
Table 3-17: Susceptibilities of polymeric Ag/AgCl hydrated and drifted in 4 M KCl solution.	138
Table 3-18: Susceptibilities of glassy Ag/AgCl hydrated and drifted in 4 M KCl solution.	139
Table 3-19: Susceptibilities of polymeric Ag/AgCl hydrated and drifted in 0.04 M KCl solution.	140
Table 3-20: Susceptibilities of glassy Ag/AgCl hydrated and drifted in 0.04 M KCl solution.	141
Table 4-1: pH ISE structure for experiment pH.1-Dielectric.....	147
Table 4-2: Sensitivities of the electrodes at different temperatures.	155
Table 6-1: Electrolyte conductivities, current levels and frequencies for experiment COND.1-Gold-15mm.....	179
Table 6-2: Electrolyte conductivities, current levels and frequencies for experiments COND.2-Gold-20 mm and COND.3-Gold-30 mm...	182
Table 6-3: Electrolyte conductivities, current levels and frequencies for experiments COND.4-Platinum-15 mm, COND.5-Platinum-20 mm and COND.6-Platinum-40 mm.	183
Table 6-4: Values of the constants A and B for linear fit to sensor conductivity response as a function of electrode spacing for gold and platinum electrodes	184
Table 6-5: Calculated cell constant expressions for gold electrodes.....	185
Table 6-6: Values of the constants A and B for different electrode spacing for gold and platinum electrodes	187
Table 7-1: Soil mixture composition.....	222
Table 8-1: Calibration points for sensors to be used for field trials.....	236

List of Figures

Figure 1-1: Climate Station (left) with the large and expensive preinstalled soil sensors (right) (Verhoef, 2011).	7
Figure 2-1: Sequence of procedures for conducting a soil test (Benton Jones, 2001).....	21
Figure 2-2: Examples of Thick-Film Printing components (Tarr, n.d.)	26
Figure 2-3: Components of Thick-Film Screen Printing procedure. (Sophocleous, 2009)	26
Figure 2-4: Proper curing profile. (Holmes & Loasby, 1976)	28
Figure 2-5: Transmitters incorporating an operational amplifier (upper left), pressure sensor in a gearbox (upper right), water quality sensor (lower left), chemical sensors (lower right) (Sophocleous, 2009)	29
Figure 2-6: Typical electrochemical cell with two electrodes	31
Figure 2-7: Construction of a typical calomel electrode. (Sophocleous, 2009)	34
Figure 2-8: Typical construction of a silver-silver chloride RE.....	36
Figure 2-9: A commercial silver-silver RE. (Glanc-Gostkiewicz, et al., 2013).....	38
Figure 2-10: The construction of a conventional pH ISE combined with a RE. ...	40
Figure 2-11: Electrical circuit of a conductivity cell explaining the ion movement completing the circuit (Radiometer, n.d.).....	45
Figure 2-12: Typical operation of a toroidal conductivity sensor (Radiometer, n.d.)	47
Figure 2-13: Circuit arrangement for a two pole conductivity cell (Radiometer, n.d.)	48
Figure 2-14: Electrode configuration for a four pole conductivity cell (Radiometer, n.d.)	49
Figure 2-15: Operable ranges for different conductivity cell types	51
Figure 2-16: Field lines between the two electrodes of a conductivity cell (Radiometer, n.d.)	53
Figure 2-17: Four electrodes conductivity cell (Nabighian, 1988).....	56
Figure 2-18: Electrode configuration of some standard conductivity cells, d is the distance between the electrodes and n is just an integer (Nabighian, 1988)	56

Figure 2-19: A cross section of the silver-silver chloride Thick-Film reference electrode. (Cranny & Atkinson, 1998).....	64
Figure 2-20: The cross section of the two different structures. (Simonis, et al., 2004)	66
Figure 2-21: The structure of the proposed electrode. (Prasek, et al., 2008) ...	67
Figure 2-22: Typical construction of a Thick-Film reference electrode. (Atkinson, et al., 2011)	69
Figure 2-23: The construction of a Thick-Film pH electrode. (Mihell & Atkinson, 1998)	71
Figure 2-24: Diagram of the electronic circuit. (Karagounis, et al., 1986).....	72
Figure 2-25: Structure of their proposed sensor. (Karagounis, et al., 1986)	72
Figure 2-26: The construction of their sensors with the microelectrode array and the gas permeable membrane. (Wittkamp, et al., 1997)	74
Figure 2-27: Structure of the potentiometric dissolved oxygen sensor. (Martínez-Máñez, et al., 2004)	75
Figure 3-1: Diagram of the experimental setup with the 36 channel multiplexer and the data logger. (Glanc, et al., 2013)	86
Figure 3-2: Experimental setup without the magnetic stirrer (left) and with the magnetic stirrer (right). (Glanc, et al., 2013)	88
Figure 3-3: Construction of the suggested Ag/AgCl reference electrode. (Glanc-Gostkiewicz, et al., 2013)	88
Figure 3-4: The substrate with six simultaneously printed electrodes. (Glanc-Gostkiewicz, et al., 2013)	90
Figure 3-5: Graphical representation of electrode susceptibility to chloride concentration for different Ag/AgCl pastes	95
Figure 3-6: Chloride susceptibility of reference electrodes without Ag/AgCl layer versus KCl concentration in KCl polymer matrix (no extra layer-blue, extra layer without KCl-red, extra layer on top with 20% KCl-green).....	99
Figure 3-7: SEM analysis of the cross section from newly made electrodes with 50% KCl polymer matrix.....	101
Figure 3-8: Hydration time of selected electrodes versus KCl percentage in the first layer	104
Figure 3-9: Lifetime of the selected electrodes as a function of the KCl weight percentage in the first layer	105

Figure 3-10: Relationship between the drift rate of selected electrodes and the KCl weight percentage in the first layer.....	106
Figure 3-11: pH buffer sequence for experiment RE.14-pH buffers.....	107
Figure 3-12: Voltage fluctuations of the selected electrode types in pH buffers 4, 7 and 10	108
Figure 3-13: Relationship between chloride susceptibility and the KCl weight percentage in the KCl polymer matrix (fired Ag/AgCl - orange, normal Ag/AgCl - blue)	111
Figure 3-14: Chloride susceptibility versus KCl weight percentage on the electrodes with glass PPCFB2 Ag/AgCl paste.....	114
Figure 3-15: Chloride susceptibilities of REs with glass PPCFC3 Ag/AgCl paste against KCl weight percentage on the electrodes	115
Figure 3-16: Voltage versus KCl solution concentration of electrodes with no KCl in the top layer (starting points - green dots, ending points - red dots)	117
Figure 3-17: Performance of electrodes with 5% KCl versus KCl solution concentration (starting points - green dots, ending points - red dots)	118
Figure 3-18: Performance of electrodes with 30% KCl against KCl solution concentration (starting points - green dots, ending points - red dots)	119
Figure 3-19: Performance of electrodes without any KCl on top layer versus KCl solution concentration after 3 days drift in saturated KCl solution (starting points - green dots, ending points - red dots).....	120
Figure 3-20: Performance of electrodes with 5% KCl on top layer versus KCl solution concentration after 3 days drift in saturated KCl solution (starting points - green dots, ending points - red dots).....	120
Figure 3-21: Performance of electrodes with 30% KCl on top layer versus KCl solution concentration after 3 days drift in saturated KCl solution (starting points - green dots, ending points - red dots).....	121
Figure 3-22: The potential of the polymeric electrodes with binder to powder ratio of 2:1 in 4 M KCl solution.....	124

Figure 3-23: The performance of the polymeric electrodes with binder to powder ratio of 1:1 in 4 M KCl solution.....	125
Figure 3-24: The performance of the polymeric electrodes with binder to powder ratio of 1:2 in 4 M KCl solution.....	126
Figure 3-25: The performance of the polymeric electrodes with binder to powder ratio of 2:1 in 0.04 M KCl solution.	127
Figure 3-26: The performance of the polymeric electrodes with binder to powder ratio of 1:1 in 0.04 M KCl solution.	127
Figure 3-27: The performance of the polymeric electrodes with binder to powder ratio of 1:2 in 0.04 M KCl solution.	128
Figure 3-28: The performance of the glassy electrodes with binder to powder ratio of 2:1 in 4 M KCl solution.....	129
Figure 3-29: The performance of the glassy electrodes with binder to powder ratio of 1:1 in 4 M KCl solution.....	130
Figure 3-30: The performance of the glassy electrodes with binder to powder ratio of 1:2 in 4 M KCl solution.....	130
Figure 3-31: The performance of the glassy electrodes with binder to powder ratio of 2:1 in 0.04 M KCl solution.	131
Figure 3-32: The performance of the glassy electrodes with binder to powder ratio of 1:1 in 0.04 M KCl solution.	132
Figure 3-33: The performance of the glassy electrodes with binder to powder ratio of 1:2 in 0.04 M KCl solution.	132
Figure 4-1: Structure of the ruthenium oxide ISE. (Soleimani, et al., 2013)....	144
Figure 4-2: Voltage vs Time showing the electrode potential drift in the two pH buffers.....	148
Figure 4-3: pH buffer sequence for experiment pH.2-Temperature.....	150
Figure 4-4: Voltage vs Time for the investigation on sensitivity changes due to temperature dependence.	151
Figure 4-5: Voltage vs pH at 25 °C.....	152
Figure 4-6: Voltage vs pH at 40 °C.....	152
Figure 4-7: Voltage vs pH at 60 °C.....	153
Figure 4-8: Voltage vs pH at 80 °C.....	154
Figure 5-1: Sensirion's prototyping kit including the LED screen, SHT21, battery and the microcontroller.	160
Figure 5-2: SHT21 units and the connections with the PCB.....	160
Figure 5-3: The two wire lengths used for the experiments.	161

Figure 5-4: Temperature error between the sensors and the chamber's reading.....	162
Figure 5-5: Humidity readings from the sensors in the chamber at a constant temperature of 25 °C.....	163
Figure 5-6: Humidity readings when the sensors are covered with PTFE and immersed in water.	164
Figure 5-7: Diagrams of the interface used for temperature (left) and humidity (right).	165
Figure 5-8: Temperature error of the sensors for various chamber's temperatures.	166
Figure 5-9: Humidity readings to compare the sensors' performance with and without PTFE membrane in a 75% RH environment.....	167
Figure 5-10: Humidity error of the first sensor at various humidity levels for all experiments.	168
Figure 5-11: Humidity error of the second sensor at various humidity levels for all experiments.....	169
Figure 5-12: Humidity error of the third sensor at various humidity levels for all experiments.....	169
Figure 5-13: Humidity error of the fourth sensor at various humidity levels for all experiments.....	170
Figure 5-14: Humidity error of the fifth sensor at various humidity levels for all experiments.....	170
Figure 5-15: Humidity error of the sixth sensor at various humidity levels for all experiments.....	171
Figure 6-1: Existing TF sensor array.....	175
Figure 6-2: Sensor array interface circuit (left), Conductivity circuit block diagram. IP+ and IP- are connected to the voltage measuring electrodes of the cell while OP+ and OP-are connected to the current driving electrodes of the cell (right).	176
Figure 6-3: Conductivity cell electrode configuration and geometry.	177
Figure 6-4: 15mm spaced gold electrode conductivity sensor output voltage levels as a function of 1 mA square wave current drive frequencies in different conductivity test solutions. (green-4 mS/cm, pink-2 mS/cm, blue-1 mS/cm, red-0.5 mS/cm, black-0.2 mS/cm).	180

Figure 6-5: 15mm spaced gold electrode conductivity sensor output voltage levels as a function of 1 kHz drive current amplitude in different conductivity test solutions. (green-4 mS/cm, pink-2 mS/cm, blue-1 mS/cm, red-0.5 mS/cm, black-0.2 mS/cm).	181
Figure 6-6: Sensor output voltage levels as a function of electrode spacing for 1 mA drive current square wave at 1 kHz in different conductivity test solutions (green-4 mS/cm, pink-2 mS/cm, blue-1 mS/cm, red-0.5 mS/cm, black-0.2 mS/cm).....	182
Figure 6-7: Output voltage levels as a function of electrode spacing for 1 mA drive current square wave at 1 kHz in different conductivity test solutions for gold electrode (left) and platinum electrode (right) sensors (green-4 mS/cm, pink-2 mS/cm, blue-1 mS/cm, red-0.5 mS/cm, black-0.2 mS/cm)	184
Figure 6-8: Sensor output voltage levels as a function of resistivity in different conductivity test solutions with 1 mA drive current square wave at 1 kHz for different electrode spacing (black-15 mm, red-20 mm, blue-30 mm, purple-40 mm).....	185
Figure 6-9: Output voltage levels as a function of resistivity with 1 mA drive current square wave at 1 kHz for gold electrode sensors for different electrode spacing (black-15 mm, red-20 mm, blue-30 mm) & values of the constants A and B for linear fit to electrode response at different electrode spacing.....	186
Figure 6-10: Output voltage levels as a function of resistivity with 1 mA drive current square wave at 1 kHz for gold (left) and platinum (right) electrode sensors for different electrode spacing in different conductivity test solutions (black-15 mm, red-20 mm, blue-30 mm, purple-40 mm)	187
Figure 7-1: TF substrate with waterproofed soldered connections before installing them in the soil columns.....	192
Figure 7-2: Experimental rig before the sensors were installed.....	193
Figure 7-3: Experimental rig after the sensors were installed including the interface on the prototype board.....	194
Figure 7-4: A photo of the complete experimental rig with the power supplies, the data logger and the computer used to run the software.....	195
Figure 7-5: Electronic circuit used for the pH sensor.....	197

Figure 7-6: Electronic circuit used for the dissolved oxygen sensor.....	198
Figure 7-7: Electronic circuit used for the PRT.....	199
Figure 7-8: Final stage of the interface with the sensors connected.....	200
Figure 7-9: Performance of the dissolved oxygen sensor in aqueous solutions.	201
Figure 7-10: Performance of the pH sensor in pH buffers using the same instrumentation.	202
Figure 7-11: Humidity readings from SHT21S in the pipes.....	203
Figure 7-12: Temperature readings from SHT21S in the pipes.....	204
Figure 7-13: Temperature readings from PRT in the pipes from the same experiment.....	205
Figure 7-14: pH sensors' performance at room temperature for the experiment using deionised water and ascorbic acid.	206
Figure 7-15: Readings from the dissolved oxygen sensors in the pipes from the same experiment with deionised water and ascorbic acid. .	207
Figure 7-16: Temperature readings from the PRT in the pipes of the same experiment with deionised water and ascorbic acid.	208
Figure 7-17: Humidity readings of SHT21S in the pipes in the same experiment for deionised water and ascorbic acid.	209
Figure 7-18: Temperature readings from SHT21S in the pipes in the same experiment with water and ascorbic acid.	210
Figure 7-19: Performance of pH sensors in modified soil rig using floral foam.....	211
Figure 7-20: Performance of dissolved oxygen sensors in modified soil rig using floral foam.....	212
Figure 7-21: Performance of PRT sensors in modified soil rig using floral foam.....	212
Figure 7-22: Damaged PVC membrane of DO ₂ sensor after pipes experiment.....	213
Figure 7-23: Evolution of new soil rig design.....	215
Figure 7-24: New soil rig, final concept design (left) and manufactured soil rig (right).....	216
Figure 7-25: Sensor arrays before and after experiments when all sensors powered from the same PCB.....	217
Figure 7-26: Schematic of the test rig with sensor orientation and positioning.....	218

Figure 7-27: Conductivity sensor output voltage levels compared with water content of the soil column as water is drained over time	220
Figure 7-28: Conductivity sensor output voltage levels compared with water content of the soil column as water is drained over time showing 24 hour fluctuation due to variation in day and night time temperatures and electrical pick up (noise spikes) from adjacent machinery	220
Figure 7-297: Altered test rig for the soil mixture test (all numbers are in centrimetres)	222
Figure 7-30: Typical resistance and water content time graph for Leighton Buzzard sand with an input current of 1 mA and a draining rate of 0.967 ml/s	224
Figure 7-31: Resistance versus water content graph for Leighton Buzzard sand. (cycle 1:blue-1.063 ml/s-1 mA, cycle 2:red-0.67 ml/s-1 mA, cycle 3:green-0.967 ml/s-0.5 mA, cycle 4:purple-0.236 ml/s-0.1 mA)	225
Figure 7-32: Builders sand resistance water content graph with three cycles (cycle 1:blue-0.047 ml/s-0.25 mA, cycle 2:red-0.322 ml/s-0.25 mA, cycle 3:green-0.352 ml/s-0.1 mA)	226
Figure 7-33: Resistance versus water content graph for custom made soil mixture for two cycles (cycle 1:blue-0.1 mA, cycle 2:red-0.25 mA)	227
Figure 7-34: Resistance versus water content graph for the first cycle of different soil types (Leighton Buzzard-blue, Builder's sand-red, Soil mixture-purple)	228
Figure 7-35: Resistance versus water content graphs for the second cycle of different soil types (Leighton Buzzard sand-blue, Builder's sand-red, Soil mixture-green)	228
Figure 8-1: IP67 box with the PCB and the wires coming out of the box	234
Figure 8-2: Four IP67 boxes with sensor array holders during initial calibration testes	234
Figure 8-3: CR1000 data logger and battery in the waterproof box	235
Figure 8-4: Existing pole on site where the waterproof box with CR1000 and the battery were connected to	237
Figure 8-5: Four drilled holes to insert the sensor arrays and boxes	238

Figure 8-6: Sensor arrays in the array holders and then they array holders were inserted in floral foam cubes.....	238
Figure 8-7: pH sensors data from field trials	239
Figure 8-8: DO2 Sensors data from field trials.....	240
Figure 8-9: PRT sensors data from field trials	240
Figure 8-10: Conductivity sensors data from field trials	241
Figure 8-11: Box with PCB after digging it out from the field	242

DECLARATION OF AUTHORSHIP

I, Marios Sophocleous

declare that this thesis and the work presented in it are my own and has been generated by me as the result of my own original research.

Thick-Film Underground Sensors

I confirm that:

1. This work was done wholly or mainly while in candidature for a research degree at this University;
2. Where any part of this thesis has previously been submitted for a degree or any other qualification at this University or any other institution, this has been clearly stated;
3. Where I have consulted the published work of others, this is always clearly attributed;
4. Where I have quoted from the work of others, the source is always given. With the exception of such quotations, this thesis is entirely my own work;
5. I have acknowledged all main sources of help;
6. Where the thesis is based on work done by myself jointly with others, I have made clear exactly what was done by others and what I have contributed myself;
7. Parts of this work have been published and these publications are listed in the following page.

Signed:

Date:

List of Publications

Conference Papers:

1. Glanc-Gostkiewicz M, **Sophocleous M**, Atkinson JK, Garcia-Breijo E. "*Performance of miniaturised Thick-Film solid state pH sensors*". Eurosensors 2012; Poland2012.
2. **Sophocleous M**, Glanc-Gostkiewicz M, Atkinson JK, García-Breijo E. "*An Experimental Analysis of Thick-Film Solid-State Reference Electrodes*". IEEE Sensors 2012; Taiwan2012.
3. J.K. Atkinson, **M. Sophocleous**, "*A Novel Thick-Film Screen Printed Electrical Conductivity Sensor for Measurement of Liquid and Soil Conductivity*". IEEE Sensors 2014; Spain.

Journal Papers:

1. Atkinson JK, Glanc M, Prakorbjanya M, **Sophocleous M**, Sion RP, Garcia-Breijo E. "*Thick film screen printed environmental and chemical sensor array reference electrodes suitable for subterranean and subaqueous deployments*". Microelectronics International. 2013; 30(2):92-8.
2. Glanc M, **Sophocleous M**, Atkinson JK, Garcia-Breijo E. "*The effect on performance of fabrication parameter variations of thick-film screen printed silver/silver chloride potentiometric reference electrodes*". Sensors and Actuators A: Physical. 2013; 197:1-8.
3. Glanc-Gostkiewicz M, **Sophocleous M**, Atkinson JK, Garcia-Breijo E. "*Performance of miniaturised Thick-Film solid state pH sensors*". Sensors and Actuators A: Physical. 2013.
4. Soleimani M, **Sophocleous M**, Glanc M, Atkinson J, Wang L, Wood RJK, R.I. Taylor. "Engine oil acidity detection using solid state ion selective electrodes". Tribology International. 2013; 65:48-56.
5. Soleimani M, **Sophocleous M**, Wang L, Atkinson J. K., Hosier I. L., Vaughan A. L., Taylor R. I., Wood R. JK. "Base oil oxidation detection using novel chemical sensors and impedance spectroscopy

- measurements". *Sensors and Actuators B: Chemical*. 2014; 199; 247-258.
6. **Sophocleous M**, Atkinson J. K. "*A Novel Thick-Film Screen Printed Electrical Conductivity Sensor for Measurement of Liquid and Soil Conductivity*". *Sensors and Actuators B: Chemical*. 2015. 213C, 417-422.
 7. **Marios Sophocleous**, John K. Atkinson, Joel Smethurst, William Powrie, Alessia Ingenito. "Simultaneous monitoring of soil electrical conductivity and water content as soil properties sensing". In preparation to be submitted in *Remote Sensing of Environment*. 2015.

Acknowledgements

This thesis is dedicated to my father Andreas Sophocleous who passed away on the 2nd of October 2015. He has been a major influence to my life as a role model during my life and especially during my PhD studies.

I would like to take this opportunity to express my deep gratitude to my supervisor Prof. John K. Atkinson for his continuous support through my PhD degree. He is the one who taught me what research means and the truthful way it is done. I would also like to thank him for his patience and his motivating talks that inspired me to move on with the research. His vast range of knowledge was an extremely helpful asset and the time he has spent with me explaining everything I have asked is highly appreciated. It is his guidance that pushed me in the right direction to complete my PhD study until now.

I would also like to thank Dr. Eduardo Garcia-Breijo, Mrs Monika Glanc and Dr Mostafa Suleimani for their help in and outside the laboratory as well as their support while I was performing the research and writing up the thesis.

List of Abbreviations

A/D or ADC	Analog to Digital Converter
AC	Alternating Current
Ag	Silver
Ag/AgCl	Silver/Silver Chloride
AgCl	Silver Chloride
C	Carbon
CE	Counter Electrode
CMOS	Complementary Metal-Oxide Semiconductor
CN	Cellulose Nitrate
CV	Cyclic Voltametry
DC	Direct Current
DFN	Dual Flat No leads
ERT	Electrical Resistance Tomography
ESL	ElectroScience Lab
FUSE	Floodplain Underground SENSors
GE	Guard Electrode
GEM	Gwent Electronic Materials
IoT	Internet of Things
ISE	Ion Selective Electrode
KCl	Potassium Chloride
LED	Light Emitting Diode
LOC	Lab-On-a-Chip
N	Nitrogen
NIST	National Institute of Standards and Technology
NPK	Nitrogen, Phosphorus, Potassium
NR	Network Rail
Op Amps	Operational Amplifiers
PA	Precision Agriculture
PC	Personal Computer
PCB	Printed Circuit Board
PIDS	Polyisophthalamide Diphenylsulfone
PRT	Platinum Resistance Thermometer
PTFE	PolyTetraFluoroethylene
PVC	PolyVinyl Chloride
RE	Reference Electrode
RH	Relative Humidity
RTV	Room Temperature Vulcanizing

RuO ₂	Ruthenium (II) Oxide
SEM	Scanning Electron Microscopy
SDM	Sigma Delta Modulation
SHE	Standard Hydrogen Electrode
SOC	Soil Organic Carbon
SQI	Soil Quality Indicators
SSCM	Site Specific Crop Management
TCR	Temperature Coefficient of Resistance
TDR	Time Domain Reflectometry
TF	Thick Film
WE	Working Electrode
WUSN	Wireless Underground Sensor Network

Chapter 1: **Introduction**

1.1 Soil Monitoring

“Soil is the world's most vital component for food and fibre production” (Papendick & Parr, 1992) therefore, protection of such a crucial natural resource is of life-threatening importance. Environmental protection and current and future population health depends vastly on soil quality (Visser & Parkinson, 1992; Merrill, et al., 2013). Initially soil conservation was linked with preventing erosion. Later on, it was recognised that maintenance of fertility is as important as physically retaining the soil, and that any decrease in fertility is perhaps more significant globally, based on the area covered times production lost (Young, 1991; Stenberg, 1999). Historical data demonstrate the necessity of soil quality protection. Ancient Mesopotamia developed and thrived due to the effective irrigation of soils. Nonetheless, issues with soil salinity and silting up of irrigation channels initiated the agricultural systems to fail (Hillel, 1992). The vast majority of farmers are greatly aware of the significance of sustainable land-use, as that our population's health depends directly upon it. Their concerns bounce back by a growing public awareness of the impacts of soil quality on agriculture and the wider environment such as ecology and the impact of climate change on soil quality (Beare, et al., 1997; Gobin, et al., 2004).

Yet, nowadays economics for sustainable agriculture place an increasing pressure on farmers to exaggerate land-use beyond the limits of what is truly sustainable. As a result, an increasing demand for more information and better tools for monitoring the sustainability of their agricultural management arises (Beare, et al., 1997; Nortcliff, 2002).

1.2 Precision Agriculture

Precision agriculture (PA), also called satellite farming or site specific crop management (SSCM), is an agricultural management concept based on monitoring and responding to inter and intra-field variability in crops (Bongiovanni & Lowenberg-Deboer, 2004; Zhang, et al., 2002; Seelan, et

1. Introduction

al., 2003). "PA is conceptualized by a system approach to re-organize the total system of agriculture towards a low-input, high-efficiency, sustainable agriculture" (Shibusawa, 1998). The desire to respond to production variability in both space and time using new emerging technologies on a fine-scale has become the goal of PA (Whelan, et al., 1997; Adamchuk, et al., 2004; Cambardella & Karlen, 1999). Agricultural industry is in need of the capability to gather more comprehensive data on such variability and being able to accurately and timely respond to those changes. (Zhang, et al., 2002; Thorp & Tian, 2004; Wang, 2001)

PA is shown to be the right way ahead for farmers of the future due to the precise crop production, input optimisation lowering costs and environmental impact and also because PA can provide an audit trail that legislation and consumers increasingly require (Stafford, 2000; McBratney, et al., 2005). Nevertheless, there are two main barriers to be overcome for its wider implementation:

- a) PA is 'information-intensive'. Mapping of several soils, crops and environmental influences within a field generates 'data overload' for the farmer. Overcoming this issue requires the development of data integration tools, expert systems and decision support systems (Sigrimis, et al., 1999; Reyns, et al., 2002).
- b) There are several techniques for data acquisition for soil, crop and environmental factors but those methods are costly and labour-intensive since most of them require soil sampling and laboratory analysis. Automatic sensor systems are needed for precision agriculture to be widely practised (Stafford, 2000; Robert, 2002).

1.3 Impact of Climate Change on Soil Quality

In recent years, attention is directed on the possibilities that atmospheric and climatic changes have an impact on plants and vegetation (Theurillat & Guisan, 2001). Several relationships between climate and soil erosion are well established and have been used by

many researchers to hypothesise the concept of probable impact of climate change on soil erosion (Imeson & Lavee, 1998). There are strong correlations between soil carbon (C) reservoirs and climate. Extensive analysis of soil C storage as well as the amounts of nitrogen (N) stored in different soils, showed that amounts of soil organic C and N are positively interrelated with precipitation, and negatively interrelated with temperature at any particular amount of precipitation. Furthermore, it was shown that similar trends along temperature gradients exist in both American and Indian soils (Kirschbaum, 1995). It is suggested that temperature is the main controlling factor responsible for N concentration reductions in soil. Nitrogen reduction in soil means an increase in nitrogen uptake by vegetation as a response to temperature increase, which is considered as critical in controlling soil solution chemistry (Ineson, et al., 1998; Keller, et al., 2004).

Real-time monitoring of soil chemical and physical parameters to assess soil quality is the best way to provide the required data to soil scientists and weather analysts to prove and confirm any existing correlations between climate changes and soil quality.

1.4 Floodplain Underground Sensors (FUSE)

Floodplain Underground Sensors (FUSE) is a multi-disciplinary project with many partners involved, each of which has a different role. As a whole, the aim of the project is to acquire information from a specific floodplain and advance the existing environmental knowledge to a higher level. The proposed study was built upon an existing hydrological monitoring network currently in place in Oxford Meadows Special Area of Conservation.

Ecosystems found in this floodplain are rare which makes it extremely interesting for further investigation. “The species composition of floodplain vegetation and their ecosystem functions (e.g. leaf CO₂ uptake and transpiration) are very sensitive to the soil hydrological

1. Introduction

regime, which is highly variable both spatially and temporally. The hydrological regime also affects the temperature and nutrient regime of the root environment, leading to indirect impacts on vegetation” (Verhoef, 2011). The importance of these parameters on the growth and vegetation’s life in general is known, but the exact mechanisms and reasons are of a huge research interest to environmentalists and scientists.

A sophisticated combination of environmental data and computer models was used to acquire the requested information from multidisciplinary state-of-the-art technologies. A Wireless Underground Sensor Network (WUSN) was used to investigate soil parameters and nutrient flows during flooding. Furthermore, related monitoring of environmental variables was a source of information, as well as high-resolution Earth Observation data.

WUSN is a recently applied technology which provides environmental scientists with the ability to continuously monitor the explored parameters in a less invasive approach. Land-based sensor networks are preferred to have few or no above-ground components for various reasons; aesthetics and security being the primary reasons, as well as avoiding interference with land management practices. Those advantages have led scientists to use WUSNs where the majority of the sensing and transmitting components are underground. However, WUSNs are not widely used until now and they haven’t been tested long-term in harsh environments. WUSN keep track of nutrients in the soil transferred from the water either because of flooding or rain. Concentrations of those nutrients are particularly important because they define the growth rate of the vegetation as well as the vegetation type.

WUSNs are only a valid solution when the sensors are cheap, miniaturised and can be placed underground to monitor important soil and water parameters that soil scientist are interested in. Soil

1. Introduction

parameters can vary with soil type, position, depth and time. Therefore, in these applications, a high density sensor network is favoured implying an extremely high cost if the existing commercial sensors are used.



Figure 1-1: Climate Station (left) with the large and expensive preinstalled soil sensors (right) (Verhoef, 2011).

In addition, most commercial sensors require a significant amount of power which is always a problem in field applications. Environmental scientists insist on using a less invasive type of sensors which suggests the miniaturisation of the sensors.

Soil parameters are clearly dependent on the weather conditions and the water quality reaching the floodplain either through flooding or through rain. Therefore, monitoring the chemical parameters of the water-soil mixture during flooding or rain is the key to understanding the vegetation growth mechanisms. Chemical parameters such as pH, nitrates, phosphates and potassium concentrations can greatly define the vegetation's growth rate. Therefore, proper monitoring of those parameters can reveal important information on vegetation growth.

Furthermore, physical parameters such as soil temperature and conductivity are vital parameters. Soil conductivity defines the amount of water content in the soil and in combination with temperature can define the vegetation type that is favoured in the area.

1.5 Network Rail (NR)

Problems with dynamic response of a soil medium under moving loads are of substantial importance in several engineering areas, especially in connection with structures of transportation facilities. Vibrations of the medium are mostly generated by vehicles or trains traveling on the ground surface (with or without a rail track system) (Theodorakopoulos, 2003). The consequences of railway traffic, in terms of environmental damage due to vibration, noise and various pollutants, are vital especially as train speeds increase. “Concerning vibration, the effect of this speed is directly connected to its relative position from waves propagating through the ground” (Picoux & Le Houedec, 2005). These vibrations induce high levels of displacement in the rail and at the ground’s surface, having no impact on passenger’s comfort, but are of significant concern for the wear and tear of the tracks and neighbouring structures (Picoux & Le Houedec, 2005).

Up to date techniques in monitoring the stability of rail tracks are labour intensive and very expensive. Rail companies such as Network Rail (NR) are in need of a reliable, real-time decision providing tool on the stability of the soil as to when maintenance needs to be executed.

This project aimed to investigate the possibility of using data from low cost sensors, to understand the important parameters affecting soil stability and model their interrelationships. The acquired knowledge will allow the prediction of changes in soil stability to help with maintenance scheduling.

1.6 Aims & Objectives of Project

The problem to be solved is to provide the technology that can overcome the limitations of existing technologies in the area of real-time soil condition monitoring. At the moment, existing technologies can offer several soil measurements but these are laboratory based and are labour intensive. Furthermore, technologies that are designed to be

1. Introduction

used in the field are very expensive in the range of several hundreds of pounds. Soil parameters can vary widely spatially and over time. Soil scientists are in need of a low cost system that can be buried underground and stay in the ground for a certain period of time (ideally more than a year) and will transmit real-time data of soil parameters. In addition, cost of the system is a major factor because a high density network is required for the environmental scientists to generate a reliable model for the vegetation growth and the monitored soil parameters.

Currently, soil parameters are monitored by soil sampling and further laboratory tests. Soil sampling is a very labour intensive procedure and requires a lot of care because each step in the process can affect the next step and the quality of the tests.

This study has as a general aim to replace the current soil monitoring technique of soil sampling and provide the technology for in-situ real-time monitoring of soil parameters that are important and that can be actually measured in the field.

The aims of the project are clearly stated below:

- Overcome existing challenges of the sensors of the sensor array.
- Measure water content of soil using either a relative humidity sensor or a conductivity sensor which can be integrated on the existing array.
- Design & fabricate the required instrumentation for the operation of the existing array and the new conductivity sensor.
- Identify an appropriate technique to deploy the sensor array in the soil in order for the sensors to perform as predicted in aqueous solutions.
- Design a soil rig to mimic the real life environment in such a way that monitored parameters can be varied in a controlled manner.
- Test the performance of the sensors and instrumentation, both in the soil rig and in the field.

1. Introduction

While these are the aims of the study, the specific objectives for each aim are separated into the different sensor types and are presented below:

- pH Sensor
 - Reference Electrodes
 - Overcome the classical stability problem of solid state reference electrodes, of maintaining a stable potential in every solution. Decrease the chloride susceptibility of the electrodes from -59 mV/decade [Cl⁻] at room temperature, to the lowest possible point. Ideally that would be 0 mV/decade [Cl⁻].
 - Increase the lifetime of reference electrodes in aqueous solutions by identifying the important factors that affect the electrode's lifetime and optimising them for maximum lifetime. A preferable lifetime for the electrode would be more than a year deployed in the soil.
 - Identify and optimise the hydration time and drift rates of reference electrodes. Ideally, hydration time should be as low as possible, in the range of several seconds up to a couple of minutes. Drift rate should be either completely characterised in order to be compensated or should be decreased to an insignificant level of several microvolts per day.
 - Characterise the performance of the electrodes in chloride solutions and investigate the effect of other ions on their performance.
 - Ion-Selective-Electrodes
 - Optimise the performance of the electrodes to have the maximum sensitivity to pH and minimum susceptibility to other ions. Maximum theoretical

sensitivity for these electrodes is approximately -59 mV/pH at room temperature.

- Investigate the lifetime of the electrodes in pH buffers. A preferable lifetime for the electrodes would be the same as the reference electrodes, of more than a year.
- Investigate the effect of temperature on the performance of the electrodes and identify any possible temperature compensation process.
- Design the instrumentation for the proper operation of the pH sensor with enough flexibility to calibrate all sensors to have 0 V at pH 7 and have the same sensitivity with respect to mV/pH on the output. The output should be a unipolar dc voltage.
- Identify an appropriate technique to deploy the sensors in soil in a way that the pH of the solution entering the soil can be monitored.
- Dissolved Oxygen Sensor
 - Design the instrumentation for the correct operation of the existing dissolved oxygen sensor where the output of the sensor would be a unipolar dc voltage.
 - Identify an appropriate technique to deploy the sensor in soil but still be able to measure the dissolved oxygen level in the solution entering the soil.
- Platinum Resistance Thermometer
 - Design the instrumentation for the proper operation of the existing platinum resistance thermometer. The instrumentation should be flexible enough to calibrate for different absolute resistance and different temperature coefficients of resistance.
- Soil Water Content Measurements

1. Introduction

- Identify a technique to incorporate an existing relative humidity sensor on the array while the sensor will maintain the manufacturer's specifications.
- If using the commercial relative humidity sensor does not meet the applications requirements to relate water content of the soil with the measured relative humidity, a new conductivity sensor will be designed and fabricated.
- Characterise the performance of the conductivity sensor in solutions of varying conductivity with respect to input current, frequency, cell constant and conductivity ranges (100 $\mu\text{S}/\text{cm}$ - 4 mS/cm).
- Obtain a correlation between measured soil conductivity and water content.
- Design the instrumentation required to input an AC square wave to the sensor and generate a unipolar DC voltage output.
- Soil Rig Design
 - Design and construct a soil rig that will mimic the real life environment in the soil.
 - The sensor arrays should be inserted in soil and solutions should be flushed through the soil while testing the performance of the sensors in the rig.
 - Modify the rig so that ideally, the sensors will perform the same way as they do in aqueous solutions.
- Field Trials
 - Prepare sets of arrays with their instrumentation in waterproof boxes and place them underground at the site under investigation to compare how the results from real life environment compare to the experimental results.

Due to the limited time, not all the objectives were completed but there has been a clear step to initiate the work towards the completion of each separate objective and aim.

1.7 Chapters Organisation

The following chapters focus on the literature review, and the experimental work giving the hypothesis and the results and discussion section for each sensor separately. A table is provided below that shows the organisation of the chapters and a general sequence of the experiments performed.

1. Introduction

Table 1-1: Chapter organisation and description of each chapter.

Chapters	Description
1. Introduction	This chapter provides the motivation for the work and the problems to be solved as well as the aims and objectives of the study.
2. Literature Review	This chapter provides information on the current monitoring techniques and then moves on to the background theory of the operation of the sensors (pH, dissolved oxygen, platinum resistance thermometer and conductivity). A comprehensive review on the reported thick film sensing technologies is also provided for all sensors.
3. Reference Electrodes	In this chapter all the experimental work on reference electrodes is provided. The sequence of the experiments is: <ul style="list-style-type: none">• The effect of Ag/AgCl paste on chloride susceptibility• Electrodes without the Ag/AgCl layer• Polymer Ag/AgCl paste• Glass PPCFB2 & PPCFC3 Ag/AgCl pastes• Effect of Ag in KCl polymer matrix• Ag to AgCl & binder to powder ratios
4. pH ISEs	In this chapter all the experimental work on pH ISEs is provided. The sequence of the experiments is: <ul style="list-style-type: none">• Investigation of the dielectric layer on electrode's performance• Temperature effect on the pH ISE's performance
5. Relative Humidity & Temperature Sensor	In this chapter all the experimental work on the relative humidity & temperature sensors is provided. The sequence of the experiments is: <ul style="list-style-type: none">• Investigation of wire length on sensor accuracy• The effect of covering the sensor with

	<p>PTFE membrane on sensor's performance</p> <ul style="list-style-type: none">• PTFE membrane as a waterproofing method• Investigation of sensor's performance consistency between sensors• The effect of PTFE membrane on SHT21S performance• Effect of PTFE on the exact same sensors
<p>6. Conductivity Cell</p>	<p>In this chapter all the experimental work on the conductivity cell is provided. The sequence of the experiments is:</p> <ul style="list-style-type: none">• Investigation of frequency and current level effects• Investigating the effect of the distance between substrates• The effect of gold electrodes instead of platinum
<p>7. Soil Rig</p>	<p>In this chapter all the experimental work on the soil rig is provided. In these experiments an existing sensing array was used that included the dissolved oxygen sensor. The sequence of the experiments is:</p> <ul style="list-style-type: none">• Investigation of sensor array performance in solutions• Investigation of sensor array in soil pipes• Investigation of sensor array performance in modified soil pipes• Investigation of water content versus conductivity curve in different soil types
<p>8. Field Trials</p>	<p>In this chapter all the experimental work on field trials is provided. In these experiments, the sensors utilised were dissolved oxygen, pH, conductivity and platinum resistance thermometer. The sequence of the experiments is:</p>

1. Introduction

	<ul style="list-style-type: none">• Sensor array calibration in solutions• Investigation of sensor array performance in the field
9. Conclusions & Further Work	This chapter summarises the most significant conclusions drawn from the experiments and will provide the reader with information on the specific outcomes of the study.

Chapter 2: Literature Review

2.1 Current Monitoring Techniques

2.1.1 Soil Quality Indicators

Soil quality fundamentally is the capacity of a soil to function (Shukla, et al., 2006; Anderson, 2003). Soil quality can be reflected by measured soil physical, chemical and biological properties, also identified as soil quality indicators (SQIs). There is an increasing interest to identify SQIs in such a way so that they:

- i. Integrate soil physical, chemical and/or biological properties and processes.
- ii. Apply under diverse field conditions.
- iii. Complement either existing databases or easily measurable data.
- iv. Respond to land use, management practices, climate and human factors (Shukla, et al., 2006; Burger & Kelting, 1999).

Monitoring changes in the key SQI with time can determine if quality of a soil under a given land use and management system is improving, stable or declining (Shukla, et al., 2006; Visser & Parkinson, 1992; Stenberg, 1999; Nortcliff, 2002).

Several soil chemical properties have been proposed as indicators of nutrient supplying capacity of soils. Those indicators can be categorised in four types. The first one is the soil organic carbon status (SOC) (Shukla, et al., 2006; Bolinder, et al., 1998). This indicator is probably the most difficult to measure and at the moment can only be measured in the laboratory with complex procedures and techniques.

The second and most widely known category is nutrients, which can be split in the three different types of fertilisers. The fertiliser types are nitrogen, phosphorus and potassium which are commercially known as NPK (Arshad & Martin, 2002; Doran & Parkin, 2011).

Soil acidity is the third category and this is measured using the soil pH. Soil pH can change by the water quality or living organisms in the soil.

2. Literature Review

Monitoring soil's pH can be of high importance since some plants only grow in specific soil acidity ranges while the growth rate is highly dependent on it (Schoenholtz, et al., 2000; Keller, et al., 2004).

Last but not least is the soil salinity which is directly related to the electrical conductivity of the soil. Soil salinity is linked to the ion concentration in water in the soil and the ability of those ions to move from one place to another in the soil (Gil-Sotresa, et al., 2005).

In conjunction to the soil chemical properties affecting soil quality, there are several physical soil properties that are also significant. These properties are split into two types, the static and dynamic indicators. Static indicators are the soil mechanical properties such as soil texture, soil bulk density, porosity and permeability. Dynamic indicators are soil properties that have to do with soil or soil/water transportation such as erosion potential and leaching potential (Karlen, et al., 1992; Parr, et al., 1992).

Putting all the pieces together, SQIs are probably the best way forward for a sustainable and highly efficient precision agriculture and even environmental management.

2.1.2 Conventional Techniques

Conventional soil testing techniques involve a sequence of steps (Benton Jones, 2001) from field sampling to laboratory analysis (wet chemistry) and ultimately the interpretation of those results as a decision providing tool to maintain optimal soil quality.

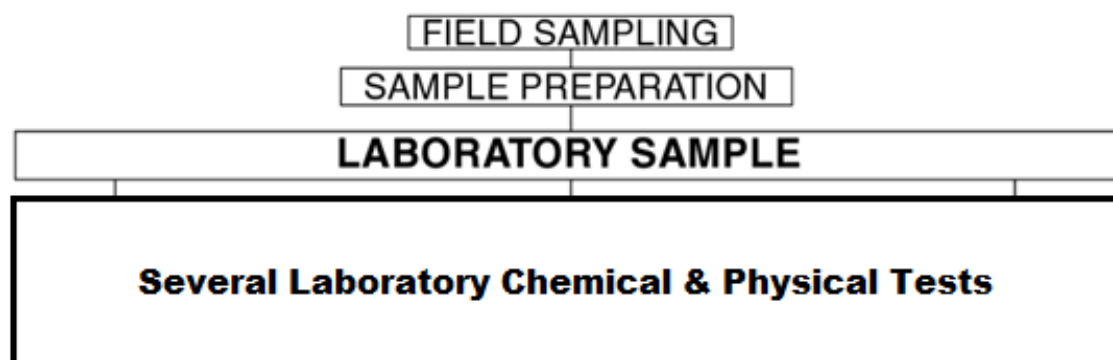


Figure 2-1: Sequence of procedures for conducting a soil test (Benton Jones, 2001)

These steps are highly interdependent and the care taken at each step can affect the result obtained at another. Consequently, conclusions drawn for one aspect must necessarily take into consideration of all others.

A soil test begins with field sampling and sample preparation before the laboratory analysis. When the soil sample is ready for laboratory analysis, several tests are performed to determine the SQIs' levels needed to evaluate the fertility and quality of the soil. The significance of a soil analysis result is as worthy as the quality of the sample analysed, whose quality is determined by (Benton Jones, 2001):

1. Field sampling technique.
2. Transportation conditions.
3. Sample preparation techniques.
4. Sample aliquot measurement.
5. Laboratory influences.
6. Sample storage.

Other on-site techniques exist to measure the mechanical properties of soil such as standard penetration, cone penetration, dilatometers, pressure meters, vanes, flat and stepped blades, hydro-fracture, borehole shear and torsional probes (Mayne, 2006).

2. Literature Review

Accurate and consistent measurements of soil pH are not easy as there are a number of aspects that can considerably affect the measurement. Usually a salt solution is used (0.01 M calcium chloride ($\text{CaCl}_2 \cdot 2\text{H}_2\text{O}$) or 1 M potassium chloride (KCl)) to overcome the “salt-effect” on pH measurement especially in the case of sandy soils or those soils with relatively low cation exchange capacities. Soil pH is also measured by chemical.

The most usual procedure is to use a pH meter made up of a reference electrode and a glass electrode (pH ion selective electrode). These electrodes may be physically separate or combined into one electrode body. When using a pH meter, the pH is determined in a soil/water slurry, which can be of various ratios, but normally 1:1 or 1:2 or in a soil slurry of either 0.01 M $\text{CaCl}_2 \cdot 2\text{H}_2\text{O}$ or 1 M KCl. If one of these salt solutions is used, the determined pH value will be different. Normally the pH determined in 0.01 M CaCl_2 is from 0.3 to 0.5 units less than that determined in water, and 0.7 to 1.0 units less when determined in 1 M KCl. Therefore, an interpretation of a pH value must be identified based on the solution in which it was determined, water or otherwise.

The determination of the soil pH is a three-step procedure:

- Prepare the soil-water, 0.01 M $\text{CaCl}_2 \cdot 2\text{H}_2\text{O}$, or 1 N KCl slurry.
- Calibrate the pH meter.
- Place the electrodes into the prepared slurry and read the pH (Benton Jones, 2001).

The level of soluble salts found in the soil solution can be measured by monitoring the electrical conductivity of the solution or the soil solution can be assessed for its elemental content. Usually the electrical conductivity of the soil solution is measured. As soluble salts increase, the usual effect is decreased plant growth; therefore, soluble salt monitoring is of vital significance. Soils affected by high soluble salt levels are also difficult to manage, particularly when sodium is the major cation contributing to the high salt level. In natural environment, soils

with high soluble salt content are found in low-rainfall areas. Soluble salt problems occur because of the use of salt-laden irrigation waters, or of improper fertilizer placement, high fertilizer application rates, or accumulation from repeated fertilizer applications. Salinity, affects about 25% of the croplands in the world and is becoming an increasing problem in most irrigated croplands. Most field crops can be damaged by fertilizer placement too close to germinating seeds or young plants. High soluble salt is a common problem in container growing, the result of accumulating applied plant nutrient element ions. Soluble salt monitoring is recommended as an important procedure for the container and hydroponic grower, indicating when containers should be leached or hydroponic solutions replenished. The cations Na^+ , K^+ , Ca^{2+} , Mg^{2+} , and NH_4^+ , and the anions Cl^- , NO_3^- , HCO_3^- , SO_4^{2-} , and CO_3^{2-} contribute to the conductivity of the soil solution or irrigation water.

The specific conductance or soluble salt level of a soil can be measured based on water saturation extract or a 1:2 soil/water extraction. An appropriate quantity of extractant is obtained and its specific conductivity is measured. The extraction procedure (soil/water ratio) chosen will yield different interpretative results; therefore, it is important that the interpretation values chosen are appropriate to the extraction procedure employed.

The various methods for determining soluble salts or salinity are described.

The steps for 2:1 Water/Soil Extraction are:

- Scoop 10 cm³ 2-mm-sieved soil into a beaker, add 20 mL water, stir thoroughly, and allow the suspension to settle for at least 30 min or long enough for the solids to settle.
- Draw the supernatant into the conductivity pipette and measure the conductivity.

The steps for 1:1 Water/Soil Extraction are:

2. Literature Review

- Scoop 20 cm³ 2-mm-sieved soil into a test tube or small container.
- Add 20 mL water, stir thoroughly, and allow the suspension to stand 15 to 20 min.
- Insert the conductivity cell into the suspension and read the electrical conductivity.

The steps for the Saturated Paste Method are:

- Weigh 250 g air-dried <10-mesh-sieved (2-mm) soil into a 400-mL beaker.
- Add water while stirring with a spatula until the soil slides freely from the surface of the spatula.
- Note: At saturation, the soil paste will glisten as it reflects light. Let stand for 1 h.
- Transfer the saturated paste to a filter funnel and draw water from the soil by applying vacuum and determine the conductivity in the obtained filtrate (Benton Jones, 2001).

2.1.3 Limitations

Conventional soil analysis techniques mentioned earlier in this chapter demonstrate several advantages and disadvantages that can restrict their use in applications where fast response is an important requirement.

Soil sampling is a very timely and labour intensive procedure. Furthermore, it is very sensitive and highly complex making it non-viable for non-experts to use (Schoenholtz, et al., 2000). Timely procedures for soil analysis result in a slow response eliminating the opportunity farmers and soil scientists to ensure on-time responses. In addition, sampling rate is another issue since soil chemical properties vary widely not only spatially but also timely. Likewise, analysing physical soil properties using the existing technologies one will face the same downsides. (Bolinder, et al., 1998; Parr, et al., 1992)

All these methods are very expensive and are off-grid techniques. In the 21st century where technological advances allow for automated systems to provide remote operation and observation, a different approach is needed to provide real-time measurements of SQIs. Nowadays, using technologies such as the Internet of Things (IoT), all the information can be brought to the farmer, environmentalists and soil scientists for a deeper understanding of nature's complex mechanisms and more efficient precision agriculture. (Verhoef, 2011)

In-situ soil condition monitoring with the use of chemical and physical sensors is an emerging research area with primary purpose to overcome the drawbacks of the past technologies. Specialised, less invasive underground sensors of low cost and wireless transmission is widely recognised as the best way forward. (Beare, et al., 1997; Young, 1991; Papendick & Parr, 1992)

2.2 Rationale of Thick-Film Technology

2.2.1 State of the art

Thick-Film (TF) Screen Printing initiated in ancient Chinese culture where silk cloth templates were used to deposit dye onto cloth in complex patterns. In the 1950s, it was proposed that, TF Technology could substitute the printed circuit board process (Holmes & Loasby, 1976; Tarr, n.d.). As the technology evolved, a whole new field of electronics, such as TF Hybrid circuits, appeared from the combined fabrication of components made by different technologies.

TF technology is defined as the successive sequential process of layer printing and firing in order to obtain the final conductor, insulator or resistive paths that are required for the specific application. Each layer is initially a paste that has a set of specific properties. Pastes' types can vary from conductors, resistors and dielectrics for crossovers, waterproofing or even capacitor pastes. (Holmes & Loasby, 1976; Haskard & Pitt, 1997; Prudenziati, 1992; Prudenziati, 1991)

2. Literature Review

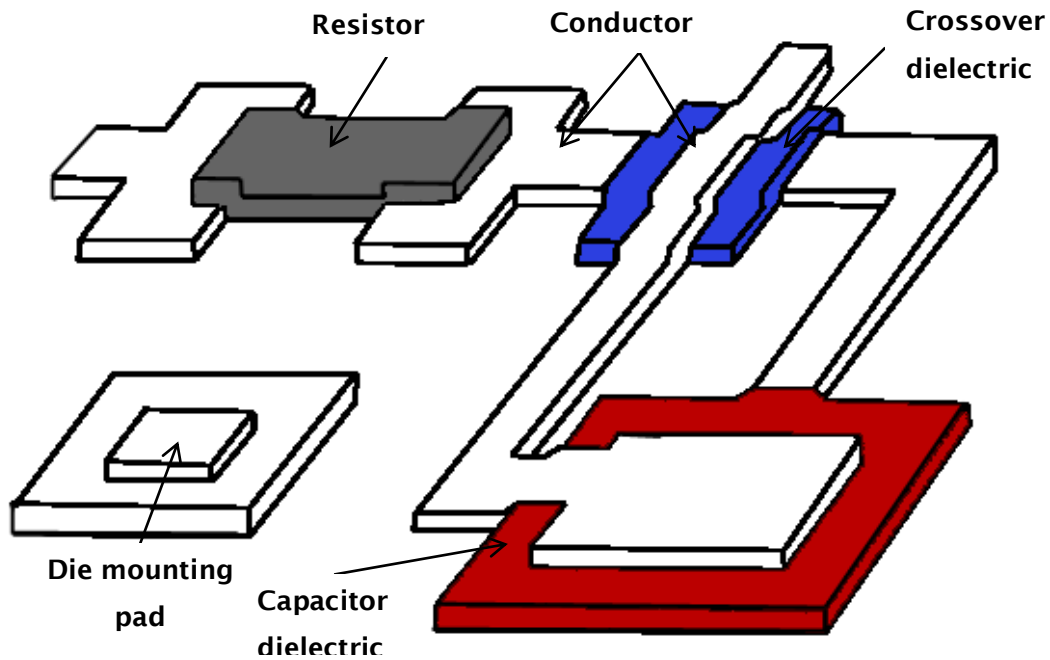


Figure 2-2: Examples of Thick-Film Printing components (Tarr, n.d.)

2.2.2 Thick-Film Screen Printing Procedure

The components used for screen printing are shown and labelled on Figure 2-3.

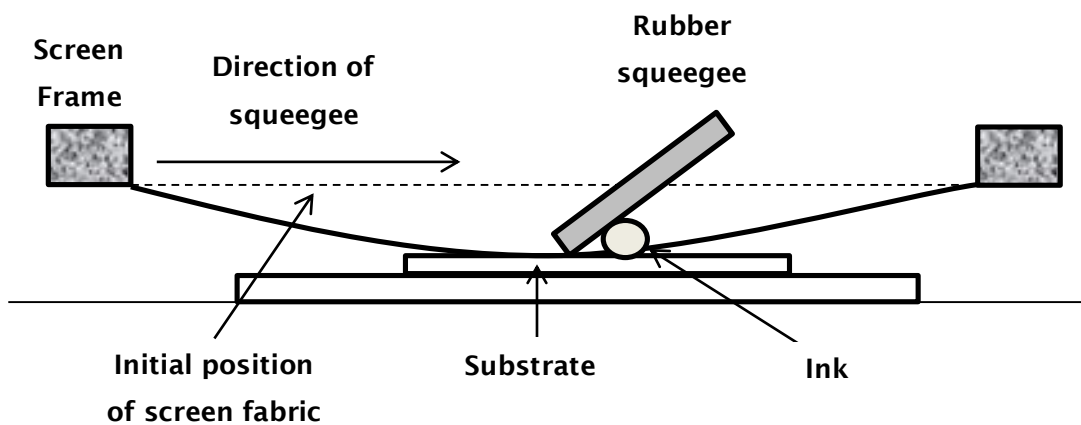


Figure 2-3: Components of Thick-Film Screen Printing procedure.

(Sophocleous, 2009)

Screen printing obeys a basic principle of operation. Ink is placed on the screen and the squeegee by moving from left to right or vice versa pushes the ink through the porous area of the screen and subsequently depositing the ink on the substrate at the desired position.

Screens are made of highly tensioned stainless steel or polyester mesh, with a relatively open weave, to allow the printing paste to pass through it and have a 'transparency' of about 40%. Stainless steel has the best dimensional stability and a greater percentage open area than polyester, making it easier for the ink to go through the screen while polyester, is less likely to be damaged and is more easily deflected. High mesh counts can provide higher resolution but lower layer thickness.

Some basic rules for screen printing are (Tarr, n.d.):

- The particle size should be less than one third of the mesh opening size.
- The filament diameter should be less than one-third of the width of the narrowest line that will be printed.
- The frame size should be at least 1½-2 times the size of the image to be printed to allow the mesh to flex during printing without distorting the image significantly.
- The wet print thickness given by a piece of mesh is approximately equal to the thickness of the mesh multiplied by the percentage open area of the mesh.

After printing, the substrates with the printed layer must first be allowed to rest at room temperature for surface stress relaxation and then dried in a dryer for the solvent to evaporate. Then, the substrates are fired in a furnace, up to a temperature where the glass frit will melt and form a cohesive and adhesive film, carrying the conductor, resistor or dielectric materials. Temperatures and timing for drying and firing are defined by the ink manufacturers but for glassy inks the temperature range is about 400°C to 1,000°C. The suggested temperature profile is shown in Figure 2-4.

2. Literature Review

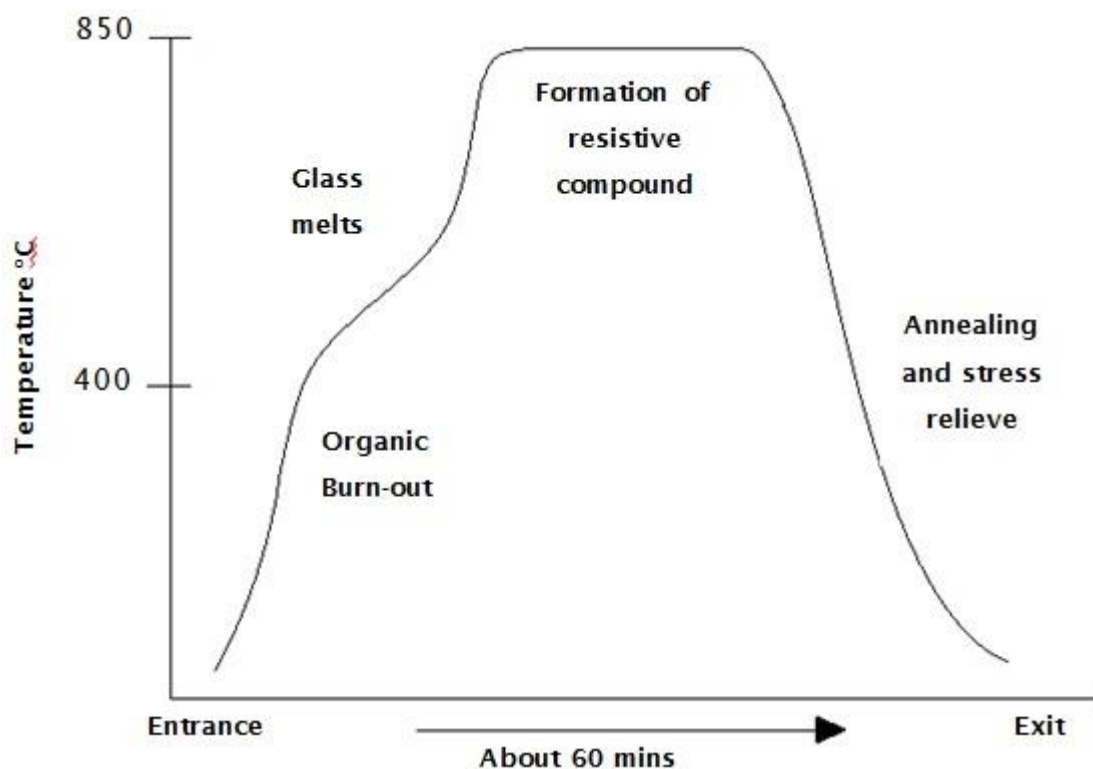


Figure 2-4: Proper curing profile. (Holmes & Loasby, 1976)

2.2.3 Lab-on-a-chip

Nowadays, TF Technology has its main use in making chemical sensors and more often biosensors but also provides support structure to other sensors (Brignell, et al., 1988). TF adds to sensor development by using a film layer as the principal sensing element. TF sensors are often characterised in groups such as mechanical, chemical and magnetic. (Morten, et al., 1995; Tarr, n.d.)

A huge number of TF sensors exist such as strain gauges, temperature sensors, pressure sensors, accelerometers, load cells, magneto-resistive sensors, thermopiles, chemical, physical and gas sensors. (Norton & Reynolds, 1985; Catteneo, et al., 1980; Atkinson, et al., 1993; Crescini, et al., 1993; Brignell, et al., 1988)

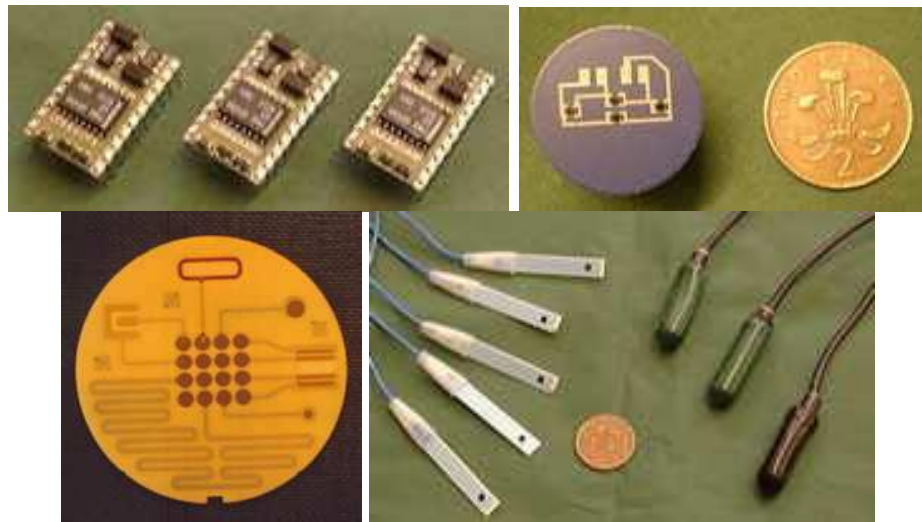


Figure 2-5: Transmitters incorporating an operational amplifier (upper left), pressure sensor in a gearbox (upper right), water quality sensor (lower left), chemical sensors (lower right) (Sophocleous, 2009)

TF technology demonstrates several advantages. These include, flexibility of design and choice of materials, easy integration with electronic circuits, low cost in infrastructure and mass production, the possibility of automation of the fabrication process and a low barrier for technological transfer (from thick-film to other technologies, and vice versa). Miniaturization is feasible, along with a high degree of electrochemical activity of the devices deriving from their high specific area and microporous structure. (Holmes & Loasby, 1976; Haskard & Pitt, 1997)

As the technological demand increases in the area of sensors, several issues arise. Sensors must follow the miniaturisation trend of this era and provide solutions compatible with users' demands. Currently, there are emerging technologies such as lab-on-a-chip (LOC), meaning a device that integrates one or more laboratory functions on a single substrate or board of only millimetres to a few square centimetres in size. LOC has become the focus of many researchers because it can provide fast, real-time data for many applications (Stone, et al., 2004). TF technology is compatible with LOC and can serve in the development and expansion of that area. (Wang, 2002)

2.3 Background Theory of Sensors

As mentioned in the previous chapters, laboratory soil testing requires a sample preparation which in most cases is a procedure to dissolve nutrients in the soil in a known volume of high purity water and measure the concentration of the nutrients of interest. (Benton Jones, 2001) Therefore, the initial step in this research was to understand the sensing theories of the existing technologies in solution. Collaborating soil scientists suggested pH, dissolved oxygen levels of the water penetrating the soil, temperature and water content or conductivity as the essential soil parameters to be monitored. The theories focusing on the sensing mechanisms of those parameters are explained in the next sections, followed by a literature review of the existing sensors.

2.3.1 Electrochemical Cells

Concentrations of chemical species can be measured in various ways. For example, pH can be measured using indicators or by electrochemical cells that use electrical properties of electrodes to calculate the parameter of interest. Although indicators are a much easier and cheaper solution, when the application requires digital data and continuous monitoring, indicators are not an option. Electrochemical cells are designed to show a relationship between one of their measurable electrical properties and the parameter of interest. A general schematic of an electrochemical cell in its simplest form is shown in Figure 2-6.

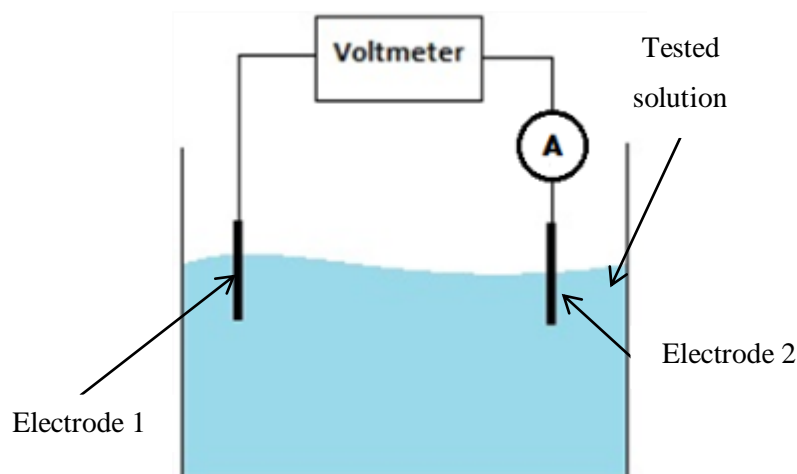


Figure 2-6: Typical electrochemical cell with two electrodes

Electrochemical cell types can range from potentiometric and amperometric to cyclic voltammetry while the most commonly and easier to use are amperometric and potentiometric cells. (Galán-Vidal, et al., 1995)

Amperometric cells are electrochemical cells where the parameter to be measured is proportional to the electrical current passing between two or more electrodes. In amperometric cells, the potential difference between the reference (RE) and working electrodes (WE) is controlled with the use of a potentiostat and a counter electrode (CE). The chosen potential difference depends on the parameter of interest while the current flowing between the RE and WE is proportional to the investigating parameter.

The most common type of amperometric cells is the Clark cell. For a Clark cell to operate properly and to be calibrated, the potential difference between the RE and WE must be always constant. CE and RE are externally connected and the potential of CE is altered in such a way to set the required potential difference between RE and WE. Once the potential difference is maintained, the current flowing between RE and WE is proportional to the parameter of interest (e.g. oxygen concentration). Clark cell always has a membrane on top of the electrodes that only allows the species of interest to penetrate. Clark cell

2. Literature Review

has the advantage that does not require the RE to have a stable potential in every solution because the electrode's potential is controlled by the potentiostat.

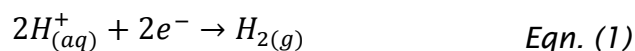
Potentiometric cells are very similar to amperometric cells with the main difference that the parameter of interest is proportional to the potential difference across the electrodes. Furthermore, in the kind of cell it is assumed that no current flows between the two electrodes. In reality, a tiny amount of current does flow in order to be able to measure a potential difference but it is insignificant to alter the output of the cell. Potentiometric cells are usually made up of two electrodes, the reference electrode (RE) and a working electrode (WE). REs are meant to have a stable potential in any solution they are immersed in. On the contrary, WEs are meant to change their potential proportionally to the parameter of interest. When the two electrodes are immersed in a solution, the electrical circuit is complete and the voltmeter will measure the potential difference between the two electrodes. The electrical circuit is complete by the flow of charged ions in the solutions. Each electrode, when immersed in a solution, generates a potential which corresponds to the chemical reaction happening at that electrode in that solution.

2.3.2 Reference Electrodes

There is a variety of different RE types, each one designed for certain applications based on its properties. Different conditions can affect the performance of one type but the performance of another might be invariant. Therefore, the decision of which RE to be used is often an important initial area for research. The properties of each type must be first understood in order to be in a position to accurately decide on the type that fits the specific application.

The standard hydrogen electrode (SHE) has been adopted as the primary standard which all other electrodes will be compared against. It is the best RE of all because it has the highest degree of reproducibility, while

it is relatively easy to prepare in a laboratory. SHE is based on the half-cell reaction (Ives & Janz, 1961):



while the associated Nernst equation is (Ives & Janz, 1961):

$$E = \frac{RT}{F} \ln \frac{a_{H^+}}{(p_{H_2}/p^0)^{1/2}} \quad \text{Eqn. (2)}$$

where R is the universal gas constant ($\text{J K}^{-1} \text{mol}^{-1}$), T is the temperature (K), F is the Faraday's constant (C mol^{-1}), a_{H^+} is the activity of hydrogen ions in the electrolyte, p_{H_2} is the partial pressure of hydrogen gas (Pa) and p^0 is the standard pressure (10^5 Pa). It is effectively an immersed platinum electrode in a solution of 1M hydrogen activity and hydrogen gas bubbling around the electrode at 1 atmosphere and 25°C. The theoretical potential of the SHE is 4.44 ± 0.02 V at 25°C (Ives & Janz, 1961).

There is another set of REs that are called electrodes of the second kind. The two most commonly used metals for REs are mercury and silver. They are called electrodes of the second kind because they are formed from mercury or silver with an excess of a sparingly soluble salt. Mercury's most common type of RE is the calomel electrode where the salt is mercury (I) chloride. It is made up of an outer glass tube fitted with a frit at the bottom to complete the circuit with the outside solution. Inside, there is another tube, the bottom of which is packed with glass wool to complete the circuit between the two liquids. The inner tube is filled with a paste of mercury and mercurous chloride dispersed in a saturated solution of potassium chloride as shown in Figure 2-7.

2. Literature Review

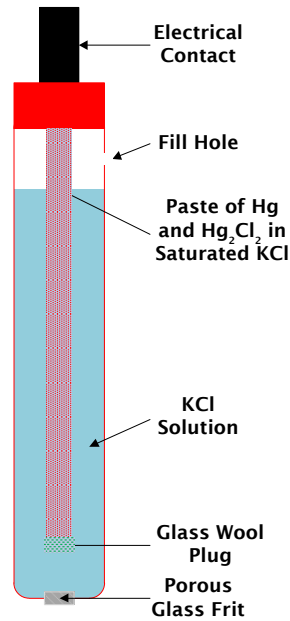
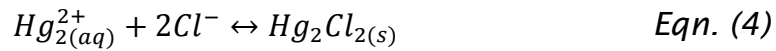


Figure 2-7: Construction of a typical calomel electrode. (Sophocleous, 2009)

The calomel electrode is based on the two following reversible reactions (Ives & Janz, 1961):



The activity of $\text{Hg}_2\text{Cl}_2(\text{s})$ in its saturated solution is constant and therefore the electrode potential is then just a function of mercury and its ion. The potential of the electrode is calculated from the Nernst equation as (Ives & Janz, 1961):

$$E = E_{\text{Hg}_2^{2+}/\text{Hg}}^o - \frac{RT}{2F} \ln \frac{a_{\text{Hg}}}{a_{\text{Hg}_2^{2+}}} \quad \text{Eqn. (5)}$$

Where $E_{\text{Hg}_2^{2+}/\text{Hg}}^o$ is the standard electrode potential for the electrode (V) and the rest of the symbols have their usual meaning. The activity of an element at its standard state is always 1 and therefore the only activity that can vary is the activity of $\text{Hg}_2^{2+}(\text{aq})$. That activity is controlled by the activity solubility product (Ives & Janz, 1961):

$$K_{sp} = a_{\text{Hg}_2^{2+}} \times a_{\text{Cl}^-}^2 \quad \text{Eqn. (6)}$$

The only variable in the Nernst equation now is the activity of the chloride ions and that is why the electrode is immersed in a saturated potassium chloride solution. By saturating the solution with potassium chloride, the activity of chloride ions is stabilized and so is the potential of the electrode being invariant of the solution that the electrode will be immersed in. This electrode has a potential of 0.2444 V at 25°C against SHE (Ives & Janz, 1961).

There is also a wider range of electrodes that can be used as references which are sensitive to specific ions. If the concentration of those ions is known or it is stable, those electrodes can be used as references. For example, the glass electrode is only sensitive to hydrogen ions or in other words pH but if the hydrogen ion concentration is known or constant the electrode can be calibrated and easily used as a reference point. Other types of REs are the quinhydrone electrode, metal oxide electrodes, membrane electrodes and more application specific electrodes such as REs for non-aqueous solution.

As SHE is not suitable for applications underground and more generally applications outside the laboratory, the only choice for a wide range of applicability are the electrodes of the second kind. From that category, mercury is again not applicable since it is a liquid and also toxic at the vapour phase, where it is also impossible to design a solid state RE based on a metal that is a liquid at room temperatures. Silver-silver halide is the chosen type since Thick-Film technology provides a wide range of inks made from silver and also silver is a solid at its standard state making the construction of the electrode and the underground applicability much easier.

The most common type of silver-silver halide electrode is the silver-silver chloride due to the ease of finding silver chloride and due to the use of potassium chloride for the electrolyte. Silver-silver chloride electrode is an electrode of the second kind and the operation of such an electrode is very much similar to that of a calomel electrode. In this case, the

2. Literature Review

electrode is constructed using a silver wire, which is electroplated with silver chloride up to a certain weight percentage and then immersed into a saturated solution of silver chloride which is usually a 3.5 M potassium chloride solution although sometimes a saturated potassium chloride solution is used. The percentage of silver that is electroplated with silver chloride is important because the performance of the electrode is affected by the thickness of the silver chloride layer. An ideal percentage is about 20% of the initial silver wire must be converted to silver chloride (Ives & Janz, 1961). Also, the time for the reaction to reach equilibrium is affected by the thickness of the silver chloride layer because silver particles take much more time to migrate to the surface of a thicker layer. The solution is in a glass tube which has a glass frit at the tip of it to allow ion exchange between the electrode and the testing liquid. A typical construction of such an electrode is shown on Figure 2-8.

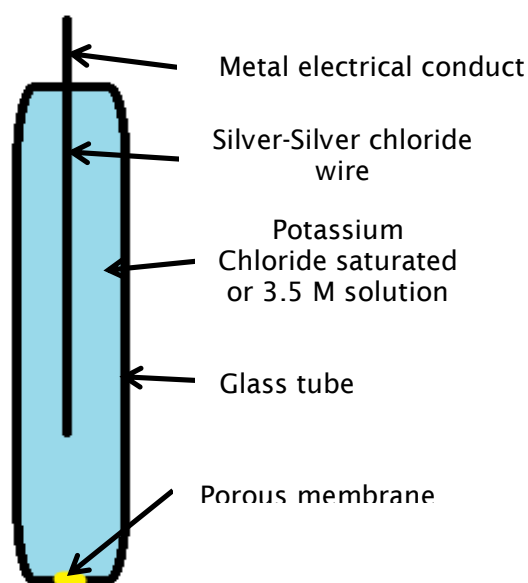


Figure 2-8: Typical construction of a silver-silver chloride RE.

The electrode is based on two simultaneous reactions on the surface in contact with the solution (Bard & Faulkner, 2001; Ives & Janz, 1961; Plambeck, 1982):





Silver metal on the electrode will form an equilibrium reaction between ionizing the element and turning it back to solid. The second reaction is reversible and it depends on the solubility of silver chloride in water. The electrode potential is defined by the Nernst equation which is modified for this specific electrode as (Ives & Janz, 1961):

$$E = E^o - \frac{RT}{F} \ln(a_{Ag^+}) \quad \text{Eqn. (9)}$$

In this case, the activity of silver chloride is controlled by the solubility of the salt in water. Therefore, the activity of silver chloride will always be constant as long as the solution that the electrode is immersed in is saturated. Since the second reaction is completely controlled by the solubility, the electrode now only depends on the first reaction. The activity of silver ions in water is also controlled by the activity solubility product of the reaction which is invariant at a given temperature. The activity solubility product for this reaction is defined as (Ives & Janz, 1961):

$$K_{sp} = a_{Ag^+} \times a_{Cl^-} \quad \text{Eqn. (10)}$$

The activity solubility product only depends on temperature and therefore the activity of silver ions is consequently dependent on the activity of chloride ions in the same solution. If the activity of chloride ions in the solution is constant then the activity of silver ions will be constant sustaining a stable potential for the electrode. That is why a saturated potassium chloride solution is often used for these electrodes. As explained before, the activity is equal to the product of the concentration and the activity coefficient which in the case of potassium chloride, at low concentrations it is close to 1 and decreases with increasing concentration up to a point where it increases again. It is always in the range of about 0.9-0.5. A conventional silver-silver chloride electrode is shown in Figure 2-9.

2. Literature Review



Figure 2-9: A commercial silver-silver RE. (Glanc-Gostkiewicz, et al., 2013)

This electrode is made up of a glass or plastic tube with a saturated potassium chloride solution, or more often 3.5 M, and an immersed silver wire, electroplated with silver chloride with a glass frit at the tip of the tube. The glass frit is a porous glass that allows a very slow ion exchange between the silver wire, the electrical conductor, and the tested electrolyte. Although the stability and performance of this construction is accurate to approximately a millivolt, it can't be used in applications where robustness and ruggedness is required. In the case of underground sensors, a glass electrode is impossible to use due to its properties but because the wire is made of silver, the electrodes are very expensive, typically more than a hundred pounds each. That by itself restricts its use where the numbers of electrodes required are high. A solid state, cheap, rugged, robust and accurate RE is required for this application, since the measurements are made in the range of millivolts.

2.3.3 Ion Selective Electrodes

Ion Selective Electrode (ISE) is defined as an electrode that changes its electrical properties proportionally to the parameter of interest only. ISEs, in the case of potentiometric cells, alter their potential proportionally to the parameter of interest (e.g. pH) and are ideally not affected by any other parameters. In order for a potentiometric cell to work it requires both a RE and an ISE. Each electrode when immersed in a solution generates its own potential based on Nernst equation and the potential difference between the two electrode potentials is recorded by the voltmeter. Since the potential of the RE is always the same in every solution, any voltage changes between the two electrodes are due to the ISE as a result of a change in the parameter of interest. A lot of ISEs have been reported until now and mainly in the area of chemical species concentration in solutions. There are ISEs for a huge variety of chemical

species such as (e.g. chloride ions, nitrates, phosphates). In this work, the only type of ISE used is the pH ISE and therefore the background for this specific type will be described in more detail in the following section.

pH was originally defined as the negative logarithm of the concentration of hydrogen ions in aqueous solution. After the development of the thermodynamic concept of activity the definition was altered to (Vonau & Guth, 2006):

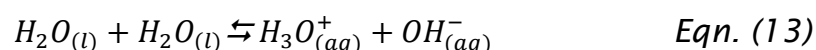
$$pH = -\log_{10}(a_{H^+}) \quad \text{Eqn. (11)}$$

where a_{H^+} is the hydrogen ion activity in aqueous solutions. Hydrogen ion activity is defined as (Plambeck, 1982):

$$a = a_c[H^+] \quad \text{Eqn. (12)}$$

where a_c is the activity coefficient (dimensionless) and $[H^+]$ is the hydrogen ion concentration (M).

While most water molecules exist as $H_2O_{(l)}$, a small percentage dissociates based on the following equation (Brett & Brett, 1993):



Arrhenius suggested that water dissociates to the hydronium ion ($H_3O^+_{(aq)}$) instead of hydrogen ions and that any substance that increases the hydronium ion concentration is an acid and any substance decreasing the hydronium ion concentration is a base.

The pH scale is based on the dissociation constant of the water but since it is pure liquid it is called self-ionisation. The constant is defined as (Brett & Brett, 1993):

$$K_w = [H_3O^+][OH^-] = 10^{-14} \quad \text{Eqn. (14)}$$

2. Literature Review

Based on the deionisation of water, the concentration of hydronium ions is equal to the concentration of the hydroxide ions (10^{-7}). Therefore, the pH of water is 7, which in reality is the negative power of the hydronium concentration. The pH range is from 0-14, while any pH below 7 is acidic and anything above 7 is alkaline.

2.3.4 pH Ion Selective Electrodes

There are different kinds of pH ISEs. The conventional pH ISE is made up of glass with an H^+ ion permeable membrane. More often, pH ISEs come together with the RE in the same structure. A simple configuration of the conventional glass pH ISE is shown in Figure 2-10.

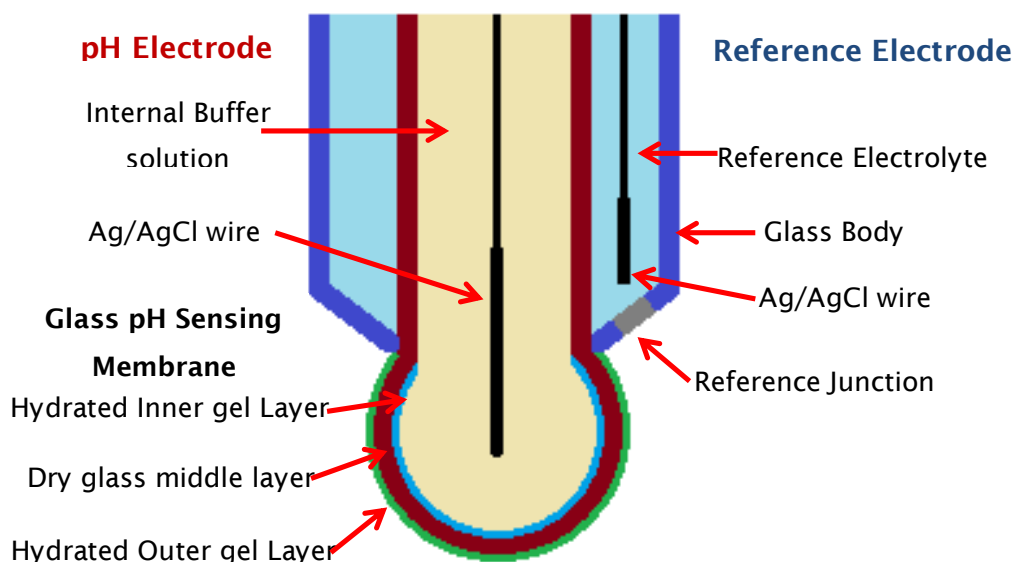
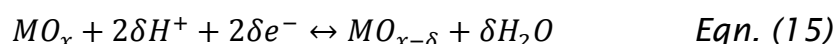


Figure 2-10: The construction of a conventional pH ISE combined with a RE.

The conventional pH ISE operates on exactly the same principle as the RE explained in detail earlier. The only difference and the point that makes it sensitive to pH only is the glass pH sensing membrane. That glass based membrane only allows hydrogen ions or hydronium ions to pass through. Any change in the concentration of hydrogen ions around the Ag/AgCl wire would change the potential of the electrode as predicted by the Nernst equation. The maximum sensitivity such a pH ISE can have is approximately 59.1 mV/pH at a temperature of 25° C.

More recent applications of the pH ISE have shown the need for a solid state ISE that could operate in more harsh environments, especially where glass casing is not an option. Solid state pH ISE would be ideal in the case of soil sensors. Furthermore, as shown in Figure 2-10 earlier, conventional pH ISEs require to be filled with inner solutions that will keep the cell in operating conditions. In a laboratory, refilling the solution is very easy but when the cell is placed underground with no access for a long time then several problems can arise.

Fog and Buck in 1984 (Fog & Buck, 1984) established the basis for metal oxide semiconductors to be used for pH sensing. They investigated the ability of some insoluble metal oxides to respond to pH by forming a reversible reaction where the equilibrium is shifted in either direction depending on the pH of the solution. The potentials were found to be stable and reliable as well as repeatable for almost all the metal oxides that were investigated for example, PtO₂, IrO₂, RuO₂, OsO₂, Ta₂O₅ and TiO₂. Most showed a Nernstian response of about 59 mV per pH at 25°C from pH values 2 to 12. This work was the basis of almost all solid state pH ISEs used in the vast majority of applications. The general reaction taking place for these metal oxides is (Fog & Buck, 1984):



where MO_x is a higher metal oxide and $MO_{x-\delta}$ is a lower metal oxide.

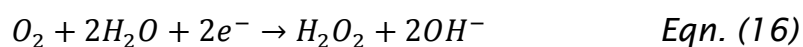
2.3.5 Oxygen Sensors

Oxygen gas, like other similar gases can dissolve in water without reacting with it. Oxygen saturation is inversely proportional to temperature. The amount of dissolved oxygen in aqueous solutions is important for water and sewage industries, food production and storage, brewing, and as a clinical tool in blood gas analysis. Deficiency of dissolved oxygen in sea water might result in fish population decrease. Therefore, monitoring of dissolved oxygen levels is essential

2. Literature Review

for every proper environmental management (Ramamoorthy & Dutta, 2003).

There are several types of oxygen sensors but the most common and most reliable is based on the Clark Cell with the use of the potentiostat. An oxygen sensor based on Clark cell has three electrodes, RE, WE and CE. CE and RE are externally connected with the use of operational amplifiers (op amps) in such a way that the input voltage of one of the op amps is equal to the potential of the RE at all times. The circuit will alter the CE potential in such a way to keep the RE potential always the same with respect to the WE. Usually, the WE is set to the 0 V of the power supply. The three electrodes are close but not touching each other and the circuit is completed by the ions in the solution. In the case of the oxygen sensor, a gas permeable membrane is placed above the electrodes and a solution of known concentration is placed between the membrane and the electrodes to complete the circuit. Gas permeable membranes only allow gas molecules to pass through and for an oxygen sensor an oxygen permeable membrane is used. When oxygen molecules pass through the membrane, the concentration of oxygen molecules in the solution changes and the current flowing between the RE and WE changes proportionally to the concentration. The reaction that most likely occurs in this type of sensor is (Glasspool & Atkinson, 1998):



2.3.6 Temperature Sensors

Temperature sensors are a very mature technology and several types of temperature sensors are widely used in many applications (e.g. thermocouples, thermistors, platinum resistance thermometers, optical thermometers) (Michalski, et al., 2002). Each temperature sensors

operates on different principles and the most extensively used type with the widest range is the thermocouple. Thermocouples are cheap and robust but are not easily compatible with TF Technology. Platinum resistance thermometers (PRT) on the other hand, are extremely simple to construct, robust and are compatible with TF Technology.

PRTs are based on the electro-thermal properties of platinum. Platinum has a temperature coefficient of resistance of approximately 4×10^{-3} ohms/ohm/°C and can be used in temperatures ranging from 300 °C to almost 1000 °C. Platinum resistance is proportional to temperature and with the use of a low constant current; the change in voltage across platinum can be used as a calibrating factor for a thermometer.

Using the equation for the resistance of the PRT of (Dziedzic, et al., 1997):

$$R_T = R_0(1 + aT) \quad \text{Eqn. (18)}$$

Where R_T is the resistance (ohms) at temperature T (°C), a is the temperature coefficient of resistance for platinum (ohms/ohms/°C). Then, using (Dziedzic, et al., 1997):

$$\Delta R = aR_0 \quad \text{Eqn. (19)}$$

the sensitivity of the platinum thermometer can be calculated. (Hrovat, et al., 1990)

2.3.7 Conductivity Cells

Measuring soil conductivity can provide vital information on the water content of the soil as well as distinguishing between different types of soil (e.g. clay, gravel, sand, limestone, coal and several combinations of them). Conductivity readings combined with porosity measurements can give information on the stability of the ground which is extremely important in applications such as train rails. Furthermore, conductivity is

2. Literature Review

related to the water content in soil, parameter that is of high value for agriculture and soil scientists (Smith & Mullins, 2000).

Although several conductivity probes are available in the market, the cost of such a probe including the instrumentation required to take a reading does not allow for a high density sensor network. TF conductivity sensors have the advantage of low cost, ruggedness, robustness and the ability to be integrated on a single substrate with other sensors. In addition, due to the simplicity of the sensor the electronic interface required is of low cost which provides the opportunity for a higher density sensor network in the investigation area.

Electrical conductivity is defined as the ability of a material to conduct an electrical current and its SI Units are Siemens/meter. In metals, current is passed by electrons while in solutions by anions and cations.

How well a solution conducts electricity depends on a number of factors (Nabighian, 1988; Radiometer, n.d.):

- 1) Concentration
- 2) Mobility of ions
- 3) Valence of ions
- 4) Temperature

Every material has a certain degree of conductivity. For example, ultrapure water has a very low conductivity due to the low levels of ionic strength. High ionic strength solutions such as concentrated acids have very high conductivities.

Conductivity can be measured by applying a constant alternating current (AC), with the use of a current source, to two electrodes immersed in the solution and then measure the potential difference (V) across them. Cations will migrate to the negative electrode and anions to the positive electrode making the solution an electrical conductor and completing the electrical circuit as shown in Figure 2-11.

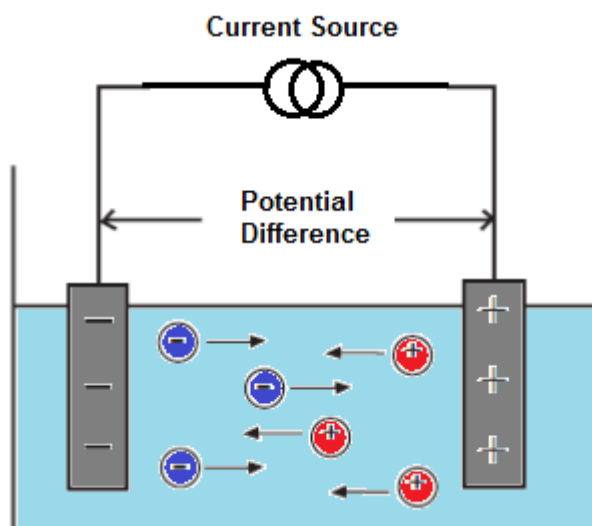


Figure 2-11: Electrical circuit of a conductivity cell explaining the ion movement completing the circuit (Radiometer, n.d.)

Usually, conductivity is important for aqueous solutions of electrolytes, substances that ionise in water. The ions formed in solution are responsible for carrying the electric current. There are strong and weak electrolytes. Strong electrolytes fully ionised in water and their solutions are highly conductive. Weak electrolytes do not fully ionise in water and have low conductivities.

The resistance of the solution (R) is calculated by Ohm's law:

$$V = IR \quad \text{or} \quad R = \frac{V}{I} \quad \text{Eqn. (20)}$$

Where V is voltage (volts), I is current (amperes) and R is the resistance of the solution (Ohms).

Conductance (G) is defined as the reciprocal of the electrical resistance (R) and it is measured in Siemens (S).

$$G = \frac{1}{R} \quad \text{Eqn. (21)}$$

A conductivity meter measures conductance, converts it into conductivity using the known cell constant of the meter. Conductivity is measured in Siemens per meter (S/m) and it is temperature dependent.

2. Literature Review

Cell constant is the ratio of the distance between the electrodes to the area of the electrodes.

$$K = \frac{d}{a} \quad \text{Eqn. (22)}$$

Where K is the cell constant (m^{-1}), a is the effective area of the electrodes (m^2) and d is the distance between the electrodes (m). Conductivity is calculated by:

$$\sigma = GK \quad \text{Eqn. (23)}$$

Where σ is conductivity (S/m). Resistivity is the reciprocal of the conductivity value and is measured in $\text{ohm} \cdot \text{m}$. It is generally limited to the measurement of ultrapure water, the conductivity of which is very low. (Nabighian, 1988; Radiometer, n.d.)

Contacting conductivity uses a cell with two metal or graphite electrodes in contact with the electrolyte solution. An AC current is applied to the electrodes by the conductivity meter, and the resulting AC voltage is recorded. This technique can measure down to pure water conductivity. Its main drawback is that the cell is susceptible to coating and corrosion, which drastically decreases the reading. In strongly conductive solutions there can also be polarisation effects, which result in non-linearity of measurements.

A toroidal conductivity cell is based on the principle of inducing a current from one coil to another. The level of the induced current will be proportional to the conductivity of the medium passing through the coils.

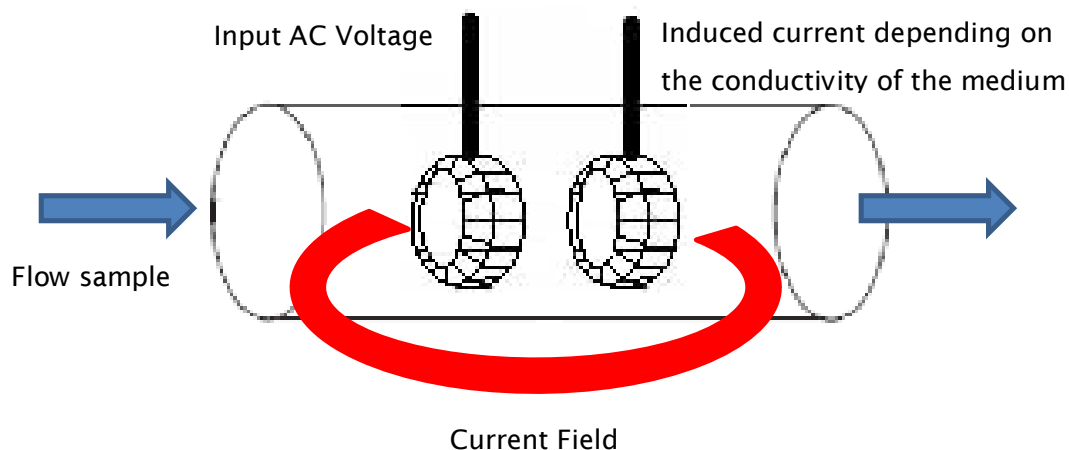


Figure 2-12: Typical operation of a toroidal conductivity sensor (Radiometer, n.d.)

The main advantage of toroidal conductivity cell is that toroidal coils do not come in contact with the solution. They are usually enclosed in a polymeric material. While this is an advantage, not coming in contact with the sample can lack sensitivity of the cell. Furthermore, toroidal sensors are typically larger than contacting sensors, and the solution current induced by the toroid occupies a volume around the sensor. Hereafter, toroidal sensors need to be mounted in a larger pipe (Radiometer, n.d.).

In a conventional two electrodes cell, an alternating current is applied between the two poles using a current source and the resulting voltage is recorded (Figure 2-13). In the attempt to measure the solution resistance (R_{sol}) only, the resistance (R_{el}) caused by polarisation of the electrodes and the field effects, interfere with the measurement, and both R_{sol} and R_{el} are measured.

2. Literature Review

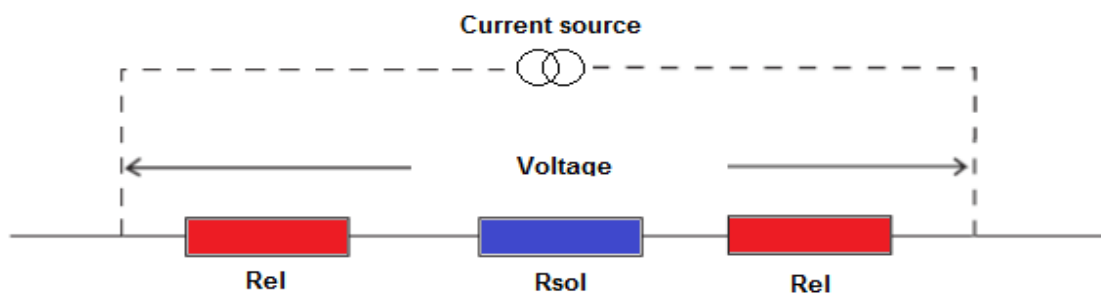
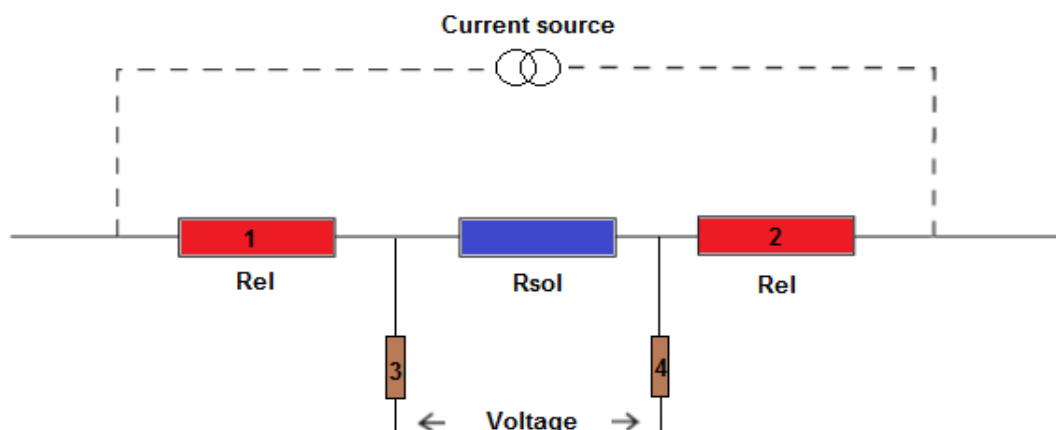


Figure 2-13: Circuit arrangement for a two pole conductivity cell (Radiometer, n.d.)

The three electrodes cell is something between the three pole and four pole cells. The advantage of this design is that the third electrode which was linked to the first electrode, allowed the field lines to be directed and restrained in an optimal manner, minimising dispersion in the measurement and reducing influences on the measurement such as pipe size and position of the cell in the pipe. It provides better reproducibility when calculating the cell constant and hence more reproducible results.

In a 4 electrodes cell (Figure 2-14), a current is applied to the outer electrodes (1 and 4) generating a constant potential difference between the inner electrodes (2 and 3). Assuming there is no current flowing, these two electrodes are not polarised. The geometry of four electrodes cells with an outer tube reduces the beaker field effect, due to the measurement volume being well defined within the tube. The position of the conductivity cell in the measuring vessel or the sample volume therefore has no influence on the measurement (Radiometer, n.d.).



*Figure 2-14: Electrode configuration for a four pole conductivity cell
(Radiometer, n.d.)*

In an attempt to decrease the effect of electrode contamination from the sample, several techniques have shown to improve the cell's performance. Covering the cell electrodes with a layer of platinum black minimises polarisation effects and decreases measurement errors. The electrochemical surface of the electrode increases, the current density decreases, and consequently the polarisation effect is reduced. Thus, the cell constant stays linear over 2-3 decades towards the higher conductivity range. Damaging platinum the black layer in any way, will change the surface of the electrodes and therefore the cell constant. However, one minor disadvantage of platinised cells is that the cell constant tends to drift faster than the constant of non-platinised cells.

2. Literature Review

Table 2-1: Selecting the right conductivity cell (Radiometer, n.d.)

Advantages	Disadvantages
2 pole	
<ul style="list-style-type: none"> 1) Simple. 2) Cheap. 3) Good with for viscous media or samples with suspension. 	<ul style="list-style-type: none"> 1) Field effects - must be in the centre of the vessel. 2) Only cells with no bridge between the plates. 3) Polarisation issues in high conductivity samples. 4) Calibration over a very small range.
4 pole	
<ul style="list-style-type: none"> 1) Linear over a wide conductivity range. 2) Allows calibration and measurement in different ranges. 3) Can be used for flow-through or immersion type cells. 4) Ideal for high conductivity medium and can be used for low conductivity measurements if cell capacitance compensated 	<ul style="list-style-type: none"> 1) Unsuitable for micro samples depth of immersion 3 to 4 cm

Different conductivity cells have different properties. The measurement range over which the cell stays linear gets broader as the number of poles increases. Platinised poles also contribute to increasing the measurement span in which the cell is linear (Figure 2-15).

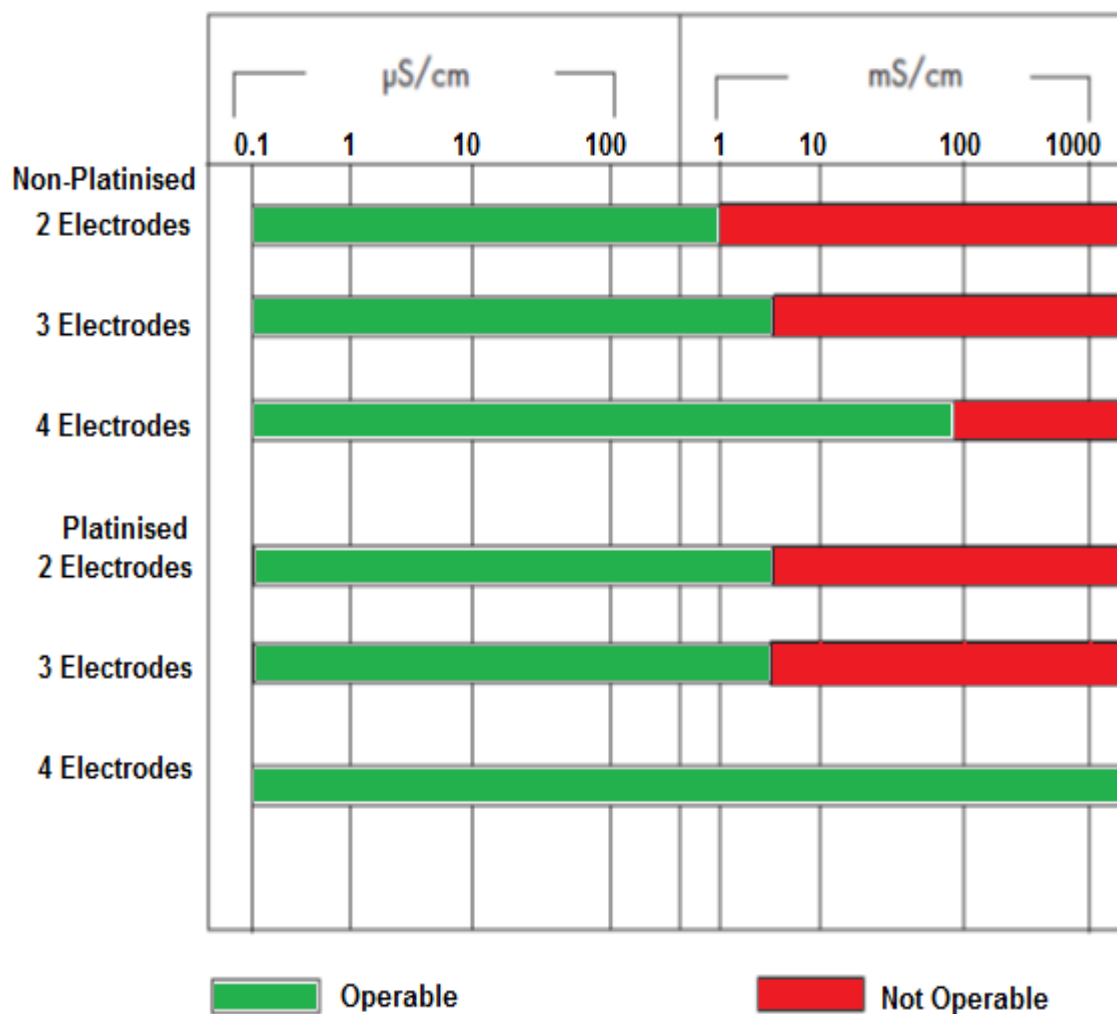


Figure 2-15: Operable ranges for different conductivity cell types

Some indicative conductivity values of common samples are shown in Table 2-2.

Table 2-2: Indicative conductivity values of some commonly used samples.

Pure water	0.055 $\mu\text{S}/\text{cm}$
Deionised water	1 $\mu\text{S}/\text{cm}$
Rainwater	50 $\mu\text{S}/\text{cm}$
Drinking water	500 $\mu\text{S}/\text{cm}$
Industrial wastewater	5 mS/cm
Seawater	50 mS/cm
1 mol/l NaCl	85 mS/cm
1 mol/l HCl	332 mS/cm

2. Literature Review

The performance of conductivity cells can be affected by the following factors (Radiometer, n.d.):

- Polarisation
- Contamination
- Geometry
- Cable resistance
- Cable capacitance
- Frequency change
- Temperature

Applying an electrical current to the electrodes in solution may cause an increase of ionic concentration near the electrode surfaces as well as chemical reactions at their surfaces. From that, a polarisation resistance arises on the electrode surface, which may lead to inaccurate results in measuring the solution's conductivity. This phenomenon is called the double layer. (Pletcher, 2009)

To overcome the problem of polarisation, an AC current can be used that will not allow the ions to stay on the electrode surface. Alternating the electrode poles will force the ions to move towards and away from the electrodes. In that way, the capacitance generated at the surface of the electrodes due to the double layer will be minimised and not affect the measurement.

Using an AC current gives the opportunity to use different frequencies. Very high frequencies will allow the cell to measure capacitance instead of resistance. Very low frequencies will allow polarisation and therefore a middle point is ideal. In low conductivity samples, low frequencies are used since there aren't many ions to form a double layer strong enough to alter the measurements. In high conductivity samples though, higher frequencies are using for the same reason.

Polarisation effect is related to the current density at the electrode's surface. If the electrode's surface is increased by the use of platinum

black for example, the current density decreases minimising the polarisation effect.

Polarisation effect is very important for the two or three electrodes cells but has almost no effect on the four electrodes cell. Since there is no current flowing through the two voltage electrodes, a double layer cannot be formed.

There is also the risk of contamination of the electrodes which arises from deposits on the electrode surface having a similar effect to polarisation errors. These effects can also be prevented with a four electrodes conductivity cell.

Errors are also caused by field effects. Field effect is the part of the measuring field that falls outside the geometric space of the cell (Figure 2-16). These field lines can affect the measurement if something interferes with the field lines, such as the beaker walls. 3 and 4-pole conductivity cells are designed to minimise this effect. There is still some field effect present for the four electrodes cell due to the fact that when field lines do not flow directly to the other electrode, the distance travelled by the current is different from the distance between the two electrodes. That can have a major effect on the cell constant.

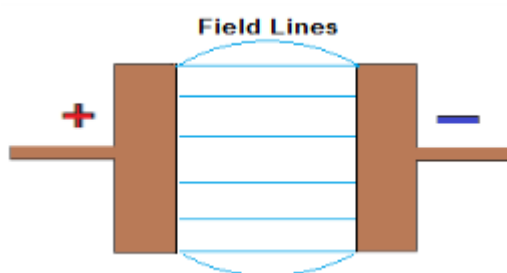


*Figure 2-16: Field lines between the two electrodes of a conductivity cell
(Radiometer, n.d.)*

Low frequencies are applied at low conductivities, where the polarisation resistance is negligible compared to resistance of the solution. They also contribute to reducing the cable capacitance effect, which is greater

2. Literature Review

when the conductivity is low. High frequencies are applied at high conductivities.

A cable has a given length, therefore a given resistance. The cable resistance induces error on the result and must be taken into account. Usually the cable resistance is compensated when the solution conductivity is high and when performing measurements using the two or three electrodes cells. For four electrodes cells, the cable resistance has no influence on the measurements. A shielded cable of a given length has a given capacity. When the measured conductance is low (below 4 μS), the cable capacitance is not negligible and must be taken into account. Usually the cable capacitance is compensated when using a four electrodes cell, measuring low conductivities and when the cable capacitance of the conductivity cell is greater than 350 pF (Radiometer, n.d.; Pletcher, 2009; Plambeck, 1982; Scholz, 2010).

Conductivity measurements are temperature dependent and the temperature is directly proportional to the conductivity. The perception of reference temperature was introduced to allow the comparison of conductivity measurements at different temperatures. The reference temperature is usually 20°C or 25°C. Temperature compensations can be done using a linear or a non-linear function used for natural waters according to ISO/DIN7888.

In moderately and highly conductive solutions, temperature correction can be based on a linear equation involving a temperature coefficient (θ). The coefficient is usually expressed as a conductivity variation ($\%/^{\circ}\text{C}$).

$$\sigma_{T_{ref}} = \frac{100}{100 + \theta \cdot (T - T_{ref})} \cdot \sigma_T \quad \text{Eqn. (24)}$$

Where $\sigma_{T_{ref}}$ is the conductivity at temperature T_{ref} , σ_T is the conductivity at temperature T , T_{ref} is the reference temperature ($^{\circ}\text{C}$), T is the sample temperature ($^{\circ}\text{C}$) and θ is the temperature coefficient. The correction is

accurate only within a limited temperature range. The temperature coefficients of the following electrolytes generally fall into the ranges shown in Table 2-3.

Table 2-3: Indicative temperature coefficients for several samples

Sample Type	Temperature Coefficient (θ) (%/°C)
Acids	1.0 - 1.6
Bases	1.8 - 2.2
Salts	2.2 - 3.0
Drinking water	2.0
Ultrapure water	5.2

The linear temperature correction is suitable only for some aqueous liquids. The temperature dependency of the rest of aqueous liquids can only be described by non-linear functions such as the non-linear function for natural waters. The principle of this correction is that the conductivity measured at the sample temperature is corrected to 25°C to give K_{25} .

$$\sigma_{25} = f_{25}(T) \cdot \sigma_T \quad \text{Eqn. (25)}$$

$f_{25}(T)$ is the temperature correction factor used for the conversion of conductivity values of natural water from T to 25°C. The temperature correction factor $f_{25}(T)$ is calculated from a 4-degree polynomial equation. This equation fits the conductivity variations against temperature for natural water stated in "Natural Water temperature correction (ISO/DIN 7888). The non-linear correction is defined by ISO/DIN7888 standard and is applicable for measurements between 0 and 35.9°C. (Radiometer, n.d.; Nabighian, 1988)

Ideally, electrodes are immersed in solutions at specific distance with a known effective surface area. For soil purposes the same principles apply and the same configuration is used. The distances between the

2. Literature Review

electrodes can define the cell constant based on the electric fields built up in the soil as shown in Figure 2-17 below.

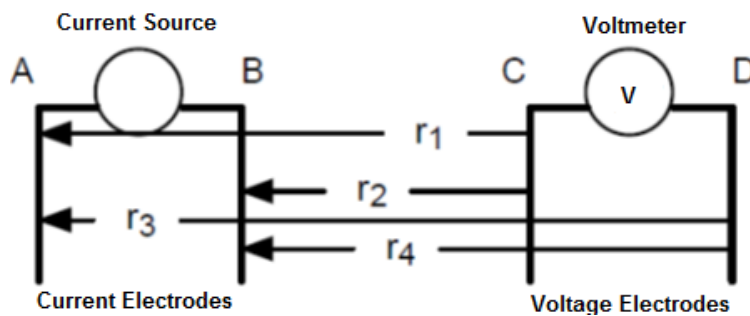


Figure 2-17: Four electrodes conductivity cell (Nabighian, 1988)

The cell constant can be calculated using Poisson's equation (Nabighian, 1988):

$$\Delta V = \frac{I\rho}{2\pi} \left[\left(\frac{1}{r_1} - \frac{1}{r_2} \right) - \left(\frac{1}{r_3} - \frac{1}{r_4} \right) \right] \quad \text{Eqn. (26)}$$

Some specific approaches are shown in Figure 2-18 where d is the distance between the electrodes and n is an integer to show that it is a multiple of d .

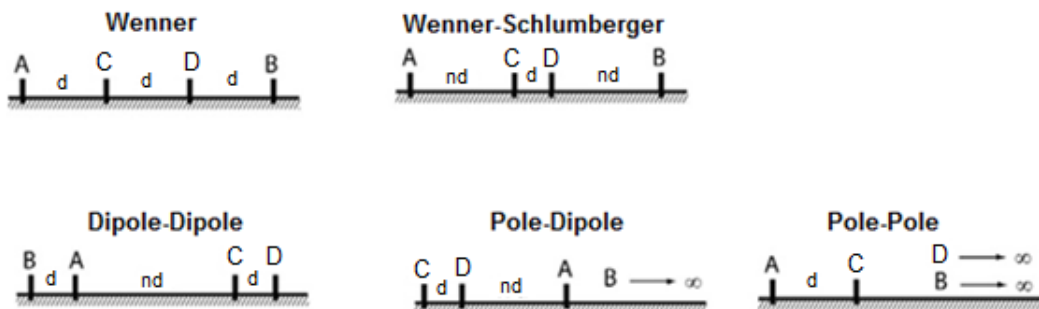


Figure 2-18: Electrode configuration of some standard conductivity cells, d is the distance between the electrodes and n is just an integer (Nabighian, 1988)

The cell constant is determined by the geometry of the cell, but in practical terms can only be measured using a standard of known conductivity. Checking the conductance measured in a known conductivity solution, the cell constant can be recalculated. The cell constant changes with time because some changes can occur due to contamination or due to physical-chemical alterations in case of

platinised cells. For high-precision measurements, it is necessary to determine the cell constant by performing a calibration measurement on a standard solution at the desired temperature. Maintaining the desired temperature constant during the calibration is very important at high precision measurements as the temperature can have an effect both on the measurements and the standard solution. In the case of a four electrodes cell, the cell constant value is generally included in the range 0.5 to 1.5 cm⁻¹.

2.3.8 Summary

This section of chapter 4 provided the theories on the operating principles of possible sensors and of existing laboratory electro-analytical equipment.

Electrochemical potentiometric pH sensors are made up of a RE and a pH ISE. REs have a stable potential in every solution they are immersed and the most common type is Ag/AgCl. The potential of the electrode is calculated using the Nernst equation. The pH ISE alters its potential to pH changes and is selective to sense only the changes in hydrogen ion activity. The potential difference between the two electrodes, measured by a high input impedance voltmeter, is proportional to the pH of the solution.

Amperometric sensors are usually based on the Clark Cell. The potential of the CE is changed by the potentiostat in such a way, that the potential difference between the RE and WE is always the same. The current flowing between the two electrodes is proportional to the parameter of interest. In oxygen sensors, a solution or gel of known concentration (e.g. potassium nitrate) is placed above the electrodes completing the circuit and an oxygen permeable membrane is deposited on top. The current flowing between the RE and WE is proportional to the diffused oxygen levels in the solution under the membrane.

2. Literature Review

PRTs are thermometers based on the thermo-electrical properties of platinum. Platinum has the ability to change its electrical resistance with temperature. Maintaining a constant current flowing in the platinum wire and measuring the voltage across it, the temperature can be calculated.

There are several types of conductivity cells with the four electrodes cell to have the most advantages in terms of range and other interferences. The four electrodes conductivity cell consists of four electrodes, a current source to drive the current through the outer two electrodes and a voltmeter to measure the potential difference across the other two. That potential difference is proportional to the conductivity of the solution which can be calculated if the cell constant is known.

In applications such as soil condition monitoring, the advantages TF technology can offer are vital. Therefore, using these background theories, fabrication of TF sensors will be ideal. Not all techniques are compatible with TF screen-printing technology and that is why the research is focused more on techniques and sensor types that can be screen-printed utilising the advantages of TF technology as well.

2.4 User Requirements & Characteristics of Existing Commercial Technologies

In this specific research application, ideal user requirements were defined by the soil scientists participating in the project and the overall project time constrains. Table 2-4 shows the user requirements for each sensor with the ideal overall cost of the substrate having all sensors integrated on it.

Table 2-4: User requirements for each separate sensor.

Measurand	Resolution	Accuracy	Range	Lifetime	Cost
pH	0.1 pH	0.1-0.2 pH	2-12 pH	> 1 year	All together should not cost more than £20 excluding interface.
Dissolved oxygen	1 ppm O ₂	1 ppm O ₂	0 – 10 ppm O ₂	> 1 year	
Temperature	0.1 °C	0.2 °C	~50 °C	> 1 year	
Conductivity	10 µS/cm	10 µS/cm	0.1 – 20 mS/cm	> 1 year	

A search for each individual sensor was performed to identify existing commercial sensors that could easily be applied to this case. Several sensors and meters came up but each one of them had some issues that could not be adjusted for soil measurements. Taking pH as the first parameter that needs monitoring, plurality of sensors have been identified but the vast majority of them required soil sampling, addition of water to make a soil water mixture and then insert the sensor which defies the purpose of a direct soil pH sensor. Table 2-5 shows three commercial sensors that claim to measure directly the pH of the soil and their specifications.

2. Literature Review

Table 2-5: Characteristics of existing technologies for direct soil pH sensing. (Specifications obtained from official websites of manufacturers)

Brand (Model)	Resolution (pH)	Accuracy (pH)	Range (pH)	Cost (GBP)	Comments
Hanna Instruments (HI99121)	0.01	@20°C ±0.02	-2 to 16	280	Only works with soft & wet soils. Brittle & made of glass
Plantcare Tools (4 in 1 Soil Meter)	0.5	Not defined	3.5 to 9	25	Unreliable
Spectrum Technologies (FieldScout pH 600 or 400)	0.01	0.01	0 to 14	450	Direct soil pH readings. 6 months warranty

pH meters are all equipped with temperature sensors for temperature compensation since pH is temperature dependent. None of the existing commercial sensors has the specifications required in this application and most importantly none of them is designed to be buried in the soil for a long period of time. All mentioned sensors are designed for insertion in soil, taking measurements and then removed for storage. Furthermore, frequent calibration is required in these meters which also defies the purpose of allowing them in the soil for an extended period of time.

Looking for commercial temperature sensors would be trivial since there is a huge variety of different types and specifications for temperature sensors. Prices can vary from several pounds to several thousand pounds depending on their specifications. In this case, a combination of pH, dissolved oxygen and temperature sensors is required and the price for the combination of the three will depend on the most expensive ones like pH and dissolved oxygen.

Dissolved oxygen sensors for direct soil measurements don't exist and the reason is that it is meaningless to measure dissolved oxygen in soil unless the actual measurements one might require are for the water flowing down in soil. No dissolved oxygen sensors for soil

measurements have been commercialised and definitely not in combination of pH and temperature. Dissolved oxygen levels are also temperature dependent therefore, all commercialised dissolved oxygen sensors include a temperature sensor for temperature compensation.

Soil conductivity sensors are beginning to receive high interest as soil conductivity measurements get increasing attention due to improved correlations between measured soil conductivity and several soil parameters. Table 2-6 shows the characteristics of the commercial conductivity meters that could be used in this application.

Table 2-6: Characteristics of existing technologies for soil conductivity sensing. (Specifications obtained from official websites of manufacturers)

Brand (Model)	Resolution (mS/cm)	Accuracy (mS/cm)	Range (mS/cm)	Cost (GBP)	Comments
Spectrum Technologies (FieldScout Direct Soil EC Meter)	0.01	±1%	0 to 19.9	270	Professional grade meter
Hanna Instruments (HI98331)	0.01	±0.05 to 0.3	0 to 4	60	Small range with temperature range of 0-50 °C
Hanna Instruments (HI993310)	0.01	±2%	0 to 20	375	Can also measure soil activity

Some of these soil conductivity meters are expensive but of high accuracy and relatively wide conductivity ranges while they all utilise a microprocessor to adjust their sensitivity depending on the conductivity range of the soil. One of the meters shown above is of lower price than the rest but the range of conductivities to be measured is narrow and does not cover the complete soil conductivity range. Again, these meters are not designed to be buried underground and left there for an extended period of time. Such usage will most probably damage the meter and its specifications will be altered. Soil conductivity is also temperature dependent and all these meters include a temperature

2. Literature Review

sensor for temperature compensation. A vast majority of soil properties is also correlated to the soil water content which is usually measured using capacitance probe. Capacitance probes are conductivity meters which utilise a high frequency (>100 kHz) AC current or voltage source. In that way, capacitance is measured instead of resistance and the dielectric constant of soil is calculated. The dielectric constant is directly related to the water content of the soil. In this specific application, a combination of soil conductivity and water content would provide useful information on soil properties and soil conditions, something that does not exist commercially or even at research level.

2.5 Sensing Technologies at Research Level

A wide variety of research groups are now interested in low-cost, solid state (SS) sensors with real-time operation. Therefore, many new sensors in this area have been reported in the last two decades. The research in this report is hence an attempt to push the borders of scientific knowledge on SS sensors, forward to a point where the sensors can be usable for soil condition monitoring. Some of the sensors are less and some more mature in their technology and the research was focused more on the areas that needed more exploration. pH ISEs, oxygen sensors and PRTs have been reported a long time ago and have a much higher level of maturity than the solid state REs and the TF conductivity sensors. In the case of the first three sensors (pH ISEs, oxygen sensors, PRTs), literature discussed in this chapter is very selective only to the researches that could help modification of the sensors for soil condition monitoring and understanding the electronics for each sensor type. In the case of REs and conductivity cells, the literature survey is much broader due of the low maturity level of the sensors. In order to utilise TF Technology's advantages in this work, literature is focused on printed or planar sensors and not in their macroscale equivalents. Some exceptions were made if the research could benefit from the way of thinking and those cases are explained in more detail.

2.5.1 Reference Electrodes

Due to the high demand for a reliable solid state RE, many attempts have been made in the past to design such an electrode but no one has ever managed to design an electrode cheap enough, non-fragile and compatible with simple electronic components. Although ISEs have been reported to be developed as miniaturised SSE, they are useless without a RE of the same size and nature. Several types of REs have been explained earlier but the most common type and the only one that is compatible with TF Technology is Ag/AgCl RE thus literature was focused only on that type.

Extensive work has been done on quasi-reference electrodes which are much easier to develop if the chloride concentration of the liquid is known or stable. In cases where the chloride concentration is not constant or known, other approaches have been reported. (Nolan, et al., 1997; Eine, et al., 1997; Desmond, et al., 1997; Shinwari, et al., 2010; Musa, et al., 2011; Fernandes & Heinke, 2015)

In most cases, ion exchange membranes have been used to withhold a constant chloride concentration under them with the use of a gel or a paste. (Mroz, et al., 1998; Huang & Huang, 2002; Simonis, et al., 2003; Simonis, et al., 2004; Ha, et al., 2005; Maminska, et al., 2006; Liao & Chou, 2006; Liao & Chou, 2008; Kisiel, et al., 2008; Rius-Ruiz, et al., 2011)

In cases where having planar electrodes was not important, macro-scale, SS REs were developed to overcome the problems with using glass electrodes in harsh environments and the need to refill the electrode when the electrolyte runs out. (Guth, et al., 2009; Vonau, et al., 2010; Shinwari, et al., 2010)

In recent years, there were some attempts to develop SS REs using conducting polymers that eliminate the need of an internal electrolyte on the electrode. (Kisiel, et al., 2005; Michalska, 2012)

2. Literature Review

There are other cases where TF technology was used to develop SS REs. TF pastes were used as chloride carriers to maintain the chloride concentration around Ag/AgCl layer constant. This type of REs is the most relevant to this work hence attempts of this kind are more detailed explained. (Cranny & Atkinson, 1998; Simonis, et al., 2003; Simonis, et al., 2004; Tymecki, et al., 2004; Martínez-Máñez, et al., 2005; Prasek, et al., 2008; Idegami, et al., 2010; Atkinson, et al., 2011)

Cranny & Atkinson in 1998 (Cranny & Atkinson, 1998), designed 3 types of reference electrodes, all fabricated using thick-film technology and only differing in their silver-silver chloride layer. One of them has a glassy silver-silver chloride layer, the other one a polymeric silver-silver chloride while the last one was a glassy silver chloride layer. The difference was the paste and the silver to silver chloride ratio. Also, the paste used for the potassium chloride layer was varied between a polymer based ink and a glass based one. The structure of the electrodes is shown on Figure 2-19.

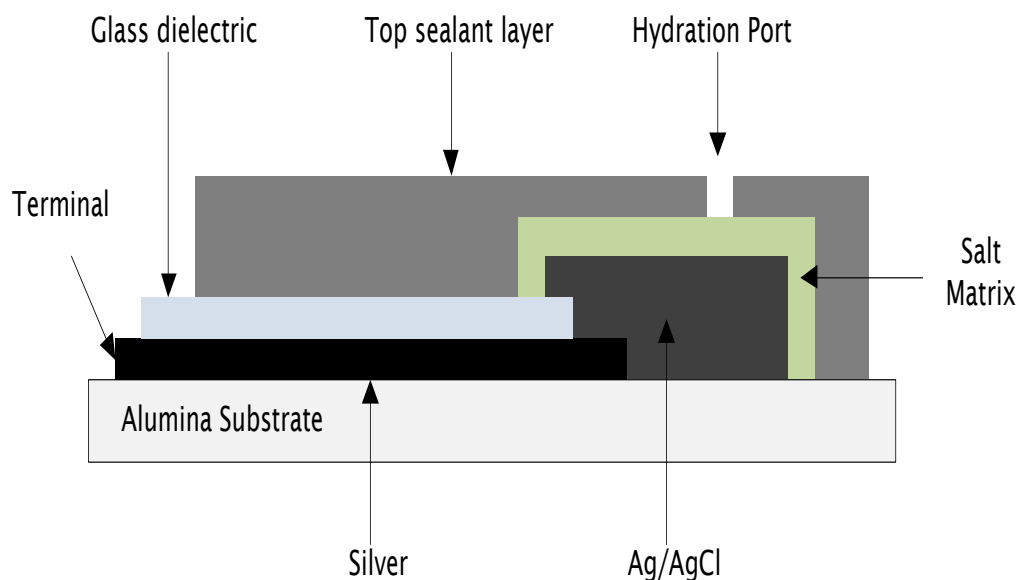


Figure 2-19: A cross section of the silver-silver chloride Thick-Film reference electrode. (Cranny & Atkinson, 1998)

A summary of the results is shown on the table below.

Table 2-7: Experimental results for each type. (Cranny & Atkinson, 1998)

Ag/AgCl Paste	Cl ion sensitivity (mV/log[Cl])	Standard potential (mV)	KCl salt matrix	Hydration time (h)	Potential drift (mV/day)	Lifetime (days)	Shelf life (months)
Polymer Ag/AgCl	-61.24	-9.94	Polymer	6	6.8	25	>6
Glassy AgCl	-60.74	-9.99	Polymer	10	4.4	40	>12
			Glassy	5	6	14	>12
Glassy Ag/AgCl	-59.99	-5.88	Polymer	4	-	-	>12
			Glassy	1	4.2	20	>12

This paper provided a basis for the fabrication of the electrodes to be designed in this project. It is a new concept and although the electrode potentials are not stable, most probably with some improvements these electrodes can provide a cheap alternative to the fragile commercial reference electrodes.

Simonis et al. in 2003 (Simonis, et al., 2003) compared the performance of REs fabricated using thin- and thick-film techniques. KCl-containing membranes were screen-printed on a layer of Ag/AgCl paste. Several coatings were used to protect the KCl from leaching into the solution. REs without the KCl-containing membranes provided stable potentials in 3 M KCl solutions for about 7 hours for thin-film electrodes and up to 90 hours for thick-film, suggesting the idea that layer thickness is directly proportional to the potential stability. REs with the KCl-containing membrane were stable for more than two months.

Simonis A. et al. in 2004 (Simonis, et al., 2004), evaluated the performance of two different types of reference electrodes fabricated using thin-film and thick-film techniques. The structures of the two types are shown in Figure 2-20.

2. Literature Review

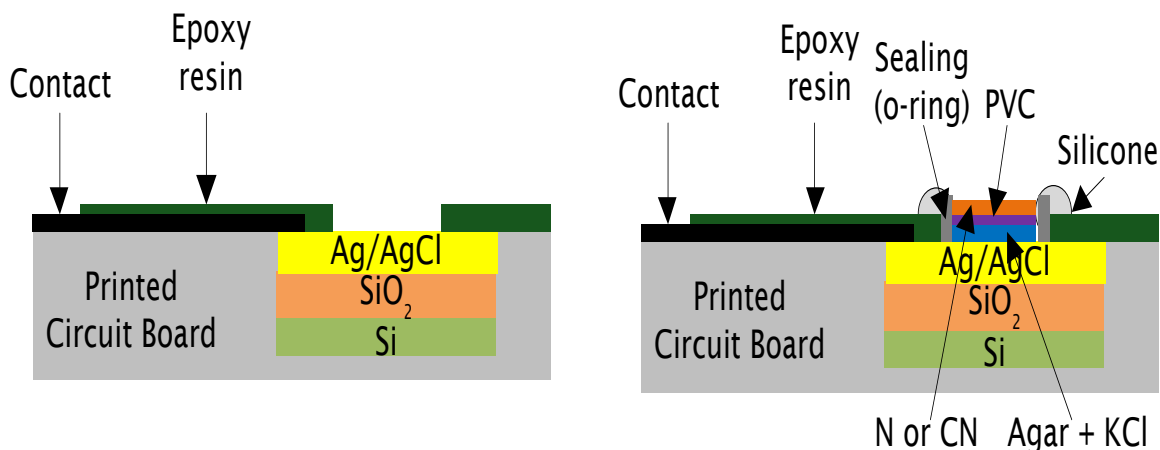


Figure 2-20: The cross section of the two different structures. (Simonis, et al., 2004)

Their main difference is the potassium chloride layer deposited on top of the silver-silver chloride layer using agar. Also, a polyvinylchloride (PVC) membrane with either Nafion (N) or cellulose nitrate (CN) on top was used, to keep the agar and potassium chloride on the electrode and decrease the diffusion rate of potassium chloride into the electrolyte. These electrodes were tested for their long term stability and the experiments revealed that the stability of the thin-film electrodes in 3 M potassium chloride solution was 7 h and 500 h for the thick-film ones without a membrane. Those that had the membrane had 2 months stability in pH 7 buffer with less than 0.1 mV drift in 10 h for the thick-film ones and 0.4 mV for the thin-film.

Trymechi L. et al. in 2004 (Tymecki, et al., 2004), tested two types of screen printed silver-silver chloride electrodes where their only difference was that one of them had a potassium chloride salt matrix on both sides of the silver-silver chloride layer while the other one it only had the matrix between the silver-silver chloride and the solution. The structures of the electrodes are shown in figure 1 of (Tymecki, et al., 2004). The long term stability was found to be 0.6 mV/h for type 1 and less than 0.2 mV/h for type 2. The continuous operating time exceeded one week while the shelf life was more than 9 months. These electrodes were tested in different concentrations of various ions and pH and revealed no effect on the performance.

Martínez-Máñez, R. et al. in 2005 (Martínez-Máñez, et al., 2005), used a reference electrode on a water quality sensor designed using thick-film technology. On this sensor, pH and many other parameters were investigated while the reference electrode was made up of silver-silver chloride and an additional upper layer of potassium chloride using dielectric paste D2020529D1 obtained from Gwent Electronic Materials, the encapsulating resin EPOTEK H77 and a simple membrane made with polyisophthalamide diphenylsulfone (PIDS). These three types were tested for their long term stability within a period of 30 days maintains a satisfactory stability to be used for the pH sensing of the water. After 6 months the drift was less than 10 mV per day.

Prasek J. et al. in 2008 (Prasek, et al., 2008), at the 31st International Spring Seminar on Electronics Technology, reported new reference electrodes which are specifically adapted for thick-film sensors. The structure of which is shown in Figure 2-21.

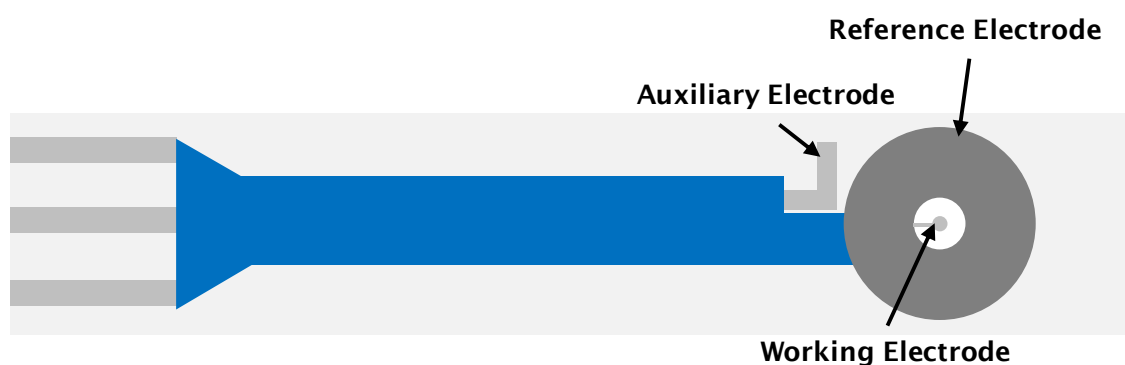


Figure 2-21: The structure of the proposed electrode. (Prasek, et al., 2008)

For the tests cyclic voltammetry (CV) was used in a potential range of -300 to 600 mV with scan rate of 20 mV/sec. Both commercial DuPont pastes with different silver to silver chloride ratio had similar response. In comparison with the classical Ag/AgCl reference electrode, the current response is comparable but there is a shift of half-wave potential in range of ~ 100 mV for these specific electrodes. Cyclic voltammetry is performed by usually gradually increasing the potential between the electrodes up to a specific voltage and then gradually decreasing back

2. Literature Review

the voltage. It is characterised by two half-waves, the forward and backwards. During that voltage alteration, the current measured between the electrodes undergoes a flat section where the current is constant. The difference between the absolute values of the two half-waves at their flat sections is the shift of half-wave potential. Also, the geometrical parameters of the electrodes in the voltammetric cell can highly affect the output responses of the electrodes.

Idegami et al. in 2010 (Idegami, et al., 2010), has proposed an accurate but disposable, planar RE having an internal electrolyte fabricated using the screen-printing process. The electrolyte paste was made up of a sodium alginate paste containing KCl. The REs could provide a potential stability of approximately 60 minutes and the chloride dependence of the electrode was in the range of ± 10 mV for chloride concentrations between 10^{-3} and 10^{-6} M.

Atkinson et al. in 2011 (Atkinson, et al., 2011), has proposed a thick-film silver-silver chloride electrode based on commercial inks and a potassium chloride matrix included in a polymeric ink on top as well as potassium chloride in a hydrogel as the stabilizing layer. They investigated the effect of potassium chloride concentration on the top layer on the stability of the electrode in different chloride concentrations and also the electrode drift after a long time of continuous operation. All the experiments were performed against a commercial silver-silver chloride electrode. The proposed structure is shown in Figure 2-22.

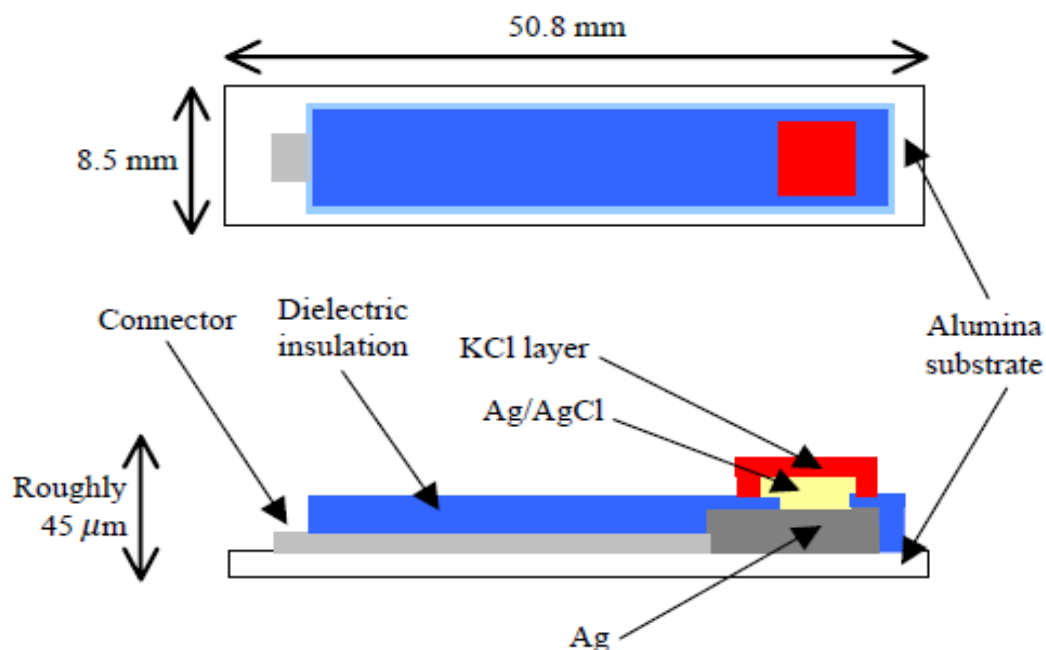


Figure 2-22: Typical construction of a Thick-Film reference electrode. (Atkinson, et al., 2011)

It was suggested that a concentration must exist which will allow almost no dependence on chloride concentration because some of the electrodes provided opposite potential trends from the Nernstian theory. Also, changes in the concentration of potassium chloride on the electrode have an effect on the step size of the electrode potential in different potassium chloride solutions. Hydrogel was proven to give somehow stable results for a wide range of concentrations while for both, hydrogel and the polymer ink, the more potassium chloride on the electrode the drift, which means leakage in the solution, increases.

2.5.2 pH Ion-Selective-Electrodes

After the work of Fog & Buck in 1984 (Fog & Buck, 1984), several successful attempts have been made in the development of a SS pH ISE. A few of them use TF technology but using different sensing materials. (Belford, et al., 1987; Davison & Harbinson, 1988; Duroux, et al., 1991; Deligianni & Romankiw, 1993; McMurray, et al., 1995; Koncki & Mascini, 1997; Marzouk, et al., 1998; Yao, et al., 2001; Wang, et al., 2002; Kampouris, et al., 2009)

2. Literature Review

Belford et al. in 1987 (Belford, et al., 1987), tested various metal oxides as pH sensitive materials in an electrochemical cell against a commercial standard calomel electrode. Platinum/Gold, platinum oxide, copper oxide and iron oxide were tested as the pH sensitive materials. Those pastes were fired at two different temperatures to evaluate the effect of the curing procedure on the sensitivity of the electrodes. The experimental results are presented in the table below.

Table 2-8: Experimental results of each type. (Belford, et al., 1987)

Contacts	Pt/Au (dil)	Pt/Au OXD	Cu	Fe
(a) Maximum temperature 900 °C				
mV/pH	51	46	56	48-52
Daily drift (mV)	~5	~5	20	~5
Longevity (days)	40	40	48	50
Crack and fissures	low/med	low	low	low
Success of fabrication	10-15%	10-15%	0.30	0.50
(b) Maximum temperature 700 °C				
mV/pH	48-50	45	56	53
Daily drift (mV)	~5	~5	~10	~5
Longevity (days)	25	23	50	40
Crack and fissures	high	high	med	med
Success of fabrication	5-10%	5-10%	~25%	~25%

McMurray et al. in 1995 (McMurray, et al., 1995), reported new composite electrodes with a RuO₂: lead borosilicate glass ratio of 1:1 show a near-Nernstian potential response between pH 2 to 12, a maximum hysteresis of 30 mV and a response time of approximately 90 s. Response rates were dependent on the diffusion of protons through the porous composite and decrease with decreasing RuO₂: glass ratio. The electrodes were insensitive to oxygen concentration changes, but revealed a small response to chloride ion concentration.

Koncki & Mascini in 1997 (Koncki & Mascini, 1997), also reported thick-film pH electrodes based on ruthenium dioxide. The pH electrodes gave a sensitivity of about -51 mV/pH, which is close to the Nernstian response while they were also tested for reproducibility with very good results. They were tested from acidic solutions up to pH 8 and showed a linear response with no affect from on any other ions but they were affected by strong reducing agents.

Mihell & Atkinson in 1998 (Mihell & Atkinson, 1998), used the fundamentals described by Fog and Buck and designed some thick-film pH electrodes based on ruthenium dioxide. The structure of the electrodes is shown in Figure 2-23.

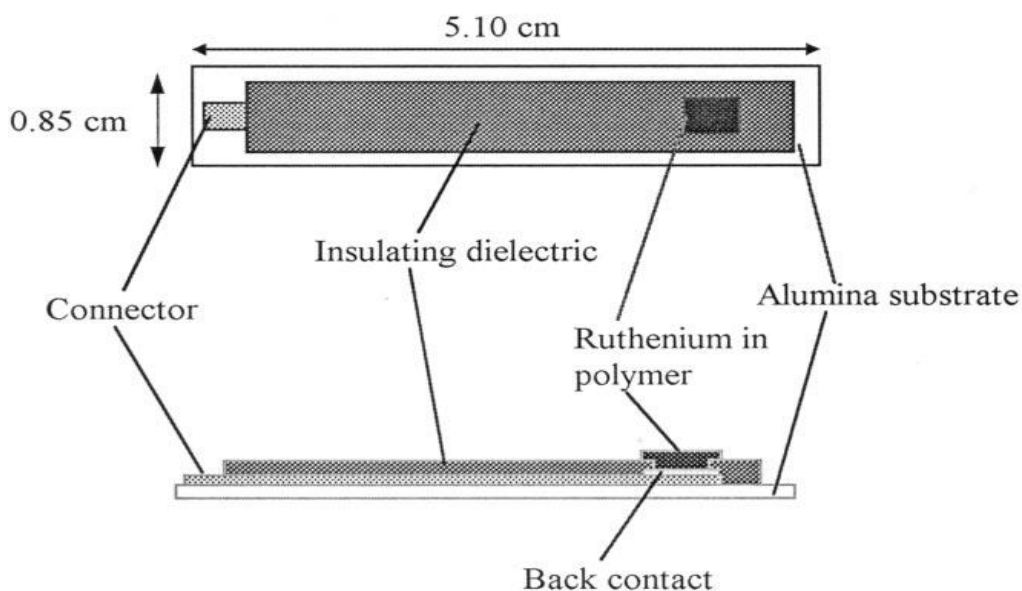


Figure 2-23: The construction of a Thick-Film pH electrode. (Mihell & Atkinson, 1998)

It was demonstrated that ruthenium oxide electrodes revealed a Nernstian response of 59 mV in pH values from 2 to 10. The mechanisms (Eqn. (15)) by which ruthenium oxide electrodes operate are not completely understood but Fog and Buck have proposed several possible mechanisms for the pH dependency and equation of the ruthenium oxide electrodes.

2.5.3 Dissolved Oxygen Sensors

There have been several attempts for a low cost dissolved oxygen sensor and some of them utilised TF technology. Work done in this report is a continuation of previous existing work; a brief survey has been done to search for different applications of such sensors. (Karagounis, et al., 1986; Chemnitius & Bilitewski, 1996; Wittkamp, et al., 1997; Atkinson, et al., 1998; Glasspool & Atkinson, 1998; Martinelli,

2. Literature Review

et al., 1999; Zen, et al., 2002; Lam & Atkinson, 2003; Martínez-Máñez, et al., 2004; Zheng, et al., 2011)

Karagkounis et al. in 1986 (Karagounis, et al., 1986), investigated the performance of a TF three electrode oxygen sensor. Using a multiple cathode electrode, the flow effects on the measured current will be minimised while the total current will be high enough to enable its use for signal processing. The three electrodes were set up as a potentiostat in the arrangement shown:

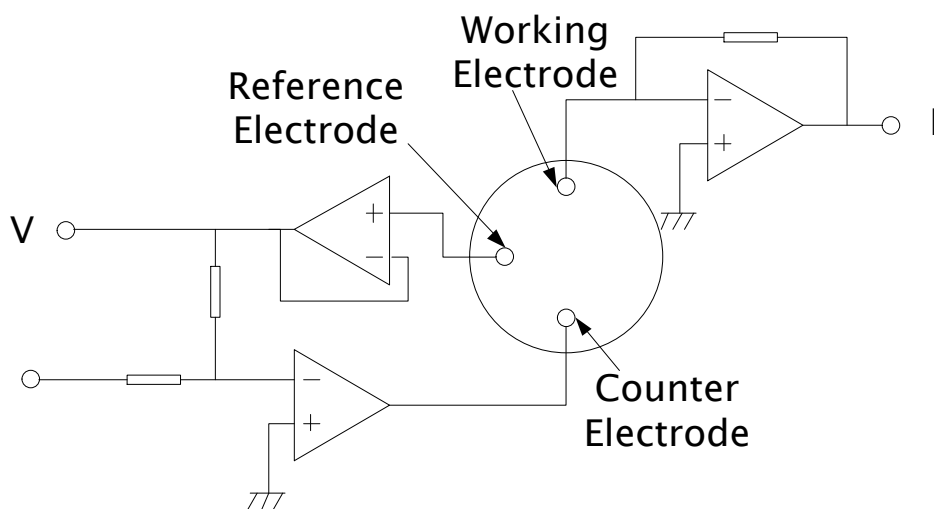


Figure 2-24: Diagram of the electronic circuit. (Karagounis, et al., 1986)

The structure of their proposed sensor is shown below:

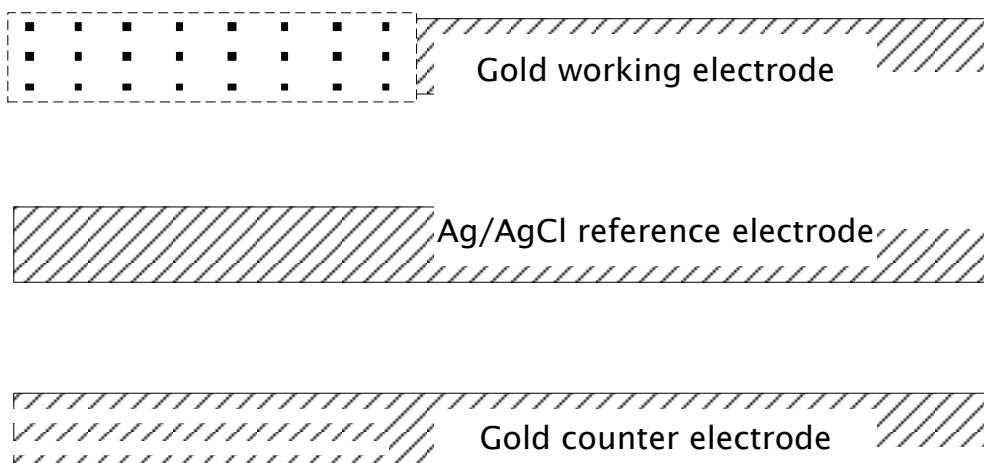


Figure 2-25: Structure of their proposed sensor. (Karagounis, et al., 1986)

Typical polarograms (Voltage vs Current graphs) were obtained indicating an operating voltage of approximately 0.8 V versus the Ag/AgCl electrode, with a scan rate of 5 mV/s. Scan rates of 5-200 mV/s were employed but there was no change to the output current. It was found that the sensor was temperature dependent from 25-42 °C with a +2.5%/°C change in the sensor's output. The sensor showed a sensitivity of 1.3 $\mu\text{A/ppm}$ of oxygen in physiological saline solution at 25 °C. The sensor was tested in the pH range of 5-9 showing no change in the output current but it can affect the operating voltage range. pH 5 showed a shorter plateau than pH 9. The long term stability of the sensor was investigated showing that it could be used for 10 consecutive days with $\pm 2.5-7.5\%$ change in sensor output from the calibration curve as compared with the initial calibration.

Wittkamp et al. in 1997 (Wittkamp, et al., 1997), demonstrated the feasibility of silicon thin-film oxygen sensors based on a Clark-type three electrode configuration with multiple cathode design. They investigated the performance of an oxygen permeable membrane on top of the sensor with the use of a gel as shown below:

2. Literature Review

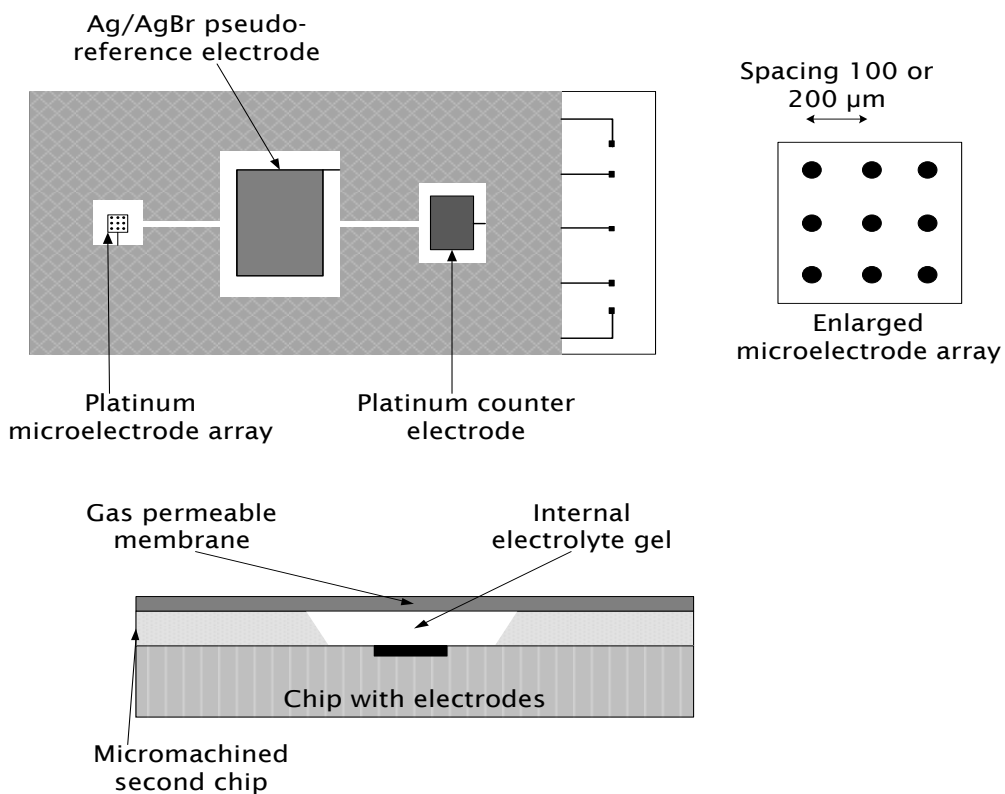


Figure 2-26: The construction of their sensors with the microelectrode array and the gas permeable membrane. (Wittkamp, et al., 1997)

The electrolyte gel was made with sodium alginate (Sigma Chemie, Deisenhofen, Germany) solution (1%) in a borax/NaOH buffer pH 10. The chip was then dipped in the same buffer containing 0.05 M CaBr₂ for 5 min, to get a calcium alginate-gel soaked with 0.1 M Br⁻ as the electrolyte. The gas permeable membrane was made of two component room temperature vulcanizing (RTV II) silicone rubber (Siloprene, Fluka Chemie, Neu-Ulm, Germany). It was demonstrated that the spacing of the multiple cathode electrode affected the peak current of the sensor for different scan rates. In addition, the plateau voltage of the sensor was found to be similar to the one without the membrane at about -875 mV. Using that voltage against a Ag/AgBr reference electrode, the sensor's sensitivity was 240 pA/mbar for 100 μm spacing and 300 pA/mbar for 200 μm. The long term stability of the sensor was also investigated for 12 hours giving a more stable output for the 100 μm spacing.

Glasspool & Atkinson in 1998 (Glasspool & Atkinson, 1998) and Lam & Atkinson in 2003 (Lam & Atkinson, 2003), have suggested a TF dissolved oxygen sensor with the use of an oxygen permeable membrane and an electrolyte gel below the membrane. The sensor was made up of three electrodes and the operation of the electrodes was based on the Clark Cell. They used a constant potential difference between the RE and WE of 0.8 V and they measured the current level which is proportional to the oxygen levels. They also used a guard electrode around the WE to only measure the oxygen penetrating the membrane and not any oxygen moving inside the electrolyte gel. The sensor showed a sensitivity of around 1 μA per ppm of oxygen and a stable lifetime of around 16 days.

Martinez-Manez et al. in 2004 (Martínez-Máñez, et al., 2004), reported a TF potentiometric dissolved oxygen sensor based on ruthenium oxide electrodes with a titanium oxide and PIDS (polyisofthalamide diphenylsulphone) gas permeable membrane. The structure of the sensor is shown below:

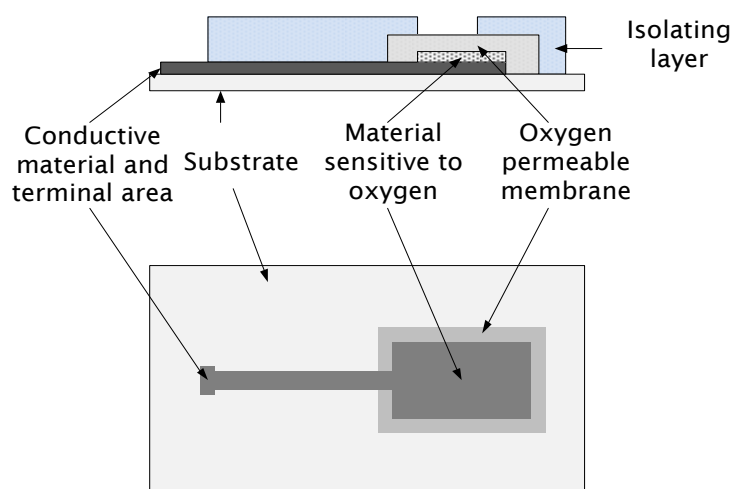


Figure 2-27: Structure of the potentiometric dissolved oxygen sensor.

(Martínez-Máñez, et al., 2004)

The electrode's potential was measured against a Ag/AgCl reference electrode in oxygen concentrations of 0.5-8 ppm in pH 7 water. Titanium oxide membranes gave a Nernstian response of 59.4

2. Literature Review

mV/decade of oxygen concentration at 25 °C on a logarithmic scale. In comparison with PIDS-coated electrodes, the sensitivity was found to be 37.4 mV/ decade of oxygen concentration indicating the reduction of oxygen with two electrons. The performance of the sensors was investigated in pH 4-10 solutions giving a large dependence of potential on the titanium oxide membrane while PIDS-coated electrodes were gave no significant potential change in that pH range.

2.5.4 Platinum Resistance Thermometers

PRTs have been around for several decades and their fabrication using TF technology is very mature. In the process of measuring humidity or conductivity accurately, temperature compensation is necessary. Furthermore, soil temperature is an important parameter and can vary widely from place to place in the same field but also the variation vertically in the soil might also be different. Hence, a PRT was used in this work. Due to the fact that this kind of sensor has a well understood operating principle, no further literature review was necessary.

2.5.5 Conductivity Cells

Conductivity meters have been around for a long time but most of them are expensive and usually contactless, missing out on sensitivity, and designed for liquids. In situations where response time and sensitivity is of higher importance, conductivity electrodes need to be in contact with the investigating medium. More often, to measure water content in soil, capacitance meters are used which are almost identical to conductivity meters but the measurements are done using a high frequency AC current. Soil conductivity can provide further information such as soil type and structure which are vital for soil scientist and farmers. (Herman, 2001; Kizito, et al., 2008)

Over the years, several conductivity meters have been reported but none of them are of low cost that can allow a dense sensor network in agricultural fields. Furthermore, soil is a very harsh environment for

sensors and not many technologies are offered for real time monitoring. Most attempts have been made for liquid electrical conductivities. (Khang & Fitzgerald, 1975; Mitchell & de Alwis, 1989; Zegelin, et al., 1989; Hanson & Kaita, 1997; Cilliers, et al., 2001; Laugere, et al., 2003; Geirinhas Ramos, et al., 2006; Ramos, et al., 2008; Lingfang, et al., 2009; Wei, et al., 2010)

Khang & Fitzgerald in 1975 (Khang & Fitzgerald, 1975), have reported a novel way to measure electrical conductivity. Usually measuring electrical conductivity follows the procedure of measuring the conductance and then changing that to conductivity by using the cell constant of the meter. That relationship is more often non-linear. The paper was concerned on eliminating any non-linearity effects, cross-talk effects, stray current effects and internal battery effects. Those effects can be eliminated by designing the probe and the electrical circuit in a specific way explained in this paper. This kind of probes can be used in metal tanks without the requirement of insulating all metal surfaces and also allow simultaneous, independent measurements in the same tank.

Zegelin et al. in 1989 (Zegelin, et al., 1989), presented a two electrode conductivity cell to also measure the volumetric water content. Although the method used was the two electrodes method, they used three electrodes in a symmetrical sense around a centre electrode to maintain the electric field around the inner electrode. They measured volumetric water content and soil electrical conductivity in situ using time domain reflectometry (TDR) in an attempt to eliminate unwanted noise and information loss due to impedance mismatch between the probe and the coaxial connecting cable. The enhanced signal clarity of the new probes extends to sample diameters of at least 0.2 m. The results indicate that electrical conductivity determined using other laboratory methods and results obtained from these probes agree for both electrolyte solutions and soil samples to $\pm 10\%$ on conductivities above 10 mS m^{-1} .

2. Literature Review

Cilliers et al. in 2001 (Cilliers, et al., 2001), developed a novel electrical resistance tomography (ERT) measurement system, which uses a switched bi-directional constant current source to generate the electric field. Voltage measurements were made on the two half cycles and subtracted, eliminating any DC components present at the measuring electrode solution interface. Resulting potential difference is a function of conductivity distribution in the medium. The use of bi-directional square waves makes the system much simpler because the current pulse is DC and the differential measurements do not require any demodulating. The Newton-Raphson (NR) algorithm was used for reconstruction. Experiments were performed on a model system of (a) non-conducting object(s) in a conducting liquid, and on liquid foams of varying bubble size. Visualizations showed that the system could resolve the position and size of the objects, and identify coarse foam regions.

Laugere et al. in 2003 (Laugere, et al., 2003), demonstrated the benefits of the use of four electrodes for contactless conductivity detection in miniaturized capillary electrophoresis devices. The influence of the electrode double layer capacitance and insulating layer capacitance on the response was minimized. Thus, at frequencies below 10 kHz, the detector response (sensitivity, linearity, accuracy) is almost independent of the measurement frequency and of the conductivity of the carrier electrolyte. Ion concentration detection limits ranging from 15 down to 5 μM (depending on the ion) were obtained. Finally, separation of six organic acids was demonstrated, extending the applicability of the contactless four-electrode detector.

Ramos et al. in 2008 (Ramos, et al., 2008), developed a low cost four electrode sensor for water conductivity measurements. The sensor was made up of a transparent tube of approximately 0.18 m long, 0.016 m internal diameter and 0.002 m tube thickness. Two current electrodes were placed 0.09 m apart and two voltage electrodes were also placed in-between at a distance of 0.02 m. The sensor could measure conductivities in the range of 50 mS m^{-1} to 5 S m^{-1} . The meter was using

sinusoidal current signals at a specific frequency and the measured voltage across the voltage electrodes was recorded. The system also included a temperature sensor in order to compensate for temperature variations in the water. This meter's main advantages include a wide measurement range, an intrinsic capability to minimize errors caused by fouling and polarization effects, and an automatic compensation of conductivity measurements caused by temperature variations.

Wei et al. in 2010 (Wei, et al., 2010), designed an intelligent conductivity meter based on a specialised microcontroller. It adopted conductivity electrodes as the sensing elements to measure the resistance of the solution. It adopted bipolar voltage pulse excitation signal to avoid effects of electrode polarisation. When being powered by the bipolar voltage pulse by the MSP430F149 microcontroller, the circuit generated an output voltage signal, corresponding to the resistance of the solution. The analog output signal was amplified by the range switching and amplifier circuit of the same microcontroller. Then it changed the waveform through the waveform transformation circuit and sent the signal to the A/D of MSP430F149. Simultaneous temperature compensation was also performed through the same controller. The system features several advantages such as easy to realization, self-compensation and self-tuning.

2.5.6 Interfaces between sensor & environment

Interfaces between sensors and soil have not been widely reported yet due to the fact that there are no soil sensors that can be inserted directly into the soil. Currently, soil analysis is made in the laboratory using soil samples that are dissolved or suspended in solutions. Therefore, there is no need for any interface between the sensors and the solution. In the case of actually inserting the sensor directly in the soil, a good physical and electrical contact needs to be maintained between the sensor and the soil. Also, since the hypothesis of directly inserting sensors in soil is to monitor the parameters of the water

2. Literature Review

flowing through the soil, some amount of that water needs to be preserved for a certain period of time so that the sensor can sense a specific parameter.

Unfortunately, such interfaces have not been reported in the literature other than the work of Cranny et al., 2011 (Cranny, et al., 2011) that used a polyurethane block at the bottom of a soil column to hold enough solution to complete the circuit for the sensor.

Prof Annie Verhoef, was the leading soil scientist of the project, mentioned that gypsum was used in the soil as an interface between the instrument and soil to measure water content. Shainberg et al. in 1989 (Shainberg, et al., 1989) and Wellings et al. in 1985 (Wellings, et al., 1985) reported the use of gypsum blocks as a medium to absorb water from soil and measure the water content of the soil indirectly. Gypsum has the ability to retain water faster than most soil types which is favoured when monitoring soil properties. The main issue when using gypsum for a long period of time was that it dissolved in the water and affected the readings of the instrument.

2.5.7 Summary

SS REs has been a major area of research of the electrochemical community and although several advancements and methods have been reported nobody has managed to solve both issues regarding the lifetime and stability of REs while maintaining the cost low enough for high density underground sensor networks. Identifying a proper solution to the problem one must first clearly understand where the problem comes from and identify how and which parameters can affect the performance of REs. The closest to TF technology REs reported that have a promising performance are those reported by Cranny & Atkinson in 1998 and Atkinson et al. in 2011 (Cranny & Atkinson, 1998; Atkinson, et al., 2011). This project will build on the existing knowledge of those REs and try to contribute to the scientific knowledge already available.

In the area of pH ISEs, there are plenty of options to use but in order to utilise the advantages of TF technology and also being able to integrate all the sensors on the same substrate, the work of Mihell & Atkinson in 1998 (Mihell & Atkinson, 1998), has been chosen since ruthenium dioxide can provide the closest to Nernstian response, having the lowest susceptibility to other species, wide operational range and being able to operate at various temperatures. The temperature effect will be a major area of investigation for pH ISEs in this report.

Dissolved oxygen sensors and PRTs have already been developed to a mature level and therefore, existing sensing technologies will be integrated on the same substrate as the other sensors to test their performance in soil condition monitoring.

Electrical conductivity or resistivity is a parameter well known for a long time but the operating principles of such a sensor are not totally clear. There are several issues still unsolved with conductivity meters and most importantly the non-linearity of conductance and conductivity as the frequency of the input signal changes as well as the conductivity of the medium. Several attempts, some of them successful have been reported to minimise or even eliminate these effects by using an intelligent design (Wei, et al., 2010) of the cell or other measures. Unfortunately, none of the mentioned techniques is compatible with TF technology which is of major importance in this research project. Designing a TF, low cost and robust conductivity sensor that can be integrated on the same substrate as the rest of the sensors, would meet the requirements of this work and will allow its use in high density underground sensor networks for soil condition monitoring.

Chapter 3: Reference Electrodes

3.1 **Instrumentation & Experimental Setup**

The performance and stability of the electrodes was tested by measuring their electro potential difference with respect to a commercial gel-filled single junction reference electrode (Beckman Coulter A57193). Three electrodes of each type were tested by soldering wires onto their exposed silver conductor layers and connecting them to the voltmeter. Initial experiments from previous people were conducted using Keithley 2000 and manual data logging. Keithley 2000 has a very high input impedance for measuring potential difference and it provides very accurate voltage readings. Keithley 2000 has a connection card that is inserted at the back of the multimeter. Each channel had as the low voltage the commercial gel-filled reference electrode while the high voltage of each channel was connected to a different TF RE or pH ISE.

The potential difference to be recorded was in the range of a couple of hundred millivolts and the changes in that potential were even smaller in the range of a couple of tenths of millivolts. Therefore, any type of noise could affect the voltage giving unstable readings. Low voltage measurements require high sensitivity instrumentation which can pick up noise from the mains through exposed conductors and interfere with the electrochemical potential of the cell. In addition, recording the potential manually involves the human error for taking a reading when the reading is relatively unstable and in addition someone's presence is required to take the readings.

In order to improve the experimental procedure, measurements were carried out using a portable data logger designed by Dr. Eduardo G. at the University of Valencia, Spain. The output signals of the multi-electrodes were acquired using a 36:1 multiplexer architecture, which was formed by two 18:1 channel MOS analogue multiplexers (MAX306, MAXIM) and one 2:1 channel analogue multiplexer (MAX308, MAXIM) thus up to 36 channels could be measured simultaneously. The selection of each channel in the multiplexer was controlled by the

3. Reference Electrodes

microcontroller (PIC18F4550). The sampling rate for the 36 channels was one electrode every 100 ms in periods of 10 s. A precision CMOS quad micro power operational amplifier (LMC6064, NATIONAL SMC), was connected to the output multiplexer as a buffer stage. This operational amplifier, working in buffer configuration, has very high input impedance and an ultra-low input bias current of less than 10 fA and hence it is suited to the signal impedance generated by the potentiometric multi-electrodes. An analogue to digital converter (ADC) (MAX128, MAXIM) with a resolution of 12-bits that can work with either unipolar or bipolar input signals was used. It uses an external or internal reference voltage in order to obtain different full scale ranges. In this case a 2.5 V external reference and a bipolar input signal were used. With this configuration the resolution (equivalent to 1 Least Significant Bit) was 1.22 mV. The PIC18F4550 microcontroller gathered the data from the ADC using the I2C bus.

The PIC18F4550 was selected for its low power consumption (sleep mode currents down to 0.1 A typical), 32 K of memory program and 2 K of RAM and USB port. The software for the PIC18F4550 microcontroller has been designed to scan the voltage for each channel. In the process of measurement, the data were sent to the PC via an RS232 serial communications. The acquisition software was developed using Visual Basic® 6.0 and Microsoft Excel® 2003 software. A block diagram of the measurement system is shown below. (Glanc, et al., 2013)

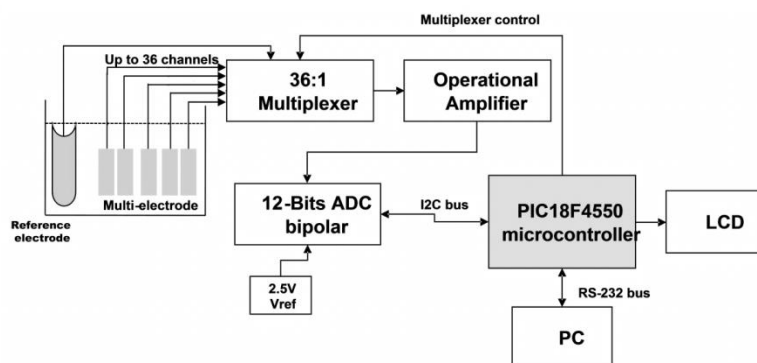


Figure 3-1: Diagram of the experimental setup with the 36 channel multiplexer and the data logger. (Glanc, et al., 2013)

3. Reference Electrodes

After a couple of experiments, it was found that the software of the device was unstable with increasing data size and the software should be restarted after a day of measurements to maintain reliability of the device. For that reason, the firmware and the software of the device were changed and another data logger with much more stable software was created. The software created was very useful as it was much more reliable and you could have a live display of the data recorded. The data could then be saved and opened as an excel file where the data processing was very convenient. Using this data logger, the sampling time was always the same at one reading every 10 seconds.

Three electrodes of each type were tested by soldering wires onto their exposed silver conductor layers and connecting them to the voltmeter. The electrodes were attached to a transparent plastic mounting plate that was designed to support the electrodes and immerse only their working part in a test solution (Figure 3-2). Different KCl solutions were made by dissolving KCl salt (Analytical Reagent, Fisher Scientific UK Ltd) in de-ionised water. Other experiments involved pH buffers to immerse the electrodes and investigate their performance especially for the pH ISEs. For later experiments the solutions were stirred constantly during testing by a magnetic stirrer to minimise the effect of mass transport from the solution to the electrodes, which is more important at lower concentrations. The experiments were all performed at room temperature of 20 ± 3 °C and it is believed that these small variations in temperature can be considered insignificant since the electrode potential sensitivity to temperature is known to be very low. The electrodes were always immersed in KCl solutions or pH buffers overnight to hydrate before any experiment was performed.

3. Reference Electrodes



Figure 3-2: Experimental setup without the magnetic stirrer (left) and with the magnetic stirrer (right). (Glanc, et al., 2013)

3.2 Proposed Reference Electrode Structure

The proposed electrode structure described below is designed to mimic the construction of a single junction electrolyte-filled Ag/AgCl commercial reference electrode.

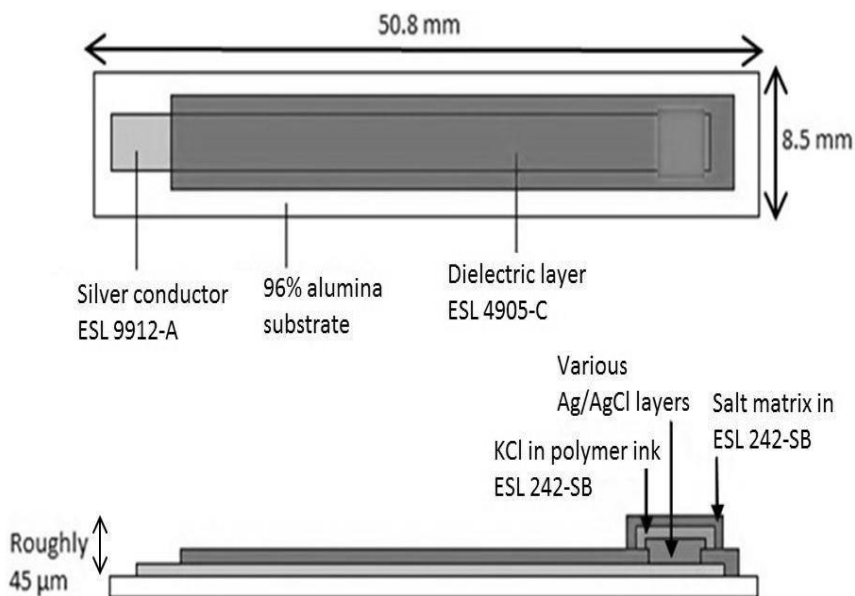


Figure 3-3: Construction of the suggested Ag/AgCl reference electrode. (Glanc-Gostkiewicz, et al., 2013)

The electrodes were screen printed onto 50 mm x 50 mm, 0.625 mm thick, 96% alumina substrates (Coorstech). Each substrate was divided

3. Reference Electrodes

into six equal sized electrodes and prescribed with laser lines so that individual electrodes could be easily snapped off along those lines. Therefore, a simultaneous six electrode fabrication was possible.

The electrodes were constructed by successive screen printing of each individual layer. The screen designs for each layer were produced using AUTOCAD to give precise dimensions of the mesh openings and each screen was designed to print a single layer of the electrode. The screens for the first three layers were made from stainless steel with 250 lines per inch, 15 micron emulsion and 45° mesh while the last two were polymer 70W PW 123-70W:133µm with photopolymer emulsion POLYCOL UNO: 113µm thickness. All the screens were manufactured for the Aurel C880 Printer by MCI Cambridge.

The first layer (Layer 1) was the silver conductor so the screen mesh opening was a rectangle with dimensions of 4.6 mm x 44.6 mm. On top of that, a waterproofing layer (Layer 2) with a rectangular shape of 6.5 mm x 43.8 mm was deposited, leaving a small window exposing the underlying silver. The window size was a square of 3.4 mm x 3.4 mm while a part of the silver, approximately 4.2 mm x 4.6 mm, was also left exposed at one end for soldering connecting wires. The screen for the Ag/AgCl layer (Layer 3) was a square window of 4 mm x 4 mm, slightly bigger than the exposed silver to ensure all the silver was covered. The last two screens, for KCl polymer matrix (Layer 4) and for the second KCl or KNO₃ polymer matrix (Layer 5) (on an attempt to mimic the double junction RE), had simple square mesh openings, like the Ag/AgCl window, but with increasing dimensions of 4.5 mm x 4.5 mm and 5 mm x 5 mm respectively, to ensure complete coverage of the previous layer. (Glanc, et al., 2013)

3. Reference Electrodes

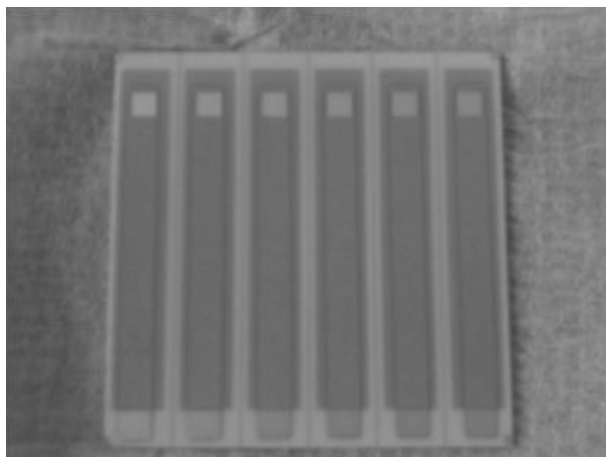


Figure 3-4: The substrate with six simultaneously printed electrodes. (Glanc-Gostkiewicz, et al., 2013)

The silver conductor (Layer 1) was printed using 9912 ink (Electro Science), on top of which a glass dielectric insulator 4905-C (Electro Science) was deposited to isolate the conductor from the electrolyte. For the Ag/AgCl layer several inks have been tested and specific information will be provided later in this chapter. The KCl polymer matrix layer was printed using a silicone based ink 242-SB (Electro Science). The reason different screen types were used was for ease of printing the polymer 242-SB with added KCl, and in order to ensure that the KCl grains would pass through the mesh opening. KCl (Analytical Reagent, Fisher Scientific UK Ltd) was milled into powder of grains smaller than 100 μm and was directly added to the ESL 242-SB paste, adding 402 solvent (Electro Science) when required to keep the paste in printable condition. All inks were dried and cured at the temperatures specified by the manufacturer. (Glanc-Gostkiewicz, et al., 2013)

This electrode operates in the same manner as the conventional gel-filled Ag/AgCl electrode. The idea was to make an all solid state electrode converting the electrolyte solution into a solid matrix layer that when placed in water will act as a layer of controlled chloride concentration. The chemical reactions taking place at the surface of the electrode are (Ives & Janz, 1961):



Based on those two reversible reactions, two different Nernst equations can be written to describe the potential of the electrode (Glanc, et al., 2013).

$$E = E^{\circ} + \frac{RT}{nF} \ln \left(\frac{(a_{Ag_{(aq)}^{+}})(a_{Cl^{-}})}{(a_{AgCl_{(s)}})} \right) \quad \text{Eqn. (29)}$$

$$E = E^{\circ} + \frac{RT}{nF} \ln \left(\frac{(a_{Ag_{(aq)}^{+}})}{(a_{Ag_{(s)}})} \right) \quad \text{Eqn. (30)}$$

For both Nernst equations the activity of a substance in its solid state is defined as unity. Also, the activity of silver and chloride ions in the solution is controlled by the activity solubility product which is invariant at a given temperature. Keeping that in mind, *eqn. (30)* will always be constant at a given temperature and therefore the equations can be changed to:

$$E = E^{\theta} - \frac{RT}{nF} \ln(a_{Cl^{-}}) \quad \text{Eqn. (31)}$$

Where E^{θ} takes into account all the constants.

Keeping the chloride concentration constant around the AgCl layer would stabilise the potential of the electrode. Adding a polymer matrix filled with KCl on top of AgCl was an idea based on previous work and understanding the electrode's operation is the most important section of this work.

3.3 Experimental Work

In all of the experiments on reference electrodes, three electrodes were tested from each kind at the same time in the same solution. The reason

3. Reference Electrodes

being, that if the experiment was to be performed again from the beginning, there will be a possibility of not getting the exact same concentration of KCl in solution which could affect the comparison between identical experiments. In order to avoid such an error, three identical electrodes from each kind were used in the same experiment and error bars were calculated from the performance of those three electrodes. In the experiment for hydration times, drift rates and lifetime only one electrode from each type was used due to shortage of channels on the data logger.

3.3.1 The effect of Ag/AgCl paste on chloride susceptibility

Preliminary experimental work, performed by Professor John Atkinson's research group at the University of Southampton, suggests that REs without the Ag/AgCl layer (layer 3) can provide a lower susceptibility to chloride concentrations. This set of experiments were focused on identifying the reason the electrodes had this unexpected performance. The first set of experiments was to investigate the performance of different Ag/AgCl pastes without any KCl matrix on top. Three different Ag/AgCl pastes were investigated as well as electrodes with no Ag/AgCl layer (bare Ag). The first type was a polymer based paste Ag/AgCl (GEM C61003P7) which has a very low curing temperature (~80 °C). The other two types of Ag/AgCl tested (PPCFB2 & PPCFC3) were both glass based with curing temperatures around 400 °C. The structure of all tested electrodes is shown in Table 3-1.

3. Reference Electrodes

Table 3-1: RE structure to investigate the effect of Ag/AgCl paste on RE's performance.

Type No.	Layer 1	Layer 2	Layer 3
1	ESL 9912	ESL 4905-C	-
2	ESL 9912	ESL 4905-C	GEM C61003P7
3	ESL 9912	ESL 4905-C	PPCFB2
4	ESL 9912	ESL 4905-C	PPCFC3
5	ESL 9912	ESL 4905-C	GEM C61003P7 - Fired
6	ESL 9912	ESL 4905-C	PPCFB2 - Fired
7	ESL 9912	ESL 4905-C	PPCFC3 - Fired

The susceptibility of the electrodes was calculated as an averaged value from each electrode and error bars were obtained when three identical electrodes were tested. Having in mind that fired polymer has provided very promising results in the past, firing the pastes above the recommended temperature was also tried to check the effect it has on the performance. The results of the experiments were tabulated and shown on Table 3-2 below. Furthermore, in order to graphically compare the performances of the electrodes, their susceptibilities were plotted on a bar chart including the error bars from each electrode type.

3. Reference Electrodes

Table 3-2: Electrode susceptibilities from different Ag/AgCl pastes and the tested KCl concentration ranges

No	Materials Used	Susceptibility (mV/decade)	Susceptibility difference between electrodes (mV)	R ²	Concentration Range (M)
1	Bare Silver	-129	2	0.998	0.0134-2
			-2		
2	Bare Polymer GEM C61003P7	-82	-	0.9586	0.0134-2
			-		
3	Bare Glass PPCFB2	-50	4	0.9991	0.0134-2
			-4		
4	Bare Glass PPCFC3	-44	17	0.9996	0.0134-2
			-17		
5	Bare Polymer GEM C61003P7 Fired	-122	20	0.9985	0.0134-2
			-13		
6	Bare Glass PPCFB2 Fired	-35	7	0.5825	0.004-4.35
			-8		
7	Bare Glass PPCFC3 Fired	-80	21	0.9331	0.004-4.35
			-35		

Chloride Susceptibility of different Ag/AgCl pastes

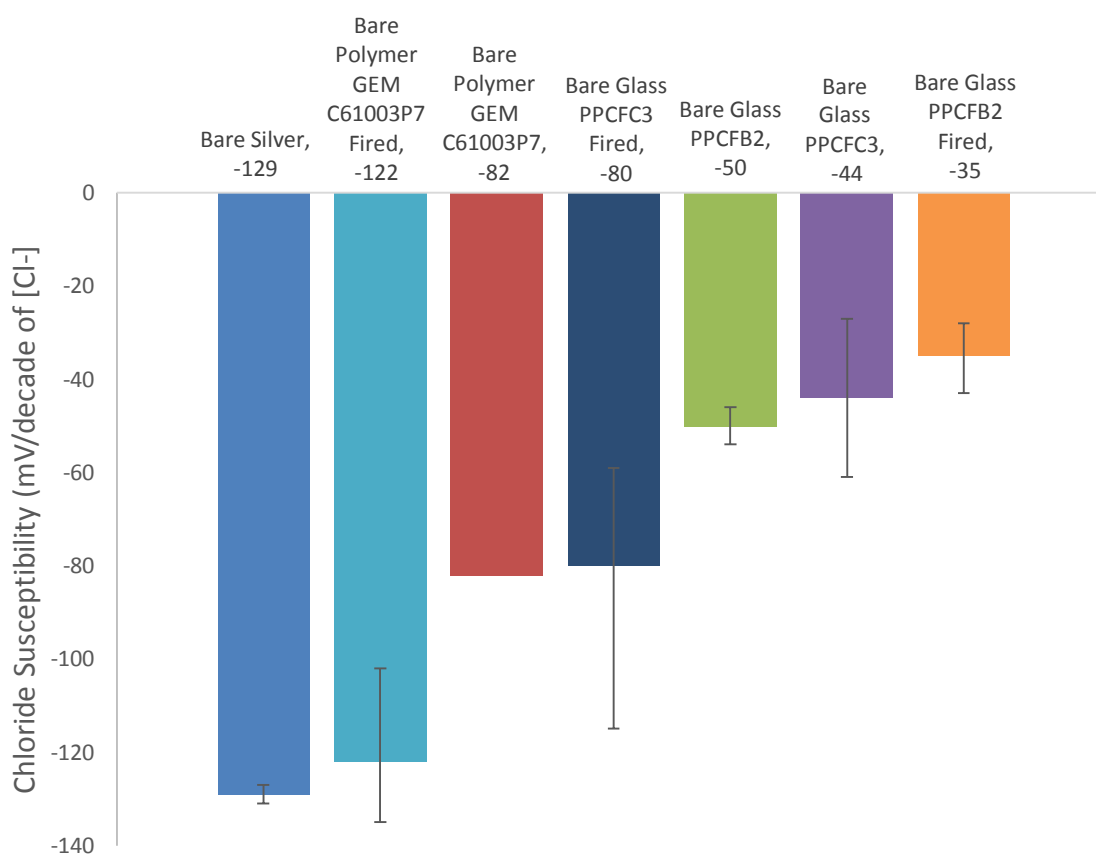


Figure 3-5: Graphical representation of electrode susceptibility to chloride concentration for different Ag/AgCl pastes

Bare silver electrodes were also tested to be able to compare with fired electrodes to check if after firing the electrodes AgCl would escape the paste and provide the same responses as bare silver electrodes. Bare silver electrodes showed a susceptibility of approximately -130 mV/decade of [Cl⁻] which is more than double from the theoretical for Ag/AgCl electrodes.

Fired polymer electrodes have a very similar performance of approximately -120 mV/decade of [Cl⁻] which suggests that once the polymer is fired at high temperatures AgCl decomposes to Ag leaving the electrodes as bare electrodes. Although other glassy pastes were fired at high temperatures their performances did not match those of bare electrodes. Most probably glass based pastes can hold AgCl much better than the polymer.

3. Reference Electrodes

The rest of the electrodes, properly cured Ag/AgCl pastes provided different performances. Polymer based paste has a susceptibility of approximately -80 mV/decade of [Cl⁻] which is higher than the theoretical. Although electrodes with super Nernstian response have been claimed in the literature, most of them ended up being just a partially understood operation. In the case of polymer based Ag/AgCl paste, it is suggested that probably the ratio of Ag to AgCl was not the correct one and again two reactions were happening at the same time, each one at a different rate. That would explain the super Nernstian response of the electrodes but a lower one than the bare silver electrodes. The ratio of Ag to AgCl in this commercial paste is about 60:40.

The two glass based electrodes provided a sub Nernstian response of approximately -50 and -44 mV/decade of [Cl⁻] with errors for the later one in the range of more than 20 mV/decade of [Cl⁻]. It is confidently assumed that the performance of those two pastes was similar but the different binder used was the reason for the larger differences between the tested electrodes. Comparing with the polymer electrodes, the ratio of Ag to AgCl in these pastes was 50:50 which comes to suggest that Ag to AgCl ratio might also have an effect on the electrodes susceptibility.

From the results of this experiment it was clear that Ag/AgCl paste can greatly affect the performance of the electrodes without any KCl polymer matrix on top. It was not yet understood how the performance of the electrodes will change once the KCl polymer matrix was added. Therefore, experiments with all kinds of Ag/AgCl pastes were performed adding the KCl polymer matrix on top.

3.3.2 Electrodes without the Ag/AgCl layer - Optimum KCl weight percentage

Looking at the performance of each Ag/AgCl paste separately, investigation focused initially at electrodes without Ag/AgCl paste. The second experiment was to investigate the optimum KCl weight

3. Reference Electrodes

percentage in the KCl polymer matrix printed on top. From previous experimental work it was found that as the concentration of KCl on the electrode increased, the susceptibility of the electrode to chloride decreased but the relationship between them was still unknown. Different KCl weight percentages were tested in various KCl solutions of different concentrations (0.004-4 M). In an attempt to improve the performance of the electrodes in some cases a second layer of KCl polymer matrix was printed on top of the first one. The same experimental procedure was followed for the electrodes with the second KCl polymer matrix. The structures of the tested electrodes are shown in Table 3-3.

Table 3-3: RE structure for electrodes without Ag/AgCl layer to find optimum KCl weight percentage in KCl polymer matrix on top.

Type No.	Layer 1	Layer 2	Layer 3
1	ESL 9912	ESL 4905-C	ESL 242-SB
2	ESL 9912	ESL 4905-C	ESL 242-SB+20% KCl
3	ESL 9912	ESL 4905-C	ESL 242-SB+66% KCl
4	ESL 9912	ESL 4905-C	ESL 242-SB+71% KCl
5	ESL 9912	ESL 4905-C	ESL 242-SB+20% KCl + ESL 242-SB
6	ESL 9912	ESL 4905-C	ESL 242-SB+20% KCl + ESL 242-SB+20% KCl
7	ESL 9912	ESL 4905-C	ESL 242-SB+50% KCl + ESL 242-SB
8	ESL 9912	ESL 4905-C	ESL 242-SB+50% KCl + ESL 242-SB+20% KCl
9	ESL 9912	ESL 4905-C	ESL 242-SB+66% KCl + ESL 242-SB
10	ESL 9912	ESL 4905-C	ESL 242-SB+66% KCl + ESL 242-SB+20% KCl

Table 3-4 shows the performance of electrodes without Ag/AgCl layer (bare Ag) but adding the KCl polymer matrix. For one electrode type, instead of KCl polymer matrix, a KNO₃ polymer matrix was printed in an attempt to mimic the operation of the double junction reference electrodes. Ideally, a double junction electrode would have a first section with KCl solution and a second section in contact with the first with KNO₃. From the results of the experiment, using only KNO₃ provides very noisy results just like when no KCl was included in the polymer based top layer.

3. Reference Electrodes

Table 3-4: REs performance without Ag/AgCl paste (bare Ag) and adding the KCl polymer matrix on top

No	Materials Used	Susceptibility (mV/decade)	Susceptibility difference between electrodes (mV)	R ²	Workable range (M)
1	ESL 242-SB	Very Noisy			
2	ESL 242-SB+20% KCl	11	7 -7	0.9652	0.0134-2
3	ESL 242-SB+66% KCl	-84	8 -4	0.9454	0.004-4.35
4	ESL 242-SB+71% KCl	-90	6 -6	0.9611	0.004-4.35
5	ESL 242-SB+20% KCl+ESL 242-SB	2	1 -1	0.8762	0.004-4.35
6	ESL 242-SB+20% KCl+ESL 242-SB+20% KCl	2	4 -5	0.6214	0.004-4.35
7	ESL 242-SB+50% KCl+ESL 242-SB	2	2 -1	0.9276	0.004-4.35
8	ESL 242-SB+50% KCl+ESL 242-SB+20% KCl	4	- -	0.8701	0.004-4.35
9	ESL 242-SB+66% KCl+ESL 242-SB	-0.3	1 -1	0.32	0.004-0.435
10	ESL 242-SB+66% KCl+ESL 242-SB+20% KCl	-3	3 -3	0.0876	0.004-0.435

The KCl weight percentage included in the polymer matrix was varied to find the optimum KCl concentration that would provide the lowest susceptibility to chloride. The susceptibility of the electrodes was plotted as a function of KCl percentage in the KCl polymer matrix.

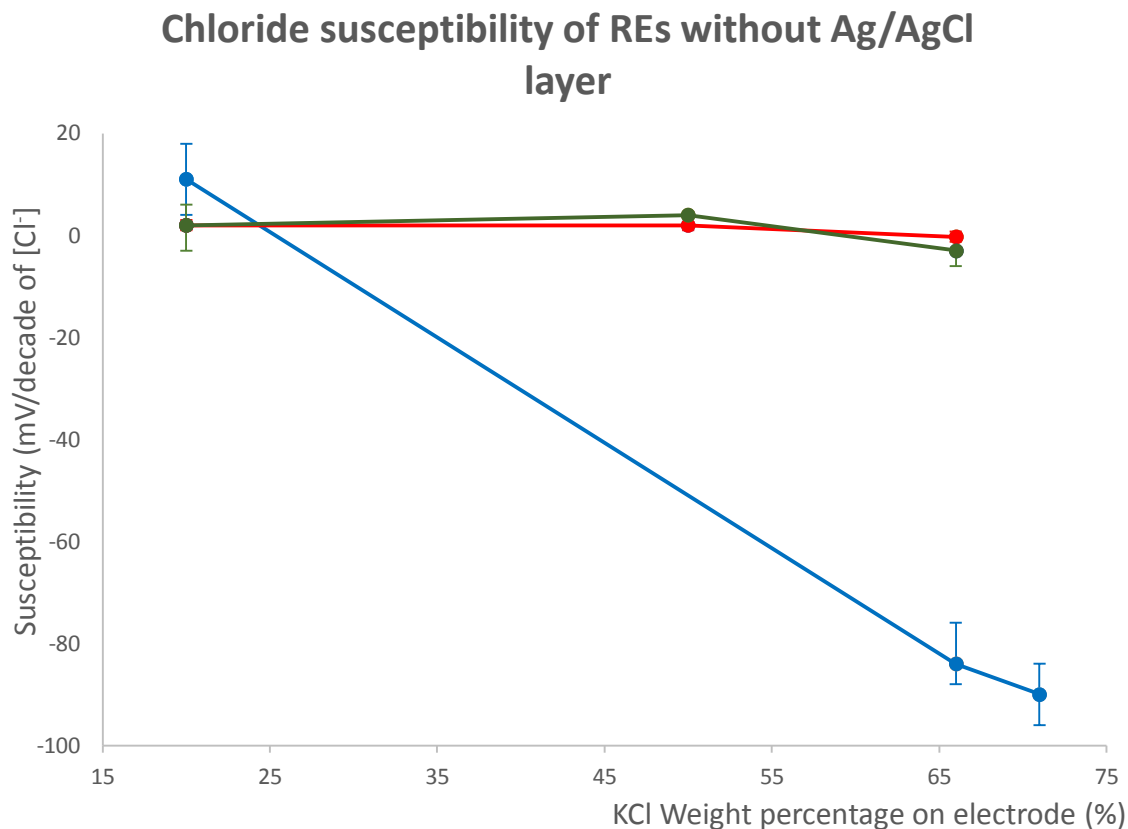


Figure 3-6: Chloride susceptibility of reference electrodes without Ag/AgCl layer versus KCl concentration in KCl polymer matrix (no extra layer-blue, extra layer without KCl-red, extra layer on top with 20% KCl-green)

It is obvious from the graph that the performance of the electrodes after adding the KCl polymer matrix has been significantly improved. In the case of using a single layer of KCl polymer matrix as the KCl concentration increases, the susceptibility to chloride concentration increases too. There is a large gap of concentrations that are not investigated which should be a part of further work and will be explained in more detail in the next chapter. It is also interesting that the electrodes with 20% KCl percentage showed an unexpected performance of opposite trend. They have a susceptibility of +11 mV/decade of [Cl⁻] which has an opposite sign from the theoretical. It is believed that in this situation, more than just one reaction takes place but the two reactions cancel each other's potential providing this unexpected performance.

3. Reference Electrodes

Electrodes with the additional layer have a further improved performance. The extra layer was added in an attempt to withhold the KCl on the electrode as long as possible. It was believed that an extra polymer layer would act as a membrane that would allow charge exchange but slow down the dissolution of KCl in the testing solution. These electrodes also showed a susceptibility opposite to the theoretical although very close to zero. Susceptibilities in the range of a couple mV/decade of [Cl⁻] could also be caused by other reasons such as noise. Furthermore, the tested KCl concentration range was extended and some of the electrodes were performing impressively. The KCl percentage in the first KCl polymer matrix did not seem to have significant effects on the performance of the electrodes.

The electrodes with the extra layer having 20% KCl in it, showed also improved performance in terms of susceptibility but in a more confined KCl concentration range.

The performances provided by the electrodes without Ag/AgCl layer after adding the KCl polymer matrix were unexpectedly improved. In an attempt to understand how an electrode without the Ag/AgCl layer can operate as a reference electrode, a SEM scan was performed on the cross section of newly made electrodes. Figure 3-7 shows the SEM scan results and the two points that the analysis was made. The first point in photo (a) (left) is the KCl polymer matrix layer and the other photo is the analysis from the surface of the Ag conductor layer.

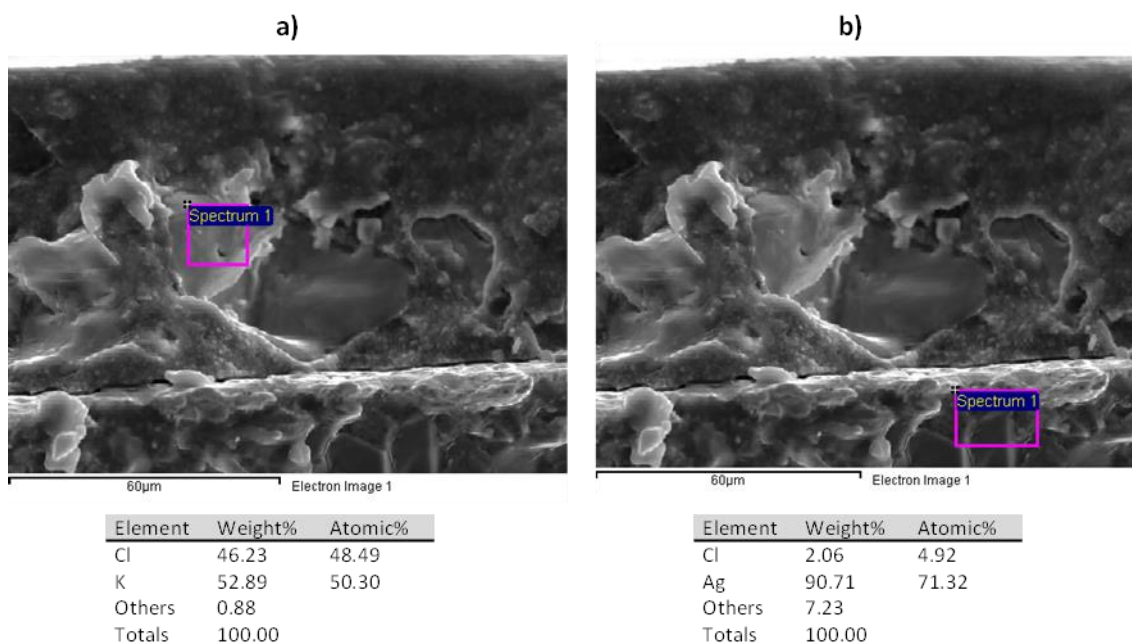


Figure 3-7: SEM analysis of the cross section from newly made electrodes with 50% KCl polymer matrix

From the analysis of the SEM scan, it became obvious that the Ag conductor layer was chloridised from the KCl layer printed on top, most probably during the curing process. Curing temperatures for ESL 242-SB are 150 °C that can trigger the chloridisation of the Ag conductor under it. This result has been the reason for further experiments to test what the ideal Ag:AgCl ratio would be for the electrodes to provide an optimum operation.

3.3.3 Electrodes without the Ag/AgCl layer - Hydration, Lifetime & Drift rate

The most stable electrodes chosen from the previous experiments were tested in a 0.04 M KCl solution for approximately 5 days. In these experiments, only one electrode from each kind was used due to shortage of channels on the data logger. Further experimentation is required to confirm the conclusions of these experiments. The electrodes chosen for the drift test are shown in Table 3-5.

3. Reference Electrodes

Table 3-5: RE structure for electrodes tested for hydration, lifetime and drift rate.

Type No.	Layer 1	Layer 2	Layer 3	Layer 4
3	ESL 9912	ESL 4905-C	ESL 242-SB+20% KCl	ESL 242-SB
8	ESL 9912	ESL 4905-C	ESL 242-SB+20% KCl	ESL 242-SB+20% KCl
9	ESL 9912	ESL 4905-C	ESL 242-SB+50% KCl	ESL 242-SB
10	ESL 9912	ESL 4905-C	ESL 242-SB+50% KCl	ESL 242-SB+20% KCl
11	ESL 9912	ESL 4905-C	ESL 242-SB+66% KCl	ESL 242-SB
12	ESL 9912	ESL 4905-C	ESL 242-SB+66% KCl	ESL 242-SB+20% KCl

Some selected electrodes with the best performances, were further experimented for lifetime, drift rate and hydration time in 0.04 M KCl solution. (Sophocleous, et al., 2012) shows the results from the experiments showing how the KCl percentage in the first KCl polymer matrix can affect other electrode parameters. Electrodes with no KCl in the extra layer provided a better performances because the top layer acted as a protective membrane to hold the KCl on the electrode.

The best performance was provided by the electrodes with 50% KCl in the first layer and no KCl in the second layer. These electrodes have a lifetime of approximately 30 hours and a drift rate as slow as 1.92 mV/hour. The hydration time required for these electrodes was approximately 0.5 hours but all these parameters can be different in different concentration solutions.

3. Reference Electrodes

Table 3-6: Lifetimes, drift rates and hydration times of the best performing electrodes.

No	Materials Used	KCl weight percentage in first layer (%)	Lifetime (hours)	Drift rate (mV/hour)	Hydration time (hours)
1	Ag+ESL 242-SB 20% KCl+ESL 242-SB	20	1.5	2.97	1
2	Ag+ESL 242-SB 20% KCl+ESL 242-SB 20% KCl	20	2	2.64	1
3	Ag+ESL 242-SB 50% KCl+ESL 242-SB	50	30	1.92	0.5
4	Ag+ESL 242-SB 50% KCl+ESL 242-SB 20% KCl	50	3	6	2
5	Ag+ESL 242-SB 66% KCl+ESL 242-SB	66	5	3.34	1.5
6	Ag+ESL 242-SB 66% KCl+ESL 242-SB 20% KCl	66	1.5	5.95	0.5

Figure 3-8 below shows the relationship between the KCl weight percentage on the electrode and their performance in terms of hydration time.

3. Reference Electrodes

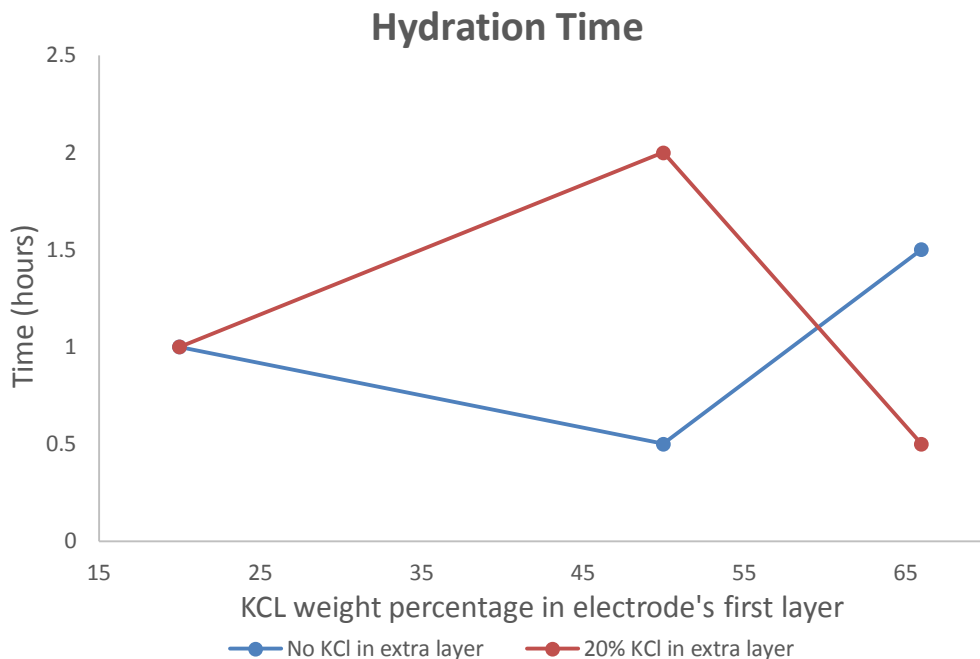


Figure 3-8: Hydration time of selected electrodes versus KCl percentage in the first layer

Ideally in real life applications, hydration time should be minimised and for an attractive measuring instrument it should be in the range of a couple of tenths of seconds. The electrodes here show hydration times of 0.5 to 2 hours. Hydration time is believed to be affected by two factors based on the existing knowledge of the electrodes. Electrodes having higher weight percentage of KCl would take longer for the KCl to hydrate. On the other hand, high amounts of KCl provide more paths for the water to penetrate the matrix and hydrate KCl.

From Figure 3-8, electrodes with no KCl on the top layer show shorter hydration times with an optimum value of 41% KCl on the first layer and no KCl on the second layer. That optimum KCl concentration on the electrode, based on curve fitting, would provide a hydration time of approximately 0.29 hours or 17 minutes.

Electrodes with KCl in the top layer showed a different trend. At low KCl concentrations, the hydration rate was the same as without KCl in top layer of approximately 1 hour. When a higher concentration of KCl was

used, the hydration time increased, suggesting that KCl concentration is a more important factor than water paths. Increasing KCl concentration even more, decreases the hydration time now suggesting that water paths are the major factor. In the case of the electrodes with no KCl on top layer the factors play the exact opposite roles allowing for an optimum point to be calculated.

Figure 3-9 shows the relationship between the lifetime of the electrodes and the KCl percentage in the first layer. In this case the relationship between lifetime and KCl weight percentage in the first layer is the same for both types of electrodes.

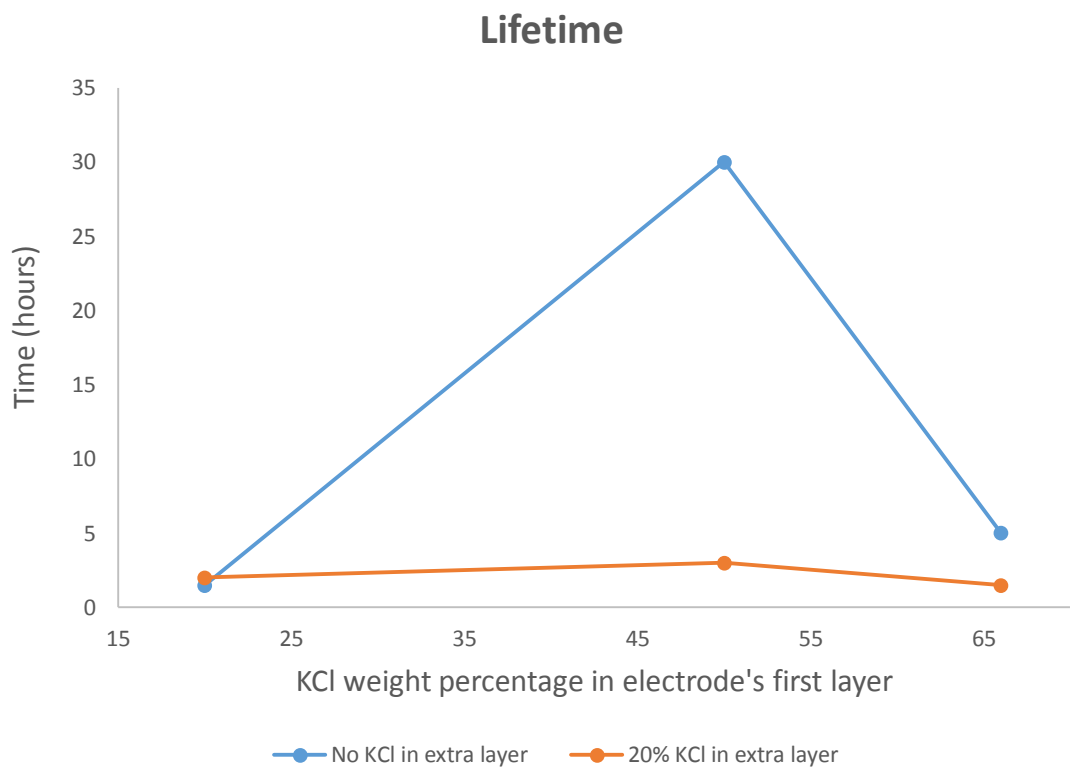


Figure 3-9: Lifetime of the selected electrodes as a function of the KCl weight percentage in the first layer

Electrodes with no KCl on the top layer provided much longer lifetimes most probably because of fewer paths for the water to penetrate and dissolve the KCl back in the solution. As mentioned earlier this relationship is only true when the electrodes are tested in 0.04 M KCl

3. Reference Electrodes

solution. The solution concentration will definitely affect the operating parameters of the electrodes.

An optimum point was calculated for electrodes with no KCl in top layer with a lifetime of approximately 32 hours and KCl weight percentage of approximately 44% KCl. The optimum point for the other electrode type was calculated the same way and having a lifetime of approximately 3 hours and a KCl weight percentage of approximately 40% KCl.

Figure 3-10 shows the relationship of the drift rate after the stable potential period (lifetime) versus the KCl weight percentage in the first layer.

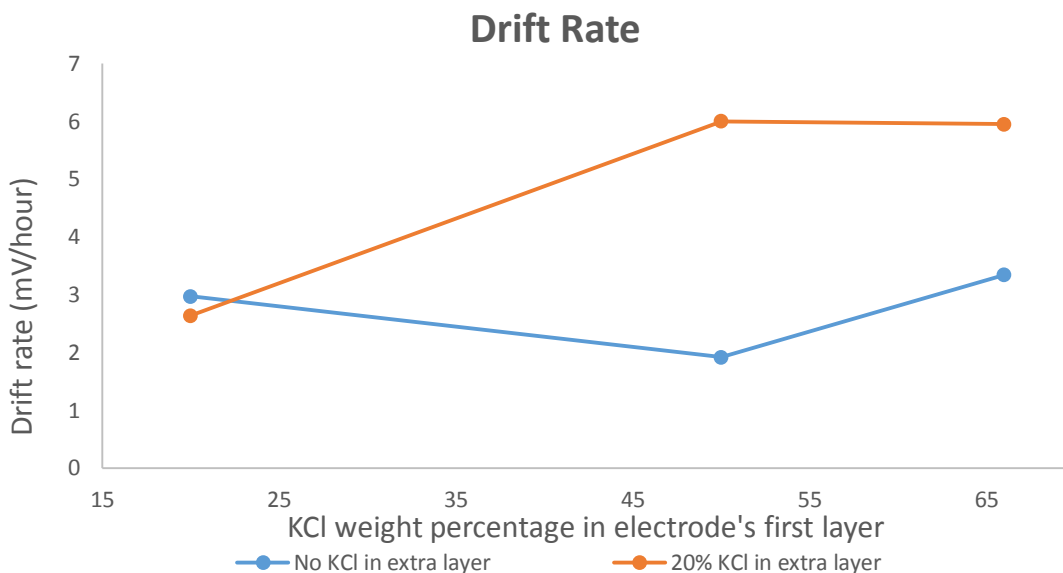


Figure 3-10: Relationship between the drift rate of selected electrodes and the KCl weight percentage in the first layer

The two types of electrodes show a different trend. Electrodes with no KCl in the top layer have a minimum point, showing the opportunity for optimisation, while the other electrodes have an increasing drift rate when the KCl weight percentage increases.

Electrodes with no KCl on top layer show an optimum point at approximately 1.7 mv/hour using a KCl weight percentage in the first

layer of approximately 41%. All parameters have a similar optimum value for the amount of KCl in the first layer approximately 40-44% KCl.

It has to be noted that this information is obtained using only three points which are not sufficient for reliable conclusions.

3.3.4 Electrodes without the Ag/AgCl layer - Electrodes' performances in pH buffers

Selected electrode types were sequentially immersed into three different pH buffers, chosen as pH4, pH7 and pH10, in a test solution sequence shown in Figure 3-11.



Figure 3-11: pH buffer sequence for experiment RE.14-pH buffers.

The averaged results from 3 electrodes of each type were calculated to minimise noise. The cyclic immersion of the electrodes in pH buffers provides useful results for the characteristics of the electrodes and more specifically their hysteresis. The electrodes were immersed in each buffer solution for approximately 1 hour to allow for their potential to stabilise and the value of the stable potential was recorded.

The electrodes were tested in pH buffers in order to understand if the voltage fluctuations were large enough to corrupt the readings from a normal pH ISE. This experiment was done in the order of pH buffers 7-4-7-10-7-4-7-10 to identify any changes on the electrodes after being submerged in different acidities. Figure 3-12 shows the voltage fluctuations from the electrodes through the whole experiment. An ideal pH ISE would give 60 mV/pH reading so voltage fluctuations of that range are quite significant.

3. Reference Electrodes

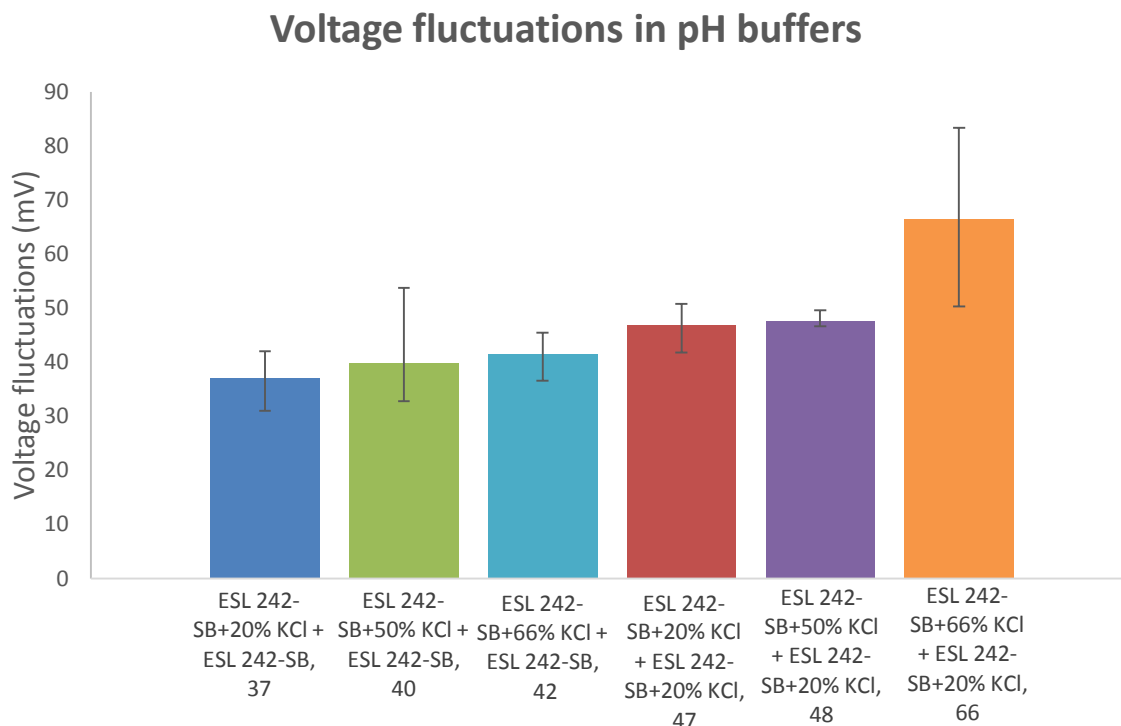


Figure 3-12: Voltage fluctuations of the selected electrode types in pH buffers 4, 7 and 10

The electrodes providing the best performances in this test were the ones without KCl in the top layer and that is probably because the fluctuations are due to KCl leaving the electrode and dissolving in the solutions altering the performance. Voltage fluctuations in the range of 40 mV are not significant since the pH range covered is 6 pH units which in pH ISE reading would be 360 mV and that will result in an inaccuracy approximately 0.1 pH units.

3.3.5 Polymer Ag/AgCl paste - Optimum KCl weight percentage

In order to find the optimum KCl weight percentage several electrode structures were used with various KCl weight percentages. Since previous work has identified that the Ag/AgCl layer can affect the performance of the electrodes, it was suggested that different optimum points of KCl percentages might exist for different Ag/AgCl pastes. The electrodes were tested in different KCl solutions (0.004-4M). Three electrodes from each type were tested to also investigate the

3. Reference Electrodes

susceptibility divergence between different electrodes of the same type. Not all of these electrodes were tested or fabricated at once which allows the possibility of fabrication procedure to affect the electrodes' performances. The structures of the electrodes tested are shown in Table 3-7 below.

Table 3-7: RE structure to find the optimum KCl weight percentage for Polymer Ag/AgCl paste.

Type No.	Layer 1	Layer 2	Layer 3	Layer 4
1	ESL 9912	ESL 4905-C	GEM C61003P7	ESL 242-SB
2	ESL 9912	ESL 4905-C	GEM C61003P7 - Fired	ESL 242-SB
3	ESL 9912	ESL 4905-C	GEM C61003P7	ESL 242-SB+6% KCl
4	ESL 9912	ESL 4905-C	GEM C61003P7	ESL 242-SB+10% KCl
5	ESL 9912	ESL 4905-C	GEM C61003P7 - Fired	ESL 242-SB+10% KCl
6	ESL 9912	ESL 4905-C	GEM C61003P7	ESL 242-SB+15% KCl
7	ESL 9912	ESL 4905-C	GEM C61003P7 - Fired	ESL 242-SB+15% KCl
8	ESL 9912	ESL 4905-C	GEM C61003P7	ESL 242-SB+20% KCl
9	ESL 9912	ESL 4905-C	GEM C61003P7 - Fired	ESL 242-SB+20% KCl
10	ESL 9912	ESL 4905-C	GEM C61003P7	ESL 242-SB+30% KCl
11	ESL 9912	ESL 4905-C	GEM C61003P7 - Fired	ESL 242-SB+30% KCl
12	ESL 9912	ESL 4905-C	GEM C61003P7	ESL 242-SB+33% KCl
13	ESL 9912	ESL 4905-C	GEM C61003P7	ESL 242-SB+50% KCl
14	ESL 9912	ESL 4905-C	GEM C61003P7	ESL 242-SB+66% KCl
15	ESL 9912	ESL 4905-C	GEM C61003P7	ESL 242-SB+71% KCl

The experiments were performed at room temperature and all electrodes were tested against a commercial Ag/AgCl electrode (Beckman Coulter). Electrodes were allowed to hydrate in 0.04 M KCl solution following the same procedure for all previous and following experiments.

Similar experiments to the ones for electrodes without Ag/AgCl layer to identify the optimum KCl weight percentage on the electrodes were performed. (Glanc, et al., 2013) shows the results of those experiments. Not all of these electrodes were tested or fabricated at once which allows the possibility of fabrication procedure to affect the electrodes' performances.

Electrodes with fired Ag/AgCl layer were also tested since they were the ones that initially provided the best performances. Less KCl weight

3. Reference Electrodes

percentages were tested for the fired polymer because those experiments were done in separate times.

Table 3-8: Susceptibilities of electrodes with polymer based Ag/AgCl layer

No	Materials Used	Sensitivity (mV/decade)	Sensitivity difference between electrodes (mV)	R2	Workable range (M)
1	ESL 242-SB	-82	1	0.9625	0.0134-2
			-1		
2	ESL 242-SB Fired	-26	1	0.9405	0.134-2
			-1		
3	ESL 242-SB 6% KCl	-54	-	1	0.0134-2
			-		
4	ESL 242-SB 10% KCl	-24.31	-	0.9989	0.004-4
			-		
5	ESL 242-SB 10% KCl Fired	-2.05	-	1	0.004-0.4
			-		
6	ESL 242-SB 15% KCl	-23.7	-	0.9994	0.004-4
			-		
7	ESL 242-SB 15% KCl Fired	-8.08	1	0.9188	0.004-4
			-2		
8	ESL 242-SB 20% KCl	-21.05	-	0.9994	0.004-4
			-		
9	ESL 242-SB 20% KCl Fired	1.9839	-	0.745	0.004-0.4
			-		
10	ESL 242-SB 30% KCl	-17.65	1	0.9996	0.004-4
			-2		
11	ESL 242-SB 30% KCl Fired	0.1523	1	0.8604	0.004-0.4
			-1		
12	ESL 242-SB 33% KCl	-48	1	0.9976	0.0134-2
			-1		
13	ESL 242-SB 50% KCl	-51	1	0.9986	0.0134-2
			-1		
14	ESL 242-SB 66% KCl	-58	-	0.995	0.004-4
			-		
15	ESL 242-SB 71% KCl	-58	-	0.9951	0.004-4
			-		

It is obvious that electrodes with fired polymer provide much better results with a much lower susceptibilities than the normally cured polymer.

Figure 3-13 shows the relationship between the chloride susceptibility of the electrodes and the KCl weight percentage in the KCl polymer matrix.

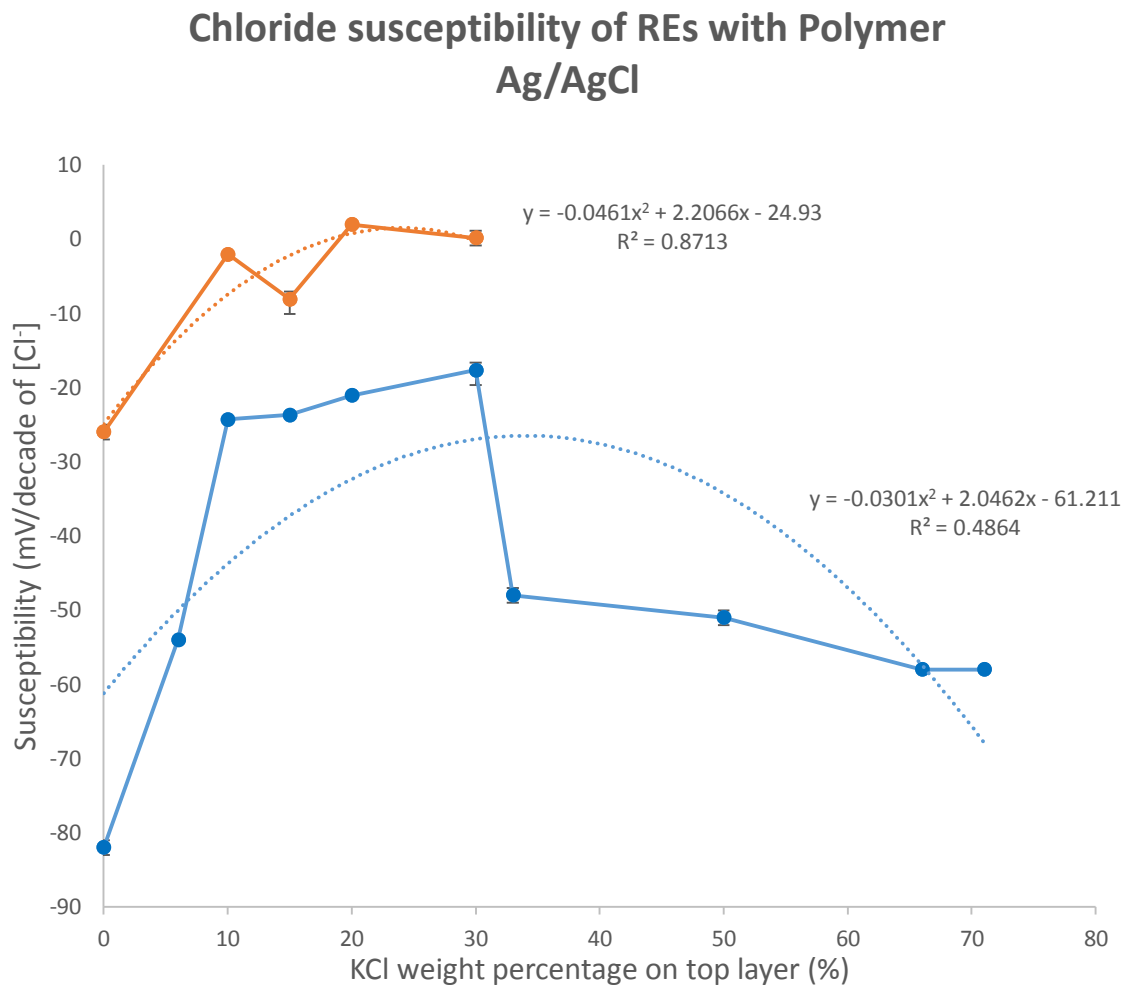


Figure 3-13: Relationship between chloride susceptibility and the KCl weight percentage in the KCl polymer matrix (fired Ag/AgCl – orange, normal Ag/AgCl – blue)

It is obvious that the electrodes with fired polymer provide a much better performance, very similar to the electrodes without the Ag/AgCl layer explained earlier. Although the results look normal in terms of error bars, it is believed that fabrication process is not very consistent in terms of KCl concentration on the electrodes as some electrodes from previous experiments with similar structures provided different susceptibilities than similar electrodes fabricated at different times.

3. Reference Electrodes

From the graph, electrodes with fired Ag/AgCl layer have an optimum point at approximately 24% KCl which provides a susceptibility of approximately 2 mV/decade of [Cl⁻]. Electrodes with properly cured Ag/AgCl paste have shown much higher susceptibilities but with more repeatable and less noisy results. An optimum point was also calculated to be approximately 34% KCl with a susceptibility of -26 mV/decade of [Cl⁻]. The R² value for the latter was very low, 0.4864 which tends to suggest again the fact that fabrication procedure is not very repeatable using the existing equipment.

3.3.6 Glass PPCFB2 & PPCFC3 Ag/AgCl pastes - Optimum KCl weight percentage

The exact same procedure, as the polymer Ag/AgCl paste, was followed to investigate the optimum KCl weight percentage for these two glass based Ag/AgCl pastes. Similarly, the experiments were performed at room temperature and all electrodes were tested against a commercial Ag/AgCl electrode (Beckman Coulter). The structures of the electrodes for PPCFB2 and PPCFC3 are shown in Table 3-9 & Table 3-10 respectively

Table 3-9: RE structure to find the optimum KCl weight percentage for Glass PPCFB2 Ag/AgCl paste.

Type No.	Layer 1	Layer 2	Layer 3	Layer 4
1	ESL 9912	ESL 4905-C	PPCFB2	ESL 242-SB+6% KCl
2	ESL 9912	ESL 4905-C	PPCFB2	ESL 242-SB+10% KCl
3	ESL 9912	ESL 4905-C	PPCFB2	ESL 242-SB+15% KCl
4	ESL 9912	ESL 4905-C	PPCFB2	ESL 242-SB+20% KCl
5	ESL 9912	ESL 4905-C	PPCFB2	ESL 242-SB+30% KCl
6	ESL 9912	ESL 4905-C	PPCFB2	ESL 242-SB+66% KCl
7	ESL 9912	ESL 4905-C	PPCFB2	ESL 242-SB+71% KCl

Table 3-10: RE structure to find the optimum KCl weight percentage for Glass PPCFC3 Ag/AgCl paste.

Type No.	Layer 1	Layer 2	Layer 3	Layer 4
1	ESL 9912	ESL 4905-C	PPCFC3	ESL 242-SB+6% KCl
2	ESL 9912	ESL 4905-C	PPCFC3	ESL 242-SB+20% KCl
3	ESL 9912	ESL 4905-C	PPCFC3	ESL 242-SB+66% KCl
4	ESL 9912	ESL 4905-C	PPCFC3	ESL 242-SB+71% KCl

Table 3-11 shows the performances of electrodes with glass PPCFB2 Ag/AgCl paste with increasing KCl weight percentage on the electrode to identify the optimum point.

Table 3-11: Performances of electrodes with glass PPCFB2 Ag/AgCl paste

No	Materials Used	Susceptibility (mV/decade)	Susceptibility difference between electrodes (mV)	R ²	Workable range (M)
1	ESL 242-SB 6% KCl	-45	1	0.9979	0.0134-2
			-1		
2	ESL 242-SB 10% KCl	-16	1	0.9999	0.004-4
			-1		
3	ESL 242-SB 15% KCl	-16	1	0.9995	0.004-4
			-1		
4	ESL 242-SB 20% KCl	-13	-	0.9913	0.004-4
			-		
5	ESL 242-SB 30% KCl	-12	-	0.9769	0.004-4
			-1		
6	ESL 242-SB 66% KCl	-62	-	0.9799	0.0134-2
			-1		
7	ESL 242-SB 71% KCl	-66	1	0.9897	0.0134-2
			-1		

Again not all electrodes were fabricated or experimented at the same time which can generate some errors on the comparisons of electrodes' performances.

Figure 3-14 shows the relationship of the chloride susceptibility and the KCl weight percentage on the electrodes. An optimum KCl percentage was calculated for this paste as well and it is approximately 31% KCl with a susceptibility of -9 mV/decade of [Cl⁻].

3. Reference Electrodes

Chloride susceptibility of REs with glass PPCFB2 Ag/AgCl layer

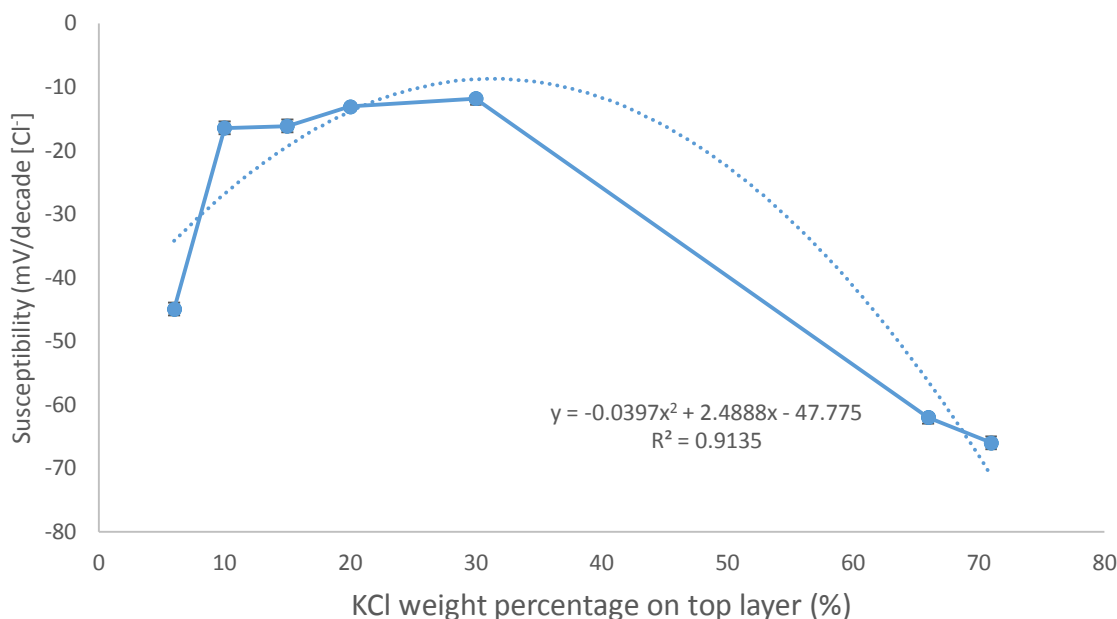


Figure 3-14: Chloride susceptibility versus KCl weight percentage on the electrodes with glass PPCFB2 Ag/AgCl paste

The exact same types of experiments were performed for the other glass Ag/AgCl paste which was more unstable with voltage deviations from the other paste.

Table 3-12 shows the performance of electrodes with glass PPCFC3 Ag/AgCl paste. This type of paste was similar to PPCFB2 with the only difference being the binder. Results with this paste tend to be noisier but having very similar susceptibilities. Noisy results can be due to the different binder affecting the electrodes' performance differently and the similar susceptibilities is a result of using the exact same Ag:AgCl ratio.

Table 3-12: Performances of electrodes with PPCFC3 Ag/AgCl paste

No	Materials Used	Susceptibility (mV/decade)	Susceptibility difference between electrodes (mV)	R ²	Workable range (M)
1	ESL 242-SB 6% KCl	-33	5	0.9984	0.0134-2
			-5		
2	ESL 242-SB 20% KCl	-29	10	0.9927	0.0134-2
			-4		
3	ESL 242-SB 66% KCl	-59	1	0.9837	0.004-4
			-1		
4	ESL 242-SB 71% KCl	-61	-	0.9903	0.004-4
			-		

Figure 3-15 shows the same relationship as before and was used to calculate the optimum KCl concentration on the electrodes. The optimum point is 20% KCl concentration on the electrodes with a -30 mV/decade of [Cl⁻].

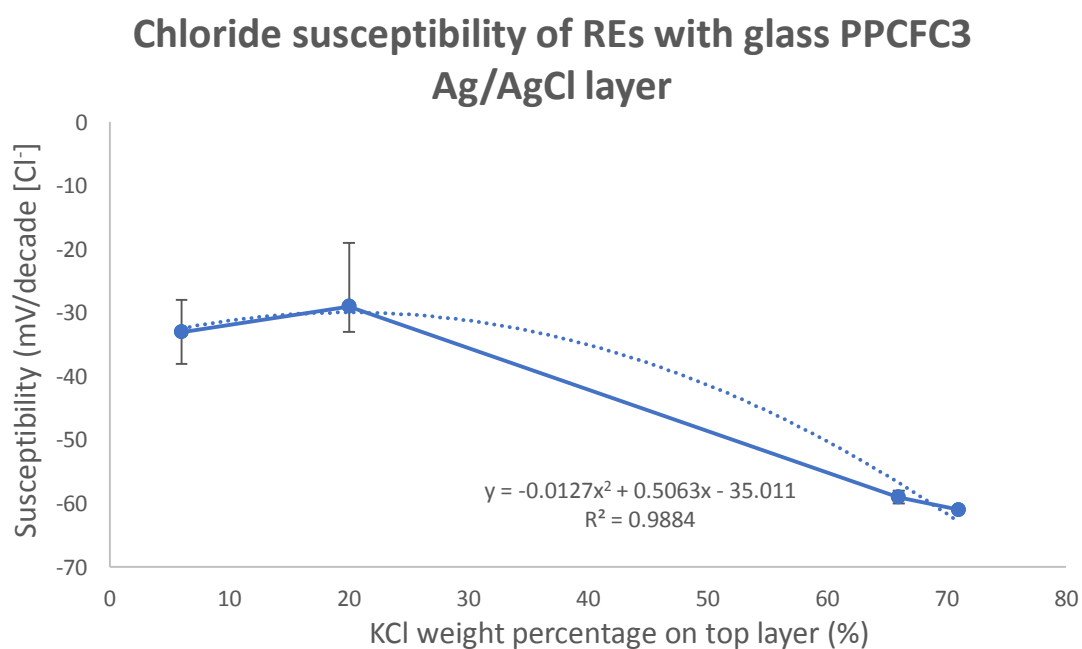


Figure 3-15: Chloride susceptibilities of REs with glass PPCFC3 Ag/AgCl paste against KCl weight percentage on the electrodes

3. Reference Electrodes

3.3.7 Effect of Ag in KCl polymer matrix

Since previous research results suggested that the Ag/AgCl layer could greatly affect the performance of the electrode, a further investigation in that area has been done. In order to also check if ESL 242-SB had an effect on the performance, electrodes with Ag weight ratios of approximately 53% (max possible) and 36% (half the Ag amount) in ESL 242-SB on top of bare Ag were tested. Another layer of KCl in ESL 242-SB was also printed to compare. The structure of these electrodes is shown in Table 3-13.

Table 3-13: RE structure for investigating the effect of Ag in KCl polymer matrix.

Type No.	Layer 1	Layer 2	Layer 3	Layer 4
1	ESL 9912	ESL 4905-C	-	-
2	ESL 9912	ESL 4905-C	ESL 242-SB+53% Ag	-
3	ESL 9912	ESL 4905-C	ESL 242-SB+53% Ag	ESL 242-SB+5% KCl
4	ESL 9912	ESL 4905-C	ESL 242-SB+53% Ag	ESL 242-SB+30% KCl
5	ESL 9912	ESL 4905-C	ESL 242-SB+36% Ag	-
6	ESL 9912	ESL 4905-C	ESL 242-SB+36% Ag	ESL 242-SB+5% KCl
7	ESL 9912	ESL 4905-C	ESL 242-SB+36% Ag	ESL 242-SB+30% KCl

For these experiments, the hydration was done in a 4 M KCl solution and then cycled through the same solutions back to 4 M again. Then, they were left in 4 M KCl solution for 3 days and then another cyclic sensitivity test was performed starting from 0.004 M KCl solution in that case. The reason for allowing a drift of 3 days and repeating the susceptibility test was to investigate if the susceptibility of the electrodes after 3 days of immersion would be affected.

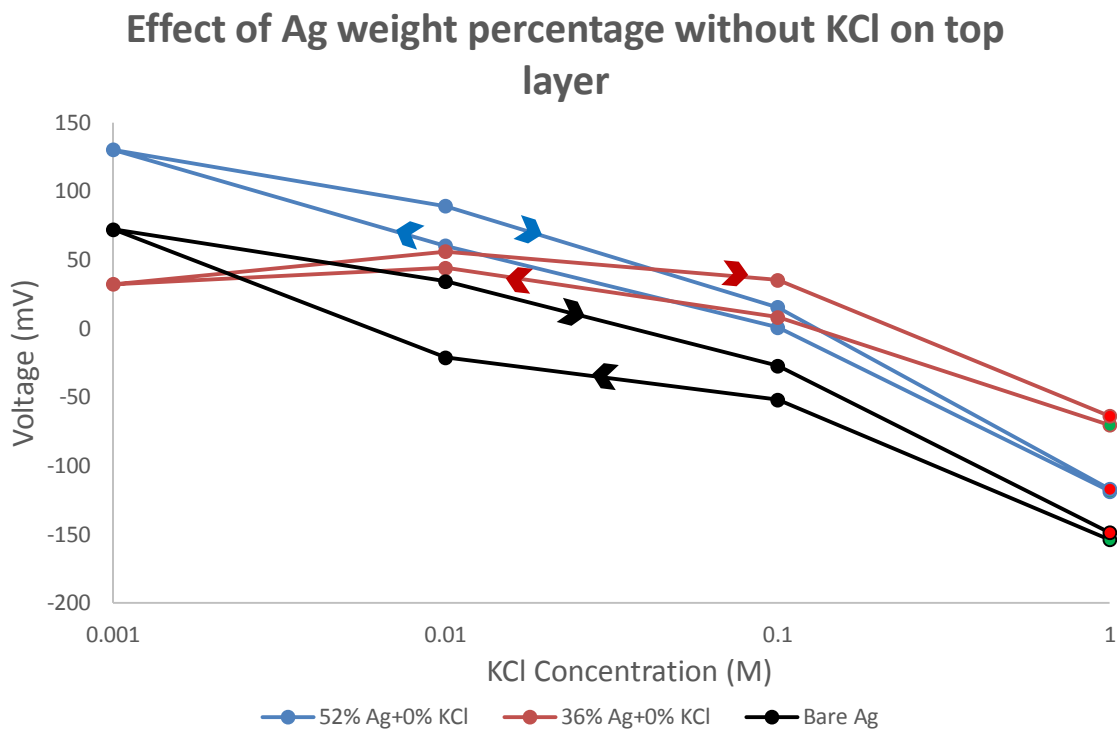


Figure 3-16: Voltage versus KCl solution concentration of electrodes with no KCl in the top layer (starting points - green dots, ending points - red dots)

In this figure, a bare silver electrode was also tested to be able to compare. Bare silver electrode performs almost identical to the 52% Ag electrode with a different absolute voltage. That is probably due to the addition of the extra polymer layer on top that changes the impedance of the electrodes. Electrodes with 36% Ag show a slightly different response that looks more like previous experiments with very low concentrations of KCl on the electrodes. That suggests that the polymer paste might also have an effect on the electrodes' performance.

Figure 3-17 shows the performance of electrodes having 5% KCl on top layer against KCl solution concentration.

3. Reference Electrodes

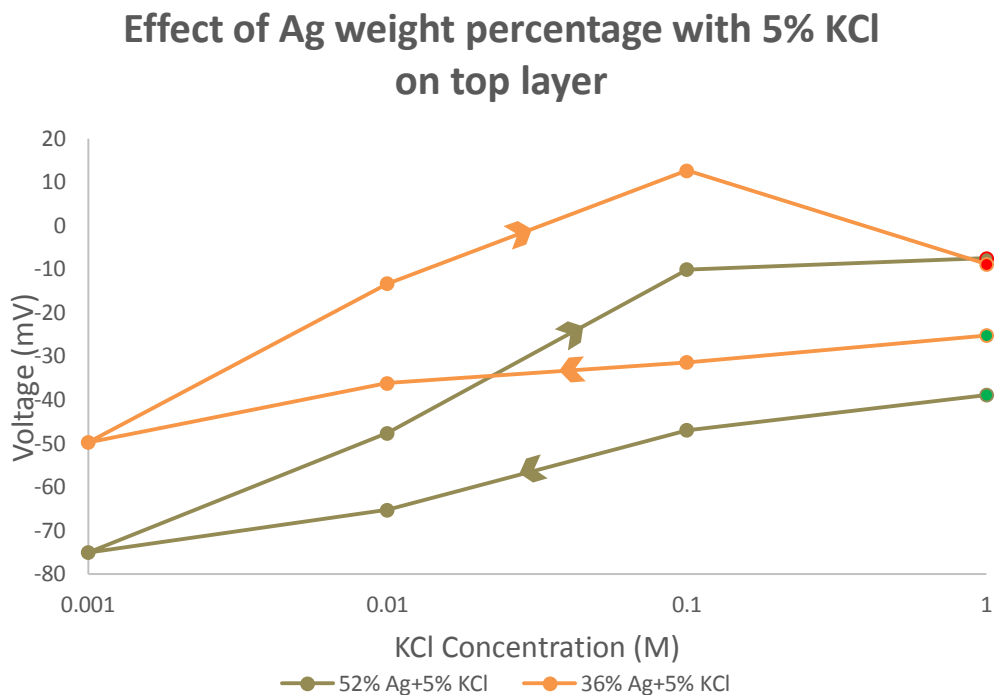


Figure 3-17: Performance of electrodes with 5% KCl versus KCl solution concentration (starting points - green dots, ending points - red dots)

The trend observed in this figure is opposite to the one observed with electrodes without KCl on top layer. Again, a difference in the absolute potential between the two electrode types is observed which is due to the different amount of silver in the top layer. A clear difference is also observed between the forward direction for solution concentration change and the reverse. There is clearly a large memory effect on the electrodes which was not seen on electrodes without KCl. That suggests that possibly the change in potential is due to KCl dissolving in the solution.

Figure 3-18 shows the performance of the electrodes with 30% KCl in the top layer.

Effect of Ag weight percentage with 30% KCl on top layer

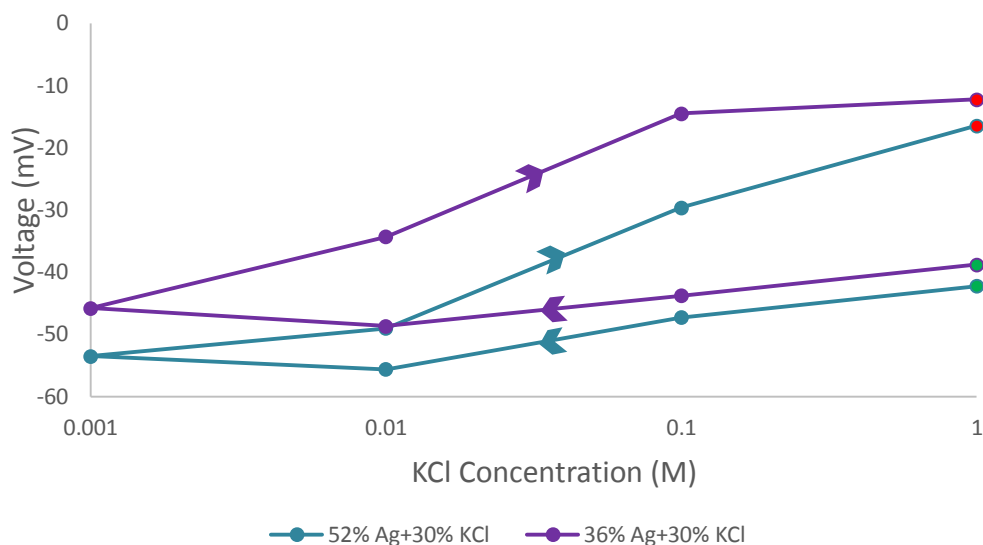


Figure 3-18: Performance of electrodes with 30% KCl against KCl solution concentration (starting points - green dots, ending points - red dots)

This electrode type presents very similar performances to the 5% KCl electrodes. Overall, these electrodes show a chloride susceptibility of approximately +10 mV/decade of $[Cl^-]$ while the electrodes with 5% KCl show a larger susceptibility of approximately +11 mV/decade of $[Cl^-]$.

The same set of electrodes was allowed to drift in saturated KCl solution for three days and then were retested for chloride susceptibility. The results are presented in Figure 3-19, Figure 3-20 & Figure 3-21.

3. Reference Electrodes

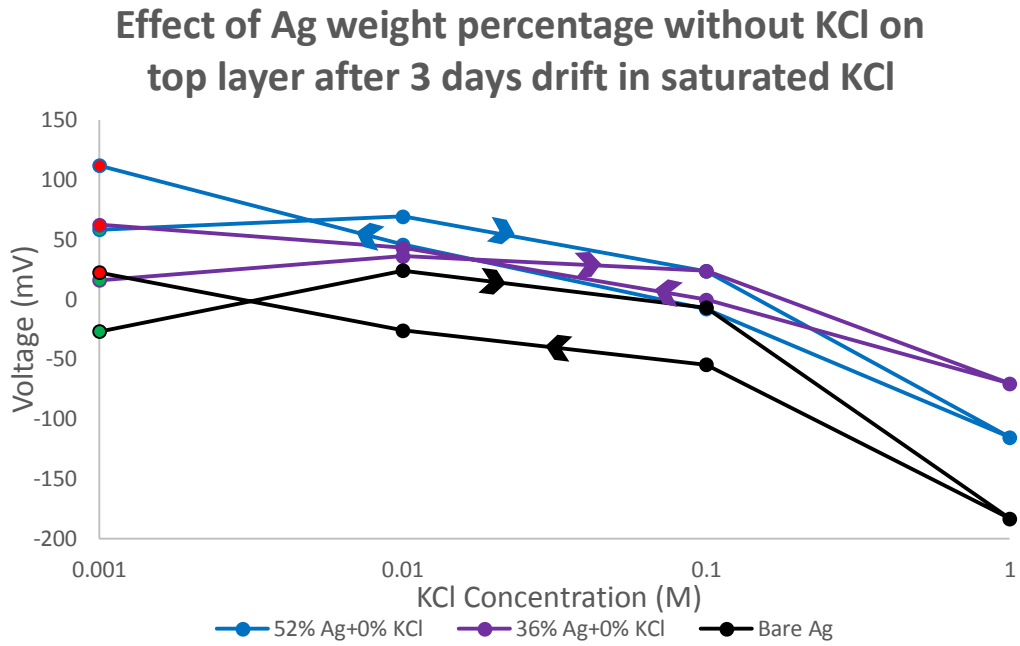


Figure 3-19: Performance of electrodes without any KCl on top layer versus KCl solution concentration after 3 days drift in saturated KCl solution (starting points - green dots, ending points - red dots)

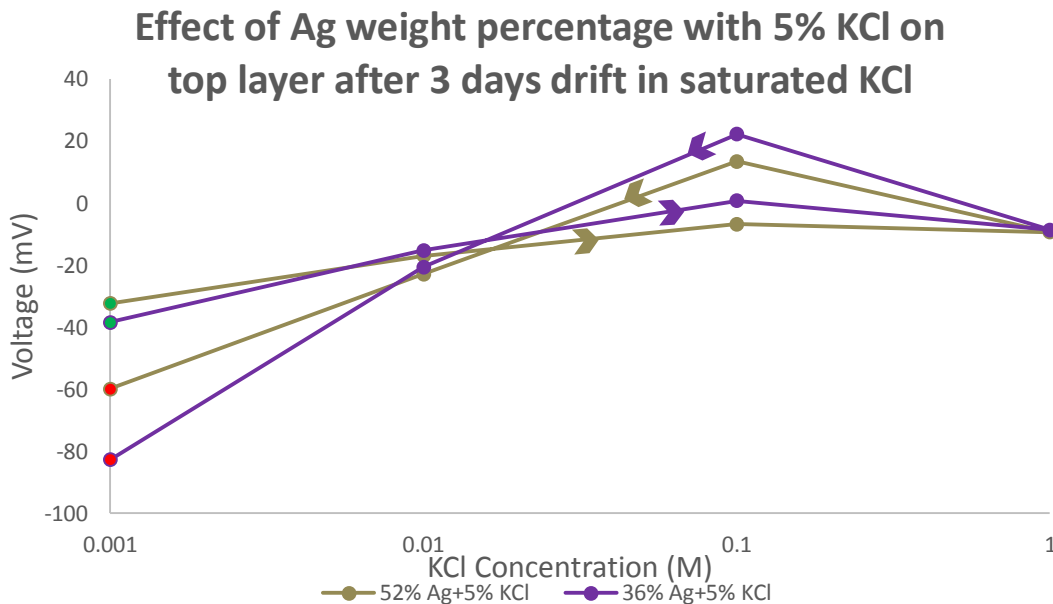


Figure 3-20: Performance of electrodes with 5% KCl on top layer versus KCl solution concentration after 3 days drift in saturated KCl solution (starting points - green dots, ending points - red dots)

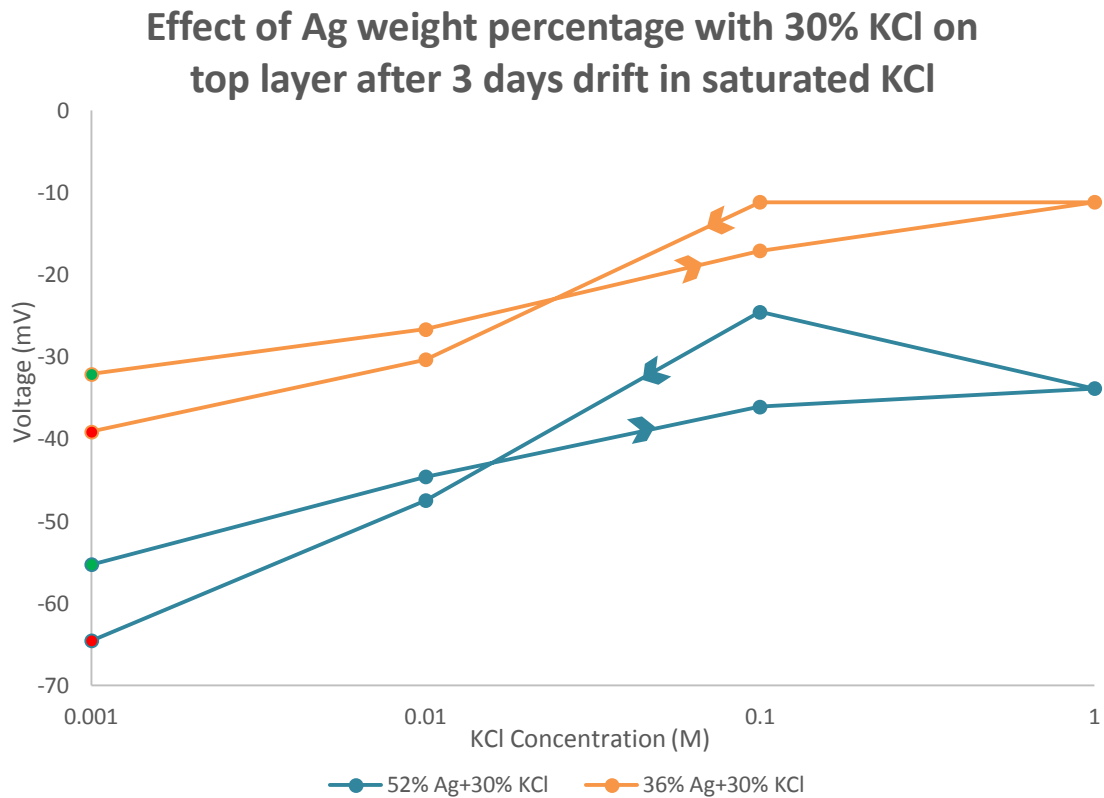


Figure 3-21: Performance of electrodes with 30% KCl on top layer versus KCl solution concentration after 3 days drift in saturated KCl solution (starting points - green dots, ending points - red dots)

After the three days drift, several conclusions could be drawn. Initially the electrodes without KCl did not show any significant difference except the fact that most probably Ag has been chloridised by the saturated KCl solution. Furthermore, the only other change observed for the rest of the electrodes is that the forward direction for solution change and the reverse provided very similar result with a much smaller hysteresis than before. Probably the saturated KCl solution affected the Ag in the paste chloridising it as well as either dissolving or absorbing KCl from or to the solution changing the structure of the electrodes to a very similar point. That can explain the smaller differences in the forward and reverse solution direction after the three day drift.

3. Reference Electrodes

3.3.8 Ag to AgCl & binder to powder ratios

In these experiments, the composition of the Ag/AgCl layer is the parameters to be investigated. Hence for this layer, the pastes were prepared manually in the laboratory by mixing appropriate amount of binder, silver and silver chloride powder. The different compositions of Ag/AgCl layer to be tested are shown in Table 3-14.

Table 3-14: Ag/AgCl paste composition for investigating Ag to AgCl & binder to powder ratios.

Electrodes Notation	Binder X	Ag/AgCl Powder Y	
	Binder to Powder ratio(X:Y)	Ag	AgCl
P/G(2:1)(0:1)	2:1 (2.0g : 1.0g)	0 (0.00g)	1 (1.00g)
P/G(2:1)(1:2)		1 (0.33g)	2 (0.67g)
P/G(2:1)(1:1)		1 (0.50g)	1 (0.50g)
P/G(2:1)(3:2)		3 (0.60g)	2 (0.40g)
P/G(1:1)(0:1)	1:1 (2.0g : 2.0g)	0 (0.00g)	1 (2.00g)
P/G(1:1)(1:2)		1 (0.67g)	2 (1.33g)
P/G(1:1)(1:1)		1 (1.00g)	1 (1.00g)
P/G(1:1)(3:2)		3 (1.20g)	2 (0.80g)
P/G(1:2)(0:1)	1:2 (2.0g : 4.0g)	0 (0.00g)	1 (4.00g)
P/G(1:2)(1:2)		1 (1.33g)	2 (2.67g)
P/G(1:2)(1:1)		1 (2.00g)	1 (2.00g)
P/G(1:2)(3:2)		3 (2.40g)	2 (1.60g)

The electrodes are notated as P(X:Y)(Ag:AgCl) and G(X:Y)(Ag:AgCl) where the first alphabet represents the binder used P for polymer (ESL 242SB) and G for glass (ESL 4905C), the second bracket (X:Y) represents the mass ratio of binder to Ag/AgCl powder and the third bracket (Ag:AgCl) represents the mass ratio of Ag to AgCl powder.

The second column of Table 3-14 shows the ratio of binder to Ag/AgCl by mass. For each binder to Ag/AgCl ratio, 4 different composition of Ag to AgCl paste were prepared in the laboratory. For each composition, two different binders were used: i) Polymer binder ESL 242-SB and ii) Glass binder ESL 4905 C. The silver powder used is from Alfa Aesar (Ag flake, 80% <20 micron, 99.9% metal basis). Hence a total of 24 different types of electrodes were tested.

3. Reference Electrodes

For each composition, the mass of binder used was fixed at 2.0 grams. Then based on the mass ratio of binder to Ag/AgCl and the mass ratio of Ag to AgCl, the appropriate mass of Ag and AgCl powder needed for each composition were determined. 2.0 grams of binder are weighted on a petri dish and the appropriate mass of Ag and AgCl powder are then added to the binder. The paste is then mixed manually with a spatula until an evenly mixed paste suitable for printing is obtained. For some compositions, thinner was added to reduce the viscosity of the paste in order to obtain a more evenly mixed paste. For polymer bound paste, ESL 402 thinner was used. For glass bound paste, ESL 401 thinner was used. Since the paste for this layer was prepared manually in the laboratory and there are no specified screen parameters designed for this paste, the screen with the smallest mesh density designed for the KCl salt matrix layer have to be used for this layer. This ensures that the pastes prepared can be drawn through the patterned area of the screen onto the substrate.

Two experiments were performed with these sets of electrodes. The first set was immersed in a 4 M KCl solution and the second set was immersed in 0.04 M KCl solution for approximately seven days to investigate the stability, drift and response time of the electrodes without the use of the extra KCl layer on top.

Drift was understood to affect the performance of the electrode so more tests were performed to characterise how each type of electrodes is affected. In the previous test it was also understood that the different pastes of Ag/AgCl could have a different response. That could be either because of the binder to powder ratio or the Ag to AgCl ratio. Therefore, polymer and glass based Ag/AgCl pastes were fabricated with different ratios of Ag to AgCl to test their performance in long time drift.

Initially the electrodes where immersed in a ≈ 4 M KCl solution and the results are shown below.

3. Reference Electrodes

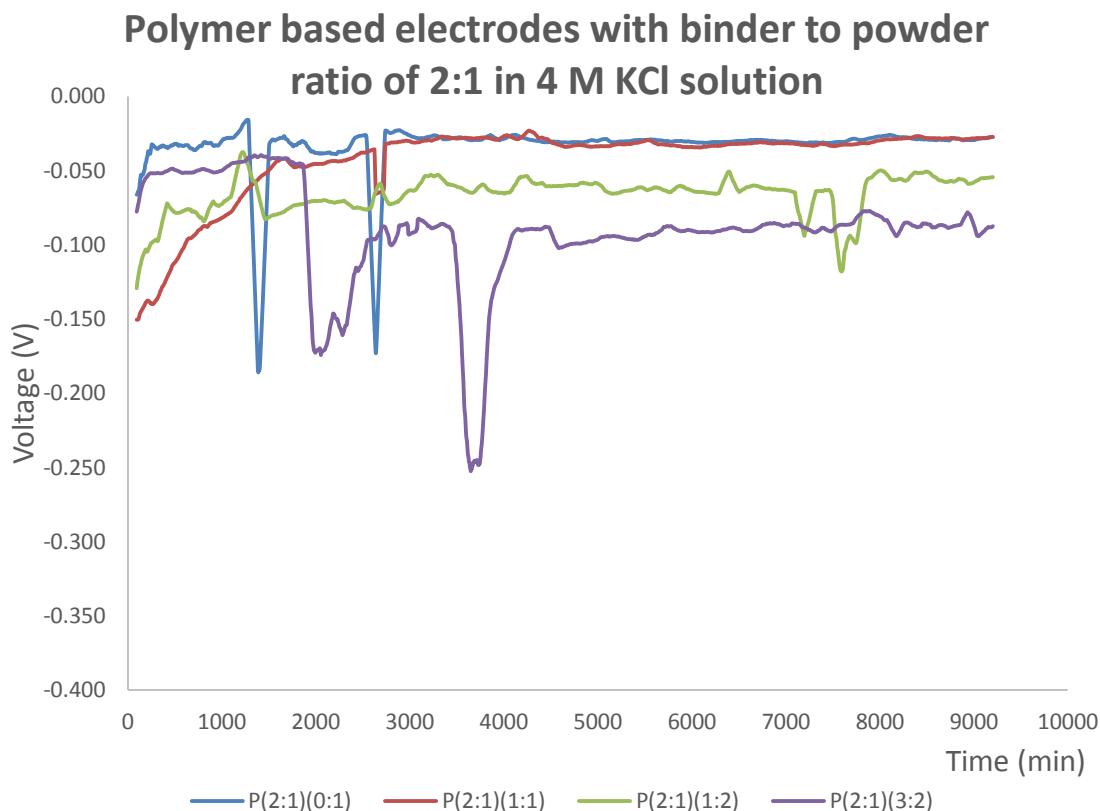


Figure 3-22: The potential of the polymeric electrodes with binder to powder ratio of 2:1 in 4 M KCl solution.

Figure 3-22 shows the performance of the polymer based Ag/AgCl electrodes. No other layer was printed on top. In the legend under the graph P stands for polymer and the first bracket shows the ratio of binder to powder while the second bracket shows the Ag to AgCl ratio. As it can be seen from the graph the electrodes are very noisy, most probably because of the high concentration of the solution, KCl crystals form on the surface of the electrode causing the potential to drop and then it re-dissolves in the solution causing the electrode to reach its normal potential. In Figure 3-22, the electrodes have different absolute potentials most probably due to the layer thickness variations. If the noise is excluded the electrodes maintain a stable potential throughout the whole experiment of about a week.

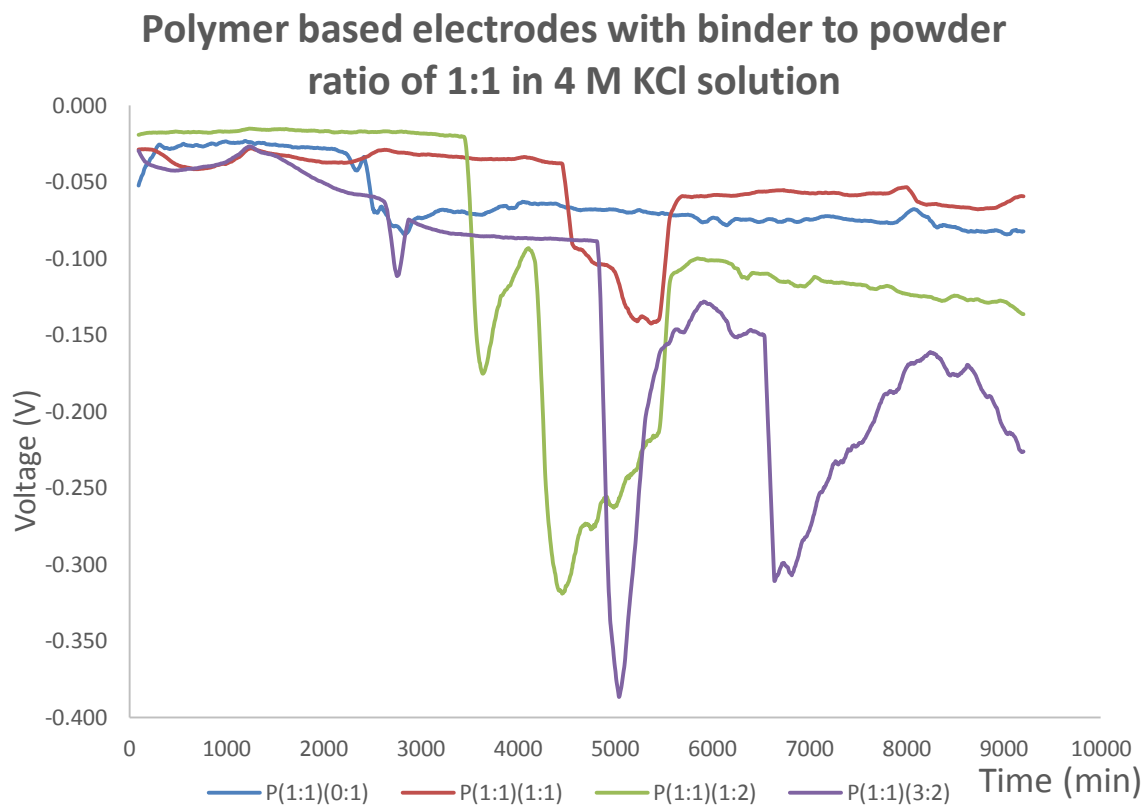


Figure 3-23: The performance of the polymeric electrodes with binder to powder ratio of 1:1 in 4 M KCl solution.

In this case, again the electrodes are very noisy for the same reason as before. Initially, the electrodes have a similar absolute potential but as the time passed they deviate from each other.

3. Reference Electrodes

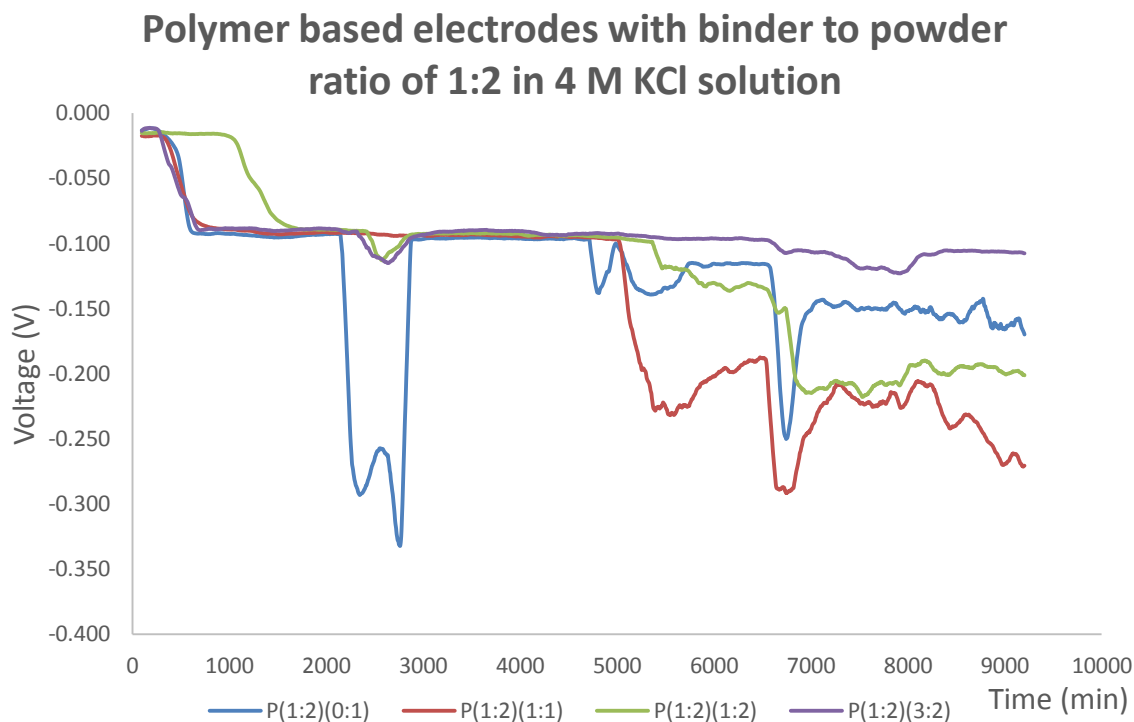


Figure 3-24: The performance of the polymeric electrodes with binder to powder ratio of 1:2 in 4 M KCl solution.

Again, the electrodes are very noisy for the same reason and their absolute potentials are very similar between them. Initially, there is a fast drop in their potential but then they all stabilise at the same potential. After some time without any noise, they become extremely noisy and again the potential deviated from each other. Overall, comparing between the three types, as the binder decreases the deviation between the different Ag to AgCl ratios increases.

Figure 3-25, Figure 3-26 & Figure 3-27 show the response of the same type of electrodes in 0.04 M KCl solution.

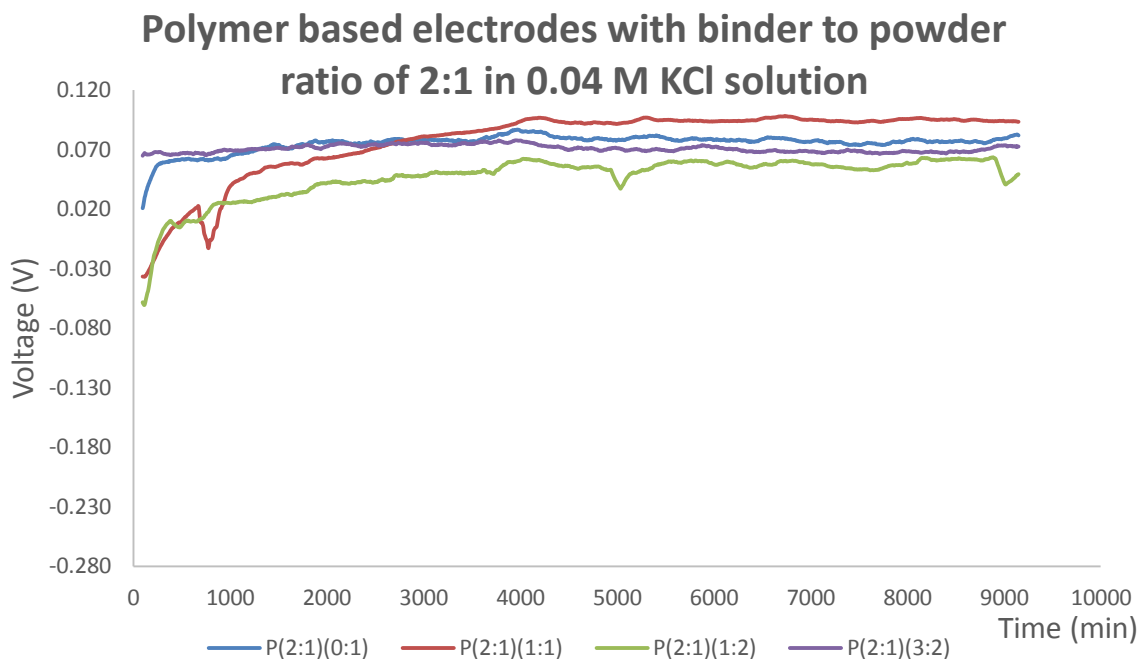


Figure 3-25: The performance of the polymeric electrodes with binder to powder ratio of 2:1 in 0.04 M KCl solution.

In this occasion, the electrodes are much less noisy from 4 M KCl solution and the potentials are closer together without any drift.

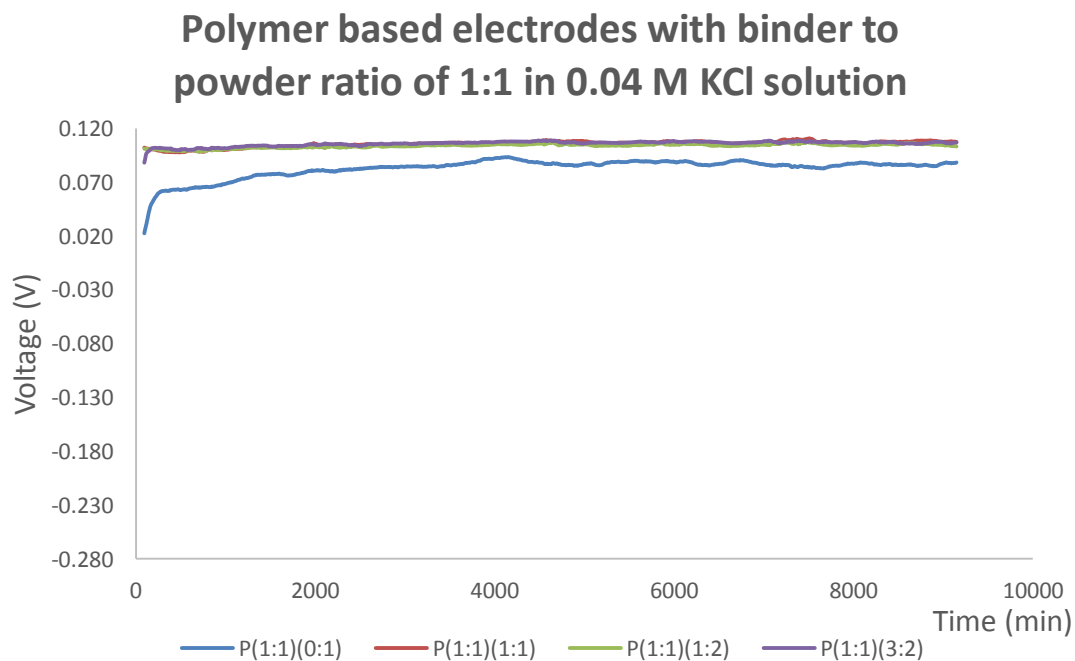


Figure 3-26: The performance of the polymeric electrodes with binder to powder ratio of 1:1 in 0.04 M KCl solution.

3. Reference Electrodes

It is clear that the potential in this solution is much more stable for all of the electrodes without any noise having much closer absolute potentials to each other. Notable is the fact that the electrode without any Ag in the top layer has a much lower potential.

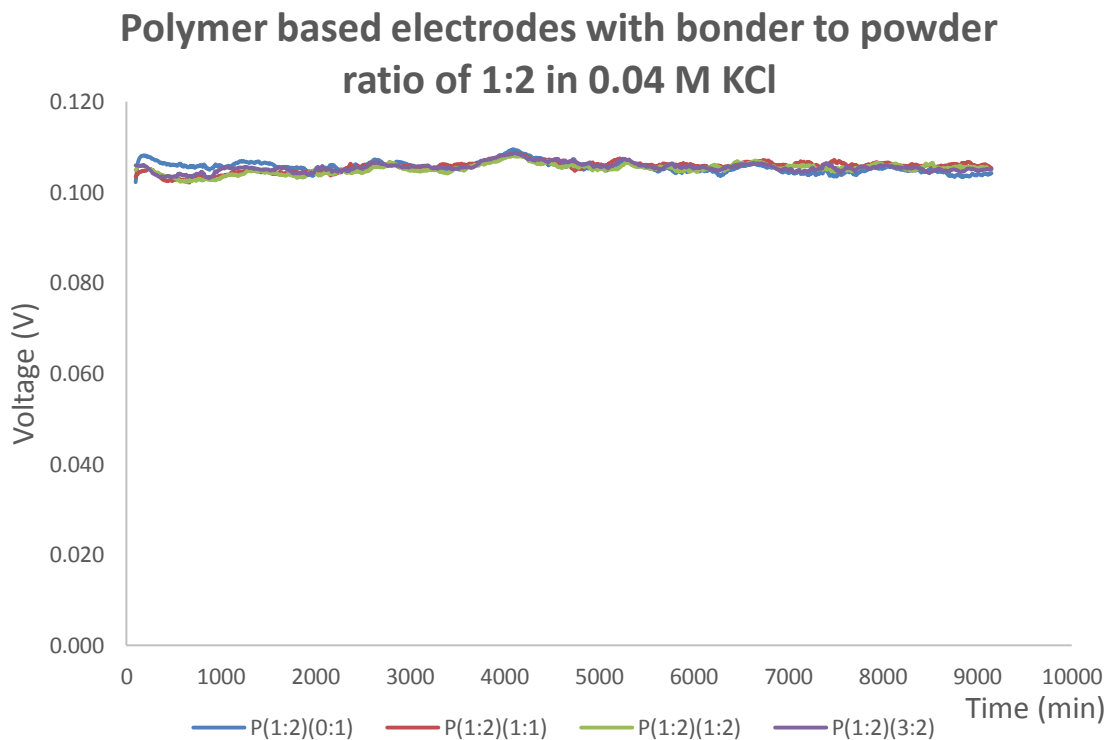


Figure 3-27: The performance of the polymeric electrodes with binder to powder ratio of 1:2 in 0.04 M KCl solution.

Again, the electrodes are even more stable with less noise and almost identical absolute potentials. As a conclusion, the less the binder the faster the electrodes stabilise their potential.

The following figures (Figure 3-28Figure 3-33) show exactly the same experiments as before but with glass based Ag/AgCl.

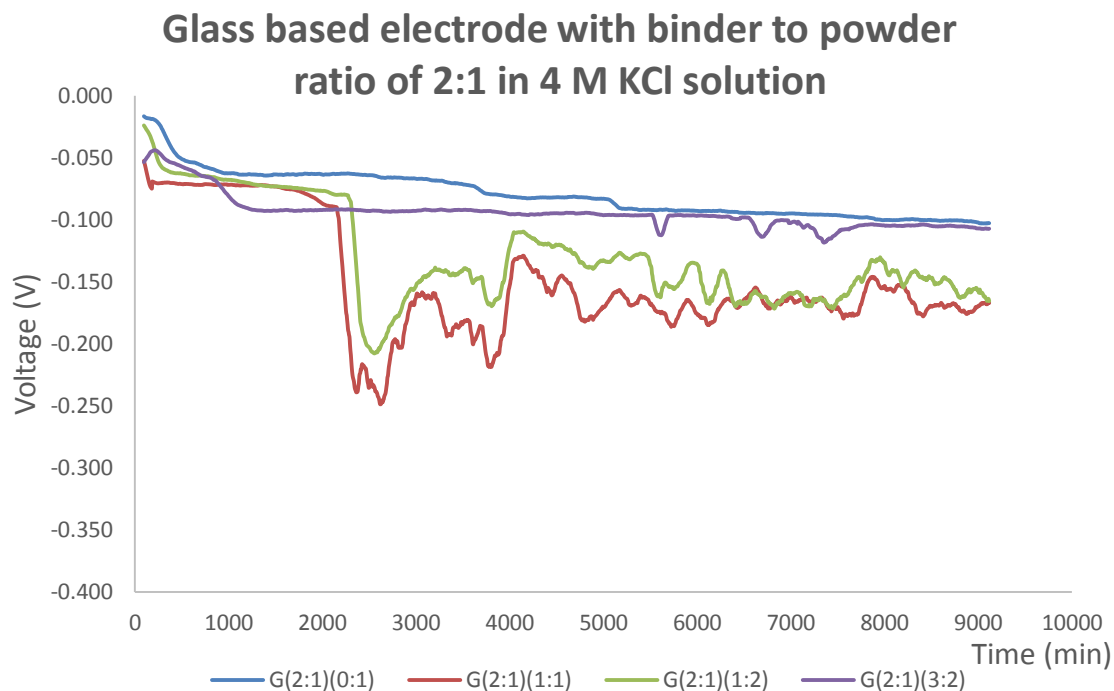


Figure 3-28: The performance of the glassy electrodes with binder to powder ratio of 2:1 in 4 M KCl solution.

These electrodes are also noisy when in 4 M KCl solution but significantly less noisy than the polymer suggesting that it is more difficult to form KCl crystals on the electrodes surface. What is important is that the electrodes' potential drops initially and then stabilises when the noise is excluded.

3. Reference Electrodes

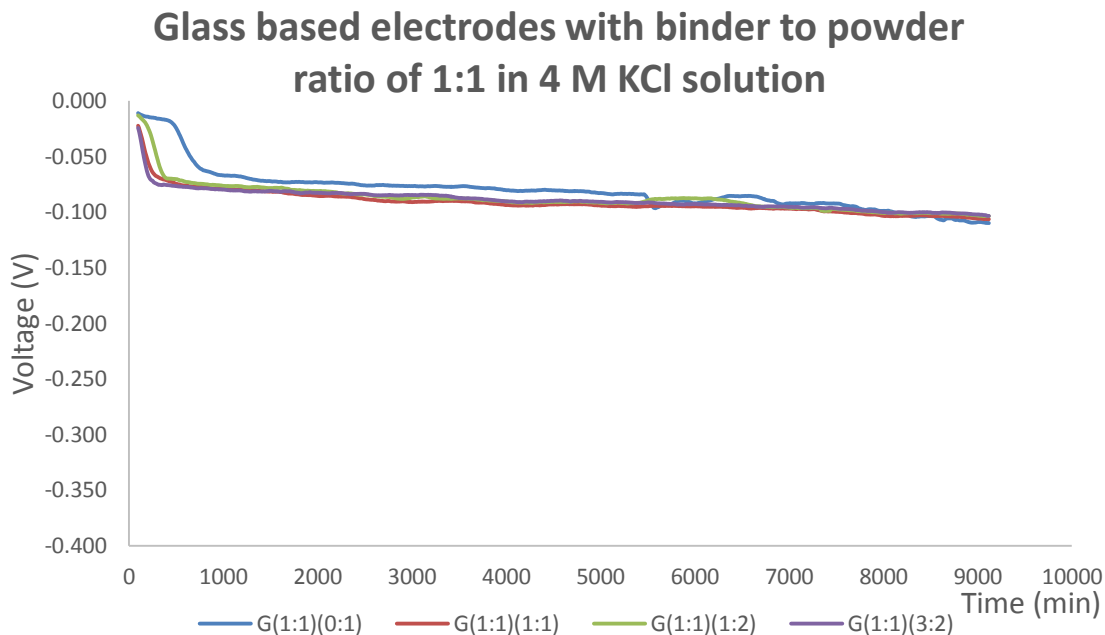


Figure 3-29: The performance of the glassy electrodes with binder to powder ratio of 1:1 in 4 M KCl solution.

These electrodes drop even more from their initial potential and after they stabilise they drift downwards, most probably due to KCl absorption on the electrodes' surface.

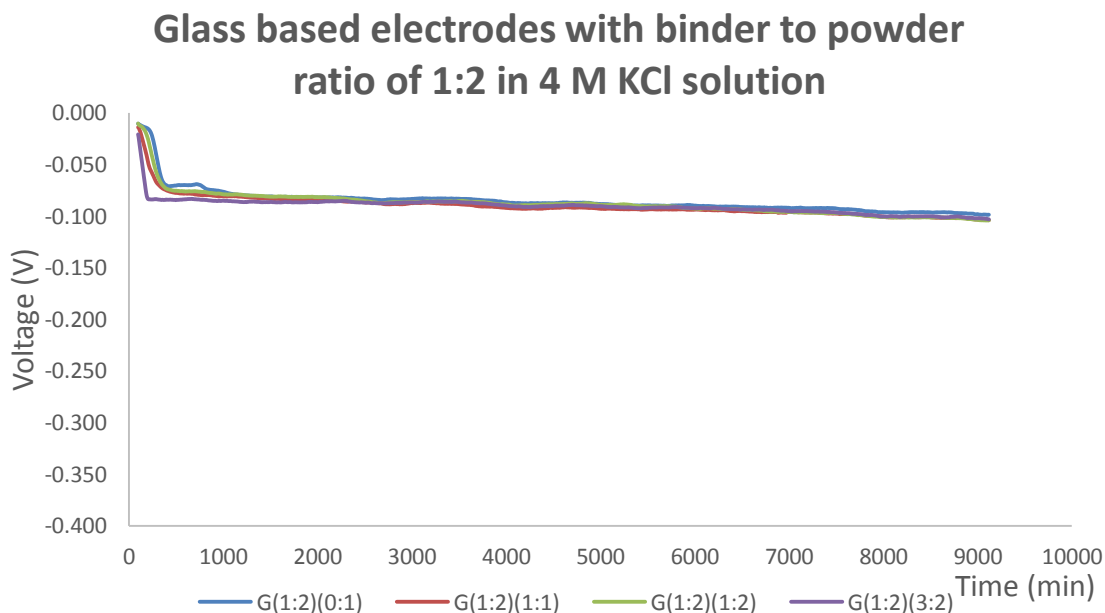


Figure 3-30: The performance of the glassy electrodes with binder to powder ratio of 1:2 in 4 M KCl solution.

3. Reference Electrodes

This set of electrodes is even more stable but there is a bigger and faster drop of initial potential. These electrodes drift less than the rest and the electrodes' potential is the same for all Ag to AgCl ratios.

From comparing the 3 graphs, the less the binder the faster they drop their potential and also the stability and noise is greatly improved. Moreover, the less the binder the smaller the effect of Ag to AgCl ratio on the electrodes' potential and stability. As the binder decreases the electrodes drift less suggesting that they can achieve equilibrium faster than at high binder ratios. Comparing with the performance of the polymeric Ag/AgCl in 4 M KCl solution, the glass based Ag/AgCl electrodes are more stable without any significant drift and much less noisy, hence more suitable for use.

The same electrodes were tested in 0.04 M KCl solution and the results are shown in Figure 3-31, Figure 3-32 & Figure 3-33.

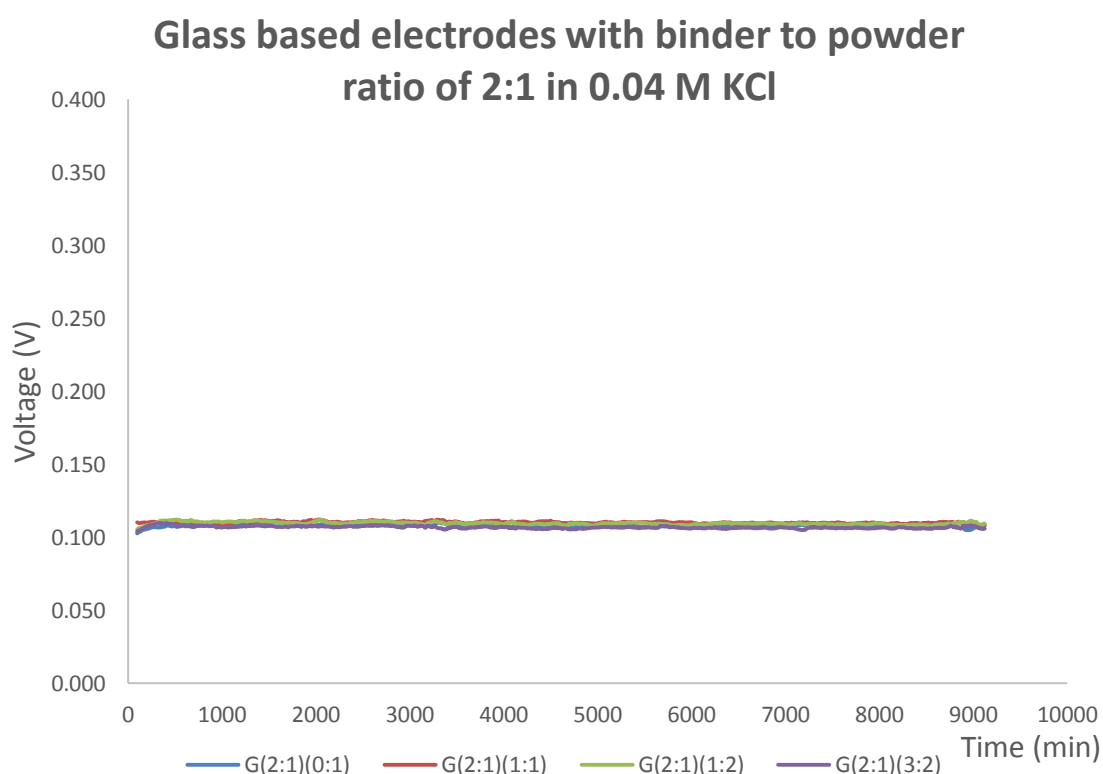


Figure 3-31: The performance of the glassy electrodes with binder to powder ratio of 2:1 in 0.04 M KCl solution.

3. Reference Electrodes

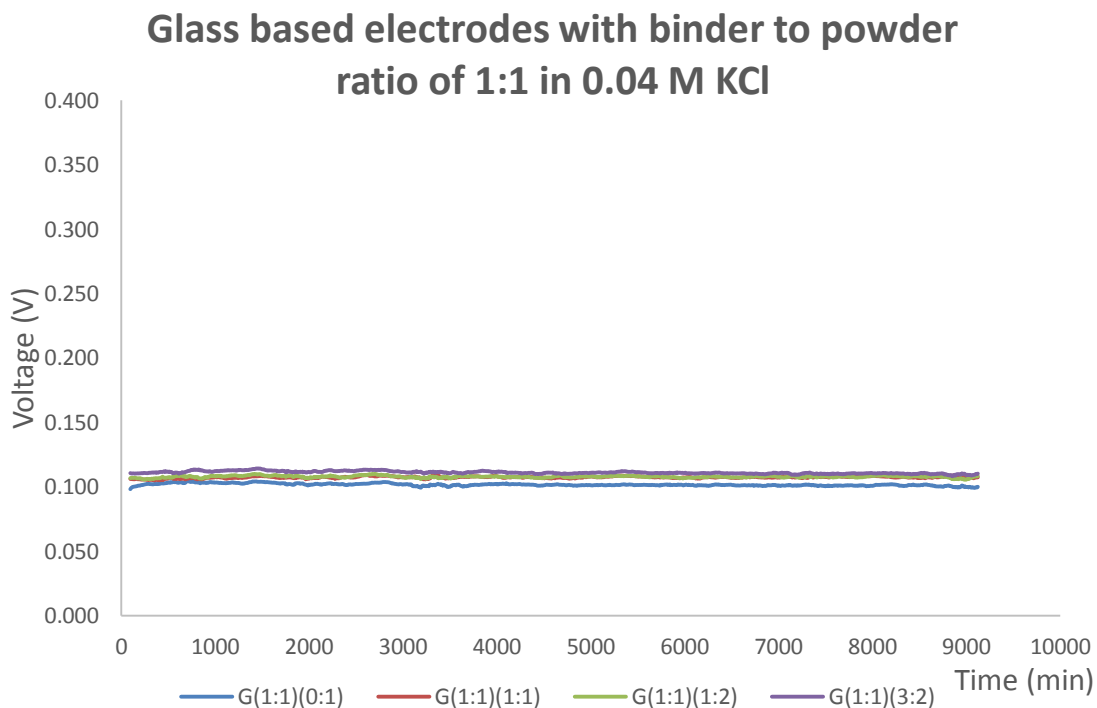


Figure 3-32: The performance of the glassy electrodes with binder to powder ratio of 1:1 in 0.04 M KCl solution.

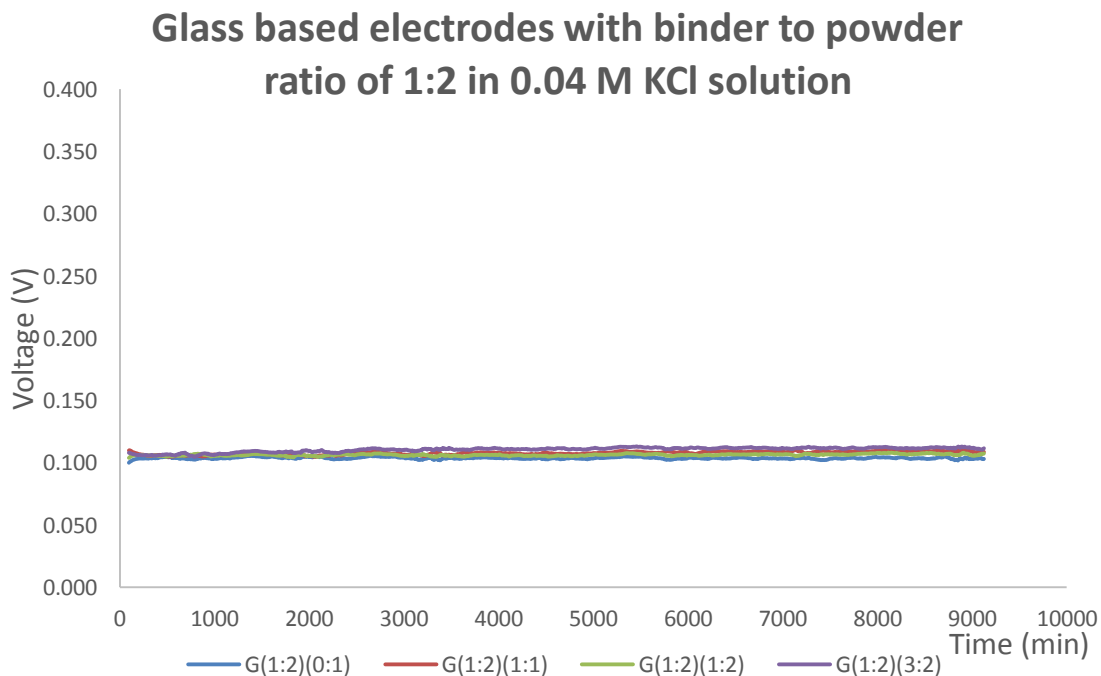


Figure 3-33: The performance of the glassy electrodes with binder to powder ratio of 1:2 in 0.04 M KCl solution.

3. Reference Electrodes

All electrodes perform almost identically in 0.04 M KCl solution, with an extremely stable potential. The absolute potential is independent of the binder to powder ratio as well as the Ag to AgCl ratio. The ensemble average potentials were calculated for the two solutions and were put in the Table 3-15 below.

Table 3-15: Averaged potentials for each electrode type in each solution.

4 M KCL				0.04 M KCl			
Electrode Type	Averaged potential (V)						
P(2:1)(0:1)	-0.029	G(2:1)(0:1)	-0.084	P(2:1)(0:1)	0.078	G(2:1)(0:1)	0.108
P(2:1)(1:1)	-0.031	G(2:1)(1:1)	-0.159	P(2:1)(1:1)	0.094	G(2:1)(1:1)	0.11
P(2:1)(1:2)	-0.062	G(2:1)(1:2)	-0.138	P(2:1)(1:2)	0.057	G(2:1)(1:2)	0.109
P(2:1)(3:2)	-0.097	G(2:1)(3:2)	-0.098	P(2:1)(3:2)	0.07	G(2:1)(3:2)	0.107
P(1:1)(0:1)	-0.073	G(1:1)(0:1)	-0.085	P(1:1)(0:1)	0.087	G(1:1)(0:1)	0.102
P(1:1)(1:1)	-0.063	G(1:1)(1:1)	-0.094	P(1:1)(1:1)	0.107	G(1:1)(1:1)	0.108
P(1:1)(1:2)	-0.14	G(1:1)(1:2)	-0.091	P(1:1)(1:2)	0.105	G(1:1)(1:2)	0.108
P(1:1)(3:2)	-0.171	G(1:1)(3:2)	-0.091	P(1:1)(3:2)	0.107	G(1:1)(3:2)	0.111
P(1:2)(0:1)	-0.131	G(1:2)(0:1)	-0.089	P(1:2)(0:1)	0.105	G(1:2)(0:1)	0.104
P(1:2)(1:1)	-0.183	G(1:2)(1:1)	-0.093	P(1:2)(1:1)	0.106	G(1:2)(1:1)	0.108
P(1:2)(1:2)	-0.145	G(1:2)(1:2)	-0.091	P(1:2)(1:2)	0.106	G(1:2)(1:2)	0.107
P(1:2)(3:2)	-0.101	G(1:2)(3:2)	-0.092	P(1:2)(3:2)	0.106	G(1:2)(3:2)	0.111

All electrodes of the polymer based Ag/AgCl in 4 M KCl solution were extremely noisy therefore any average will be wrong to use for comparisons. Glass based electrodes had a very similar potential in 4 M KCl solution except G(2:1)(1:1) and G(2:1)(1:2) which behaved randomly. This suggests that the potential doesn't depend on the binder to powder ratio or the stoichiometry of the electrode. In the 0.04 M KCl solution, polymeric Ag/AgCl, excluding 2:1 binder ratio, had similar potential of just above 100 mV while the glassy ones all had approximately 105 mV suggesting that the potentials are independent of the Ag to AgCl ratio. It is more possible that the varying thickness of the layer affects the absolute potential of the electrode. Thickness variation can affect the amount of materials which in turn can affect the E_0 value in the Nernst equation, changing the absolute potential of the electrode.

3. Reference Electrodes

3.3.9 Ag to AgCl & binder to powder ratios - Effect of adding KCl layer

The next set of experiments was designed to test the effect of printing the KCl polymer matrix on top of the Ag/AgCl layer. The electrode structure used for this experiment is shown in Table 3-16.

Table 3-16: *Ag/AgCl paste composition for investigating the effect of adding the KCl polymer matrix on electrodes' performance.*

Electrodes Notation	Binder X	Ag/AgCl Powder Y		ESL 242-SB+KCl Concentration
	Binder to Powder ratio(X:Y)	Ag	AgCl	KCl Concentration
P/G(2:1)(1:2)	2:1 (2.0g : 1.0g)	1 (0.33g)	2 (0.67g)	5%
				30%
P/G(2:1)(3:2)	2:1 (2.0g : 1.0g)	3 (0.60g)	2 (0.40g)	5%
				30%
P/G(1:1)(1:2)	1:1 (2.0g : 2.0g)	1 (0.67g)	2 (1.33g)	5%
				30%
P/G(1:1)(3:2)	1:1 (2.0g : 2.0g)	3 (1.20g)	2 (0.80g)	5%
				30%
P/G(1:2)(1:2)	1:2 (2.0g : 4.0g)	1 (1.33g)	2 (2.67g)	5%
				30%
P/G(1:2)(3:2)	1:2 (2.0g : 4.0g)	3 (2.40g)	2 (1.60g)	5%
				30%

Two sets of experiments were performed. First experiment was performed with the hydration in 4 M KCl solution and in the second hydration was performed in 0.04 M KCl solution. The electrodes were hydrated until they have reached a stable potential (approximately 4 days) and then tested for susceptibility (4-0.004-4 M). For the second set of experiments, where the hydration was in 0.04 M KCl solution, a 3 day drift was allowed after the first susceptibility tests and another test was also performed to investigate the effect of drift on the electrodes' susceptibility.

The next set of experiments was designed to test the effect of the KCl layer on top. Only two types of Ag/AgCl layer were used both for polymer and glass for each binder to powder ratio, 1:2 and 3:2. The

3. Reference Electrodes

electrodes were immersed in ≈ 4 M KCl solution until they have reached a stable potential and then tested for susceptibility (4-0.004-4 M).

Electrodes with the 3:2 30% KCl electrode were extremely noisy most probably due to a bad connection, although three electrodes were tested from that type and all of them responded in that way. Also, electrodes 1:2 5% KCl takes a long time to reach a potential and it doesn't even stabilise after the susceptibility test. Since the other 1:2 electrode reaches stability very fast it is assumed that is due to inconsistencies during the printing process. Moreover, some of the electrodes while decreasing the KCl concentration of the solution their potential decreases instead of increasing.

Again, one type of electrodes (1:2) 5% KCl this time shows a very noisy response. In this case the electrodes during the susceptibility test increased their potential with decreasing KCl concentration in the solution.

Here, the electrodes have very similar absolute potentials and perform as expected during the susceptibility test. What is important is that the potential steps get bigger when moving from 0.004 M to 4 M than the other way around. As the binder to powder ratio decreases, the electrodes seem to respond with less noise but with biggest steps.

The same experiments were performed with the same types of electrodes but in 0.04 M KCl solutions. Also, another set of susceptibility tests were performed after a 3 day drift.

The electrodes seem to increase their potential and never stabilise, not even after the 3 day drift. They do seem to converge to a certain potential though after the 3 day drift. The susceptibility tests provided results showing a strange behaviour of the electrodes in 0.004 M KCl since the potential decreased instead of increasing.

Electrodes with 1:2 5% KCl responded based on the theory but the other two types decreased their potential in the 0.004 M solution.

3. Reference Electrodes

Furthermore, the absolute potential of the electrodes seems to converge after the 3 day drift suggesting that the electrodes are conditioned during the experiment reaching the same Ag/AgCl and KCl percentage on the electrode. They all seem to drift to approximately 100 mV with respect to a commercial (Beckman Coulter) Ag/AgCl RE.

These electrodes seem to converge to the same potential faster than the rest suggesting that as the binder to powder ratio decreases a stable Ag/AgCl ratio is achieved faster reaching again around 100 mV. Also, the electrodes with 5% KCl respond properly during the susceptibility test while the other 2 show a drop of potential in the 0.004 M KCl solution. During the second susceptibility test the responses look closer together for all the electrodes.

In terms of stability, the electrodes perform really well and reach a similar potential for all of them of approximately 0 mV with respect to a commercial (Beckman Coulter) Ag/AgCl RE. The main issue with these experiments is the susceptibility tests were the electrodes sometimes respond in the opposite way than they are expected to.

The same absolute potential has been reached of about 0 mV from all the electrodes. They are very stable and very close to each other but still presenting the same issue as before during the susceptibility tests.

Again, the electrodes reach a stable potential of approximately 0 mV suggesting that the absolute potential of the electrodes does not depend on the binder to powder or the Ag to AgCl ratios, not even the KCl percentage. Maybe those factors can affect the response time of the sensors rather than the absolute potential of them.

Comparing the results from the glassy Ag/AgCl electrodes to the polymeric ones, the glassy ones are much more stable and less noisy. They reach a stable potential faster and they do not drift.

It is obvious that the electrodes start at different absolute potentials but as time goes by, the potentials converge to about 100 mV with no

3. Reference Electrodes

significant noise. In this solution the electrodes take much longer to stabilise their potential when compared to the 4 M KCl solution. The same issue still holds for the susceptibility tests.

The electrodes are reaching about 100 mV again as the time goes by but when compared to the binder to powder ratio of 2:1, these electrodes stabilise faster and their potentials are closer together. This suggests conditioning of the electrodes from the solution they are immersed in. Susceptibility tests continue to show the same performance of an opposite of the theoretical trend.

These sets of electrodes take longer to stabilise but again around 100 mV and after the 3 day drift their potentials are very close to each other. This also suggests that the time required to stabilise might be affected by the fabrication procedure or the thickness of the layers. This is well explained if one looks into the paste preparation of Thick-Film pastes. A lot of effort is invested by paste companies to achieve a uniform spread of the material in the paste. A weak dispersion of the powder in the paste results in a non-uniform concentration of any material (in this case Ag or KCl) in the paste which means that during printing the electrodes will not have a constant concentration. That will clearly affect the absolute potential and the hydration time of the electrodes.

The sensitivities from all the electrodes during all the experiments were calculated and inserted in the tables below for a better comparison between the electrode types. It has to be reminded that some electrodes did not perform as expected during the susceptibility tests and therefore comparisons may not be true if one does not keep in mind the actual potential trend recorded.

Table 3-17 shows the sensitivities calculated from polymeric Ag/AgCl electrode when hydrated and drifted in 4 M KCl solution.

3. Reference Electrodes

Table 3-17: Susceptibilities of polymeric Ag/AgCl hydrated and drifted in 4 M KCl solution.

Electrode type	Susceptibility (mv/decade Cl-) saturated to 1:1000	Susceptibility (mv/decade Cl-) 1:1000 to saturated	Average Susceptibility (mV/decade Cl-)
P(2:1)(1:2) 5%	-17.6	-9.2	-13.4
P(2:1)(1:2) 30%	-4.4	-1.9	-3.15
P(2:1)(3:2) 5%	10.6	13.7	12.15
P(2:1)(3:2) 30%	-63.1	-118.1	-90.6
P(1:1)(1:2) 5%	-79.5	-112.9	-96.2
P(1:1)(1:2) 30%	-31.5	-30.4	-30.95
P(1:1)(3:2) 5%	-16.4	-15.1	-15.75
P(1:1)(3:2) 30%	-23.5	-21.6	-22.55
P(1:2)(1:2) 5%	-41	-40.3	-40.65
P(1:2)(1:2) 30%	-36.7	-36.5	-36.6
P(1:2)(3:2) 5%	-37.8	-38.2	-38
P(1:2)(3:2) 30%	-22.6	-21	-21.8

Excluding the two types of electrodes (2:1 3:2 30% KCl and 1:1 1:2 5%), the rest have very similar sensitivities when moving 4-0.004 M and back. What is also noticeable is that as the binder to powder ratio decreases the sensitivity (slope) of the electrodes increases becoming more negative. Also, adding more KCl on the electrode makes the sensitivity (slope) decrease, becoming more positive when compared to the same type of Ag/AgCl layer. Taking all the observations into account, the most probable explanation is that the different binder to powder ratios as well as Ag to AgCl ratios can only affect the response time of the electrodes during susceptibility tests but does not affect the absolute potential of the electrodes when left in the solution for a long time.

3. Reference Electrodes

Table 3-18: Susceptibilities of glassy Ag/AgCl hydrated and drifted in 4 M KCl solution.

Electrode Type	Susceptibility before 3 days drift (mV/decade Cl ⁻)			Susceptibility after 3 days drift (mV/decade Cl ⁻)			Total averaged susceptibility (mV/decade Cl ⁻)
	Sat to 1:1000	1:1000 to Sat	Average	Sat to 1:1000	1:1000 to Sat	Average	
G(2:1)(1:2) 5%	1.5	11.6	6.55	0.2	6.5	3.35	4.95
G(2:1)(1:2)30%	9.3	15.2	12.25	5.4	11.5	8.45	10.35
G(2:1)(3:2)5%	-4.3	3.9	-0.2	-5.9	1.2	-2.35	-1.275
G(2:1)(3:2)30%	1.1	6.5	3.8	4	10	7	5.4
G(1:1)(1:2)5%	-13.4	-10	-11.7	-9	-5.1	-7.05	-9.375
G(1:1)(1:2)30%	-13.3	-10.7	-12	-13.8	-10.14	-11.97	-11.985
G(1:1)(3:2)5%	-5.2	-0.3	-2.75	-2.1	1.8	-0.15	-1.45
G(1:1)(3:2)30%	-5	-0.4	-2.7	-3	1.6	-0.7	-1.7
G(1:2)(1:2)5%	-	-	-	-	-	-	-
G(1:2)(1:2)30%	-17.1	-14	-15.55	-17.6	-15.1	-16.35	-15.95
G(1:2)(3:2)5%	-5.6	-0.2	-2.9	-4.3	0.4	-1.95	-2.425

Table 3-18 shows the susceptibilities of the glassy Ag/AgCl electrodes when hydrated and drifted in 4 M KCl solution. Sensitivities (slopes) before the 3 day drift increase, becoming more positive when moving 0.004-4 M than in the forward direction suggesting conditioning of the electrodes. After the 3 day drift the sensitivities (slope) also increase, becoming more positive during the backward direction compared to the forward. Overall before and after the 3 day drift the electrodes have very similar sensitivities. Changing the KCl on the electrode doesn't seem to have an effect on the electrodes' performance but as the binder to powder ratio decreases the sensitivity (slope) increases, becoming more negative.

Comparing to the polymeric Ag/AgCl electrodes, the sensitivities of the glassy Ag/AgCl are much smaller and taking also into account their stability, more suitable as reference electrodes.

3. Reference Electrodes

Table 3-19: Susceptibilities of polymeric Ag/AgCl hydrated and drifted in 0.04 M KCl solution.

Electrode Type	Susceptibility before 3 days drift (mV/decade Cl ⁻)			Susceptibility after 3 days drift (mV/decade Cl ⁻)			Total averaged susceptibility (mV/decade Cl ⁻)
	Sat to 1:1000	1:1000 to Sat	Average	Sat to 1:1000	1:1000 to Sat	Average	
P(2:1)(1:2) 5%	-15	-14.4	-14.7	-10.4	-9.1	-9.75	-12.225
P(2:1)(1:2)30%	2.4	3.1	2.75	-2	-2.4	-2.2	0.275
P(2:1)(3:2)5%	-12.1	-8.3	-10.2	-1.5	-0.3	-0.9	-5.55
P(2:1)(3:2)30%	-7.3	-0.5	-3.9	-2	4.6	1.3	-1.3
P(1:1)(1:2)5%	-41.8	-41.6	-41.7	-37.4	-37	-37.2	-39.45
P(1:1)(1:2)30%	-19.7	-19.3	-19.5	-19.7	-18.8	-19.25	-19.375
P(1:1)(3:2)30%	-16.8	-16	-16.4	-14.7	-13.3	-14	-15.2
P(1:2)(1:2)5%	-47.1	-46	-46.55	-32.8	-30.7	-31.75	-39.15
P(1:2)(1:2)30%	-18.3	-20.5	-19.4	-19.1	-18.7	-18.9	-19.15
P(1:2)(3:2)5%	-41.2	-40.8	-41	-30.7	-29.9	-30.3	-35.65
P(1:2)(3:2)30%	-19.7	-21.1	-20.4	-22.8	-22.9	-22.85	-21.625

Table 3-19 shows the sensitivities for the polymeric Ag/AgCl electrodes hydrated and drifted in 0.04 M KCl solution. The sensitivities (slopes) tend to decrease, being more positive moving 0.004-4 M but with very small changes which can be due to noise. Also, the sensitivities before and after the 3 day drift decrease, becoming more positive which again can be noise due to the very small changes. It is clearer though, that as the binder to powder ratio increases the sensitivities increase, becoming more negative and as the KCl on the electrode increases the sensitivities decrease, becoming more positive. Most probably the high binder to powder ratio helps to hold the Ag to AgCl ratio more on the electrode without allowing it to shift the equilibrium to either side.

3. Reference Electrodes

Table 3-20: Susceptibilities of glassy Ag/AgCl hydrated and drifted in 0.04 M KCl solution.

Electrode Type	Susceptibility before 3 days drift (mV/decade Cl ⁻)			Susceptibility after 3 days drift (mV/decade Cl ⁻)			Total averaged susceptibility (mV/decade Cl ⁻)
	Sat to 1:1000	1:1000 to Sat	Average	Sat to 1:1000	1:1000 to Sat	Average	
G(2:1)(1:2) 5%	-1.5	-2.7	-2.1	-11.6	-12.7	-12.15	-7.4
G(2:1)(1:2)30%	8.5	10.1	9.3	7.2	6.9	7.05	8.1
G(2:1)(3:2)5%	-5.1	-2.1	-3.6	1.1	-2.1	-0.5	-2.85
G(2:1)(3:2)30%	9.1	9.6	9.6	7.9	7	7.45	8.3
G(1:1)(1:2)5%	-4.2	-5.9	-5.05	-10	-10.6	-10.3	-7.825
G(1:1)(1:2)30%	-13.33	-14	-13.665	-16.5	-14.3	-15.4	-13.9825
G(1:1)(3:2)5%	-1.9	-1.6	-1.75	-7.1	-7.8	-7.45	-4.775
G(1:1)(3:2)30%	1.1	0.5	0.8	-6.9	-7.2	-7.05	-3.2
G(1:2)(1:2)5%	-4.9	-6.8	-5.85	-13.3	-14.4	-13.85	-10.125
G(1:2)(1:2)30%	-16.7	-17.2	-16.95	-14.1	-15.5	-14.8	-16.225
G(1:2)(3:2)5%	-13.4	-14.8	-14.1	-17.4	-17.2	-17.3	-15.65

Table 3-20 shows the sensitivities for glassy Ag/AgCl hydrated and drifted in 0.04 M KCl solution. The sensitivities do not change significantly during the forward or backward direction but there is a small change before and after the drift which seems to be random. Also, the Ag to AgCl ratio seems to have no effect on the electrodes' performance and neither does the KCl amount on the electrode. In general though, as the binder to powder ratio increases the sensitivity increases, becoming more negative.

Comparing the glass and polymer electrodes, the glass electrodes show a smaller sensitivity to KCl concentration changes and are more stable in their potential. Therefore, for both solutions glass electrodes perform better than polymer while the most appropriate combination requires further investigation in order to check clearly how the KCl layer affects the performance of the electrodes.

Chapter 4: **pH ISEs**

4. pH ISEs

4.1 Proposed pH Ion Selective Electrode Structure

In this study, pH ISEs were based on ruthenium oxide as the active layer. The structure of the electrodes was exactly the same as the Ag/AgCl reference electrodes and the same screens were used with the exception that different printing pastes were used.

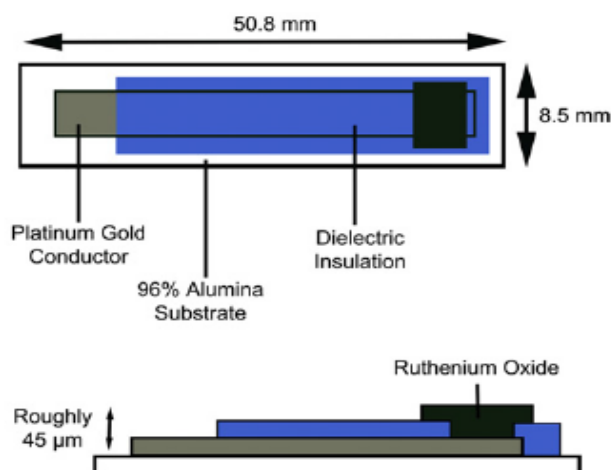
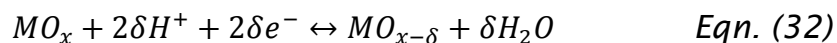


Figure 4-1: Structure of the ruthenium oxide ISE. (Soleimani, et al., 2013)

In this case, various conductors were investigated with the best found to be a platinum gold (ESL 5837) mixture. On top of the conductor the same dielectric layer was printed to protect the electrode and in the small window a ruthenium oxide paste (C50502D7) was printed. In all the experiments pH ISEs were tested against a commercial Ag/AgCl electrode (Beckman Coulter) using the same instrumentation used for REs.

This ISE operates on the basis that it will change its potential proportionally with the pH of the solution into which the electrode will be immersed. When Fog and Buck initially published their work on metal oxides to be used as pH ISEs, five different mechanisms were proposed as to how the metal oxides react with the solution. In the case of ruthenium oxide, they suggested that the most probable mechanism would be represented by the reaction [30]:



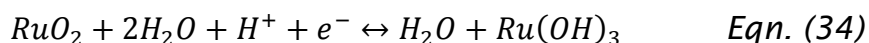
Where MO_x is a higher metal oxide and $MO_{x-\delta}$ is a lower metal oxide.

The electrode's potential is given by the Nernst equation [35]:

$$E = \frac{RT}{F} \ln a_{H^+}^l + \frac{RT}{2F} \ln a_O^s + \text{constant} \quad \text{Eqn. (33)}$$

Where $a_{H^+}^l$ is the proton activity in the liquid phase and a_O^s the activity of oxygen in the solid phase. Activities of solids are defined as unity and therefore that part of the equation is equated to zero.

McMurray et al, used The Pourbaix Atlas to present another mechanism of only one redox equilibrium between two insoluble ruthenium oxides [35]:



And the potential of the reaction is given by [35]:

$$E = E^o - 0.0591pH \quad \text{Eqn. (35)}$$

Taking the activity coefficients to be constant and close to unity, both mechanisms suggest a Nernstian response of -59 mV/pH.

4.2 Experimental Work

In all of the following experiments three electrodes were tested from each kind at the same time in the same solution. The reason being, that if the experiment was to be performed again from the beginning, there will be a possibility of having variations in the pH of the solution which could affect the comparison between identical experiments. In order to avoid such an error, three identical electrodes from each kind were used in the same experiment and error bars were calculated from the performance of those three electrodes.

4. pH ISEs

4.2.1 Investigation of the dielectric layer on electrode performance

Some previous work was also done in this area so any experiments were to further understand and characterise the behaviour of the electrodes.

Initial experiments were done to investigate the sensitivity of the electrodes in various pH buffer solutions. It was suggested that, the conducting layer made of platinum-gold was too expensive and the feasibility of using silver conductors was investigated. The electrodes with silver conductor had a lower absolute potential and also lower sensitivity of approximately 35 mV/pH when compared to the platinum-gold of approximately -60 mV/pH. It was also noticed that the stabilisation time of the silver conductor electrodes was longer and that together with the sensitivity was the reason silver conductor was not a good idea for pH electrodes. It is known that silver ions are very mobile making them able to enter the ruthenium oxide layer and affecting the electrode's potential while platinum-gold conductor is more inert in every way being a much better response.

The next step of the research was the dielectric window layer deposited between the conductor and the ruthenium oxide layer. It was realised that the curing temperature of the dielectric paste was the same as the one for ruthenium oxide. It is understood for TF technology, the top layer shouldn't cure at higher temperatures than the underlying layer in order not to destroy it. Therefore, the idea of changing the polymer dielectric layer to a glass based layer was also tested. Experiments have shown that the performance of the electrodes was very similar except the sensitivity of the electrodes. It was found that electrodes with polymer dielectric layer had an approximate sensitivity of 50 mV/pH while the electrodes with glass 40 mV/pH. It was suggested that because the polymer dielectric and ruthenium oxide layers cure at the same temperature the two layers had a better adhesiveness to each other when compared to the glass. Therefore, water could not infiltrate between the two layers and affect the electrode's potential.

Having the existing knowledge in mind, more experiments using the glass and polymer dielectric layers were done. It was believed that the water getting in-between the two layers would have an even more significant effect on the electrodes' drift. The structure of the tested electrodes is shown in Table 4-1.

Table 4-1: pH ISE structure for experiment pH.1-Dielectric.

Type No.	Layer 1	Layer 2	Layer 3
1	ESL 5937	ESL 4905-CH	C50502D7
2	ESL 9912	GEM 2020823D2	C50502D7

The electrodes were tested in pH buffers 4 and 7. The electrodes were tested in pH 7 buffer for 28 days while in pH 4 buffer for about 50 due to the higher stability of the electrodes in pH 7 buffer compared to pH 4 buffer.

pH ISEs were tested against a commercial (Beckman Coulter) Ag/AgCl RE and three pH ISEs were tested. In all of the following experiments, the custom made data logger from the University of Valencia was used.

This experiment was performed to investigate the effect of using different types of dielectric paste on the performance of the ISEs. More details on the experimental methodology can be found in Chapter 5.

Figure 4-2 below shows the results from testing in pH buffers 4 and 7. The electrodes were tested in pH 7 for only 28 days while in pH 4 for about 50 days because the potential was very stable for pH 7.

4. pH ISEs

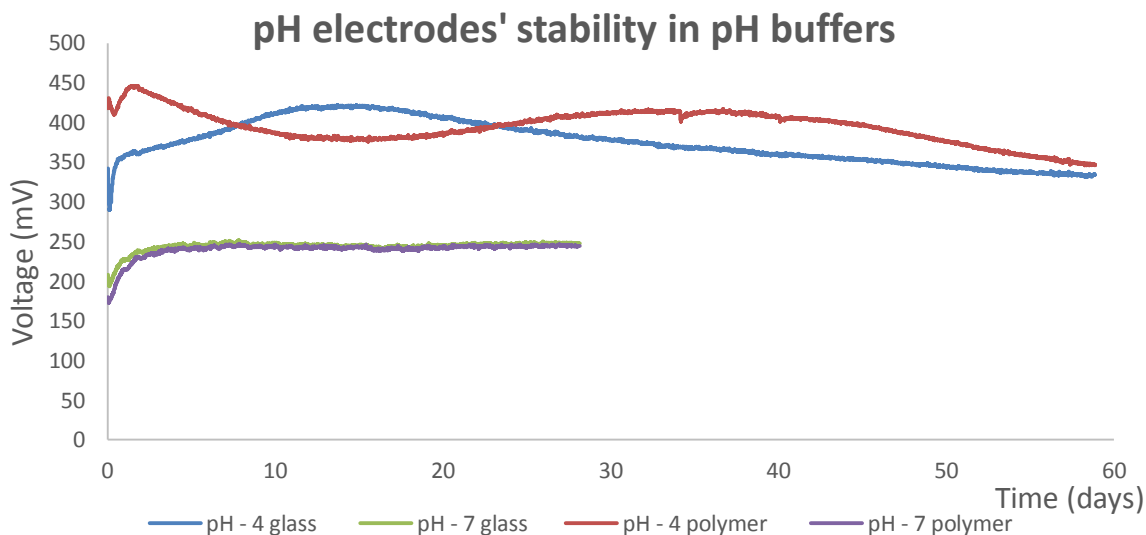


Figure 4-2: Voltage vs Time showing the electrode potential drift in the two pH buffers.

Both electrodes perform exactly as expected in pH 7 buffer with a very stable potential of approximately 245 mV with respect to a commercial Ag/AgCl reference electrode. Also the stability time of the electrodes is very similar with the glass electrodes reaching a constant potential faster than the polymer. In pH 4 buffer solution, the electrodes respond differently which is strange. The electrodes with polymer dielectric start at a higher absolute potential and show a potential moving from about 350 to 430 mV. The glassy electrode's potential is initially lower and increases with time but then it drops back again to a similar potential as the polymer one. It is believed that low pH values in the long term can affect the glass dielectric-ruthenium oxide connection differently than with the polymer and that is why a very different response is observed.

4.2.2 Temperature effect on the pH ISEs' performance

Temperature is another factor known to affect the pH of the buffer changing the dissociation constant of most salts. The performance of the electrodes at different temperatures was investigated in a cyclic manner giving the opportunity to also look for hysteresis of the electrodes. The temperature of the solutions was varied using a water

bath and an external thermometer to monitor the actual temperature of the buffers. In this experiment only electrodes with polymeric dielectric layer were used. The electrodes were tested in pH 4-7-10 at 25-40-60-80 °C and were left immersed in each buffer for approximately 1 hour. It is well known that TF technology is not affected by low temperatures but depending on the inks used, electrodes can be greatly affected by high temperatures. Polymer based Ag/AgCl is cured at 80 °C which means that the polymer used as a binder melts at that temperature. Therefore, any higher temperatures would affect the adhesiveness of the layer to the substrate. Temperature range from room temperature to the highest temperature possible was chosen to cover the range with the highest possible risk for the electrodes. Taking room temperature as the starting point and 80 °C as the maximum point, the steps of 25, 40, 60 and 80 °C were used. These experiments were performed in parallel with other tests that required operation of the electrodes in base oil. Base oil has a very low conductivity at room temperatures but its conductivity increases dramatically above 50 °C (Soleimani, et al., 2013). For potentiometric sensors to operate, the input impedance of the voltmeter must be remarkably greater than that of the oil. Therefore, the electrodes' performance was tested at higher temperatures up to the ink's limit so that the experiments could be performed using existing instrumentation. Although these temperatures are not met in soil monitoring, a better understanding was achieved, with respect to the behaviour of the electrodes at various and extreme temperatures. Room temperature was used as the reference temperature since the behaviour of the electrodes was known, and the range up to the ink's limit was covered by another two temperature points. The temperature intervals were large (25-40-60-80 °C) due to time restrictions for further experiments but at the same time having uniform distribution of temperature points. pH buffers of 4-7-10 were tested because this experiment was not used to identify the limits of the electrodes on the pH range but rather test their sensitivity in a normal range. Furthermore, Fog & Buck (Fog & Buck, 1984) have identified that the pH sensing range

4. pH ISEs

of ruthenium oxide was from 2-12. Testing the electrodes in that range would most probably damage them and not allowing for testing electrodes' hysteresis. The buffer sequence used in the experiment was important and shown in Figure 4-3 in order to check for any hysteresis when the buffers were cycled and how that hysteresis is affected by temperature.



Figure 4-3: pH buffer sequence for experiment pH.2-Temperature.

During the experiment at 80 °C the wire from the reference electrode was accidentally disconnected and then re-soldered and therefore during the initial pH 4 period the data are missing. Errors for the whole experiment were in the range of $\sim\pm 10$ mV which can be incorporated in the noise levels of the instrumentation used. Figure 4-4 shows the potentials recorded during the test.

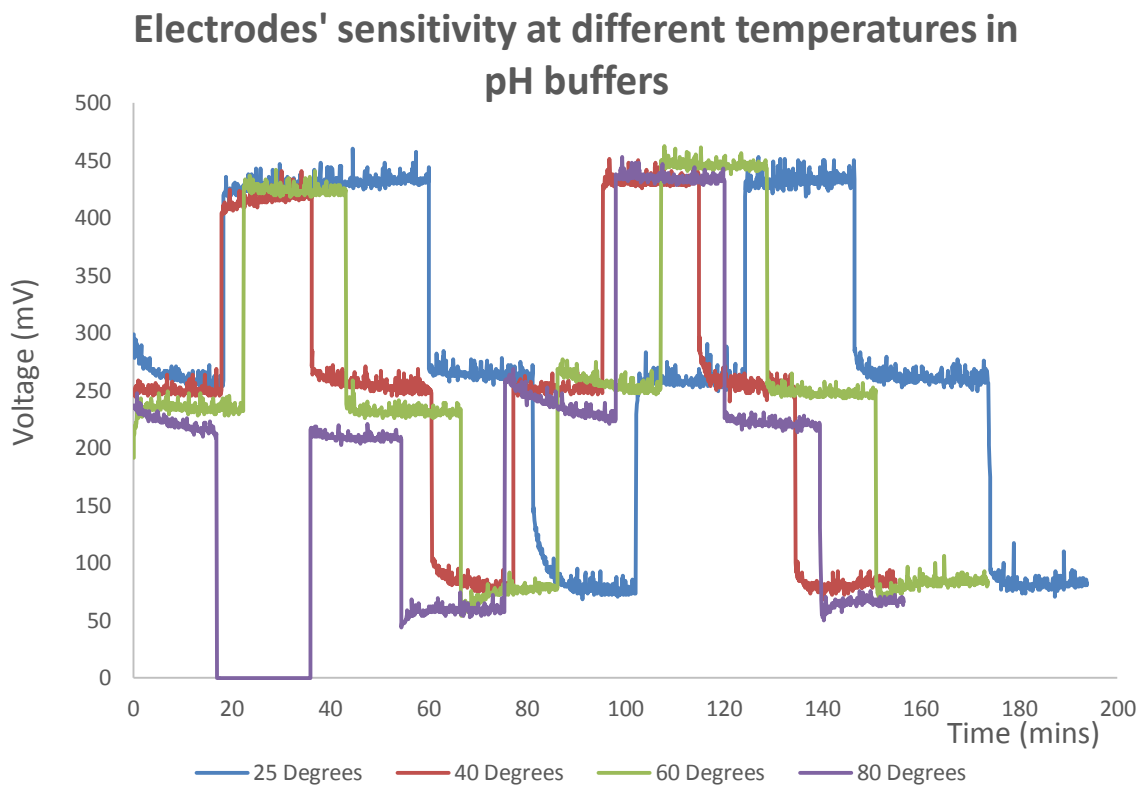


Figure 4-4: Voltage vs Time for the investigation on sensitivity changes due to temperature dependence.

From the graph, it is understood that electrodes perform satisfactory to all temperatures without breaking down. The tests were done for only 50-60 minutes in every solution. In this experiment the electrodes show a sensitivity of approximately -58 mV/pH , which is very close to the Nernstian. The data from the experiment were averaged for each pH and then plotted on voltage-pH graphs. Figure 4-5 below shows the performance of the electrodes in $25 \text{ }^\circ\text{C}$.

4. pH ISEs

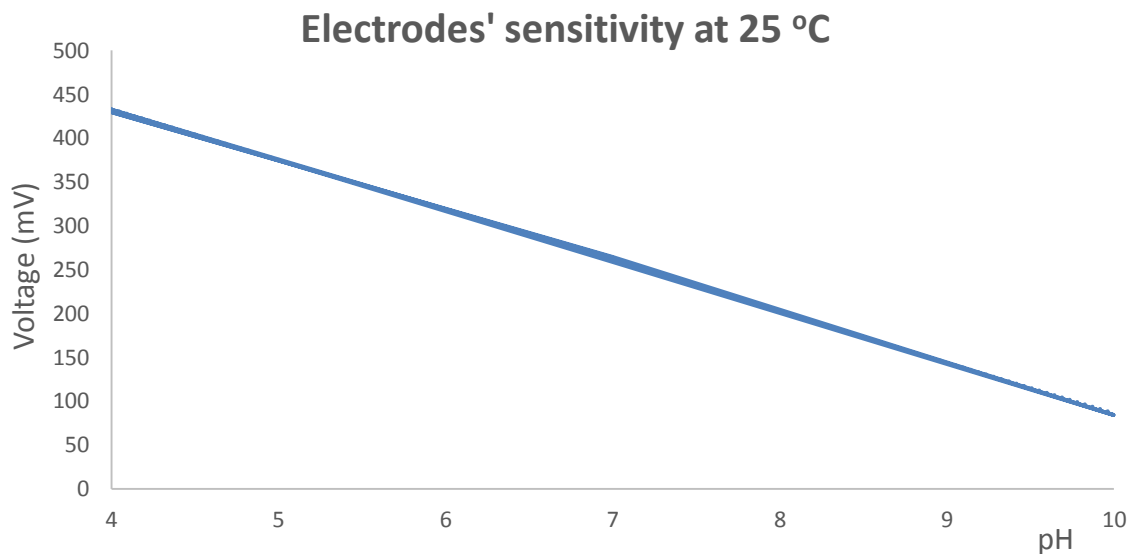


Figure 4-5: Voltage vs pH at 25 °C.

The electrodes at 25 °C show a sensitivity of approximately -58 mV/pH (Nernstian) and they experience almost no hysteresis.

Figure 4-6 show the performance of the same electrodes at 40 °C after they have been used for the 25 °C test.

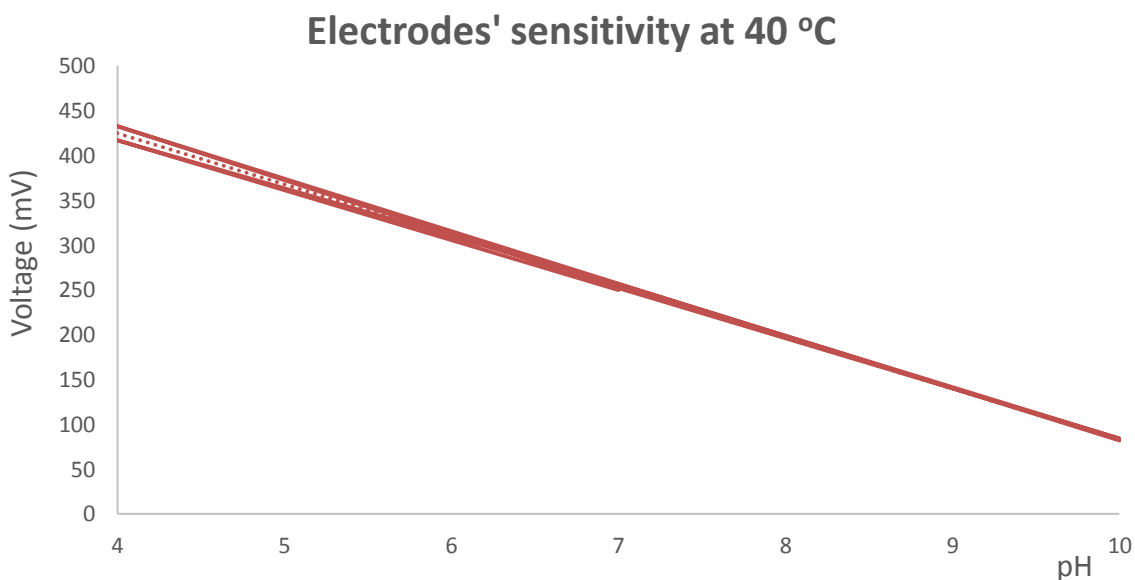


Figure 4-6: Voltage vs pH at 40 °C.

The electrodes perform very well showing an initial sensitivity during the first cycle of approximately -55 mV/pH while during the second cycle the sensitivity drops to approximately -58 mV/pH.

Figure 4-7 below shows the performance of the electrodes in 60 °C of the same experiment.

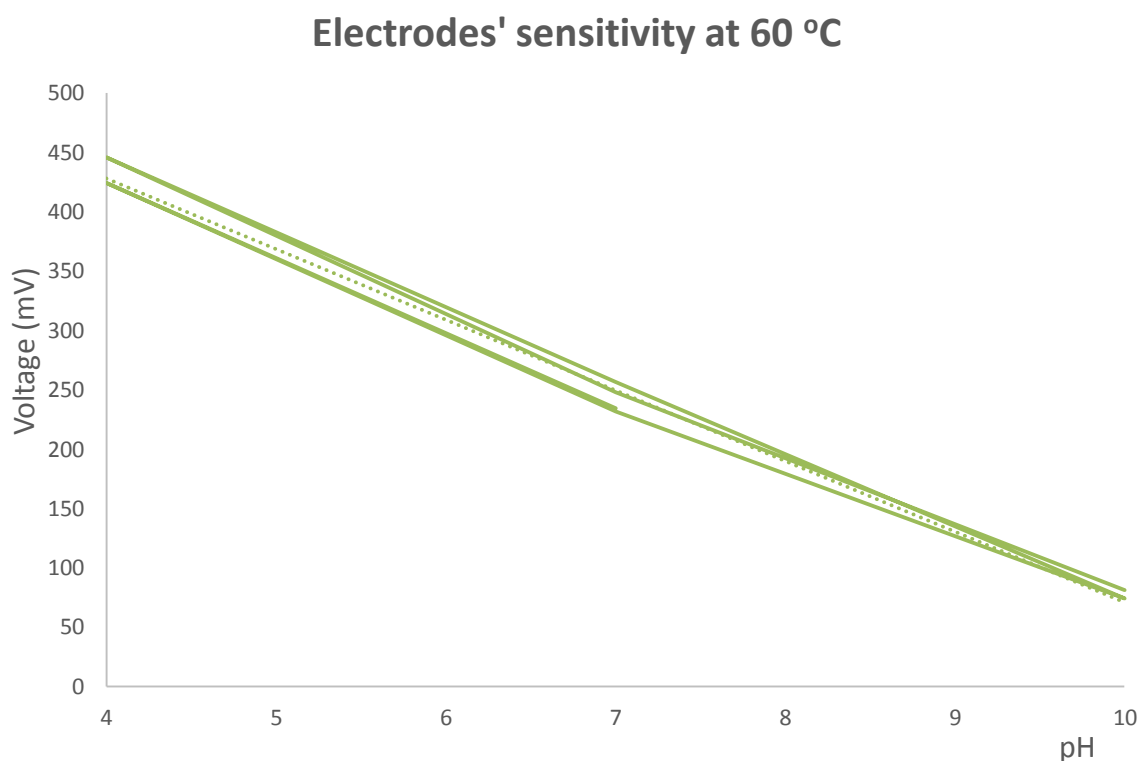


Figure 4-7: Voltage vs pH at 60 °C.

Again, the electrodes perform very well with a sensitivity of approximately -58 mV/pH during the first cycle and -60 mV/pH during the second. The two sensitivities are very close to the theoretical and the difference could be because of outside noise. The fact that initially the potential of the electrodes is higher for the same pH buffer and then as the electrodes are rotated through different pH buffers the potential drops is most probably due to hydration of the electrodes as every temperature test was done in a different day. It is also observed that as the temperature increases that potential drop during the experiment increases up to a point where the electrodes it is believed to reach their maximum operating range.

Figure 4-8 shows the response of the electrodes at 80 °C.

4. pH ISEs

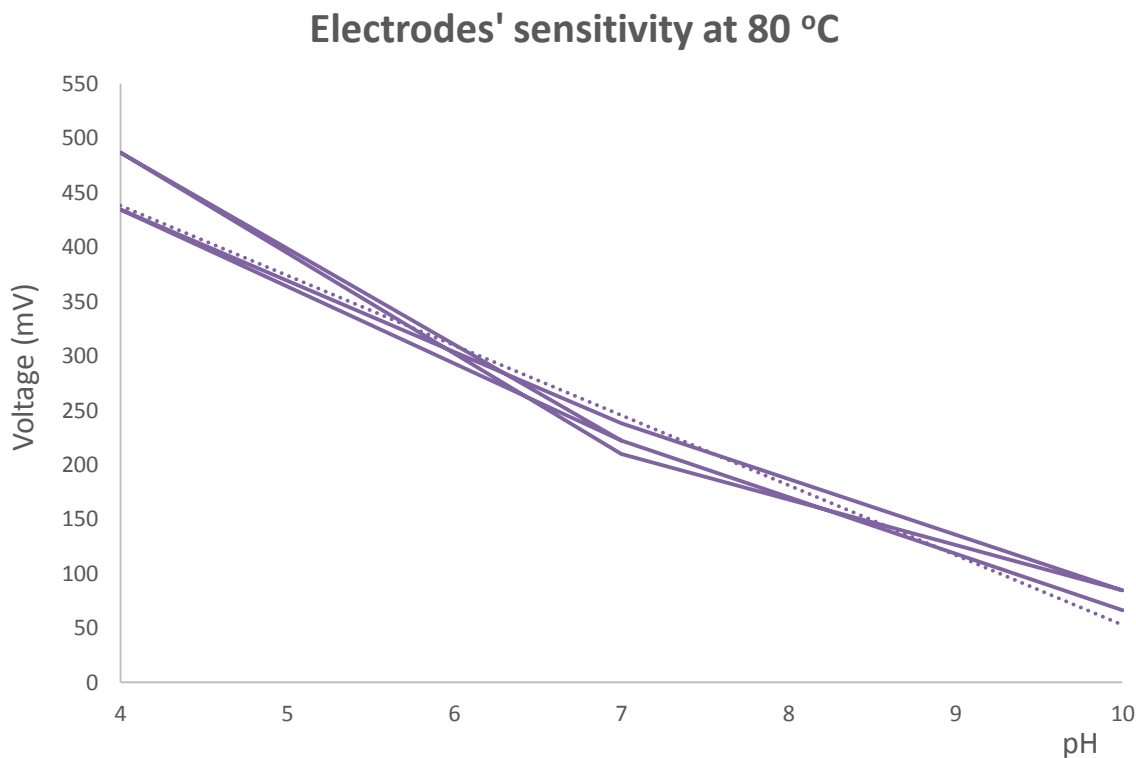


Figure 4-8: Voltage vs pH at 80 °C.

As the temperature increases the sensitivity of the electrodes increases which corresponds to the theory that at higher temperatures acidic solutions tend to be more acidic and alkaline solutions more alkaline. The main difference of the response in 80 °C is that the graph is not a straight line anymore because maybe high temperatures affect the electrode differently in different pH numbers.

Overall, the electrodes presented a very good sensitivity of approximately -58 mV/pH which is in correspondence to the Nernstian theory. Moreover, the electrodes showed no significant signs of hysteresis when cycled through various pH buffers in the range of 4-10. It was observed that as the temperature increased the potential of the electrodes in mainly pH 4 was decreasing during the second cycle rather than the first.

Table 4-2: Sensitivities of the electrodes at different temperatures.

Temperature (°C)	Equation (Linear)	R ²
25	Y=-57.781x+664.62	0.9994
40	Y=-56.992x+652.65	0.9986
60	Y=-59.618x+666.92	0.9918
80	Y=-64.28x+695.52	0.9611

From Table 4-2 it is observed that the sensitivity of the electrodes increases with temperature which is in correspondence with the theory. Furthermore, as the temperature increases the R² value decreases indicating a variation of the electrodes potentials in the same pH buffers in different cycles. This can be caused by the pH buffers changing due to the water evaporating at higher rates at higher temperatures or due to a higher conditioning rate of the electrodes or due to both reasons at the same time. The potential variations are more noticeable in pH 4 buffer and less noticeable as the pH value increases most probably due to the pH changing rates being different for each buffer and the conditioning rate of the electrodes being also different in each buffer.

Chapter 5: **Relative Humidity & Temperature Sensor**

5.1 SHT21

The idea behind the use of a combined humidity and temperature sensor was to monitor the water content in the soil. The investigation was based on the approach that the water content will be related to the humidity levels at that specific temperature.

Relative humidity is defined as the ratio of the water vapour present in the air divided by the maximum amount of water vapour that can be absorbed by air at a specific temperature. During temperature changes, the maximum water vapour level changes which in turn changes the relative humidity. Therefore, a combined humidity and temperature sensor was required. Since such a sensor would be used underground and the case of water short circuiting the sensor was highly possible, the final design should include a way to waterproof the sensor and the circuit but still allowing air reaching the sensor. The sensor had to be low cost to fit the project's restraints and the future plan was to integrate the sensor on the same TF substrate with all the rest of the sensors.

SHT21 is a humidity and temperature sensor of Sensirion. It is embedded in a reflow solderable Dual Flat No leads (DFN) package of 3x3 mm foot print and 1.1 mm height and it provides calibrated, linearized signals in digital, I²C format. It is a reworked capacitive type humidity sensor with an improved band gap temperature sensor. The resolution of SHT21 can be changed by command (8/12bit up to 12/14bit for RH/T), low battery can be detected and a checksum helps to improve communication reliability.

Initially a prototype sample was used shown in Figure 5-1 below. On the Printed Circuit Board (PCB), there was the SHT21 sensor connected to a microprocessor taking readings and converting them into temperature and humidity. There was also an LED screen to present the values.

5. Relative Humidity & Temperature Sensor



Figure 5-1: Sensirion's prototyping kit including the LED screen, SHT21, battery and the microcontroller.

The PCB was used to get the readings manually from the sensor, so the sensor was removed from the PCB using a hot air gun and wires were soldered on the pads which were in turn connected to the TF substrate. In order to be able to switch between different sensors the wires from the PCB were soldered on a male RS232 connector and the wires from the TF substrates on female RS232 connectors as shown in Figure 5-2 below.



Figure 5-2: SHT21 units and the connections with the PCB.

5.2 Experimental Work

5.2.1 Investigation of wire length on sensor accuracy

The first set of experiments (RH.1-Wires) was performed in an environmental chamber where the temperature and humidity could be controlled. Unfortunately, the humidity of the chamber could not be controlled at that moment so the experiments in the chamber were confined to temperature control. Due to the fact that the chamber has

5. Relative Humidity & Temperature Sensor

the only opening on the side, 4 sensor samples were tested, in order to eliminate the temperature distribution in the chamber, two types of wires were used. As shown in Figure 5-3, two wire lengths were used splitting the sensors into 2 groups.



Figure 5-3: The two wire lengths used for the experiments.

All 4 sensors were placed in the chamber and the temperature of the chamber was varied. Once the temperature on the LED screen of the chamber stabilised to the required temperature a reading was taken for all the sensors.

The experiments were performed to investigate the possibility of using SHT21 as a humidity and temperature sensor to monitor the water content of the soil. For the soil application, the sensor needs to be waterproofed and incorporated on the TF sensor array, therefore experimentation was needed to find a way of doing that while maintaining sensor's performance.

5. Relative Humidity & Temperature Sensor

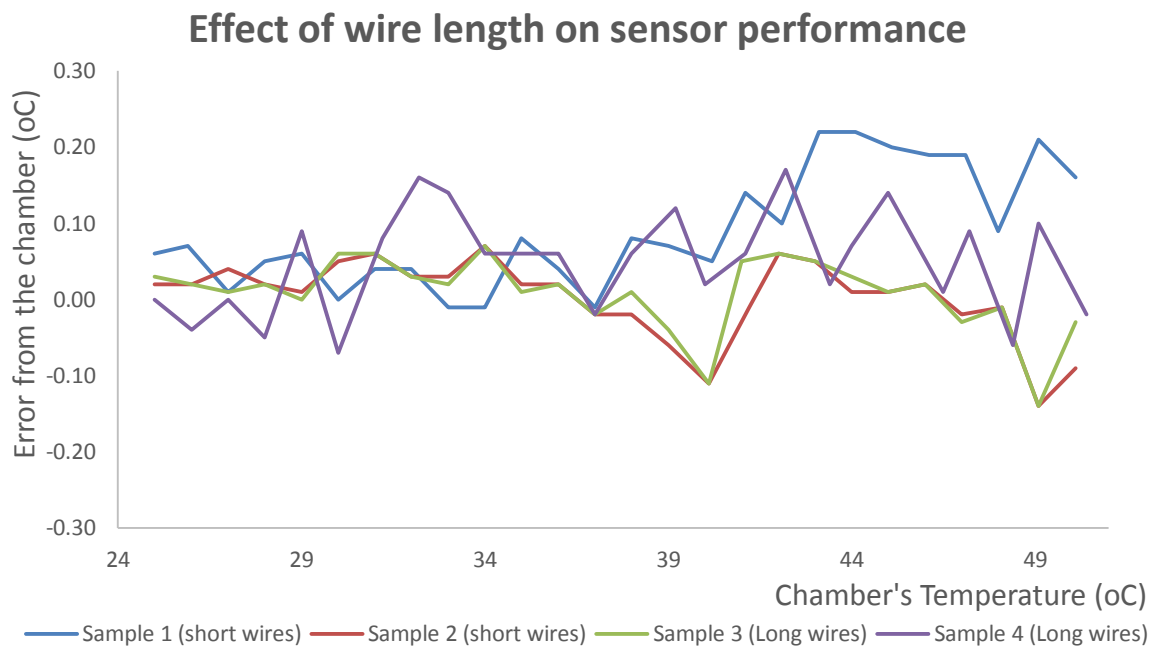


Figure 5-4: Temperature error between the sensors and the chamber's reading.

The error calculated falls within the ± 0.3 °C accuracy of the SHT21 sensor which means that soldering the sensor on the TF substrate does not alter its specifications provided by the manufacturer. It also proves that the temperature in the chamber is uniformly distributed.

5.2.2 The effect of covering the sensor with PTFE membrane on sensor's performance

Further experimentation was done for humidity measurements at a constant temperature (RH.2-PTFE-Performance). The effect of adding polytetrafluoroethylene (PTFE) membrane on top of the sensor was to be investigated, therefore one sensor with short wires was sealed using 2 windings of PTFE and another sensor with short wires was sealed in the same way.

Figure 5-5 below shows the humidity reading recorded from the SHT21 display at 25 °C in the chamber from all the sensors.

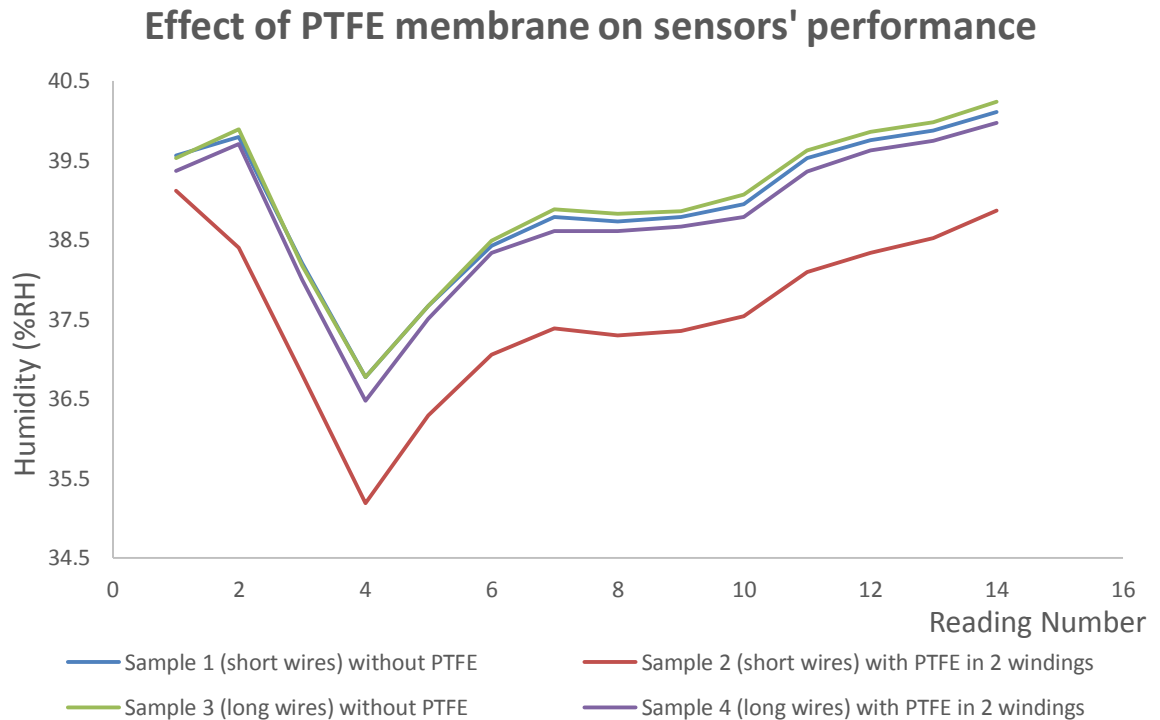


Figure 5-5: Humidity readings from the sensors in the chamber at a constant temperature of 25 °C.

From the graph, the sensors perform within the ± 2 %RH accuracy specifications of the manufacturer. All sensors with and without PTFE are providing very similar results which suggests that the addition of PTFE membrane on top of SHT21 has no effect on its performance.

5.2.3 PTFE membrane as a waterproofing method

The next experiment (RH.3-PTFE-Waterproofing) was to check if the addition of the PTFE membrane is a valid method for waterproofing the sensor. Therefore, two sensors with the same wire lengths were immersed in water after they had been wound with PTFE. One of them had 1 winding and the other one had 2. The temperature of the chamber was gradually increased until it stabilised at the temperature of interest and the readings were recorded until humidity reached 100%.

Figure 5-6 below shows the humidity readings from SHT21 versus the temperature of the chamber.

5. Relative Humidity & Temperature Sensor

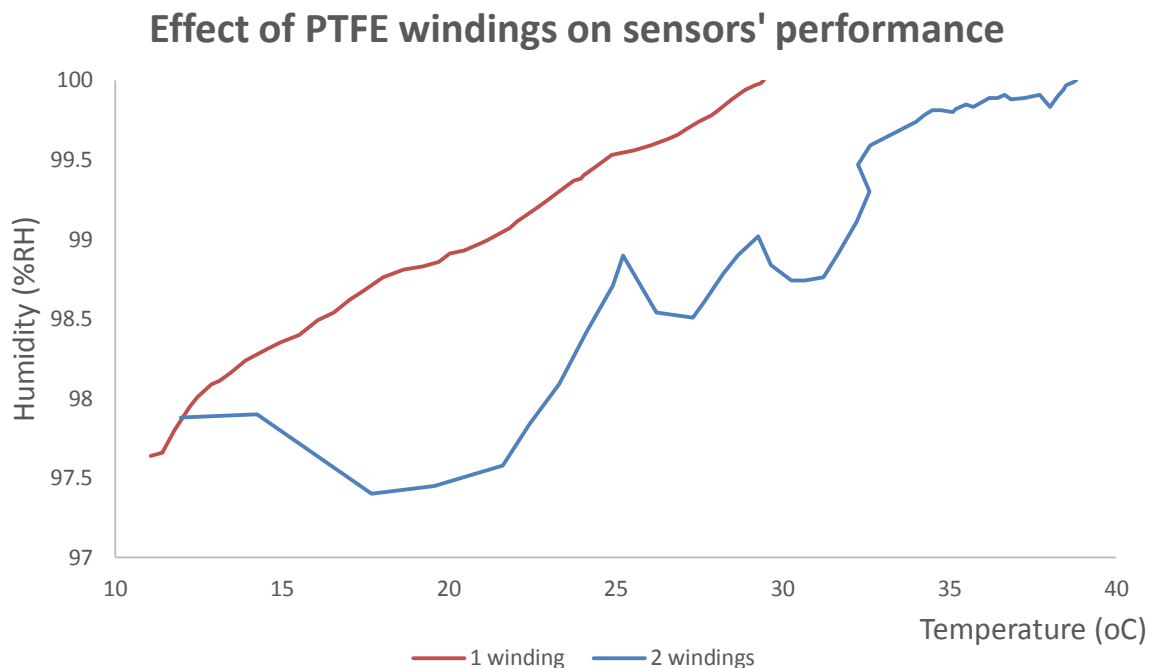


Figure 5-6: Humidity readings when the sensors are covered with PTFE and immersed in water.

It was found that PTFE membrane is a successful way to waterproof the sensors since they did not short circuit. The response of the sensor in water was satisfactory with the main difference between the winding number to be the temperature and time required to achieve the 100% RH. The sensor with 1 winding of PTFE reached 100% RH at 30 °C, while the sensor with 2 windings at 40 °C. Moreover, the trend the maximum humidity was reached for the sensor with 1 winding was very linear but for the sensor with 2 windings was very noisy. It did follow an increasing trend with temperature but most probably a higher pressure was required to allow the water vapour to penetrate the PTFE membrane twice. It is possible that air pockets with different humidity or temperature levels are formed between the PTFE layers. As the humidity and temperature varies, the changes are not linear because they have to go through those air pockets and then finally reach the sensor. Having a single winding will only form one air pocket with is linearly proportional to the change as seen from the graph. Therefore, a single winding PTFE sensor will be more suitable to be used for such an application.

5.3 SHT21S

In this set of experiments, another version of the sensor was used. SHT21S is the same sensor but with a Sigma Delta Modulation (SDM) interface which is convertible to analog output. The output was translated using the formulas from the sensors datasheet. An interface was required in order to get an analog output from the sensor as shown in Figure 5-7 below for temperature and humidity. The sensor reads temperature when the clock is connected to low and humidity when connected to high.

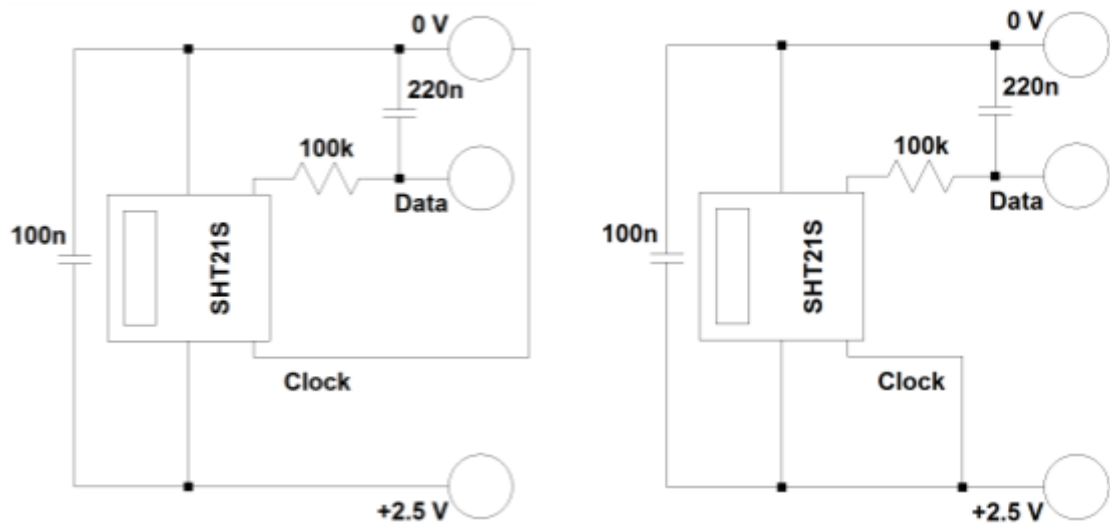


Figure 5-7: Diagrams of the interface used for temperature (left) and humidity (right).

The resistor and capacitor (CR) circuit acts as a low pass filter with a cutoff frequency of $\frac{1}{2\pi CR}$ which is equal to approximately 8 Hz. The data output of the sensor is a Sigma Delta Modulation described in the sensor's datasheet. The more high pulse values the higher the value of the measurement. Adding a low pass filter will average the output and using the provided equations the direct current (DC) voltage is translated to the physical parameter to be measured.

5. Relative Humidity & Temperature Sensor

5.3.1 Investigation on sensors' performance consistency between sensors

In the next experiment (RH.4-Consistency), 6 sensors were soldered on the TF substrate without any PTFE membrane. There was an experimental mistake during this test. The operating power supply range suggested by the manufacturer is 2.1-3 V but the experiments were performed using a 5 V power supply with the sensor still operating normally. Of course, the fact that the sensors were operated outside the recommended range could affect the sensors' performance. Also, during these experiments, the environmental chamber was fixed to be able to control humidity but the temperature could not be completely controlled since it had variations of ± 2 °C.

Figure 5-8 below shows the temperature error of the sensors when compared to the temperature shown on the LED screen of the chamber.

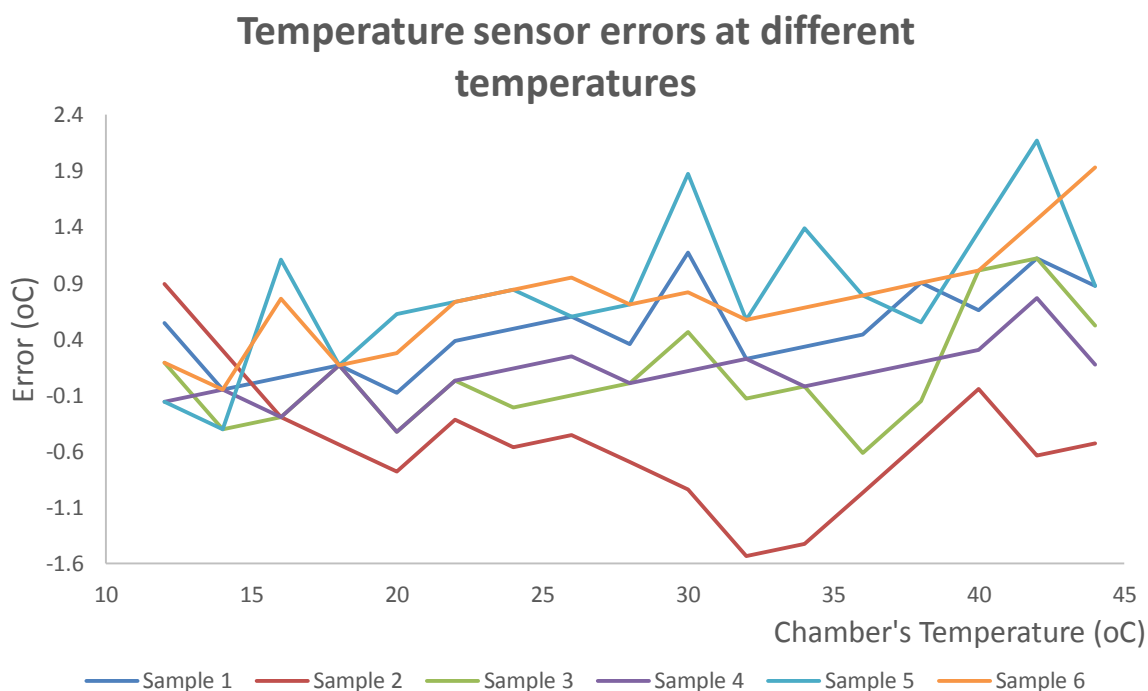


Figure 5-8: Temperature error of the sensors for various chamber's temperatures.

The sensors' accuracy for temperature is ± 0.3 °C as defined by the manufacturer but it is obvious that the error was sometimes more than

5. Relative Humidity & Temperature Sensor

2 °C. The error slightly increases as the temperature increases but that can be explained by the time the sensors were allowed to reach that temperature. Readings were recorded when the chambers LED screen had a stable value and maybe the sensors didn't have enough time to actually reach that point. In addition, the sensor was operating outside the recommended supply voltage range so that can also be a source of error.

5.3.2 The effect of PTFE membrane on SHT21S performance

The next experiment (RH.5-PTFE-NaCl) was to test the sensors' performance for humidity with and without the PTFE membrane. This test was performed in a saturated sodium chloride environment and that is defined to be 75 %RH. The performance of the sensors in that environment without PTFE membrane, with one winding of PTFE and with two windings was investigated. Two sensors from the previous experiment were used from each type and an average value from those two sensors was recorded.

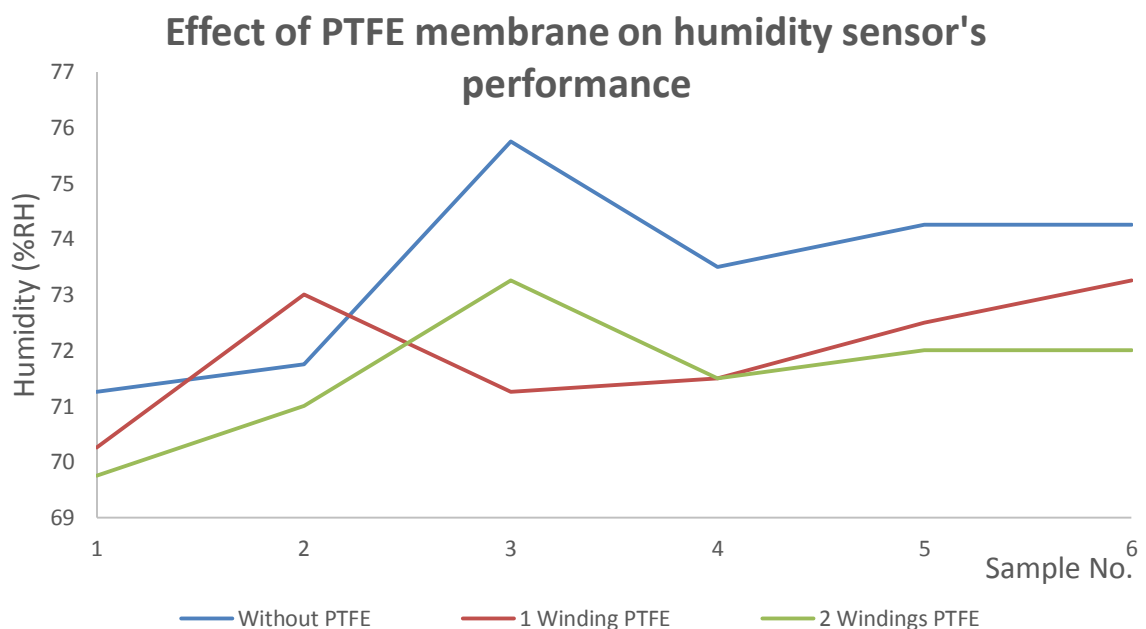


Figure 5-9: Humidity readings to compare the sensors' performance with and without PTFE membrane in a 75% RH environment.

5. Relative Humidity & Temperature Sensor

Sensors with two windings of PTFE membrane showed a lower humidity than the other two sensor arrangements. The readings were more erroneous from the actual humidity and the accuracy increases as the PTFE windings were getting less. Sensors without the PTFE membrane had the most accurate results but if the readings between the sensors were compared the 3 different types fall in the accuracy range of the sensor of ± 2 %RH.

5.3.3 Effect of PTFE on the exact same sensors

Another experiment (RH.6-PTFE-25°C) was performed with the same 6 sensors from the previous experiment, in the chamber with varying humidity from approximately 35 % to 80 % at 25 °C. Each sensor was tested in the chamber three times, once without PTFE, once with one winding and once with two windings.

The results are shown in Figure 5-10, Figure 5-11, Figure 5-12, Figure 5-13, Figure 5-14 & Figure 5-15 below.

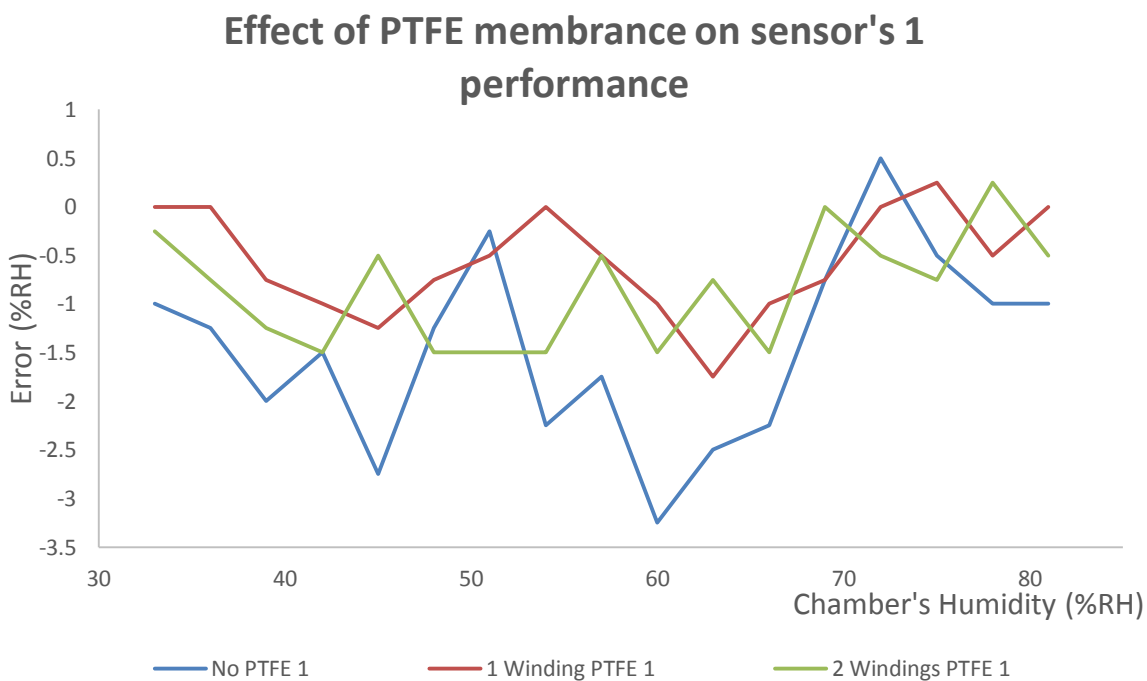


Figure 5-10: Humidity error of the first sensor at various humidity levels for all experiments.

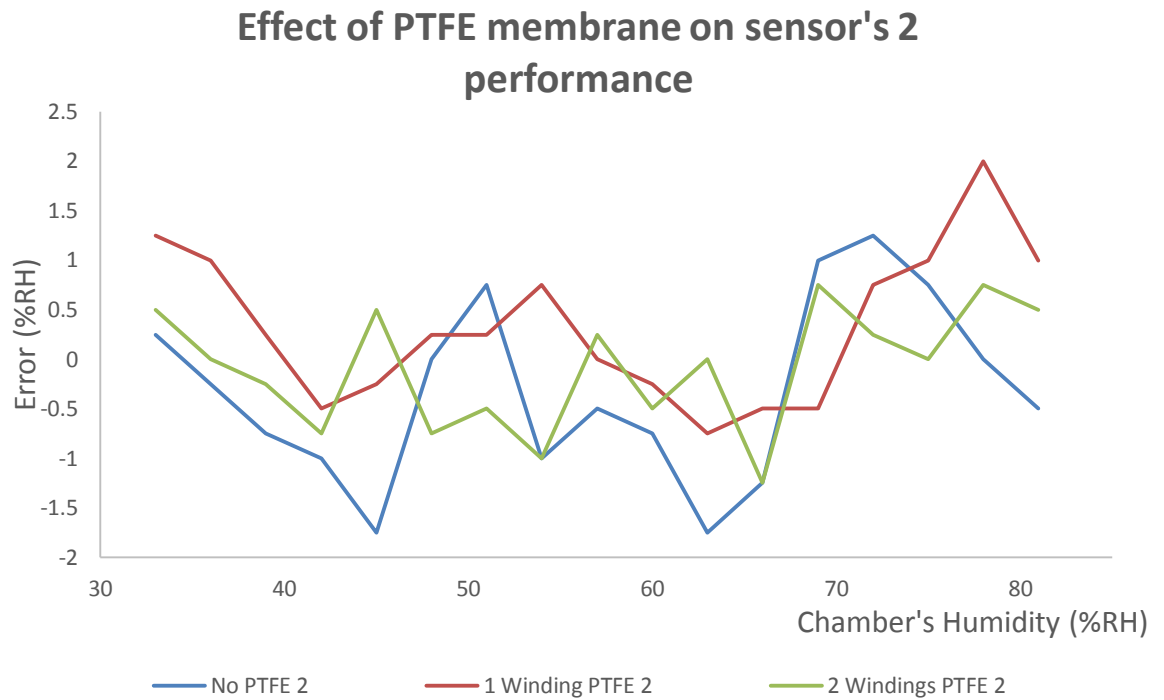


Figure 5-11: Humidity error of the second sensor at various humidity levels for all experiments.

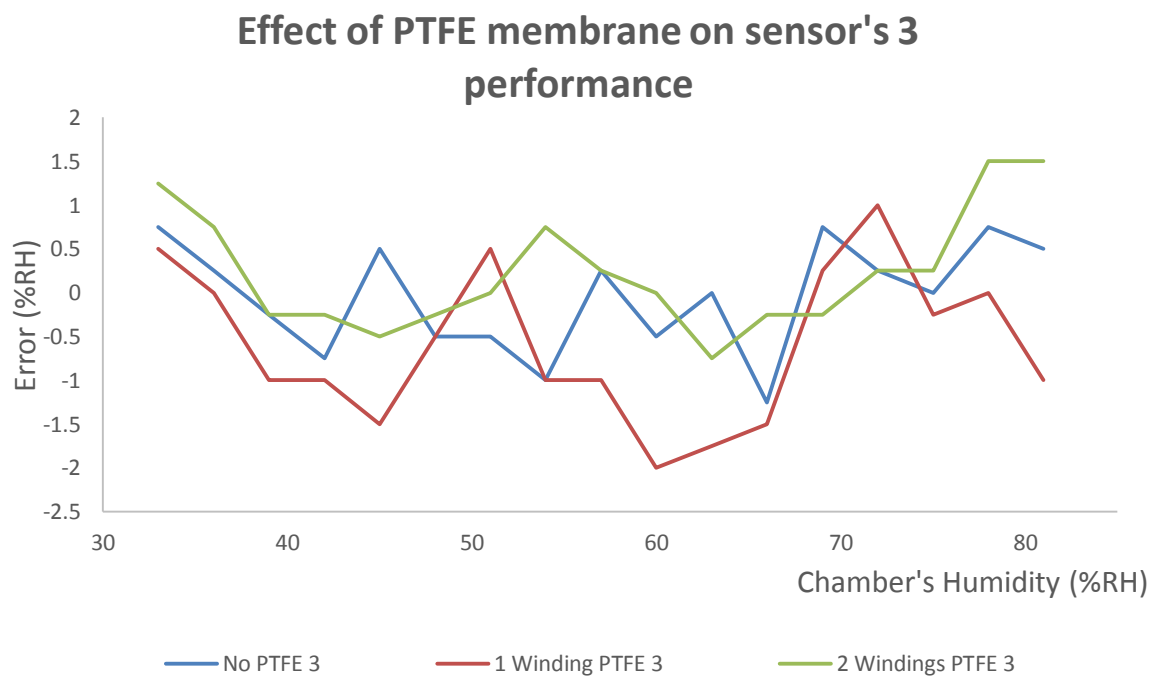


Figure 5-12: Humidity error of the third sensor at various humidity levels for all experiments.

5. Relative Humidity & Temperature Sensor

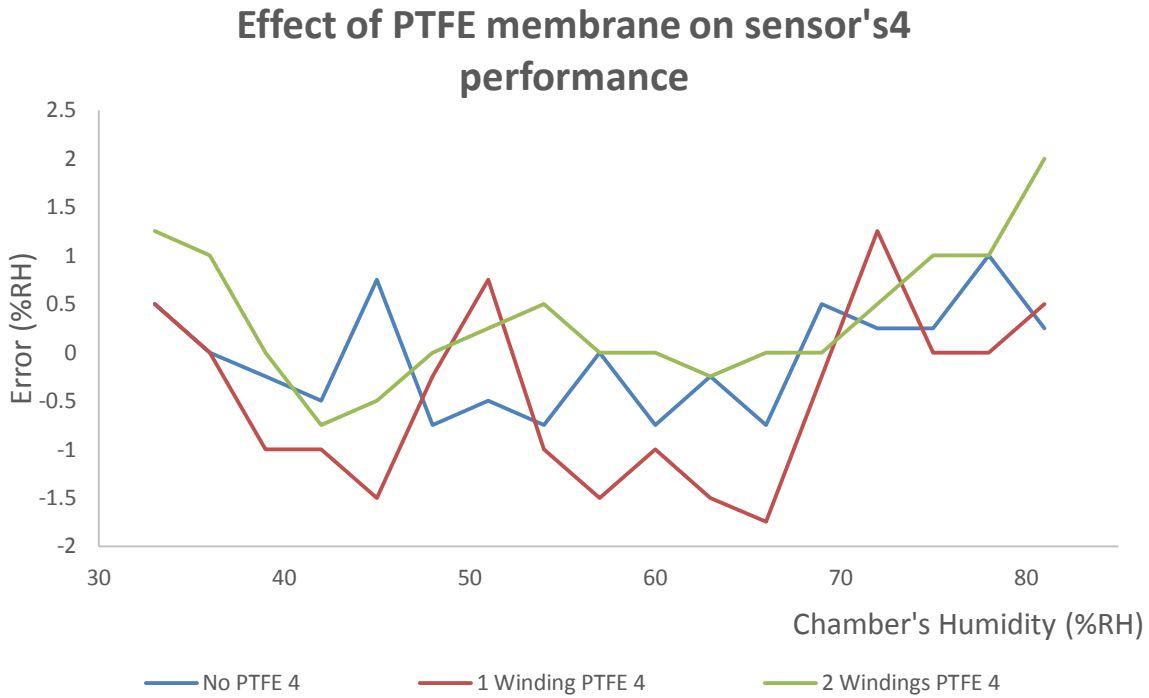


Figure 5-13: Humidity error of the fourth sensor at various humidity levels for all experiments.

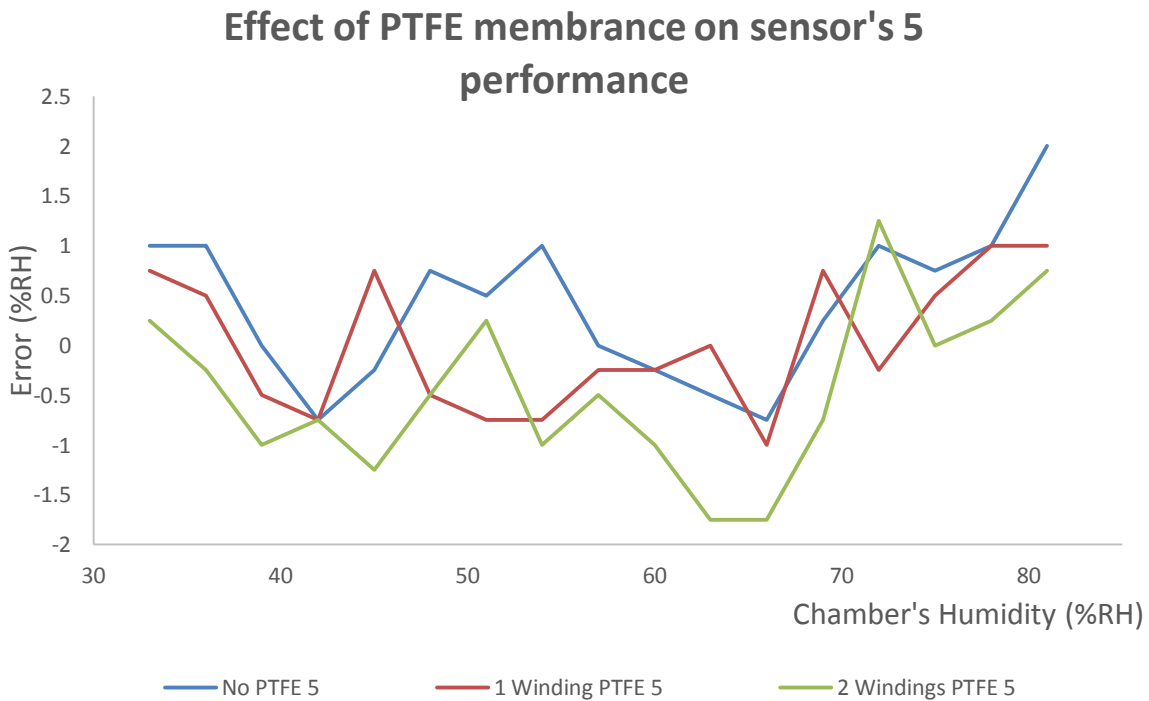


Figure 5-14: Humidity error of the fifth sensor at various humidity levels for all experiments.

Effect of PTFE membrane on sensor's 6 performance

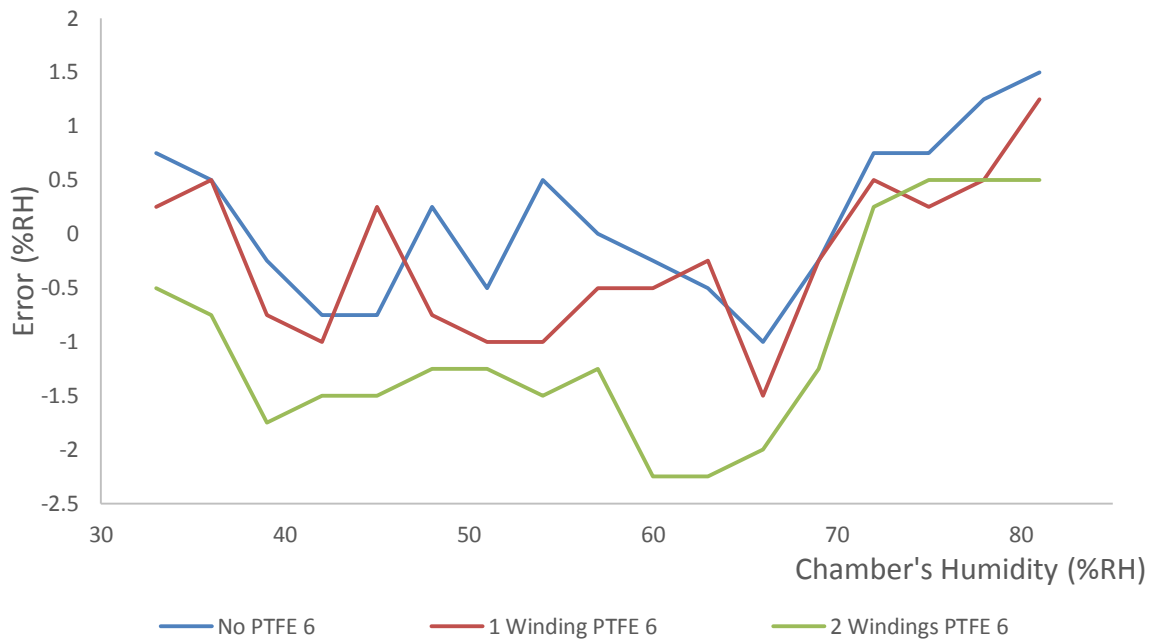


Figure 5-15: Humidity error of the sixth sensor at various humidity levels for all experiments.

From the figures presented above, no obvious trend was recognised and it is believed that the deviations between the sensors are not due to the PTFE membrane but fall in the accuracy range of the sensors or because of the higher than recommended supply voltage.

Chapter 6: **Conductivity Cell**

6.1 Instrumentation

Conductivity measurements were decided to be made using an AC square wave current source that would minimise any polarisation effects but at the same time it would eliminate any phase shift issues if a sinusoidal wave was used. In order to provide the conductivity cell with the correct signal, a printed circuit board (PCB) was designed and fabricated. The PCB was designed to include all the instrumentation required for the rest of the sensors of the existing TF sensor array shown in Figure 6-1 as well as the conductivity cell.

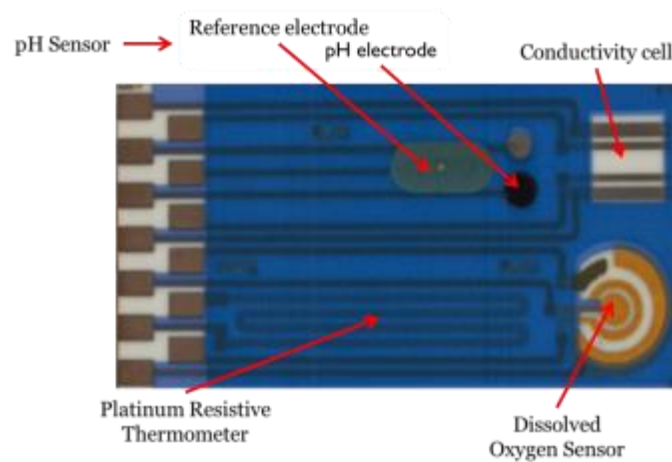


Figure 6-1: Existing TF sensor array

The interface circuits on the PCB have been designed to produce dc voltages that correspond to the real-time measured values of pH, dissolved oxygen, temperature and conductivity in such a way that they can be easily interfaced to a data logger or microprocessor analogue to digital converter. The PCB carries various circuit board jumpers and adjustable components to allow gain setting and offset compensation for easy calibration of the various sensors on the array to allow maximum flexibility of use.

The conductivity sensor interface circuit allows for drive signal frequencies in the range 100 Hz to 5 kHz and also allows varying of the drive current amplitude up to a maximum of 10 mA. Operating frequency, drive current level and gain sensitivity of the detecting

6. Conductivity Cell

amplifier are set by variable resistors on the PCB. The drive current signal used is a simple alternating polarity square wave and the resulting output square wave voltage from the sensor is converted to a single ended dc voltage proportional to conductivity by a multiplexed chopper rectifier circuit, as shown in Figure 6-2. Full details on the PCB circuit are given in Appendix A.

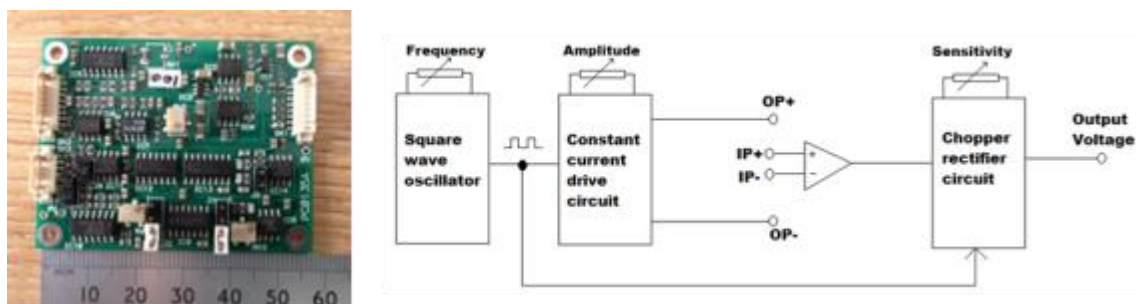


Figure 6-2: Sensor array interface circuit (left), Conductivity circuit block diagram. IP+ and IP- are connected to the voltage measuring electrodes of the cell while OP+ and OP- are connected to the current driving electrodes of the cell (right).

The output of the PCB was connected to a data logger, initially connected to the same data logger used for the pH sensor experiments explained earlier in this chapter. Later experiments were performed using another commercial data logger (Campbell Scientific, CR1000) and all the data were recorded automatically using custom coded software where you can alter the sampling frequency and the measuring range unlike the previous data logger.

6.2 Proposed Cell Geometry & Fabrication

Due to significant issues with variable fringing at different analyte conductivities the cell geometry was changed in a subsequent design to that of the three dimensional model depicted in Figure 6-3, using a supporting structure that was produced on a 3D printer to space two substrates, each carrying three electrodes, facing one another across the volume of analyte to be measured.

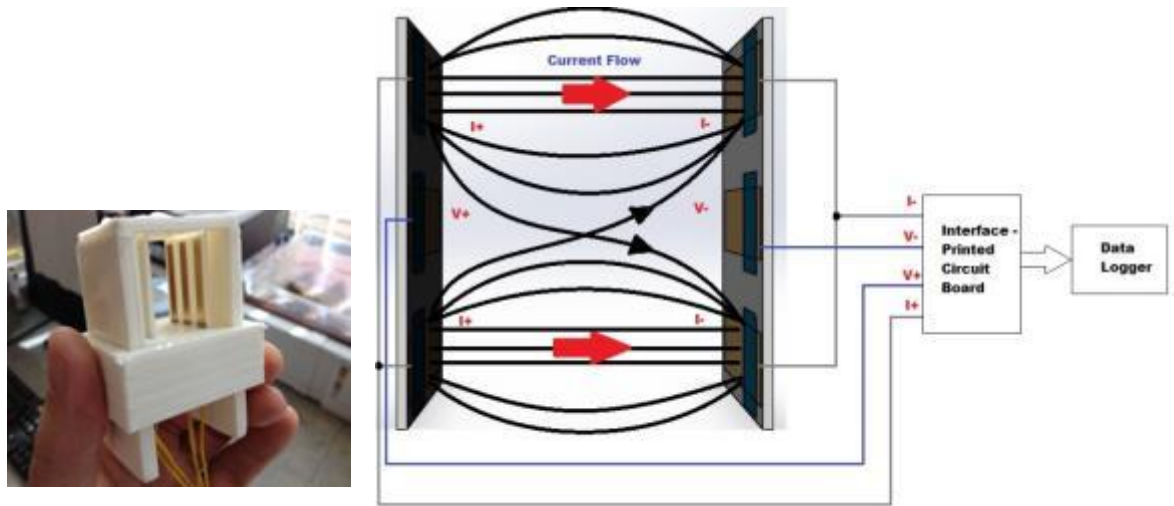


Figure 6-3: Conductivity cell electrode configuration and geometry.

The design of the sensor is such that the drive current is applied across the two outer sets of electrodes, while the resulting potential across the cell is measured by the inner electrode on each substrate. This approach also facilitated the printing of one half of the conductivity cell onto the back of an existing sensor array (Atkinson, et al., 2013) with an identical electrode pattern printed on a second substrate mounted opposite and facing the first. By using this geometry, any fringing will be minimised because of the positioning of the voltage measuring electrodes in between the two oppositely driven outer electrode pairs, additionally any rotation or tilting of the two substrates relative to one another will be cancelled out. In order to decrease the printing cost of the new design the use of gold electrodes, in addition to platinum, was investigated to check for any difference in performance. The electrodes for the new sensor design were screen printed onto 50 mm × 25 mm, 0.625 mm thick, 96% alumina substrates (Coorstech) using stainless steel screens with a mesh count of 250 lines per inch, 15 μm emulsion thickness and a 45° mesh. The screen designs for each layer were produced using AUTOCAD and the screens were manufactured by MCI Cambridge for the Aurel C880 Printer. The first layer deposited was the gold or platinum conductor with rectangular screen mesh openings with dimensions of 4.5 mm × 45 mm. A waterproofing layer with a rectangular shape of 6.5 mm × 14 mm was deposited on top of that; leaving an exposed area of

6. Conductivity Cell

26 mm × 4.5 mm of the underlying gold or platinum to comprise the individual electrodes. The distance between each electrode on the same substrate is approximately 5 mm. A part of the conductor, approximately 5 mm × 4.5 mm, was left exposed at one end for soldering connecting wires. The gold electrodes were printed using 8844 ink (Electro Science) while the platinum electrodes were printed using 5545 ink (Electro Science), on top of which a glass dielectric insulator 4905-C (Electro Science) was deposited to isolate the electrode connection pads from the measurement surface and to expose a precise surface area of the electrodes. All layers were held at room temperature for 10 min after printing to allow relaxation of surface stresses and then dried in a DEK 1209 infrared mini dryer at suitable temperatures. The layers were then cured in a 6 zone belt furnace (BTU VQ41) at temperatures specified by their manufacturer.

6.3 Experimental Work

6.3.1 Solution Experiments - Investigation of frequency and current level effects

The newly designed conductivity cell was tested in KCl solutions of various conductivities of which the conductivities were measured using a commercial conductivity meter and the conductivities were also correlated with KCl concentration versus conductivity graphs from the National Institute of Standards and Technology (NIST) (Shreiner & Pratt, 2004). The temperature of the experiments was also recorded and was maintained at 25 ± 5 °C. In all the experiments, noise levels were seen as spikes with maximum values of lower than ± 9 mV for any point in any experiment. Spikes of that amplitude are expected and arise due to noise from other electrical equipment around the experimental setup as well as the mains. The graphs in this section were plotted using another curve fitting software.

The first set of experiments was performed to identify any frequency effect on the performance of the cell. The cell was immersed in solutions of various conductivities to check if the output voltage from the cell was frequency dependant. This set of experiments also investigated the proportionality of the cell with respect to the input current levels. The same set of frequencies was tested in different solutions and at different current levels. The results of this experiment were recorded using the custom made data logger and were obtained every ten seconds while the test was performed for ten minutes for every parameter to be changed. The distance between the two substrates was 15 mm. The electrolyte conductivities tested are shown in Table 6-1. In every conductivity solution various current levels were tested and for each current level various frequencies were also tested. The current levels and frequencies used are shown also in Table 6-1.

Table 6-1: Electrolyte conductivities, current levels and frequencies for experiment COND.1-Gold-15mm.

Solution No	Conductivity (mS/cm)	No	Current (mA)	No	Frequency (Hz)
1	0.2	1	0.1	1	100
2	0.5	2	0.5	2	200
3	1	3	1	3	400
4	2	4	2	4	700
5	4	5	4	5	1000
				6	2000
				7	3000
				8	4000
				9	5000

Table 6-1 shows the output voltage as a function of 1mA current square wave at different drive frequencies resulting from placing the 15mm spacing gold electrode conductivity sensor in different conductivity test solutions. With slopes of less than $9 \times 10^{-7} \text{V/Hz}$ it can clearly be seen that there is no significant frequency effect on output voltage levels.

6. Conductivity Cell

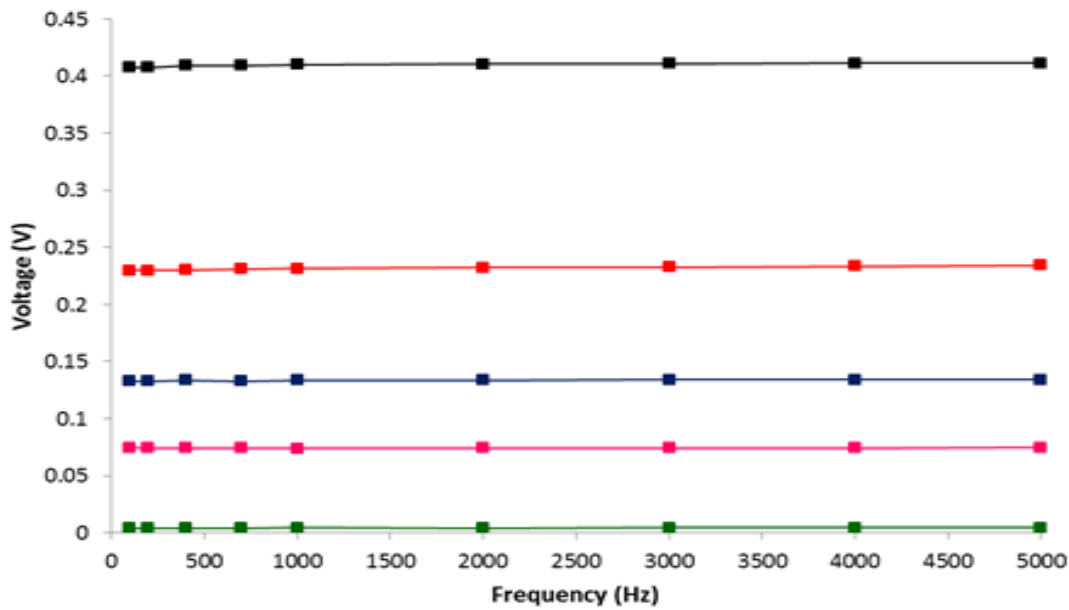


Figure 6-4: 15mm spaced gold electrode conductivity sensor output voltage levels as a function of 1mA square wave current drive frequencies in different conductivity test solutions. (green-4 mS/cm, pink-2 mS/cm, blue-1 mS/cm, red-0.5 mS/cm, black-0.2 mS/cm).

The sensor output voltage was found to be directly proportional to current and highly linear as shown in Figure 6-5, exhibiting linearly increasing slopes in different conductivity test solutions. R^2 values better than 0.9996 were obtained for linear fits to plots of voltage outputs for all combinations of electrode spacing and drive frequencies.

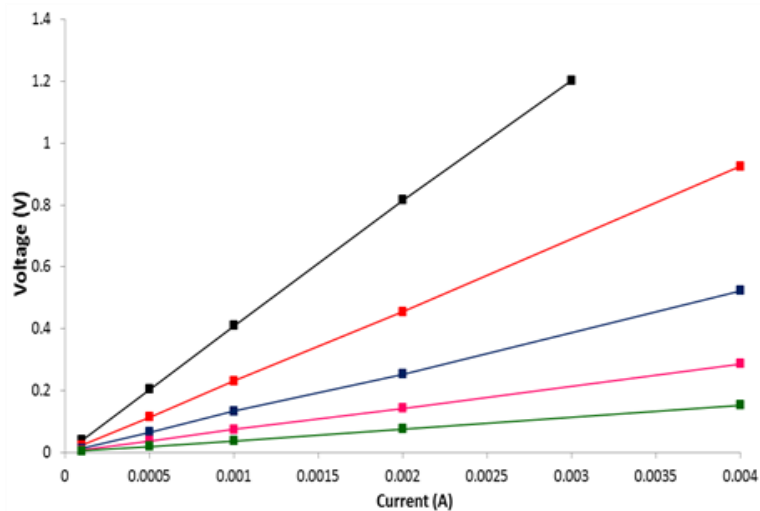


Figure 6-5: 15mm spaced gold electrode conductivity sensor output voltage levels as a function of 1kHz drive current amplitude in different conductivity test solutions. (green-4 mS/cm, pink-2 mS/cm, blue-1 mS/cm, red-0.5 mS/cm, black-0.2 mS/cm).

6.3.2 Solution Experiments - Investigating the effect of the distance between substrates

This second set of experiments was the same as the previous experiment but the distance between the substrates was altered from 15 mm to 20 mm and then 30 mm. This experiment was to identify the relationship between the sensor output and the distance between the substrates. The previous experiment had a very large number of readings and was very time consuming. In order to decrease the duration of the experiment, only three current levels and three frequencies were tested ().

6. Conductivity Cell

Table 6-2: Electrolyte conductivities, current levels and frequencies for experiments COND.2-Gold-20 mm and COND.3-Gold-30 mm.

Solution No	Conductivity (mS/cm)	No	Current (mA)	No	Frequency (Hz)
1	0.2	1	0.5	1	100
2	0.5	2	1	2	1000
3	1	3	2	3	5000
4	2				
5	4				

Experiments for 30 mm spacing, 0.2 and 0.5 mS/cm were performed using the custom made data logger and the recording interval was again 10 seconds. The rest of the experiments were recorded using CR1000 and the recording interval was one second.

Figure 6-6 shows plots of sensor output voltage in different conductivity solutions as a function of electrode spacing driven with 1mA current square wave at a drive frequency of 1kHz. The sensor output voltage was found to be linearly proportional to distance between the substrates with R^2 values of better than 0.99 suggesting that fringing does not depend on the distance between the substrates.

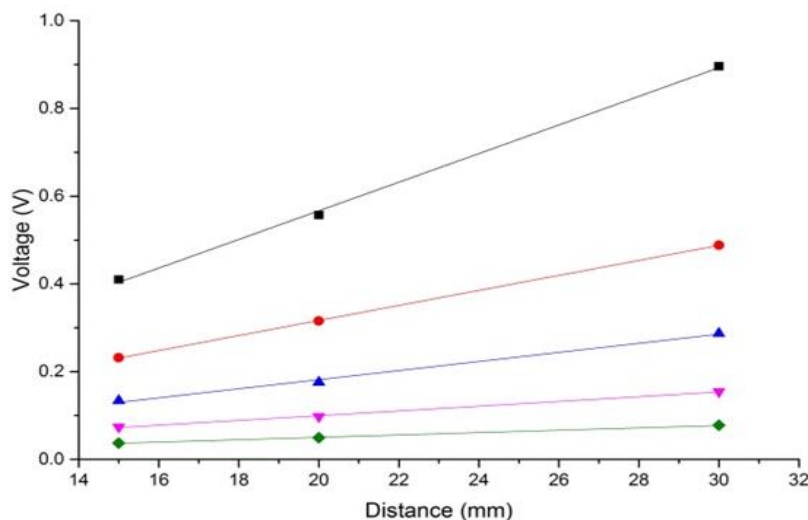


Figure 6-6: Sensor output voltage levels as a function of electrode spacing for 1mA drive current square wave at 1kHz in different conductivity test solutions (green-4 mS/cm, pink-2 mS/cm, blue-1 mS/cm, red-0.5 mS/cm, black-0.2 mS/cm)

6.3.2.1 Solution Experiments - The effect of gold electrodes instead of platinum

This set of experiments was designed and performed to identify any difference in the performance of the cell if gold or platinum was used as the electrode material. The exact same cell was fabricated but instead of gold, a platinum ink was used (Electro Science 5545). Conductivity solutions, current levels and frequencies tested are shown in Table 6-3. A larger spacing was also tested for platinum to see if there is any threshold above which the cell is not performing as expected.

Table 6-3: Electrolyte conductivities, current levels and frequencies for experiments COND.4-Platinum-15 mm, COND.5-Platinum-20 mm and COND.6-Platinum-40 mm.

Solution No	Conductivity (mS/cm)	No	Current (mA)	No	Frequency (Hz)
1	0.2	1	0.5	1	100
2	1	2	1	2	1000
3	4	3	2	3	5000

In order to save time on the experiment, only three conductivity solutions, three current levels and three frequencies were tested. All the readings were recorded using CR1000 and the recording interval was again one second.

Figure 6-7 shows plots of sensor output voltage as a function of electrode spacing for platinum electrodes driven with 1mA current square wave at a drive frequency of 1kHz.

6. Conductivity Cell

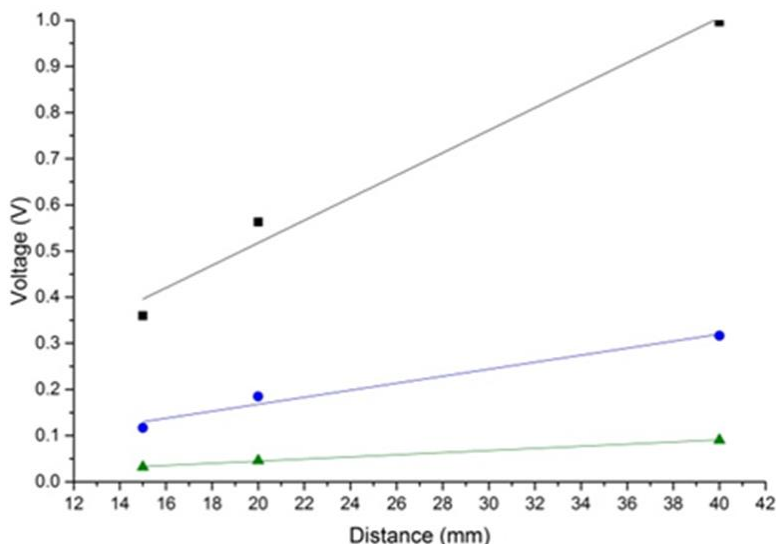


Figure 6-7: Output voltage levels as a function of electrode spacing for 1 mA drive current square wave at 1 kHz in different conductivity test solutions for gold electrode (left) and platinum electrode (right) sensors (green-4 mS/cm, pink-2 mS/cm, blue-1 mS/cm, red-0.5 mS/cm, black-0.2 mS/cm)

The sensor output voltage was found to be linearly proportional to distance with R^2 values for gold of better than 0.99 while for platinum R^2 values were better than 0.95. The sensor with gold electrodes exhibited higher slope factors (A) than those with platinum electrodes but with less than 10 mV/mm difference shown in Table 1. Platinum paste was not pure and contained other metals like copper and iron, which could corrode and change the sensor's performance while gold paste was of very high purity ensuring a more stable performance.

Table 6-4: Values of the constants A and B for linear fit to sensor conductivity response as a function of electrode spacing for gold and platinum electrodes

$V = A * L + B$								
	Gold					Platinum		
	0.2 mS/cm	0.5 mS/cm	1 mS/cm	2 mS/cm	4 mS/cm	0.2 mS/cm	1 mS/cm	4mS/cm
A	0.03262	0.01714	0.01036	0.0054	0.0027	0.02438	0.00759	0.00231
B	-0.0857	-0.02627	0.02562	0.00853	0.00378	0.03003	0.01612	0.00146
R^2	0.99773	0.99988	0.99157	0.99626	0.99706	0.96713	0.95443	0.99816

Graphs of voltage versus resistivity were plotted and the relationship between sensor output and resistivity was obtained as shown below.

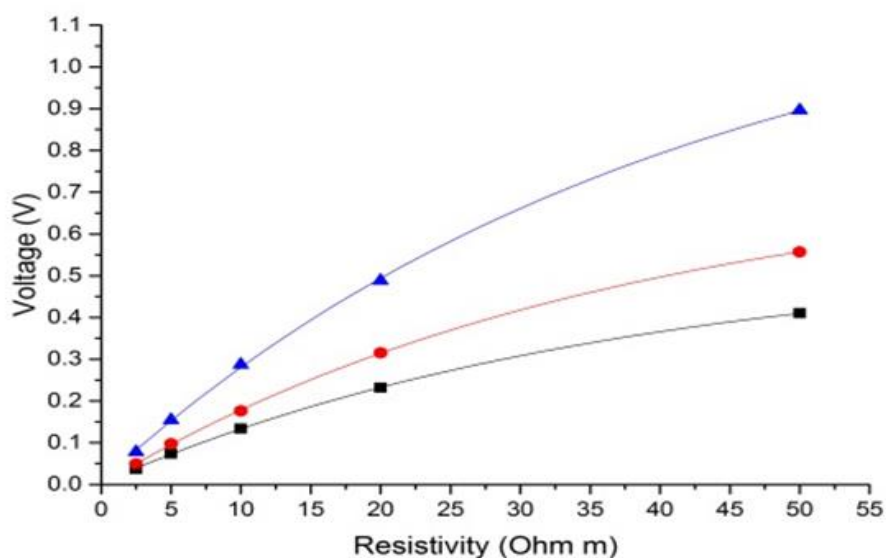


Figure 6-8: Sensor output voltage levels as a function of resistivity in different conductivity test solutions with 1 mA drive current square wave at 1 kHz for different electrode spacing (black-15 mm, red-20 mm, blue-30 mm, purple-40 mm)

Figure 6-8 shows the sensor output voltages as a function of resistivity for different electrode spacing. It was observed that the relationship between voltage and resistivity is of the form:

$$V = A \cdot \exp(-\rho/B) + V_0 \quad \text{Eqn. (36)}$$

with R^2 values better than 0.999 being obtained for both gold and platinum electrode types. Values of the constants A and B for different electrode spacing are as shown in Table 6-5 as well as expressions for the calculated cell constant for each distance.

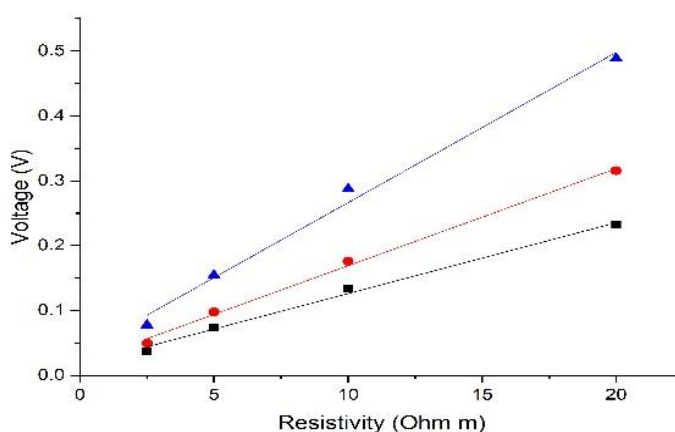
Table 6-5: Calculated cell constant expressions for gold electrodes

$dR/d\rho = -(A/(I \cdot B)) \cdot \exp(-\rho/B)$			
	15 mm	20 mm	30 mm
A	-0.54777	-0.75185	-1.26085
B	36.79427	37.08662	41.07856
Cell Constant (m^{-1})	$14.89 \cdot \exp(-\rho/36.79)$	$20.27 \cdot \exp(-\rho/37.09)$	$30.69 \cdot \exp(-\rho/41.08)$
R^2	0.99988	0.99985	0.99951

6. Conductivity Cell

This non-linearity in the cell constant is due to fringing of the electric field in low conductivity solutions, below approximately 0.5 mS/cm.

Figure 6-9 shows the detail of the sensor output voltage versus resistivity plot for gold electrodes with 1 mA drive current at 1 kHz over the range 2 to 20 Ω m, where an approximately linear relationship can be observed with R^2 values better than 0.988. Values of cell constant for various gold electrode spacing are as shown in Table 3.



$V = A \cdot \rho + B$			
	15 mm	20 mm	30 mm
A	0.01093	0.015	0.02315
B	0.01663	0.0189	0.03479
R^2	0.99134	0.99543	0.98808

Figure 6-9: Output voltage levels as a function of resistivity with 1 mA drive current square wave at 1 kHz for gold electrode sensors for different electrode spacing (black-15 mm, red-20 mm, blue-30 mm) & values of the constants A and B for linear fit to electrode response at different electrode spacing.

Figure 6-10 shows the sensor outputs for platinum electrodes as a function of resistivity.

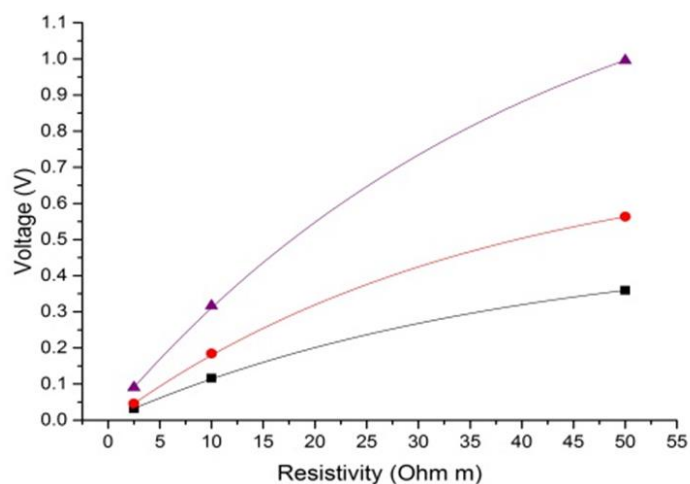


Figure 6-10: Output voltage levels as a function of resistivity with 1 mA drive current square wave at 1 kHz for gold (left) and platinum (right) electrode sensors for different electrode spacing in different conductivity test solutions (black-15 mm, red-20 mm, blue-30 mm, purple-40 mm)

It can be seen that the relationship between voltage and resistivity is of the form $V = A \cdot \exp(-\rho/B) + V_0$ with R^2 values are better than 0.999 for both gold and platinum electrode types. Values of the constants A and B for different electrode spacing for both gold and platinum electrodes are as shown in Table 6-6. This apparent non-linearity in the cell constant is the result of fringing of the electric field in low conductivity solutions, i.e. below approximately 0.5 mS/cm.

Table 6-6: Values of the constants A and B for different electrode spacing for gold and platinum electrodes

	$V = A \cdot \exp(-\rho/B) + V_0$					
	Gold			Platinum		
	15 mm	20 mm	30 mm	15 mm	20 mm	40 mm
V_0	0.55054	0.75259	1.26855	0.49405	0.7456	1.41958
A	-0.54777	-0.75185	-1.26085	-0.49264	-0.75122	-1.41142
B	36.79427	37.08662	41.07856	38.56012	35.33241	41.52998
R^2	0.99988	0.99985	0.99951	1	1	1

Chapter 7: **Soil Rig**

7.1 Soil Columns for Multi-sensor Arrays

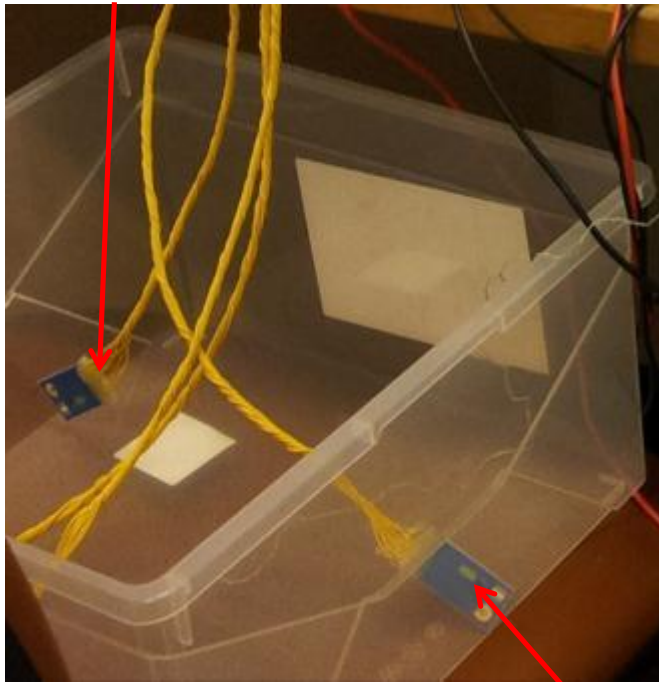
Since the final application of the sensors will be underground, an experimental rig has been designed to mimic the real life environment for the sensor. It has been explained earlier that all sensors are to be printed onto a single TF substrate and therefore printed substrates from previous work have been used to test the sensors and their interface with the data logger. In the field a CR1000 Campbell Scientific data logger will be used but in the lab the same data logger used for the pH sensor tests was to be used. The previously prepared TF sensor is shown in Figure 6-1 where a conductivity sensor is also printed. The conductivity sensor was not used at all in this set of experiments but it is the subject of investigation of experiments described later in this chapter. On the substrate, a platinum electrode was printed as a redox sensor but for these experiments it was not used.

Humidity and temperature sensors (SHT21S) were also used to back up the platinum resistive thermometer and to check if the humidity reading could be correlated with the water content in the soil. In these experiments, the SHT21S sensors were covered with a manufacturer provided waterproof PTFE cap which was attached to the substrate using the hot glue gun.

All sensors had their connections waterproofed using the hot glue gun as shown in Figure 7-1.

7. Soil Rig

Waterproofed
connections



TF Sensor

Figure 7-1: TF substrate with waterproofed soldered connections before installing them in the soil columns

7.1.1 1st Soil Columns Design

The experimental rig was made up of two PVC pipes of 7.5 cm in diameter and 60 cm in length which were placed vertically in a closed plastic box to hold them in that position and prevent any fluid spilling on the electronic circuit. The bottom of the pipes was sealed with tape and holes were made in the tape for the fluids to flow out. Then, two 3 cm holes were drilled in the pipes at different points on the pipe with 30 cm space difference. The holes were drilled to insert the sensors in the pipes and the hole was sealed with plasticine. Two different types of soil were used to fill up the two pipes, sand and top soil. Sand is mainly silicon oxide which is almost unreactive to anything while top soil is enriched with various substances to help the flora growth. In that way, a comparison could be made and the performance of the sensors in different soils could be tested. At the bottom of the plastic box another hole was drilled and a drainage pipe was installed. The box was then

tilted slightly making a slope for the fluids to flow out of the drainage pipe which was directly pointed in the sink. Figure 7-2 below shows the experimental test rig before the sensors were inserted.

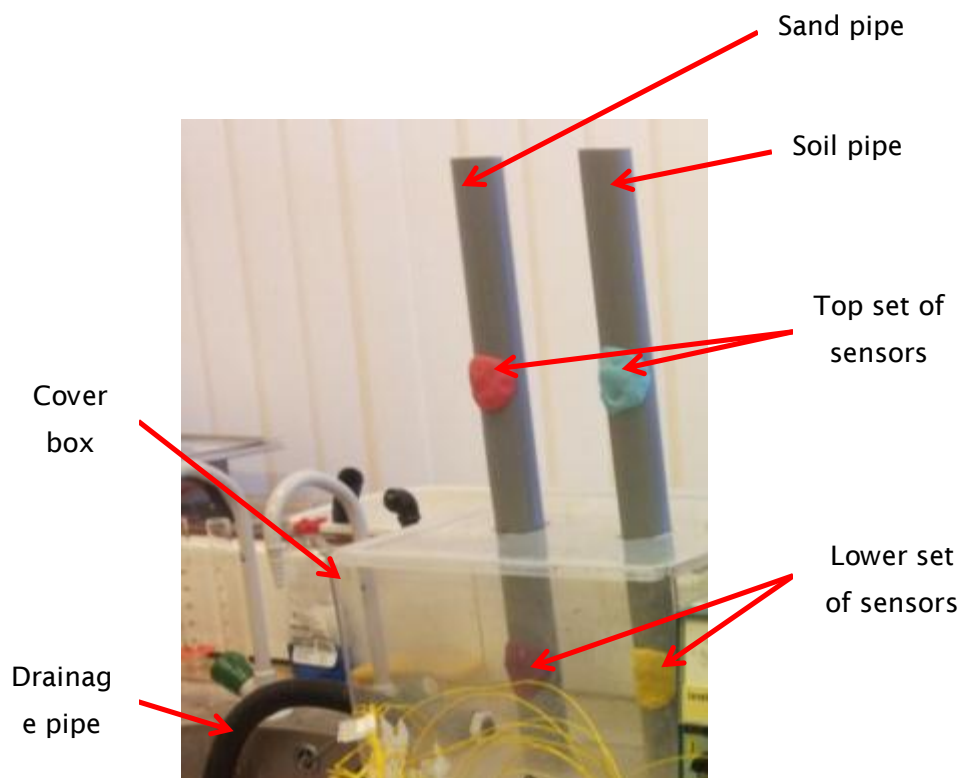


Figure 7-2: Experimental rig before the sensors were installed.

The next step was to insert the sensors in the pipes in an approximately 45° angle in order for the fluid to flow away from the sensor but still allowing enough time for the sensor to get the readings. Figure 7-3 below shows the rig after the sensors were inserted in the pipes and also shows the electronic circuits prepared to be able to get the readings from the various sensors using the same data logger used for the pH sensor experiments.

7. Soil Rig

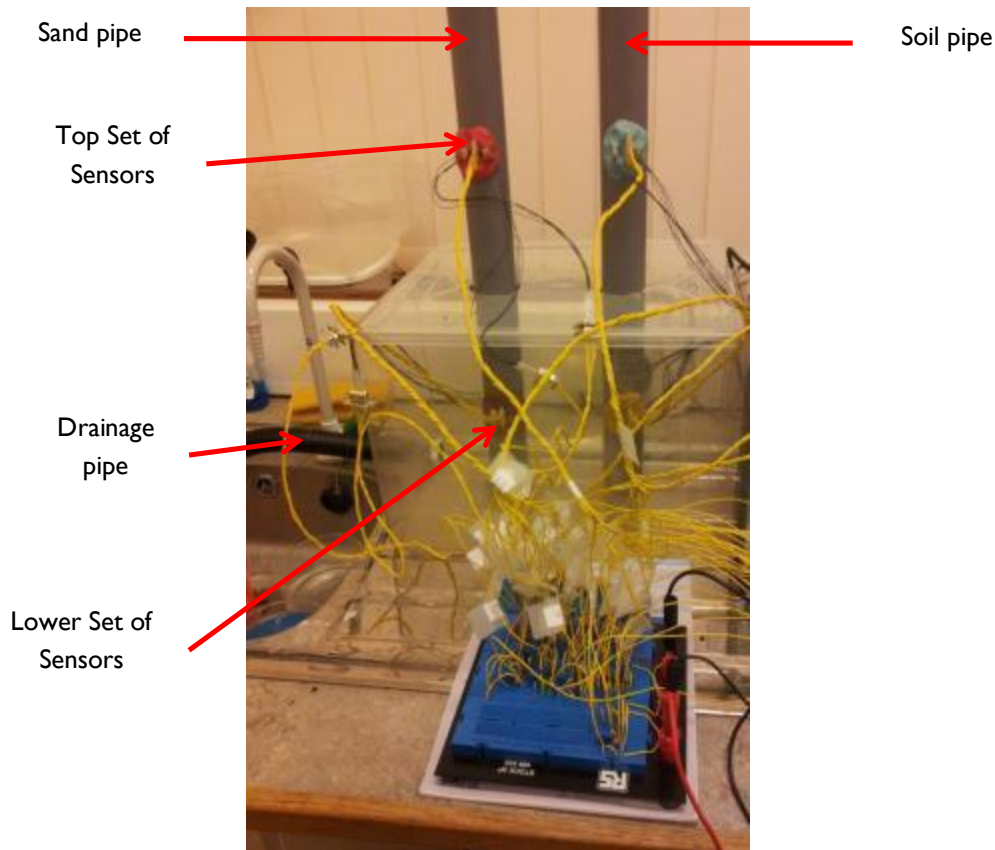


Figure 7-3: Experimental rig after the sensors were installed including the interface on the prototype board.

Since the interface is required for the sensors to operate and also some sensors require power supply, a dual DC power supply was used to power the amplifiers of the circuit and another single DC power supply for the SHT21S since the power supply range of SHT21S was lower than the power supply range of the amplifiers. Figure 7-4 below shows the final design of the experimental rig including the power supplies, the data logger and the computer used to acquire and save the data.

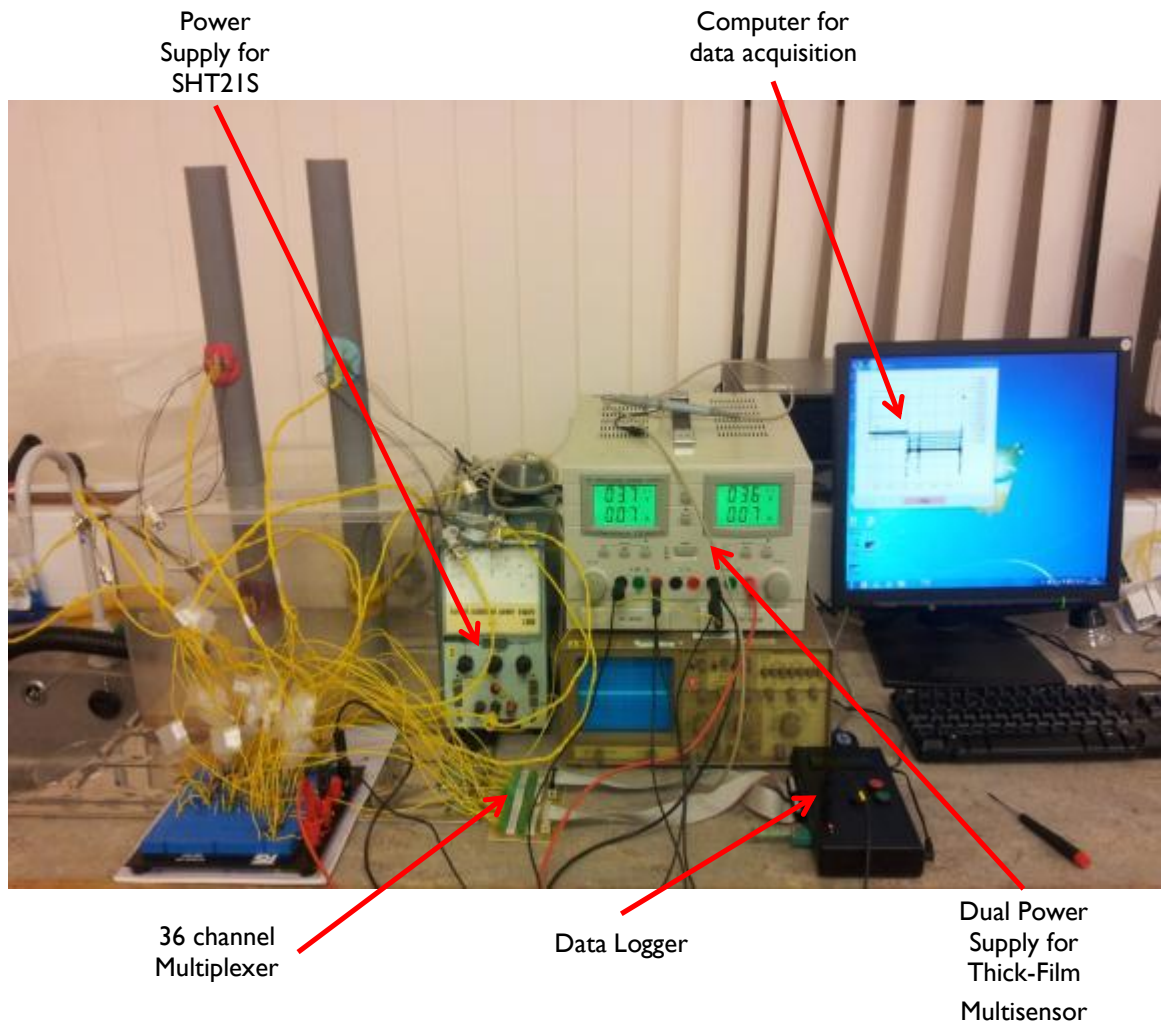


Figure 7-4: A photo of the complete experimental rig with the power supplies, the data logger and the computer used to run the software.

For the experimental rig shown previously, initial experiments were to be performed using the same data logger as before. Although in the field the data logger to be used will be different the instrumentation was designed for the laboratory data logger with the plan that it will be adjusted when a field data logger will be purchased for use in the laboratory. The main difference between the two data loggers is that the one already owned in the laboratory has only one reference point with a multiplexer of 36 channels, all being measured against the same reference point. The data logger to be used in the field (Cambell Scientific CR1000) has channels with a reference point for every single channel. In that case, the interface design needs to be slightly modified.

7. Soil Rig

The interface circuit for the pH sensor, a combination of a Ag/AgCl RE and a Ruthenium Oxide ISE, was the first to be constructed. For a pH sensor, the potential difference between the two electrodes is to be measured but that voltage has to be measured against the 0 V of the power supply which is connected to the reference point of the data logger. Therefore, a single output was required from the interface to connect to the logger.

An instrumentation amplifier was used (INA121) on a prototype board and was powered to ± 3.6 V. Both power supply wires were connected in parallel with a 0.1 μ F capacitor to reduce any noise in the power supply signal. The reference pin of the amplifier was connected to the 0 V of the power supply which means keeping the same reference point for the data logger too. The output pin of the amplifier was connected to a low pass filter of a 150 k Ω resistor and a 1 μ F capacitor in parallel. The CR filter connected to the output was introduced to reduce noise.

The INA121 instrumentation amplifier has two pins where a resistor can be placed in between, which can set the gain depending on the resistor's resistance. The equation to calculate the gain is given in the data sheet of the amplifier. In this case, since the change for every pH unit is ~ 60 mV, for 14 units it will give a change of approximately 850 mV. Taking the worst case that the electrodes will have an initial offset then the change of 14 units will lead to 1 V change but if the gain is set to 2 then the change will be close to 2 V which approaches the saturation point of the amplifier when operated at ± 3.6 V. The reason 3.6 V supplies were chosen was to keep the supply current as low as possible. The two electrodes were connected to the amplifier as shown in Figure 7-5 with a 1 M Ω resistor connected in parallel to the ground to allow for bias current of the amplifier. pH sensing is potentiometric and therefore ideally there shouldn't be any current flowing through the electrodes and that's why high value resistors were used.

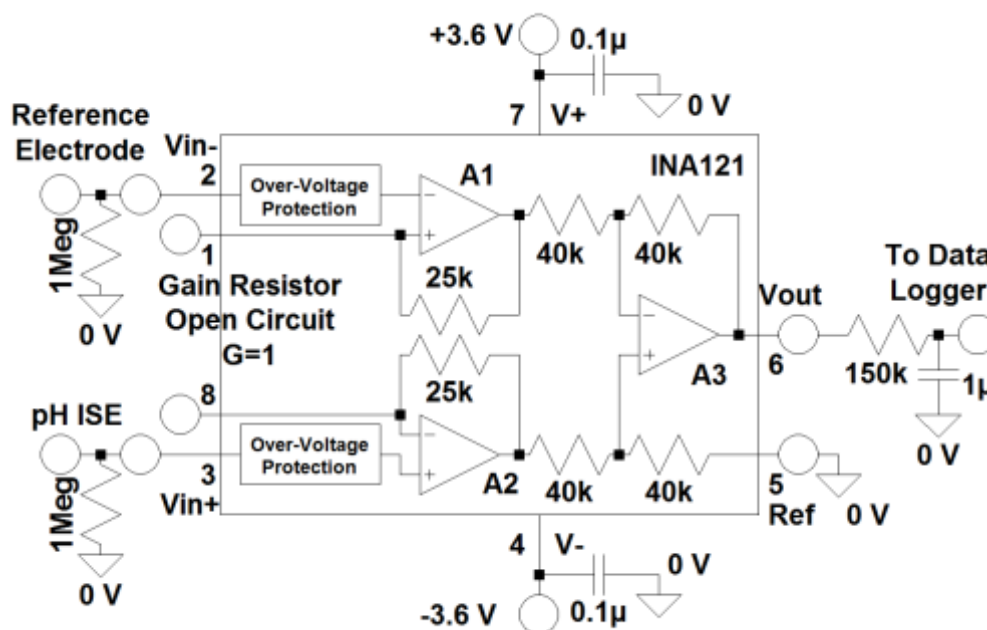


Figure 7-5: Electronic circuit used for the pH sensor.

The dissolved oxygen sensor interface was mainly the circuitry required for the sensor to operate. A TL074 chip was used which contains four individual operational amplifiers. In order to use just one power supply for all the amplifiers, the chip was powered using ± 3.6 V.

Based on previous work (Glasspool & Atkinson, 1998), the oxygen sensor performs best when the reference electrode is set to 0.8 V. A potential divider was used using the two resistors of 56 k Ω and 15 k Ω to set the input voltage of the first amplifier to 0.8 V and based on the rule suggesting that in the feedback arrangement shown the two inputs of the amplifier need to have the same potential, the reference electrode connected to amplifier 4 is also forced to 0.8 V. As shown in Figure 7-6, the working electrode is held at 0 V by the virtual earth of amplifier 3 and since no current can flow through the amplifier, any current flowing between the reference electrode and the working electrode has to pass through that 150 k Ω resistor generating a voltage to be measured from the data logger versus the 0 V of the power supply. The guard electrode is held at 0 V to prevent lateral diffusion of O₂ beneath the sensors' membrane.

7. Soil Rig

Previous investigation (Glasspool & Atkinson, 1998) suggests a slope of approximately $-2 \mu\text{A/ppm O}_2$, which will give a sensitivity of approximately -0.3 V/ppm O_2 with the $150 \text{ k}\Omega$ resistor used.

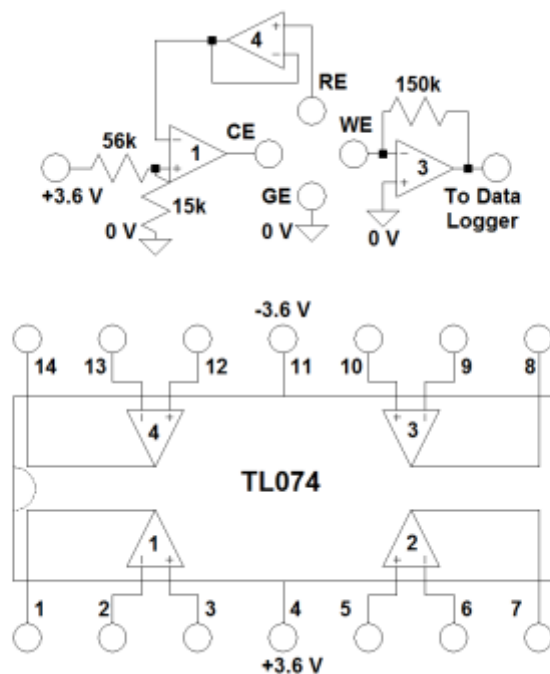


Figure 7-6: Electronic circuit used for the dissolved oxygen sensor.

The idea of a platinum resistive thermometer is very simple and very well established but the interface of a TF PRT is not that straight forward due to the low resistance value of the thermometer. The same power supplies were used to power the instrumentation amplifier with a similar configuration as before.

In the case of PRT, the temperature coefficient of resistance (TCR) for platinum is $\sim 0.004 \Omega/\Omega/^\circ\text{C}$. In Figure 7-7, the circuit diagram shows how the TF PRT is connected to the amplifier. The reason for connecting the PRT in series with a 390Ω resistor is to set the initial input to approximately zero since the resistance of the TF PRT at 0°C is approximately 390Ω . Every TF PRT has a slightly different total resistance and that is why a variable resistor was connected to the INA121 reference pin to change the reference voltage and set the voltage output to zero at approximately 27°C . In this arrangement the PRT will measure the temperature change from 27°C allowing for a

temperature range of -15 to approximately 50 °C covering the whole range of atmospheric temperatures. The calibrating temperature will always be in the middle of the operating range using this interface. The gain resistor was a 10 kΩ resistor setting the gain to 6.

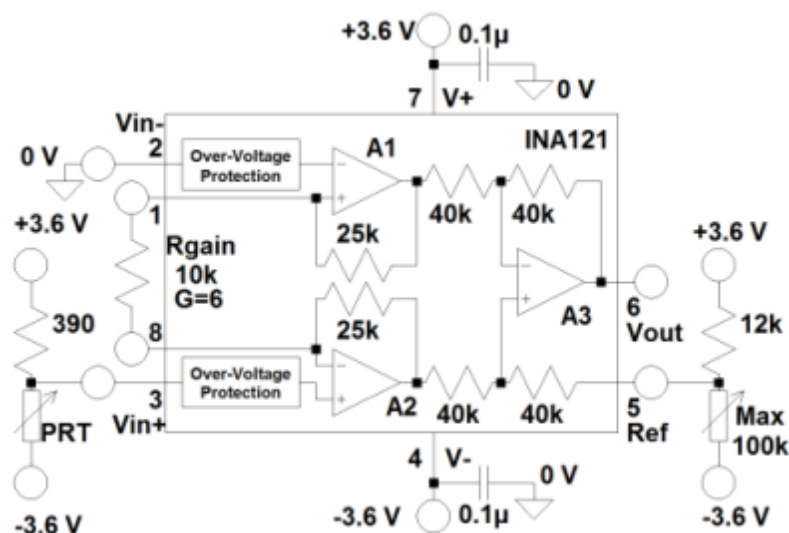


Figure 7-7: Electronic circuit used for the PRT.

All the circuit design calculations are shown below:

$$TCR = \frac{R_T - R_0}{TR_0} = 0.004 \Omega/\Omega/^\circ\text{C} \quad \text{Eqn. (37)}$$

$$R_{20} = \sim 410 \Omega \quad \text{Eqn. (38)}$$

$$\Rightarrow R_0 = \sim 380 \Omega \quad \text{Eqn. (39)}$$

$$V_O = V_S \left(\frac{R_{PRT}}{R_{PRT} + 390} \right) \quad \text{Eqn. (40)}$$

$$V_O = V_S \left(\frac{R_{PRT} + dR}{R_{PRT} + dR + 390} \right) \quad \text{Eqn. (41)}$$

$$\frac{\Delta V_O}{V_S} = \frac{R_{PRT} + dR}{390 + R_{PRT} + dR} - \frac{R_{PRT}}{390 + R_{PRT}} \quad \text{Eqn. (42)}$$

$$\text{IF } R_{PRT} = \sim 390 \Omega \Rightarrow \frac{\Delta V_O}{V_S} = \frac{dR}{4R_{PRT} + 2dR} \quad \text{Eqn. (43)}$$

7. Soil Rig

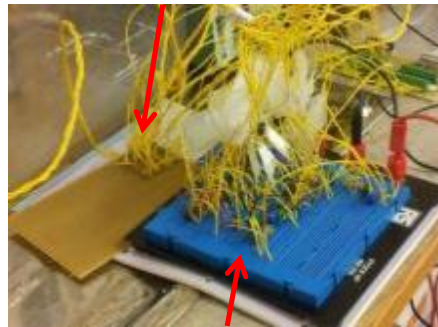
$$2dR \ll 4R_{PRT} \Rightarrow \frac{\Delta V_O}{V_S} = \frac{dR}{4R_{PRT}} \quad \text{Eqn. (44)}$$

$$\Rightarrow V_O = V_S \left(\frac{TCR}{4} \right) = 7.2 \left(\frac{0.004}{4} \right) = 7.2 \frac{mV}{^\circ C} \quad \text{Eqn. (45)}$$

$$IF G = 6 \Rightarrow \text{Sensitivity} = \sim 43.2 \text{ mV}/^\circ C \quad \text{Eqn. (46)}$$

The final stage of the interface with all the circuits for 4 TF sensors and 8 SHT21S (4 measuring temperature and 4 measuring humidity) is shown in Figure 7-8. SHT21S interface was moved to a veroboard due to unreliability of the circuit and also making it easier to move.

Veroboard used for SHT21S



Prototype Board used for Thick-Film Multi-sensor

Figure 7-8: Final stage of the interface with the sensors connected.

7.2 Experimental Work

7.2.1 Investigation of sensor array performance in solutions

Initial experiments (SOIL.1-pH Buffers) were performed in solutions to first test the electrical connections of the interface and the electrodes and to make sure that everything was operating as expected. In this set of experiments, the TF sensor array was connected to the interface and tested in pH buffers (pH 4 and pH 10 buffers) and the dissolved oxygen sensor was tested in the same pH buffers where air was pumped using a fish tank pump to saturate the water with oxygen.

The results are shown in Figure 7-9 for the oxygen sensor and in Figure 7-10 for the pH sensor.

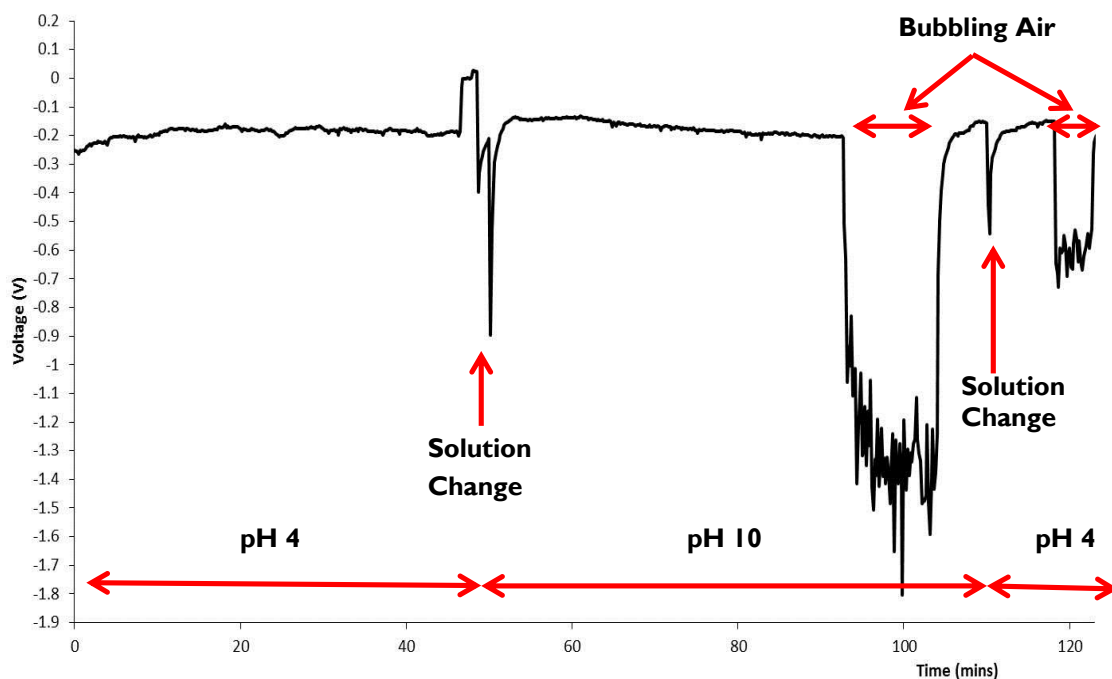


Figure 7-9: Performance of the dissolved oxygen sensor in aqueous solutions.

The TF sensor was immersed in pH buffers of pH 4 and pH 10 and the oxygen level was changed to test the oxygen sensor's performance in different solutions. The first solution was pH 4 buffer as shown in Figure 7-9 and the sensor output was showing an initial dissolved oxygen concentration of approximately 1 ppm O_2 which is in the appropriate level of pH buffers. Then, the solution was changed to pH 10 buffer with the potential of the sensor to remain the same as expected showing no susceptibility to the different pH buffers. Air was bubbled through the solution using a simple air pump and the sensor's output moved to somewhere in the range of 5 ppm O_2 . Water can reach a maximum of approximately 8 ppm O_2 when it is air saturated. In this case, because the air pump would only pump air at a single point, the dissolved oxygen level was not uniform and bubbles were surrounding the sensor causing the very noisy signal observed. The reason the sensor only read 5 ppm O_2 might be due to a reaction between the pH buffer and oxygen decreasing the dissolved oxygen level in the solution.

7. Soil Rig

The pH buffer was then changed to pH 4 and air was also bubbled through the solution. In this case, the sensor read approximately 2 ppm O₂ and that can also be explained from the high probability of pH buffer reacting with the pumped air affecting the dissolved oxygen level.

Figure 7-10 below shows the response of the pH sensor in the same experiment at the same time. The sensor's potential in pH 4 buffer is approximately 285 mV and it drops to -80 mV in pH 10 buffer. That suggests a sensitivity of -60.8 mV/pH, which is very close to the theoretical Nernstian response. The experiment suggests that both sensors operate normally and as expected in aqueous solutions and that the pH sensor is not affected by the bubbled air at all.

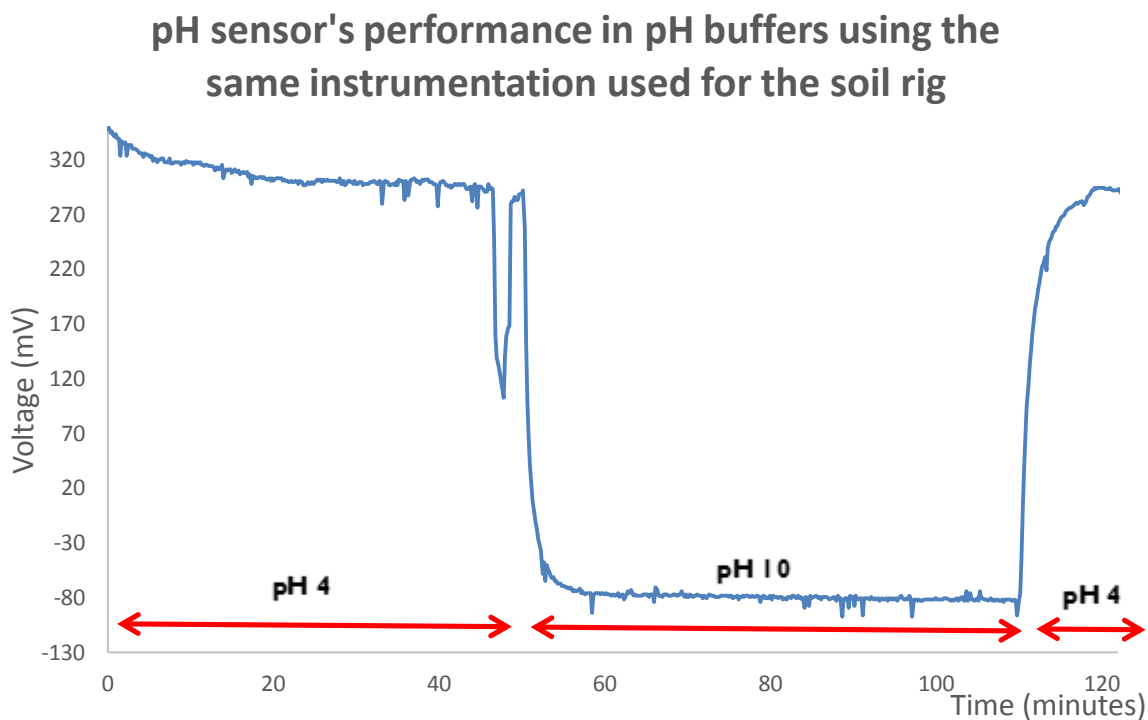


Figure 7-10: Performance of the pH sensor in pH buffers using the same instrumentation.

7.2.2 Investigation of sensor array in soil pipes

After the experiment in solution has successfully shown that the instrumentation and the sensors were operating as expected, the sensor array was inserted directly in the soil pipes as explained earlier. In this

experiment (SOIL.2-Pipes-pH Buffers), pH buffers 4 and 7 were flushed through the soil pipes several times and the sensor output was recorded. In these experiments, SHT21Ss were also used and their performance was investigated simultaneously with the rest of the sensors.

In Figure 7-11, the humidity recorded from the SHT21S is plotted against time. Surprisingly, the sensors indicated a more than 100% RH which is physically impossible but after checking the specifications of the sensors, if the sensor is placed for some time in extreme conditions of more than 95% RH then an offset of 3-4% RH is observed which is what is shown on the graph. It is also possible that the sensor is short circuited due to possible leakage of water under the waterproof layer. That was contrasted by the performance of the SHT21S temperature sensors which provided accurate results.

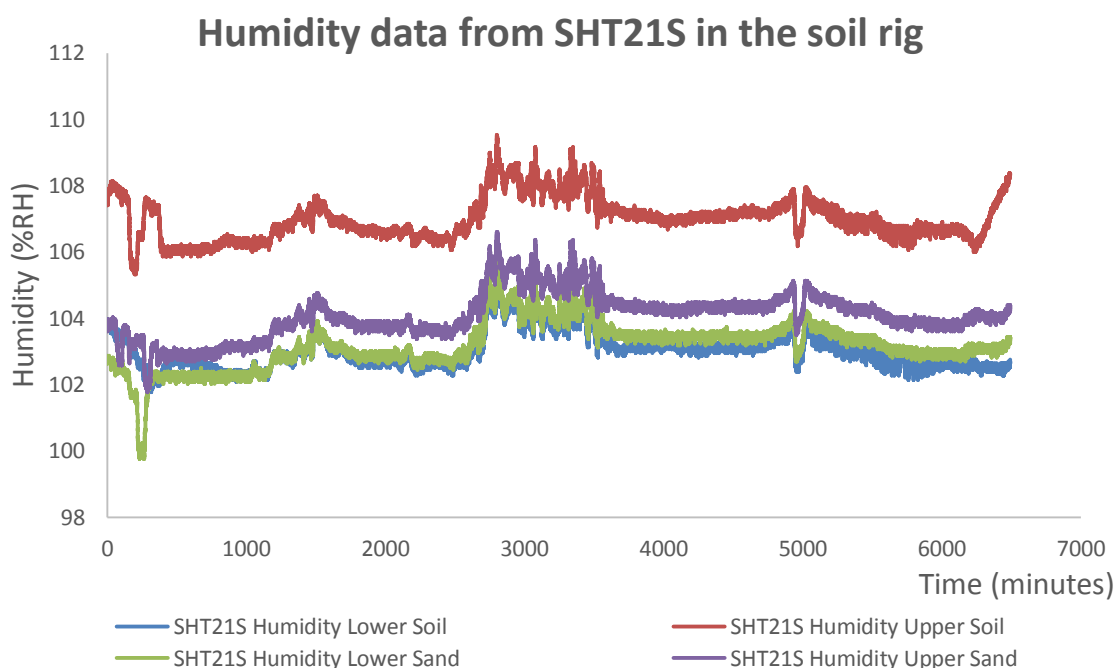


Figure 7-11: Humidity readings from SHT21S in the pipes.

In Figure 7-12, the temperature recorded from the SHT21S sensors is plotted against time providing normal results which were also tested using a thermometer in the room where the experiments were taking place.

7. Soil Rig

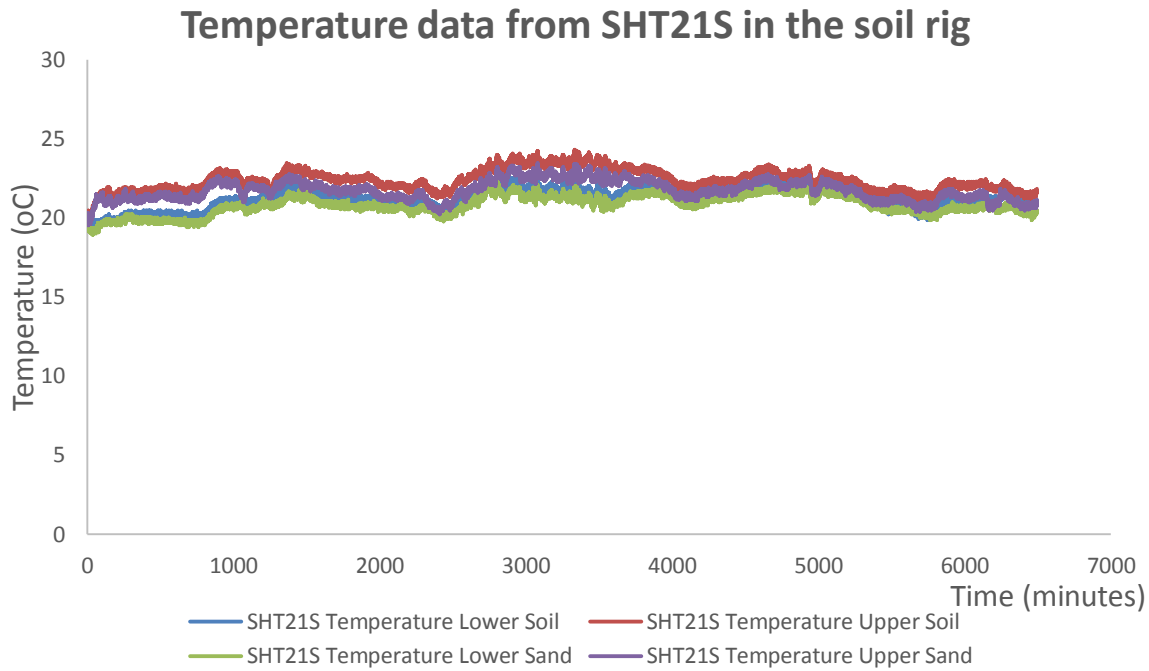


Figure 7-12: Temperature readings from SHT21S in the pipes.

After plotting the results from the PRT sensor, the performance of the 2 temperature sensors were compared and there was only a very small offset between them which could easily be due to not accurately calibrating the electronic circuit for the PRT. These results suggest that the PRT sensor is reliable for use in this application and it also has the advantage of not requiring waterproofing since it is included on the TF substrate at very little incremental cost to the sensor design.

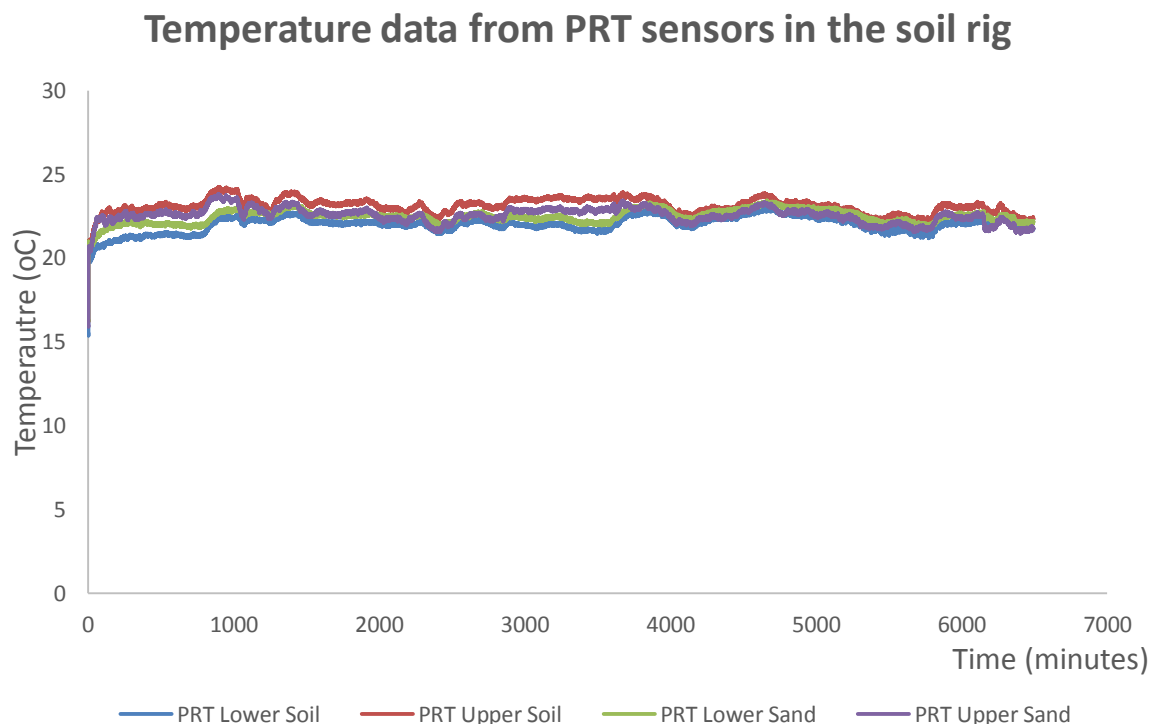


Figure 7-13: Temperature readings from PRT in the pipes from the same experiment.

The next set of experiments was performed with deionised water and 0.125 M ascorbic acid (vitamin C) with an approximate pH value of 3.5. Vitamin C is also used as an oxygen scavenger in boilers to reduce the dissolved oxygen level increasing the lifetime of the boiler. The idea was to use a solution that simultaneously alters the pH and the dissolved oxygen level of the solution-soil mixture. The experiment started on the first day flushing deionised water down the pipes for approximately 440 minutes. The next day the experiment was restarted using 0.125 M vitamin C for approximately 250 minutes. The combination of the results of the two experiments was plotted on graphs of the investigating parameter against time.

7. Soil Rig

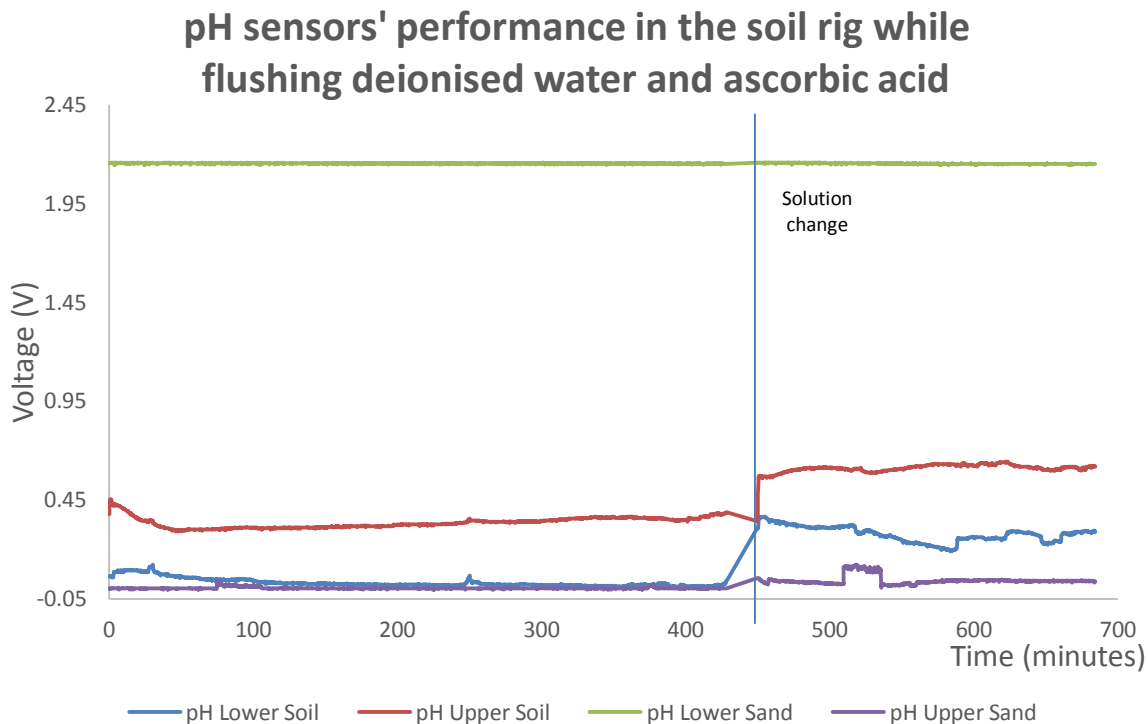


Figure 7-14: pH sensors' performance at room temperature for the experiment using deionised water and ascorbic acid.

Figure 7-14 shows the performance of the TF pH sensors in the two pipes. It is quite obvious that one of the sensors (bottom sand) is giving an extremely high voltage which is most probably the saturation point of the amplifier used and that is most probably due to a bad connection of the sensor to the prototype board. This by itself suggests an unreliability of the prototype board and a more reliable type of interface being required. The next interesting point from the graph is that the higher sensor in sand shows almost no change to the pH while a small peak around the 520th minute is observed. This could be explained again by a bad connection or even suggesting that there is not enough time for the sensor to interact with the solution before it runs out of the pipe. The two pH sensors used in top soil showed a change of approximately 220 mV which can be translated using a sensitivity of 60 mV/pH to a pH change of 3.6 pH units giving a pH value of 3.4 for vitamin C. What is interesting is the offset observed between the pH sensors although their sensitivity was the same. The reason might be a difference to the

thickness of the active layer on the electrodes changing the initial impedance of the electrode generating an offset between them.

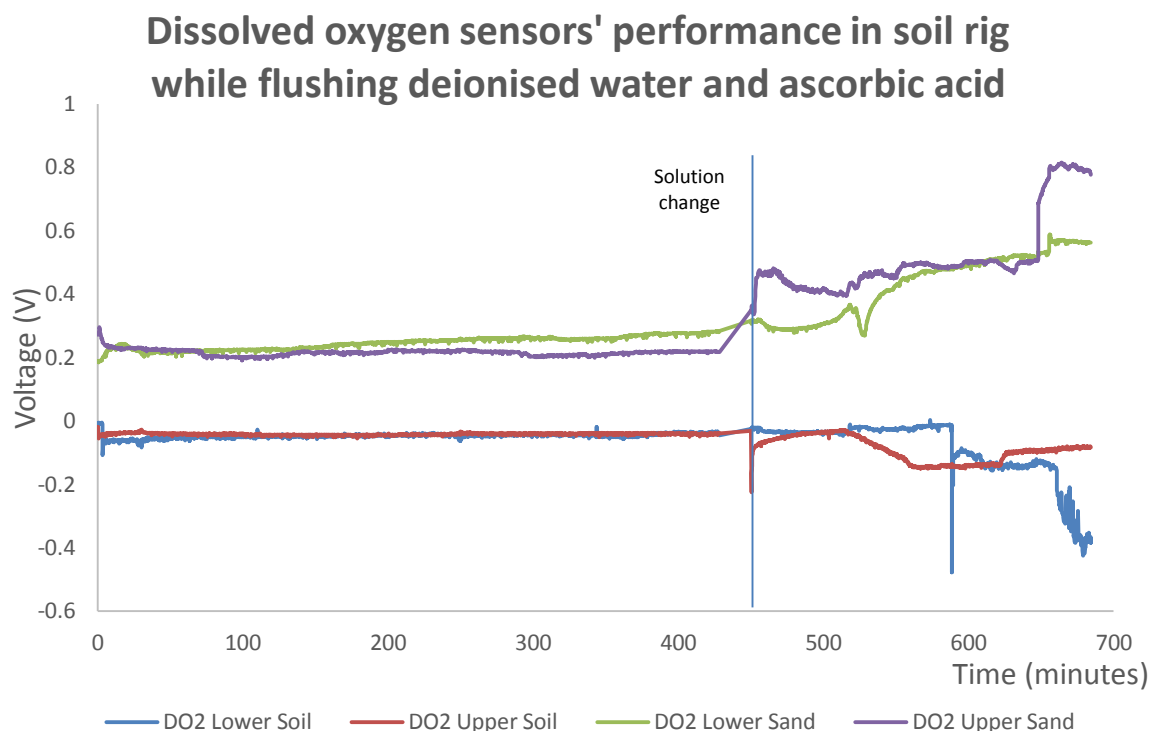


Figure 7-15: Readings from the dissolved oxygen sensors in the pipes from the same experiment with deionised water and ascorbic acid.

Figure 7-15 shows the performance of the dissolved oxygen sensors in the two pipes. What is very interesting is the fact that with deionised water the sensors read approximately zero volts for the soil but 0.2 V in sand. Sensors from the sand pipe are providing a positive voltage which is most probably an offset of the sensor. The reason this offset is observed is unknown unless the sensor is somehow damaged from the sand and gives unpredicted values. Dissolved oxygen sensors in the soil might have provided more meaningful results in deionised water but when the solution was changed, the voltage decreases, which under normal circumstances means an increase in oxygen level. On the other hand, the strange positive offset of the sensors in the sand provided more meaningful results when the oxygen level was decreased from vitamin C. The only possible explanation is that deionised water already had a very low dissolved oxygen level and when vitamin C was added it

7. Soil Rig

reacted as an open circuit providing very noisy results like the ones shown in Figure 7-15. Moreover, the unreliability of the prototype board can also be the reason for those unexpected results which does not allow for proper analysis of the sensors' performance and characterisation.

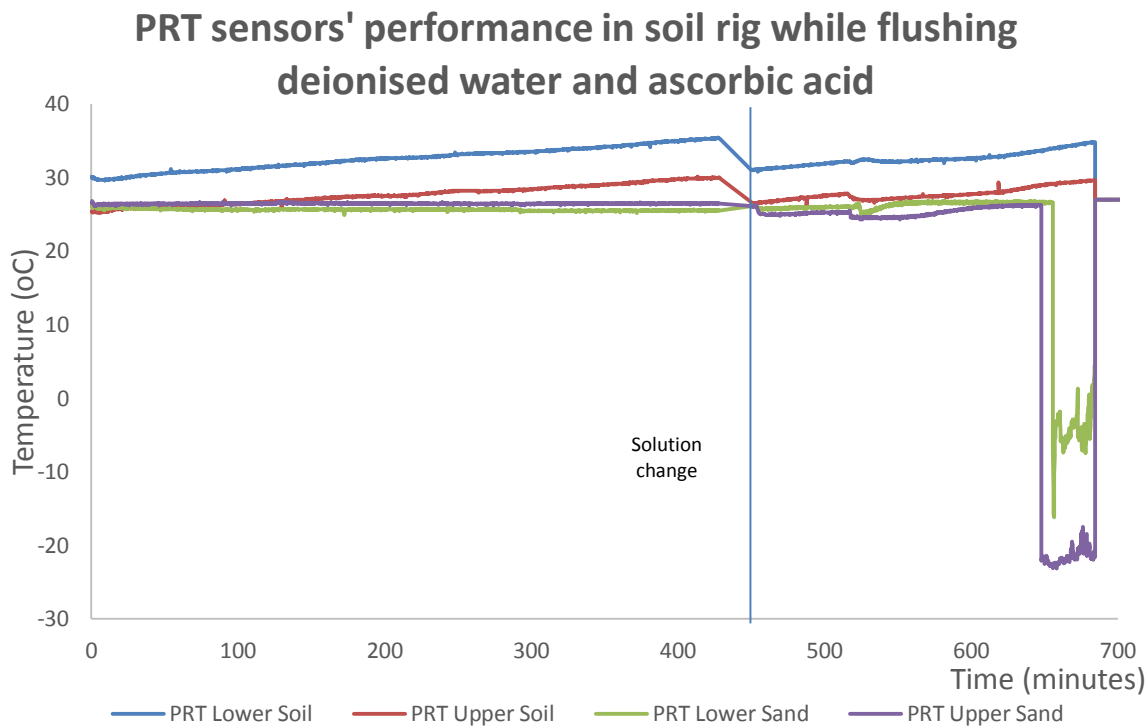


Figure 7-16: Temperature readings from the PRT in the pipes of the same experiment with deionised water and ascorbic acid.

Figure 7-16 shows the performance of the PRT during the same experiment. Sensors performed satisfactory but an offset between them could be seen which can suggest a need for a more accurate calibration of the electronic circuit used. That again brings up the need for a more trusted way to construct the interface. A small increase in temperature during the experiments can be seen which might be due to two reasons; either the temperature of the room was increasing since the experiment started in the morning and stopped in the afternoon or the sensor exhibits a self-heating effect due to the current flowing in the platinum film. Furthermore, the two negative peaks near the end can be observed which are most probably due to the unreliable connections e.g. someone

maybe touching the wires disconnecting them from the prototype board. After the experiment was finished all the results show approximately 28 degrees which is due to the algorithm used to translate the voltage into temperature.

Figure 7-17 & Figure 7-18 show the performances of the SHT21S sensors for temperature and humidity in the same experiment. The interface used for this chip was soldered on a veroboard to increase the reliability of the interface. The sensors were in the soil for a long time exposed to humidity values approaching 100% RH which turns out can destroy the active material. These random and illogical readings recorded can only suggest that the sensors were destroyed from the high levels of humidity and in turn that humidity measurements in the soil could not be achieved since the only solution being poured down the pipes are aqueous solutions and any gas evolved will be water vapour.

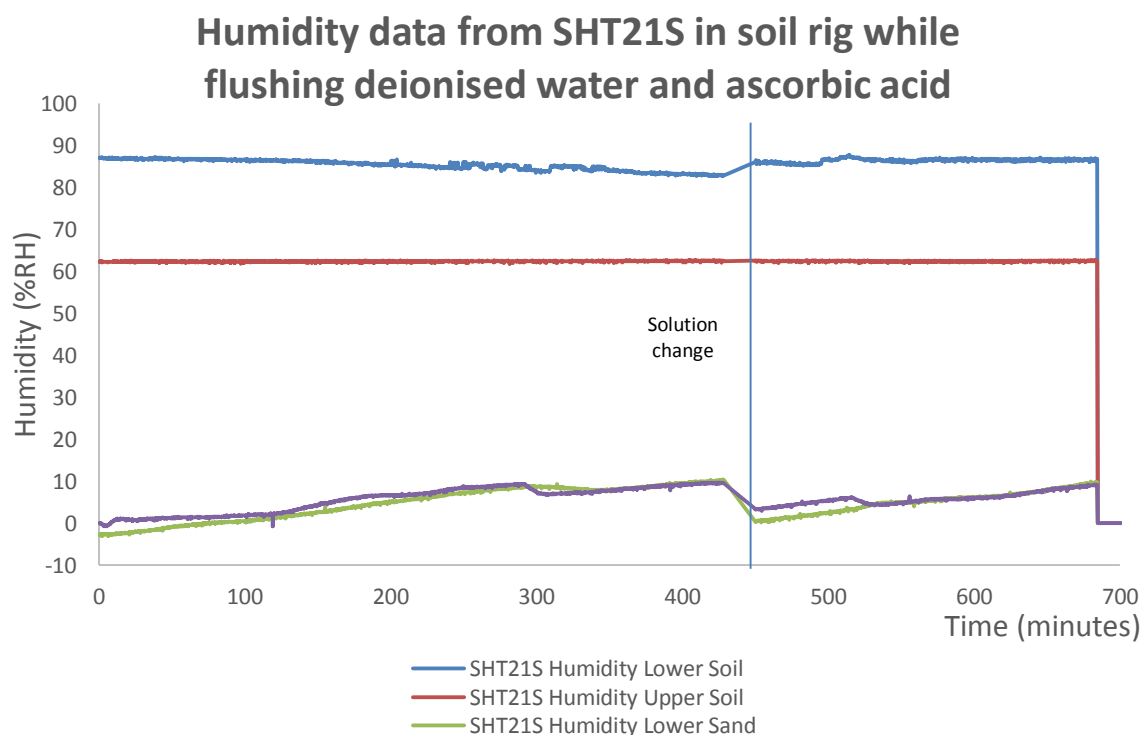


Figure 7-17: Humidity readings of SHT21S in the pipes in the same experiment for deionised water and ascorbic acid.

7. Soil Rig

Temperature data from SHT21S in soil rig while flushing deionised water and ascorbic acid

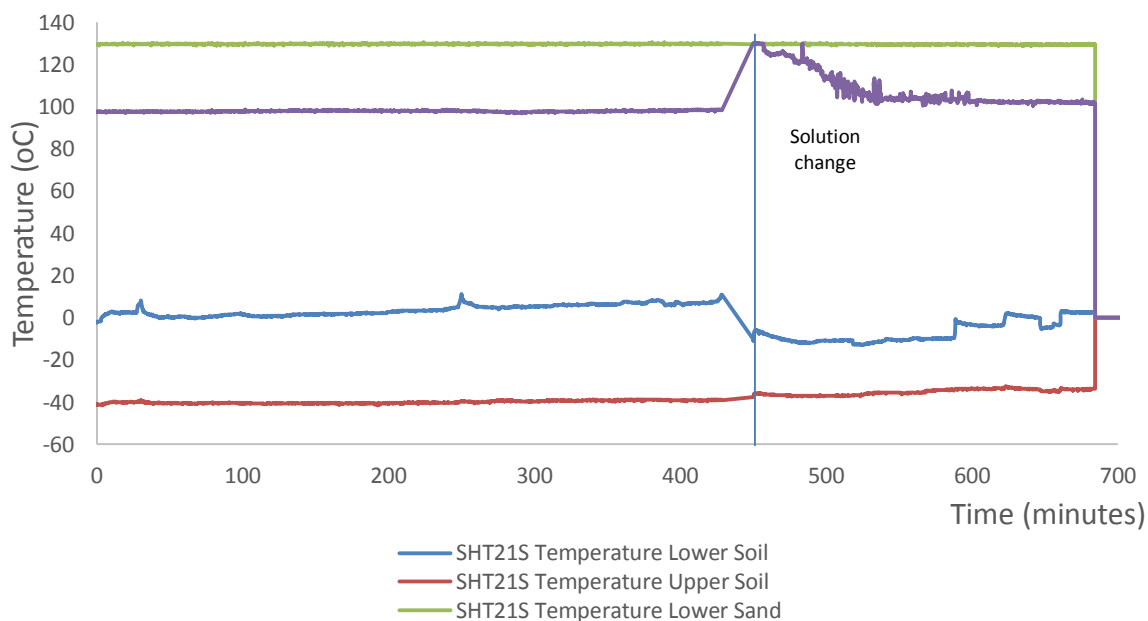


Figure 7-18: Temperature readings from SHT21S in the pipes in the same experiment with water and ascorbic acid.

7.2.3 Investigation of sensor array performance in modified soil pipes

Due to the unclear results obtained from the previous set of experiments, it was suggested that the sensors required more time in contact with the flushing solutions and at the same time keep the sensors protected from the soil. Furthermore, it was realised that pH buffers did not have an effect on the dissolved oxygen sensor and another solution was chosen. Ascorbic acid (vitamin C) is known to be an oxygen scavenger and depending on the concentration can have a low pH value. Therefore, in this set of experiments (SOIL.3-Pipes-Ascorbic Acid) ascorbic acid was flushed through the pipes. The flushing solution was altered between deionised water and ascorbic acid so that the sensors would show the difference. In order to protect the sensor from the soil, the sensor array was inserted in small cylindrical shaped pieces of floral foam that has the ability to absorb a significant amount of the solution and stay wet for a significant amount of time.

In this experiment, SHT21Ss were not used due to conclusions drawn from the previous set of experiments.

The main modification of the experimental rig was the addition of the green foam (Floral Foam) usually used as an artificial soil for flowers in the house. It is ideally inert but it can absorb huge amounts of solutions for a long time. The reason for using the foam was provide more time for the sensors to respond to the solution changes since now the solutions would surround the sensors in the foam for a much longer time. The sensors were inserted in a cylindrical piece of the foam which was inserted in the soil at the same depths as before.

The performances of the sensors are shown in Figure 7-19, Figure 7-20 & Figure 7-21.

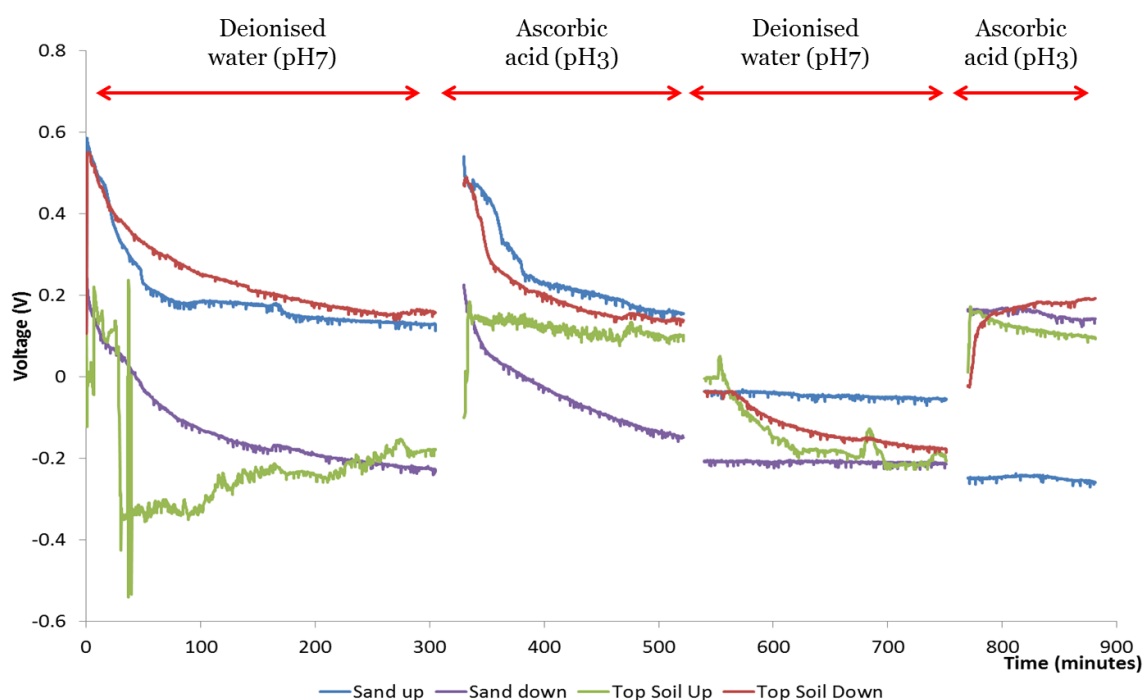


Figure 7-19: Performance of pH sensors in modified soil rig using floral foam

7. Soil Rig

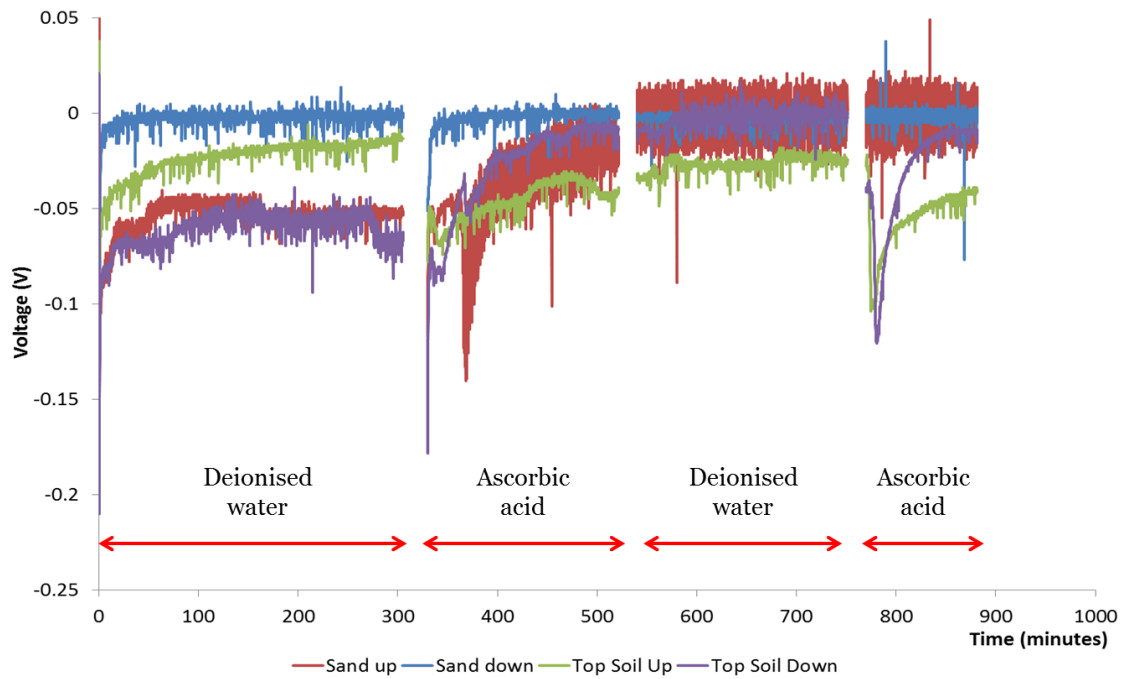


Figure 7-20: Performance of dissolved oxygen sensors in modified soil rig using floral foam

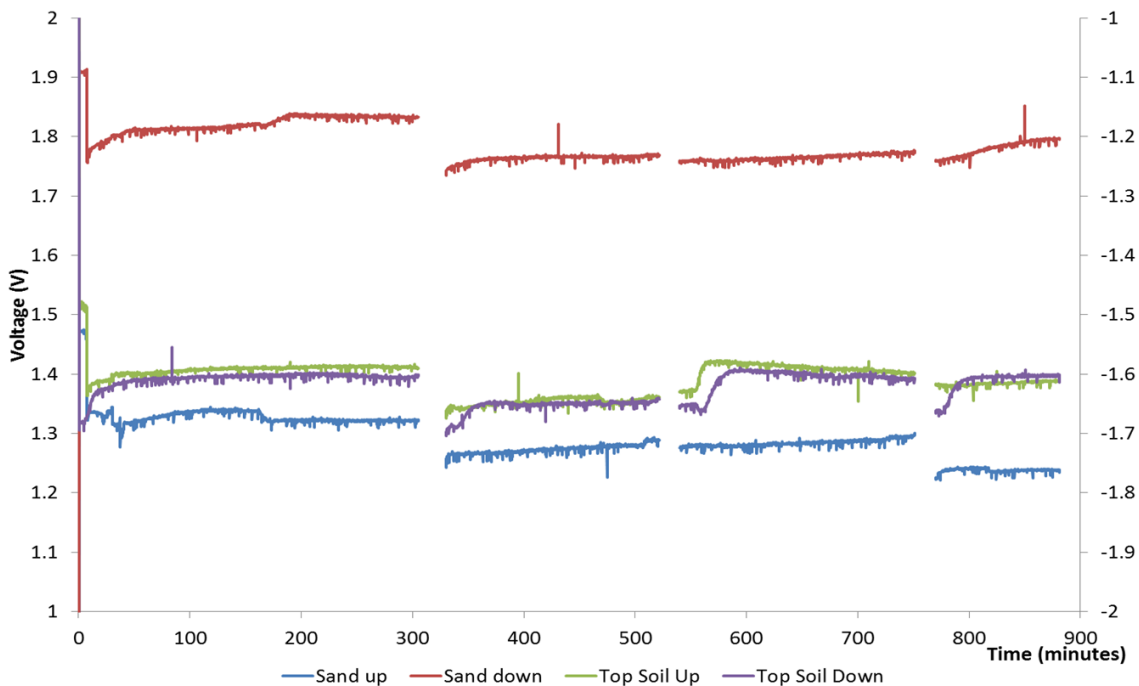


Figure 7-21: Performance of PRT sensors in modified soil rig using floral foam

The performance of the sensors has been obviously improved especially the pH sensor but once again the unreliability of the breadboard does not allow for satisfactory performances. Now, the solution changes are

more profound and the sensor output remains at a constant potential. Although the performance has been improved it doesn't yet correspond to the expected performance. Just to check that the sensor was not damaged, another test was performed with the same sensor in a solution of ascorbic acid showing a very slow pH response to ascorbic acid while a much faster response to pH buffers (4, 7 and 10).

The DO₂ sensor's performance was really troubling at the beginning but once we took the sensors out of the foam the problem was obvious. Ascorbic acid is an organic salt and it affected the PVC membrane of the sensor as shown in Figure 7-22 below.

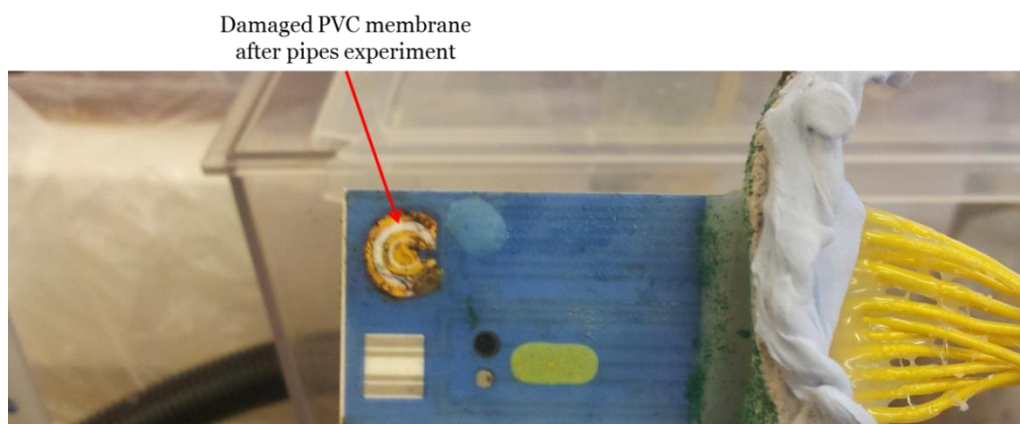


Figure 7-22: Damaged PVC membrane of DO₂ sensor after pipes experiment.

The PRT performed as expected and it was not affected by any damage on the rest of the sensors of the same tile. The only disadvantage the PRT has is the instrumentation used which drives a high current causing the platinum to self-heat and show a very slight increase in temperature. Difficulties with the breadboard existed for the PRT too because all the calibrations needed were extremely difficult when wires come off the board.

From these experiments several conclusions had been drawn:

- The experimental rig and soil pipes needed further modification for the sensors to perform as expected.

7. *Soil Rig*

- Ascorbic acid was not a good solution to test the sensors because it affected the PVC membrane of the DO₂ sensor and has a very slow response with the pH sensor. Fortunately, ascorbic acid is not found in nature in the soil.
- Soil pipes need redesign to trap solutions instead of flushing them in order to mimic real life application more precisely.
- The interface needs to be moved from breadboard to a Printed Circuit Board (PCB) to increase the reliability of the interface.
- The interface circuits, especially for the PRT needs to be improved.

7.3 2nd Soil Column Design

Previous experiments in soil pipes have suggested that the flushing time of the solutions was too small for the sensor to respond to the solution properties. Based on those experimental difficulties and some more explained in the next chapter, another soil rig was designed in conjunction with an MSc project.

The design of the new soil rig has evolved from a costly and highly complicated but more functional design to a much simpler and cheaper

design as shown in Figure 7-23.

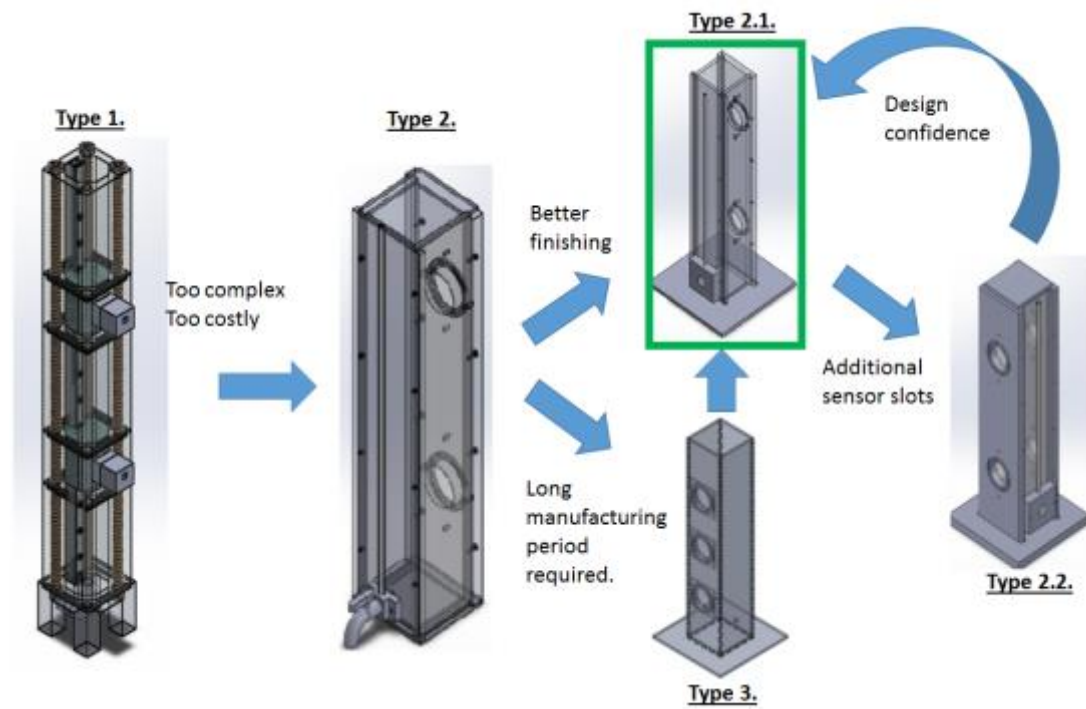


Figure 7-23: Evolution of new soil rig design.

Due to the high cost and the long time for the manufacturing of the initial designs, it was decided to move to something simpler to decrease the cost but still have the properties required for the sensors to operate properly. The last soil rig concept and the manufactured new soil rig are shown in Figure 7-24.

7. Soil Rig

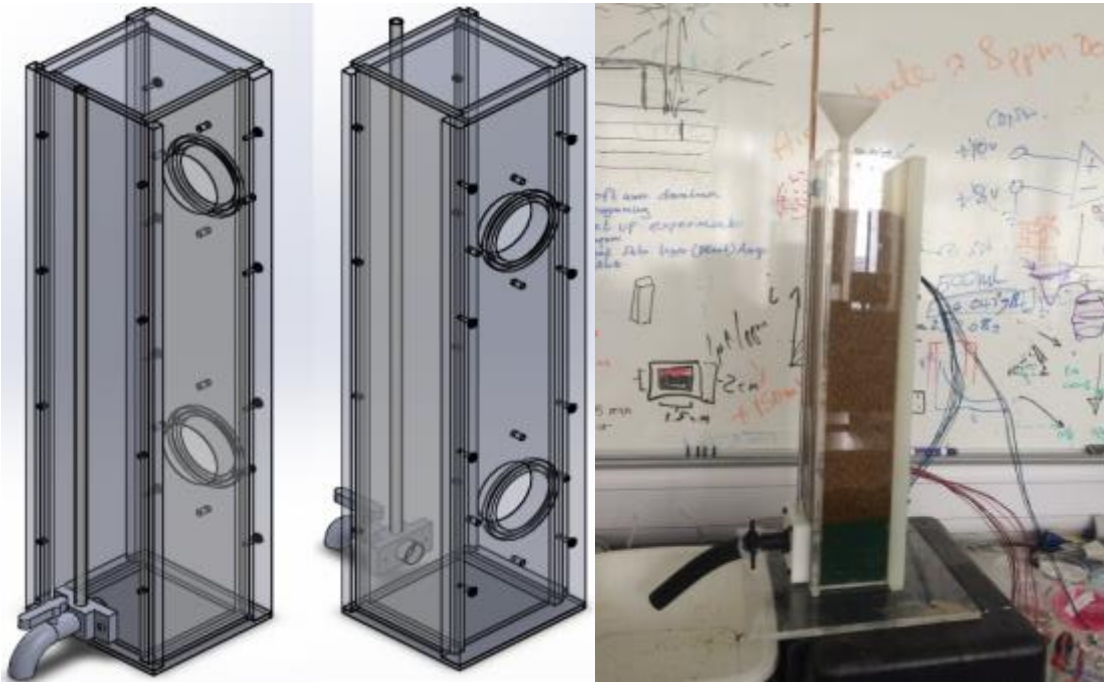


Figure 7-24: New soil rig, final concept design (left) and manufactured soil rig (right).

Experiments performed in the new soil rig were performed by the MSc student and can be found elsewhere (Pang Yew WEE, 2014). Although the experiments and experimental results are not shown or discussed in this thesis, the conclusions drawn from that work were used for further experimentation. When all the sensors on the TF sensor array were used together with the conductivity, all powered from the same PCB, several problems arose. Oxygen sensors and conductivity electrodes were stripped off the substrate most probably due to electrolysis happening from interference between electrodes of different sensors. Due to the fact that each sensor's electronics were not completely isolated from each other, most probably a complete circuit was formed between different sensors. A comparison of the sensor array before and after use is shown in Figure 7-25.

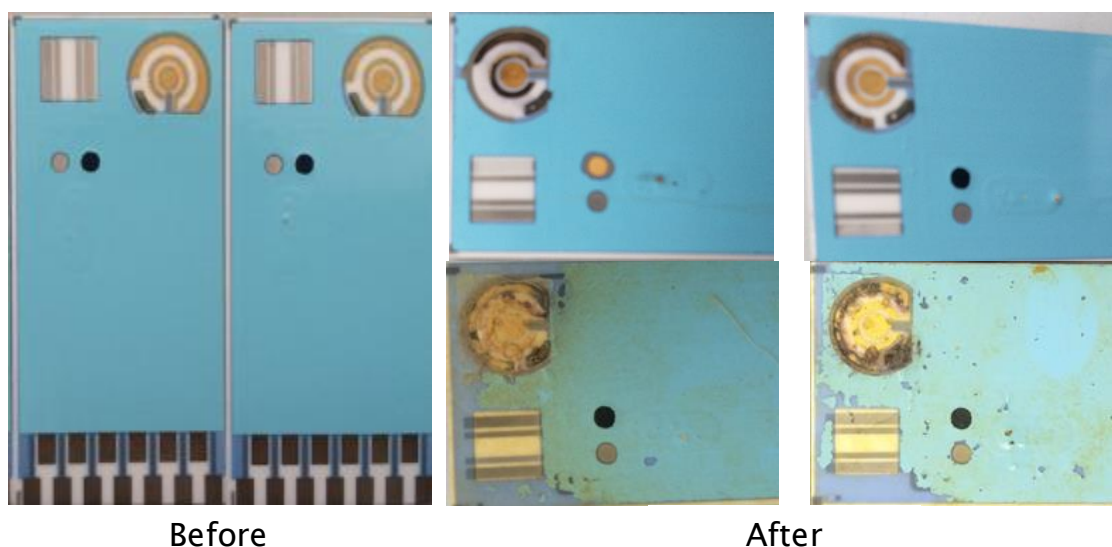


Figure 7-25: Sensor arrays before and after experiments when all sensors powered from the same PCB.

7.4 Soil Column for Conductivity Measurements

Based on the conclusions drawn from previous experiments, separate experiments were performed for conductivity sensor in soil but this time the experiments were performed in conjunction with another MSc student (Alessia Ingenito) in the Civil Engineering department. In this set of experiments, the conductivity sensor was tested together with a commercial water content soil probe in different types of soils.

7.4.1 Instrumentation

A test rig was manufactured to test several soil parameters using different commercially available measuring instruments (Theta probe) and compare their performance with the newly made lower cost Thick-Film sensors. The test rig is made up of a 1 m tall cylindrical column with a diameter of approximately 0.3 m having several holes on the sides to allow the sensors to be inserted at the correct height. As shown in Figure 7-26 below, the column was filled with 0.06 m of gravel to allow for faster drainage speeds and geotextile filters were used to separate the tested soil sample with gravel and to prevent any drainage blockage. The soil sample was poured in the column between 0.06-0.34

7. Soil Rig

m and the sensors were inserted in the soil sample around 0.3 m from the bottom of the column being completely covered from the soil sample but still be high enough to get faster results. Theta probe (Delta-T ML2x) was inserted at the same height as the Thick-Film conductivity sensor to ensure readings synchronisation. The column was then filled with de-aerated water using a peristaltic pump through the drainage pipe to prevent the formation of bubbles in the water. The column was filled with water up to 0.5 m completely covering the sensors. Once the column was filled with water, the pump was removed and the column drainage speed was controlled through a valve at the drainage pipe. Readings were recorded right before the drainage valve was opened and continued until the column was completely empty of water, although soil samples were always left wet. This was repeated several times for the same soil type without refilling the column to test for the relationship of soil properties and cycle number.

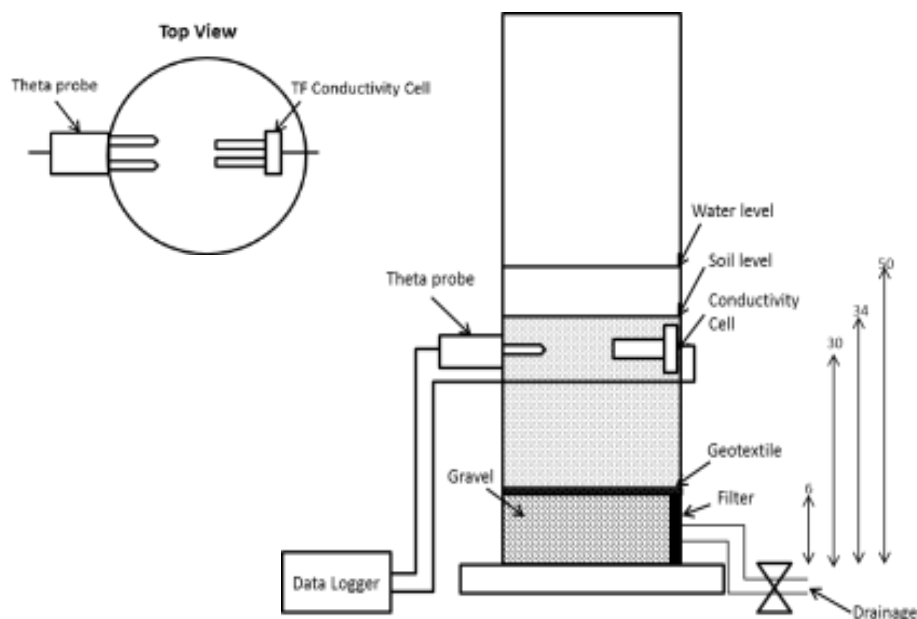


Figure 7-26: Schematic of the test rig with sensor orientation and positioning

Readings from Theta probe was recorded using a data logger provided by Delta-T (GP2 Data Logger) and the probe was calibrated for each soil sample independently according to the manufacturer's instructions. The Thick-Film conductivity sensor is based on the 4 electrodes method with

a current source of a square wave input with a frequency of 1 kHz for the current electrodes and measuring the potential difference across the voltage electrodes. Current levels can be altered in order to allow different sensitivities for different conductivity ranges. More details on the construction, fabrication and operation of the conductivity sensor can be found elsewhere. Readings from the conductivity sensor were recorded using a Campbell Scientific CR1000 data logger.

7.4.2 Initial Soil Experiments with Conductivity Cell and Theta Probe

Conductivity sensor was tested in a soil column in parallel with a theta probe (Delta-T) to investigate the relationship of water content and conductivity sensor's output. Several experiments were performed with different soil types to also investigate any relationships or trends between soil types and sensor's output. Soil column was filled with water and readings were recorded as soon as the drainage pipe was opened.

Figure 7-27 shows a plot of sensor output voltage levels compared with water content for the 20mm spacing gold electrode conductivity sensor operating at 0.25mA drive current amplitude at 1kHz square wave while submerged in the soil column and as the water is drained over time.

7. Soil Rig

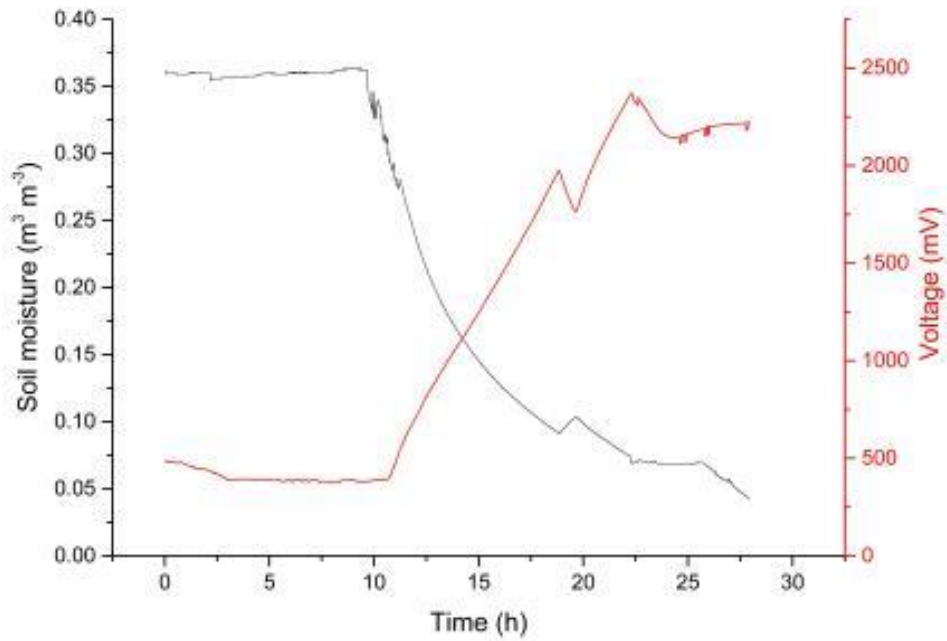


Figure 7-27: Conductivity sensor output voltage levels compared with water content of the soil column as water is drained over time

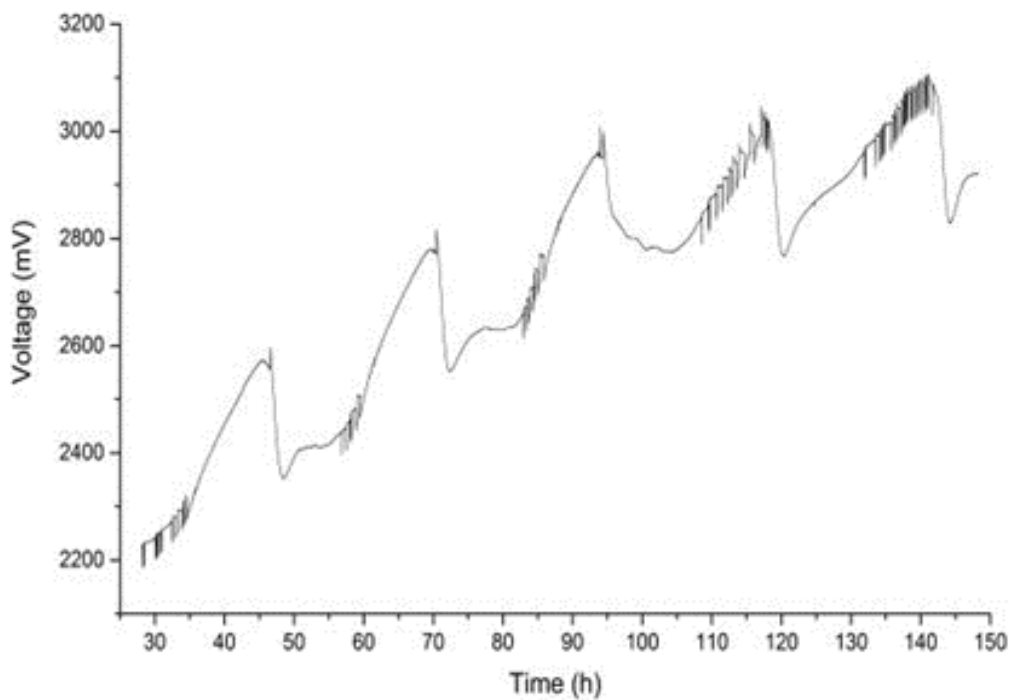


Figure 7-28: Conductivity sensor output voltage levels compared with water content of the soil column as water is drained over time showing 24 hour fluctuation due to variation in day and night time temperatures and electrical pick up (noise spikes) from adjacent machinery

The correlation between water content and conductivity can clearly be observed, with the decreasing water content causing the sensor output voltage to increase indicating an increase in soil resistivity. The artefacts at around 20 hours and 22 hours were due to a backing up caused by temporary blockages in the flow of water out of the soil column.

Examination of the sensor output voltage from the 30 hour point onwards shows fluctuation on a 24 hour cycle due to day and night time temperature variations experienced by the soil column. Electrical interference due to switching of electrical machinery in close proximity to the soil column can also be seen as a series of noise spikes during the day time portion of the plot. The latter are unlikely to be encountered in many of the application areas for these sensors but can be easily filtered out with the use of electrical screening of the sensor connection wires, which was not done in this case. The variation of electrical conductivity due to temperature will however need to be compensated for and the included temperature sensor on the sensor array would need to be used for this purpose.

7.4.3 Investigation of water content versus conductivity curve in different soil types

Three different soil types were used, Leighton Buzzard type E (Experiment CONDSOIL.1-LB), Builder's sand (Experiment CONDSOIL.2-BS) and a Soil Mixture made up of Sand, Silk and Clay (Experiment CONDSOIL.3-SM). Leighton Buzzard type E sand while it has the ability to retain water, allows the test to run quickly. The sand was poured through a pluviation tube in 4 steps, each one from a falling height of 7 cm. In this way a homogeneous density of $1,43 \text{ Mg/m}^3$ has been ensured.

Unlike the Leighton Buzzard sand, the Builder's Sand is characterized by a greater particle size and by being less homogeneous. Builder's Sand was also inserted in the column using the pluviation tube. In analogy with the previous experiments, the column has been filled in 4 steps, by

7. Soil Rig

a falling height of 7 cm. The Builder's Sand experiments were characterized by a greater density, equal to $1,71 \text{ Mg/m}^3$. The column has been slowly filled ($0,87 \text{ ml/s}$) with the de-aerated water from the bottom until the height of 50 cm, just like Leighton Buzzard sand.

The soil mixture is characterized by a greater capacity to retain water. The mixture is formed by soil Leighton Buzzard (fractions B,C and D), silt (HPF5) and clay (Hymod Prima). Table 7-1 summarizes the soil composition.

Table 7-1: Soil mixture composition

SAND			SILT	CLAY
Leighton Buzzard fraction B [%]	Leighton Buzzard fraction C [%]	Leighton Buzzard fraction D [%]	HPF5 [%]	Hymod Prima [%]
(Particle size 1,18 mm to 600 μm)	(Particle size 600 μm to 300 μm)	(Particle size 300 μm to 150 μm)		
51	11	11	19	8

The test rig configuration was different this time. Due to the different nature of the soil, in order to avoid a too slow test, the gravel filter has been increase to 28 cm height, while the soil is located in a band of 7 cm around the sensors. Figure 7-29 summarizes the test rig changes.

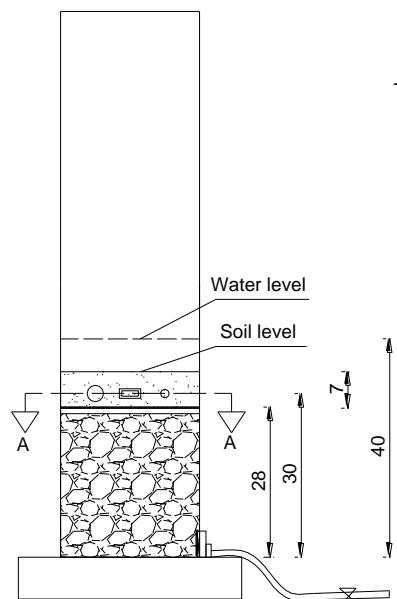


Figure 7-297: Altered test rig for the soil mixture test (all numbers are in centrimetres)

The soil has been first mixed by hands in plastic bags with the exact percentage of the different soil kinds with an initial water content of 8%. In order to ensure the hydration process of the clay and silt and prevent evaporation of water, the mixture has been left in sealed plastic bags for at least 24 hours. Then, the mixture was poured into the column in two steps. In order to control the soil density, the usual Proctor compaction rules has been used. The Proctor method suggests to use 40mm deep layers, using the 2.5 kg metal rammer falling through 300 mm and so the column has been poured in 2 steps, each one of 4 cm. However there isn't a specific calibration between strokes number and density. Moreover, Proctor method controls the number of blows, but as the sample size is much larger, that may be difficult to scale. For these two reasons an average density calculation was chosen. An average density based on weight and volume was calculated to be 2,09 Mg/m³. Two tests were carried out, each one lasted 10 days.

Initial experiments have identified an operational detail dependence of the TF conductivity sensors. The orientation of the sensor, although having no overall effect on the performance or the readings from the sensor, could generate a voltage output drop that would disappear when the orientation was altered. Having the substrates facing each other horizontally, would generate a voltage output drop when the water level in the soil column was as the sensor level. It is believed that when the water level decreases lower than the level of the two upper voltage electrodes, the electric field measured was only the one from the two lower voltage electrode because of the vast difference in impedance of the two sides. Once the level of the water decreases below the sensor level the voltage output would match the output to be the same as when the sensor orientation was changed to vertically facing plates.

Leighton Buzzard sand was used as one of the soil types and deionised water was flushed through the column at measured average rates. Resistance time graphs were plotted together with the water content measured using the commercial meter (Delta-T Theta probe) and the two

7. Soil Rig

were compared. Figure 7-30 below shows the typical resistance time graph for almost all the soil types including the water content graph. The relationship of water content versus conductivity is shown as inversely proportional since as the water level increases charge carriers in the water soil mixture decrease causing the conductivity to decrease. Resistance readings start to decline earlier than the water content and that is probably because the conductive particles of the water soil mixture move down the column as the water starts to drain out of the column.

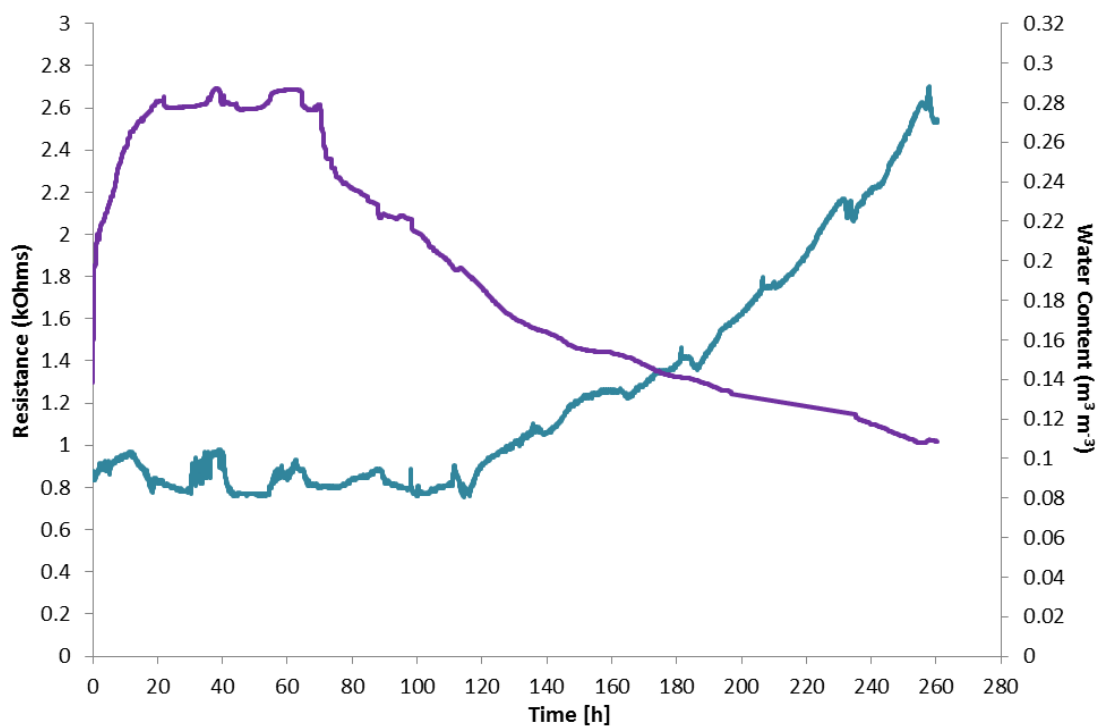


Figure 7-30: Typical resistance and water content time graph for Leighton Buzzard sand with an input current of 1 mA and a draining rate of 0.967 ml/s

After the soil column was prepared with Leighton Buzzard sand, deionised water was flushed through the column several times without changing the sand. It was very interesting to observe that each cycle would give different resistance changing rates while the water content rate would remain relatively stable. Figure 7-31 below shows the resistance water content relationship during water drainage. Resistance was obtained by dividing the voltage output by the input current to normalise the data. The experiment was repeated for four cycles and the

results were all plotted on the same graph. The input current was altered depending on the resistance of the soil to make sure the output voltage was in the operating range of the instrumentation.

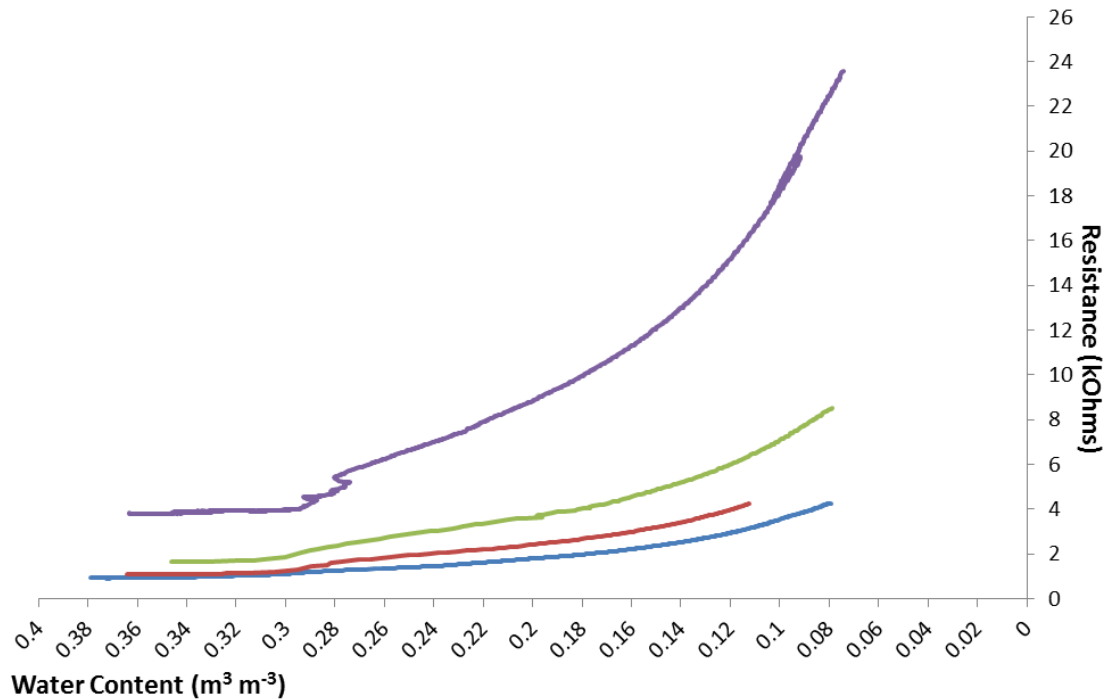


Figure 7-31: Resistance versus water content graph for Leighton Buzzard sand. (cycle 1:blue-1.063 ml/s-1 mA, cycle 2:red-0.67 ml/s-1 mA, cycle 3:green-0.967 ml/s-0.5 mA, cycle 4:purple-0.236 ml/s-0.1 mA)

The first cycle in this soil type has provided the lowest resistance readings and the resistance kept increasing as the cycles' number increases. This is most probably due to the use of new deionised water every time and the conductive ingredients dissolved in the water from the soil were washed out decreasing the conductivity of the mixture. It is very important to mention that although the absolute relationship between water content and resistance was changing the shape of the graph was similar for all cycles suggesting the possibility of being related to another property of the soil type used.

Keeping that possibility in mind, the soil type was changed into something more complicated than Leighton Buzzard sand. Builder's sand is not a single type of soil and contains different grain sizes that

7. Soil Rig

would change the packing of the soil and therefore soil's porosity and permeability. Figure 7-32 shows the relationship of resistance and water content for builder's sand for three consecutive cycles.

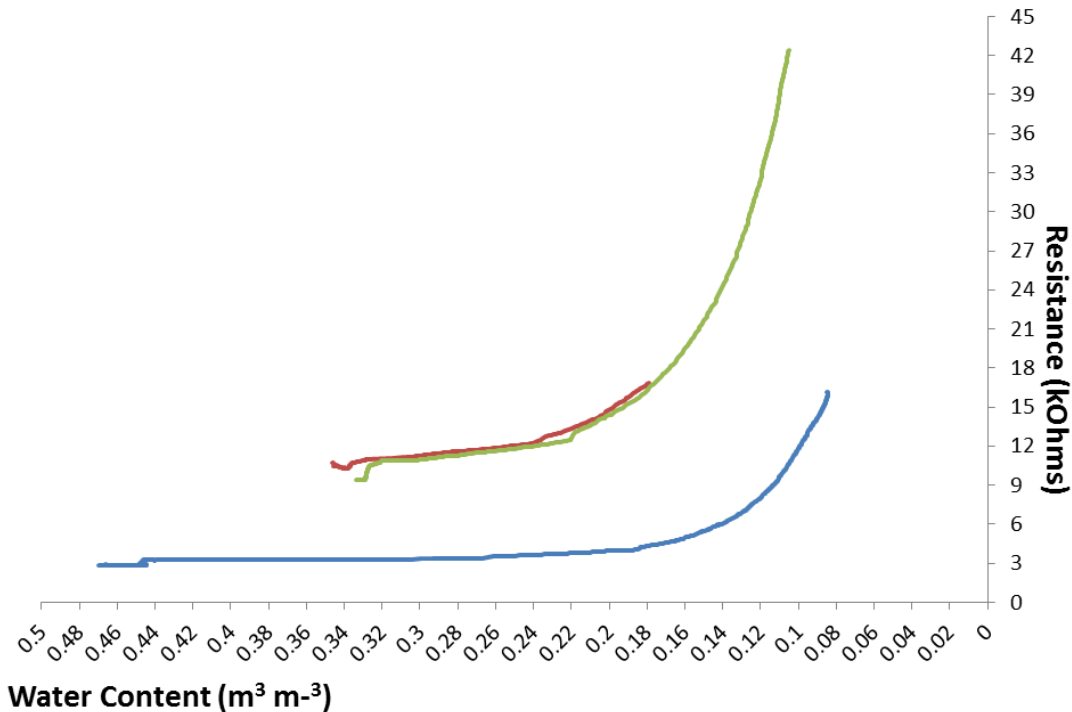


Figure 7-32: Builders sand resistance water content graph with three cycles (cycle 1:blue-0.047 ml/s-0.25 mA, cycle 2:red-0.322 ml/s-0.25 mA, cycle 3:green-0.352 ml/s-0.1 mA)

In this case, the initial cycle provided again a lower resistance reading than the second and third cycle. Cycles two and three were almost identical which is most probably because of the non-existence of any remaining conductive ingredients in the soil mixture. Furthermore, the shapes of the graphs were again similar but different from the Leighton Buzzard sand type.

The next experiment was to investigate how cycles can affect the resistance of a soil mixture. The preparation of this soil type was explained in detail in chapter 5. For this soil type, only two cycles were performed due to an unexpected issue with the soil column.

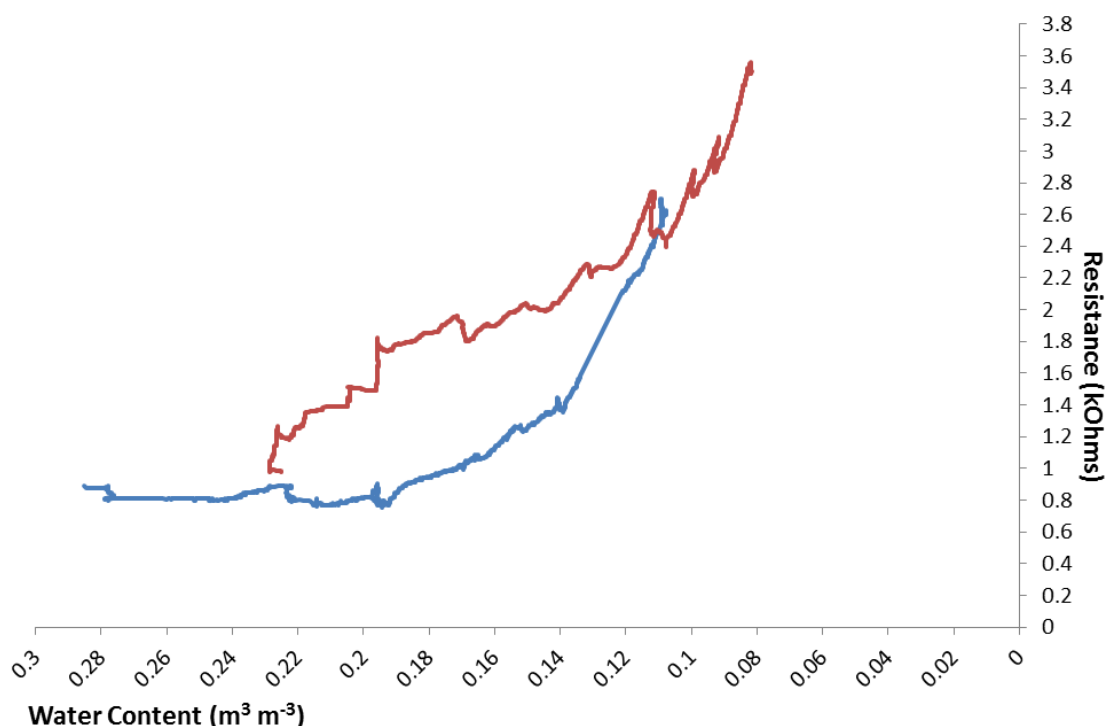


Figure 7-33: Resistance versus water content graph for custom made soil mixture for two cycles (cycle 1:blue-0.1 mA, cycle 2:red-0.25 mA)

Figure 7-33 shows the relationship of resistance and water content for the custom made soil mixture. Again the resistance of the soil mixture measured increased from the first cycle to the second probably for the same reason as the rest of the soil types. It is important to mention that the shape of the graphs in this case was not the same. In the previous soil types the shape of the graph was very similar for all cycles. This soil mixture was made from several soil types and grain sizes. The difference in the shapes can be a result of washing out very fine particles which would clearly affect the packing of the soil mixture and eventually the soil mixture mechanical properties like porosity and permeability. In addition, different types of soil are affected differently from washing cycles and that can change the resistance of the soil differently at different water content levels.

Comparing the resistance versus water content graphs from different types of soils at the same cycle has provided very useful conclusions and ideas for further work. Figure 7-34 & Figure 7-35 show the

7. Soil Rig

relationship of resistance and water content for the first and second cycles of different soil types.

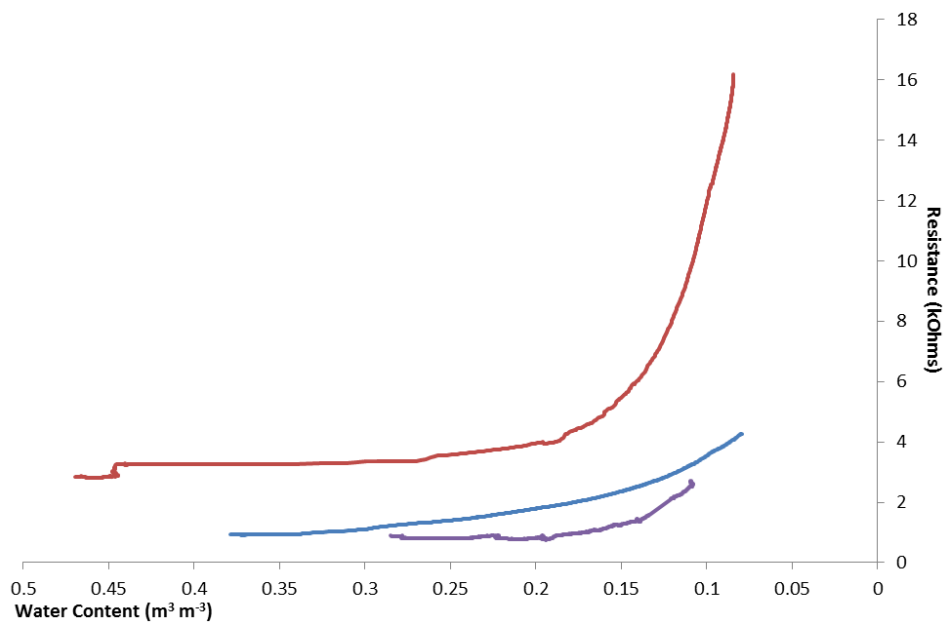


Figure 7-34: Resistance versus water content graph for the first cycle of different soil types (Leighton Buzzard-blue, Builder's sand-red, Soil mixture-purple)

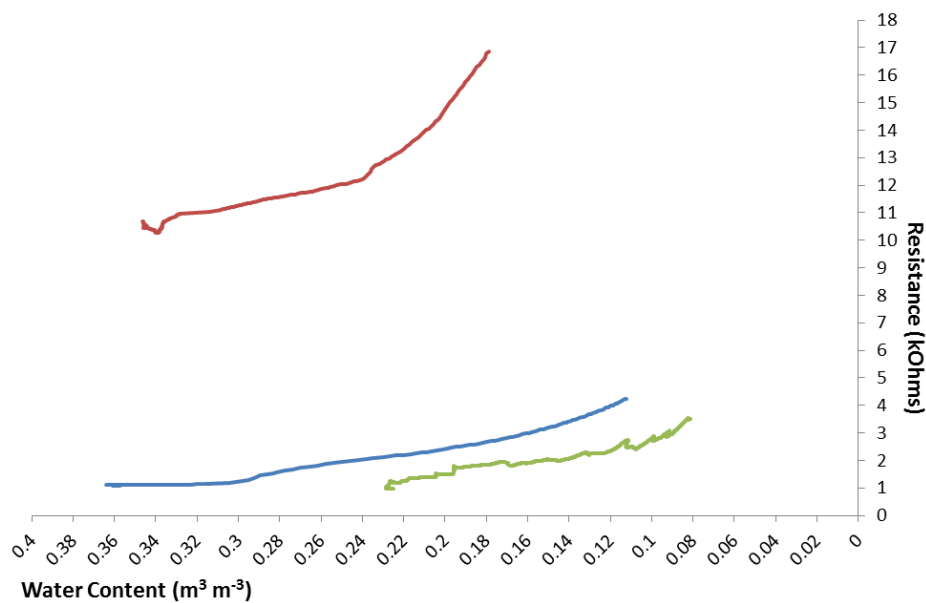


Figure 7-35: Resistance versus water content graphs for the second cycle of different soil types (Leighton Buzzard sand-blue, Builder's sand-red, Soil mixture-green)

Those three different soil types provided three different resistance water content graphs when comparing the same cycle number. The resistance range for the builder's sand is clearly the highest while the soil mixture has the lowest resistance range. It is believed that this relationship is a result of mechanical property of the soil such as porosity or permeability or perhaps even a chemical property of the soil such as salinity. Looking at the absolute values for resistance obtained as specific water content range, it can also provide information on the packing or structure of the soils in the column. Furthermore, the maximum amount of water level in the column immediately before the beginning of drainage might provide an indication of the porosity since the higher the water content the lower the resistance. This work requires further experimentation in order to provide satisfactory evidence that the pre-mentioned suggestions are valid or not.

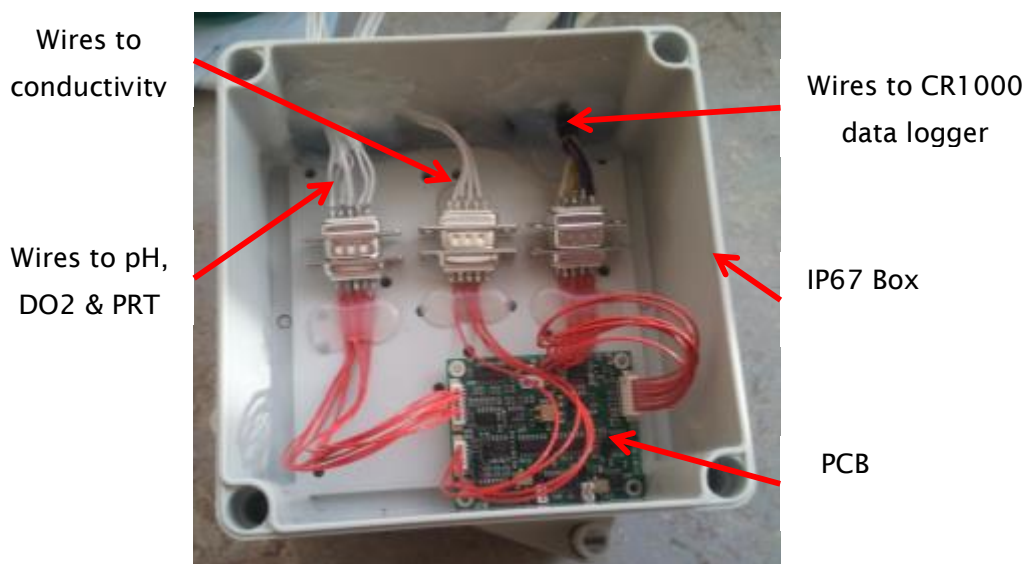
Chapter 8: **Field Trials**

8.1 Field Trials

As the last step of this research, the sensor arrays were prepared for field tests at Yarnton Meadow in Oxford where the FUSE project area of interest is. The existing TF sensor arrays were used instead of printing new and improved arrays to firstly test the instrumentation and the way the sensor will be placed in the soil.

8.1.1 Instrumentation

Eight sensor arrays were connected to four PCBs. Four of the sensor arrays only had their conductivity sensor connected while the other four had the pH, dissolved oxygen and temperature sensor connected. Conductivity sensors were used in separate arrays to prevent the problems arose in the case of using a single PCB for all the sensors (Pang Yew WEE, 2014). The soldered connections between the electrodes and the wires were waterproof using the hot glue gun and then each PCB was placed in an IP67 box which was drilled to pass the wires inside and the holes were filled again with the hot glue gun.



shows the boxes where the PCBs were placed in with the sensor arrays coming out.

8. Field Trials

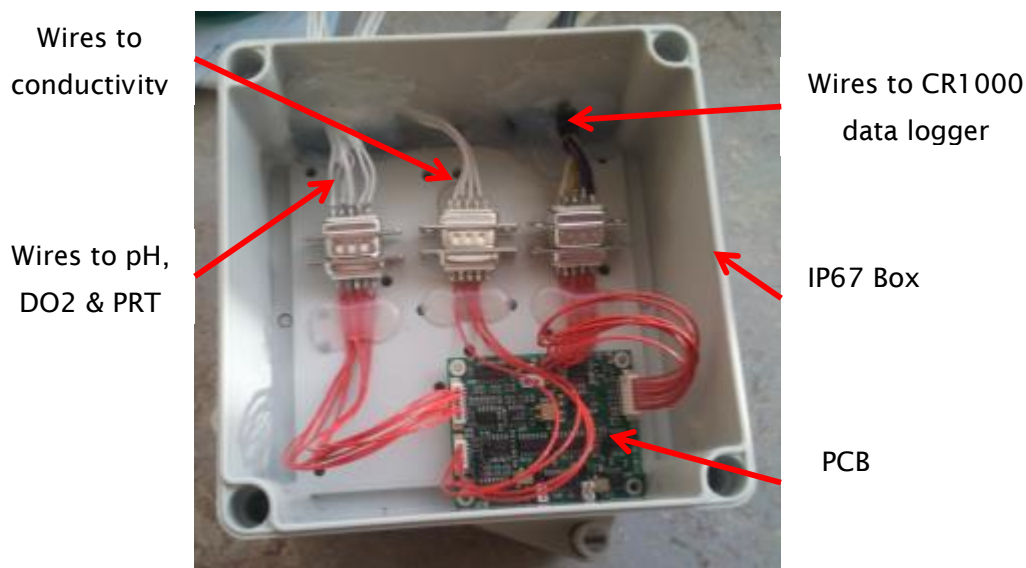


Figure 8-1: IP67 box with the PCB and the wires coming out of the box.

The sensor arrays were then placed in to 3D printed array holders, designed to protect the substrate from breaking and to provide an enclosure for the electric field of the planar conductivity sensor to improve its performance as shown in Figure 8-2.

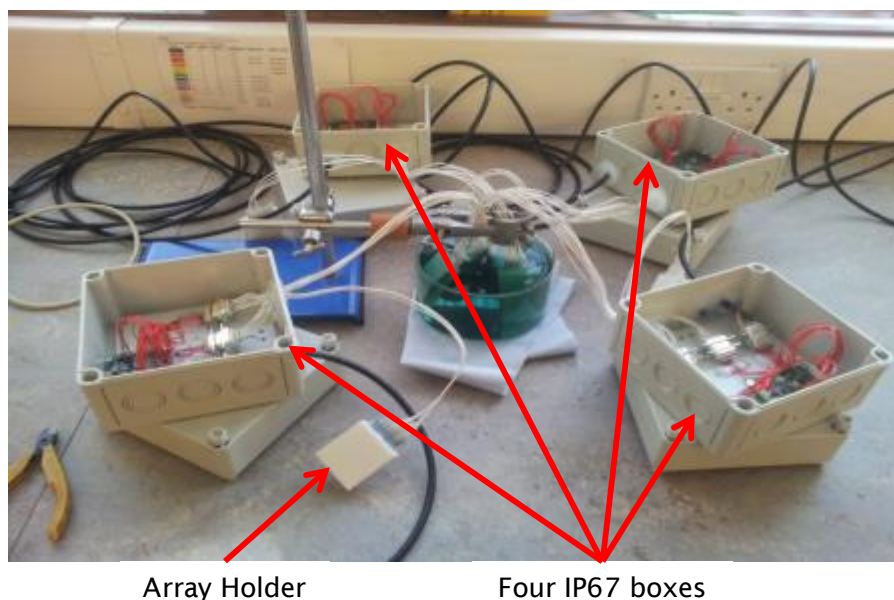


Figure 8-2: Four IP67 boxes with sensor array holders during initial calibration tests.

All the sensors' outputs were connected to a CR1000 data logger which was powered by a 13 V battery (Campbell Scientific) and where both

placed in a commercially obtained waterproofed box (Campbell Scientific) as shown in Figure 8-3.

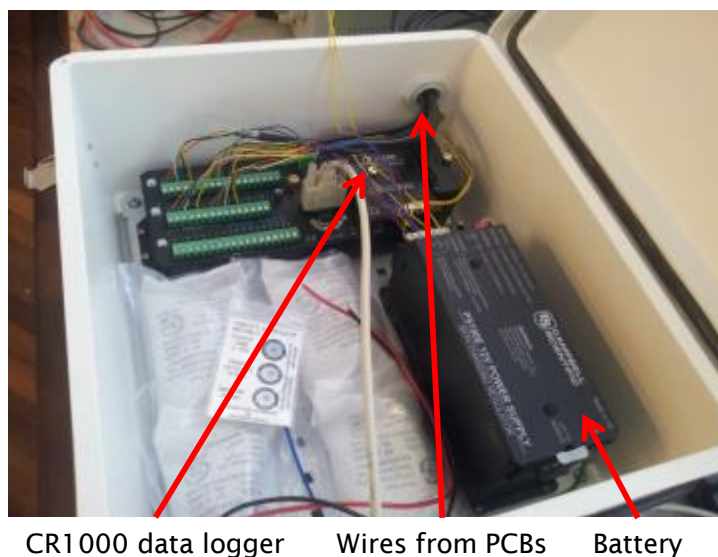


Figure 8-3: CR1000 data logger and battery in the waterproof box.

The battery will be connected to an already existing solar panel (Campbell Scientific) at the site. The solar panel was used to recharge the battery when required. The array holders with the sensor arrays will go into a cube of floral foam to protect them from the soil when placed at Yarnton Meadows.

8.2 Experimental Work

8.2.1 Sensor array calibration in solutions

Before placing the sensors in the field, initial calibration experiments were performed for every array and for every single sensor. The sensors with the array holders were calibrated in pH buffers 4 and 7 and their initial values for dissolved oxygen and temperature at 25 °C were recorded. Furthermore, conductivity values were obtained in the two pH buffers to provide a base line for the conductivity sensor and those values were also measured using a commercial conductivity meter.

8. Field Trials

Voltage output from each sensor was recorded and the data is shown on Table 8-1 below. The sensors were planned to be buried at two different depths. Two sensors would go deeper and two shallower to check if a time delay is observed.

Table 8-1: Calibration points for sensors to be used for field trials

	pH Deep 1	pH Deep 2	pH Shallow 1	pH Shallow 2
mV/pH	-130	-150	-190	-163
	DO ₂ Deep 1	DO ₂ Deep 2	DO ₂ Shallow 1	DO ₂ Shallow 2
pH 7 (no bubbling)	0.165	0.29	0.24	0.19
	PRT Deep 1	PRT Deep 2	PRT Shallow 1	PRT Shallow 2
25 oC	1.83	1.82	1.82	1.81
	Conductivity Deep 1	Conductivity Deep 2	Conductivity Shallow 1	Conductivity Shallow 2
mV/(mS/cm)	-82.9	-92.4	-87.7	-97.2

There are clearly differences between the several sensors as expected. Fabrication of the sensors can highly affect their performance and due to the non-industrial manufacturing process an inconsistency is observed in the fabrication process.

In the case of pH sensors, the thickness of the ruthenium oxide paste is important and can affect the sensitivity and the settling time of the sensor. The PCB used in this calibration was designed to amplify the sensor output by three times. Taking that into consideration the sensitivity of the sensors is acceptable.

Dissolved oxygen sensors were calibrated with a single point calibration since the sensitivity of the sensor is controlled by the instrumentation used.

Platinum resistance thermometers were calibrated using single point calibration since the platinum temperature coefficient of resistance is known and the voltage should be adjusted to a point that can cover most of the environmental temperature range.

Conductivity sensors were very close to each other and it is believed that differences are due to noise during the calibration process.

8.2.2 Investigation of sensor array performance in the field

The sensors and instrumentation was implemented at Yarnton Meadows inside a protected area where other scientist used other types of sensors to monitor the plant growth under FUSE too. The waterproof box with the data logger and the battery were connected to an already existing pole (Figure 8-4) and the wires were guided to the drilled holes where the sensor arrays were buried.

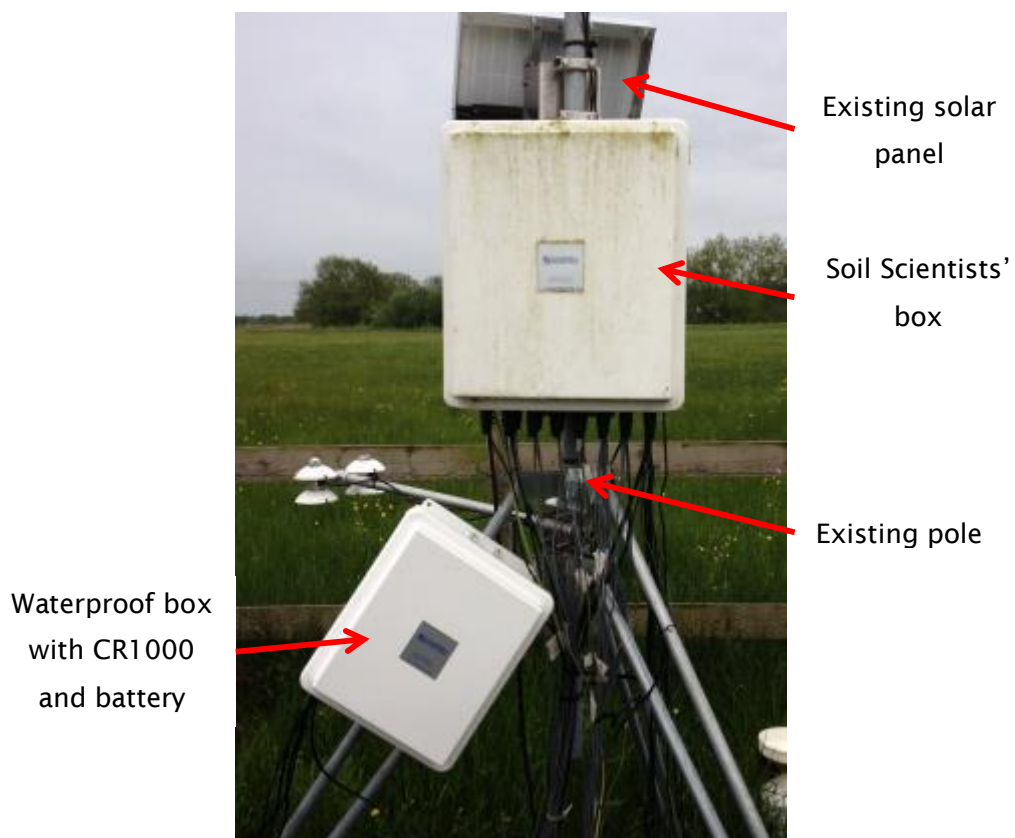


Figure 8-4: Existing pole on site where the waterproof box with CR1000 and the battery were connected to.

Four different holes, next to each other were drilled. Two of them were approximately 50 cm deep and the other two were approximately 30 cm deep (Figure 8-5).

8. Field Trials



Figure 8-5: Four drilled holes to insert the sensor arrays and boxes.

The IP67 boxes were also buried in the holes with only the wires going to the data logger coming out from next to the pole. That was done to compare if the drilling height might have a difference in the soil properties and to check if there will be a time difference between the readings. The sensors were placed in cubes of floral foam (Figure 8-6) to protect them from the soil and allow enough time for the sensors to monitor any changes in the soil water.



Sensor arrays in the array holders
and then in the floral foam cubes

Figure 8-6: Sensor arrays in the array holders and then they array holders were inserted in floral foam cubes.

The data logger was set to take readings every 30 minutes from all the sensors and save them to an external memory card of 2 GB.

8. Field Trials

The sensors were buried in the field and the power for the data logger was obtained for the battery from a photovoltaic panel that was installed at the site bought by Campbell Scientific from the University of Reading. After some time the sensors were buried in the field our colleagues from the University of Reading informed us that the battery of the photovoltaic panel has run out and probably a short circuit in our sensors was the reason. Fortunately, some of the data from the sensors were obtained before the battery run out and they are presented in the figures below.

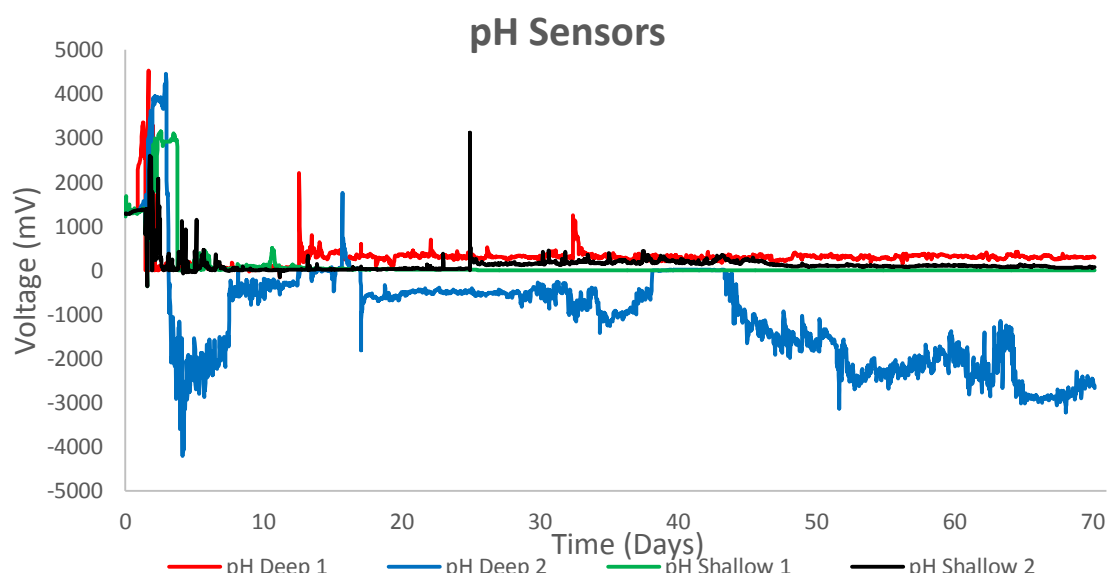


Figure 8-7: pH sensors data from field trials

8. Field Trials

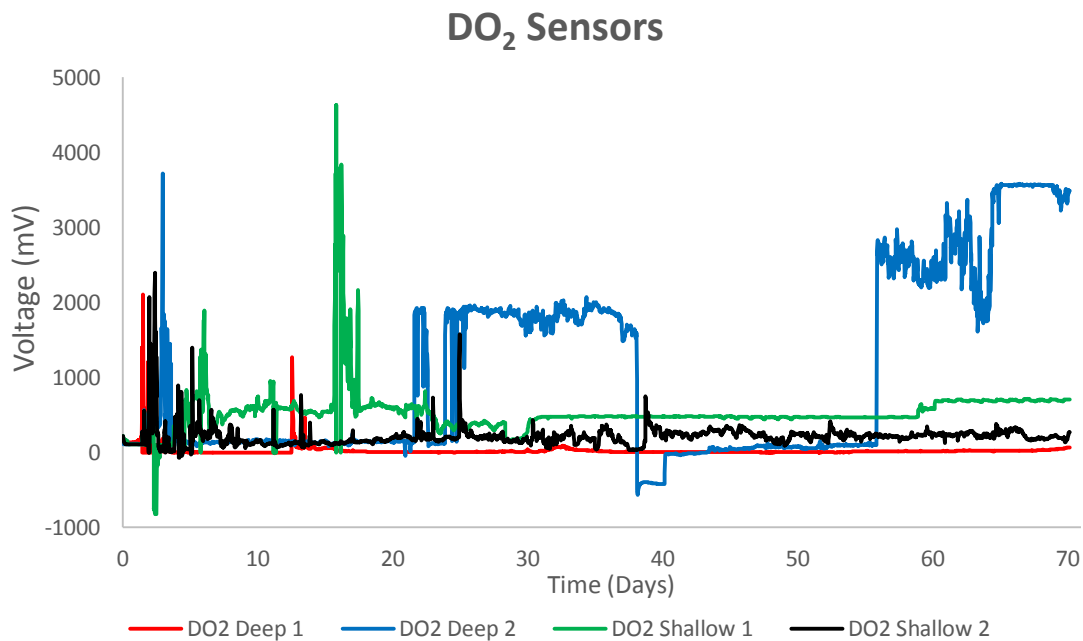


Figure 8-8: DO2 Sensors data from field trials

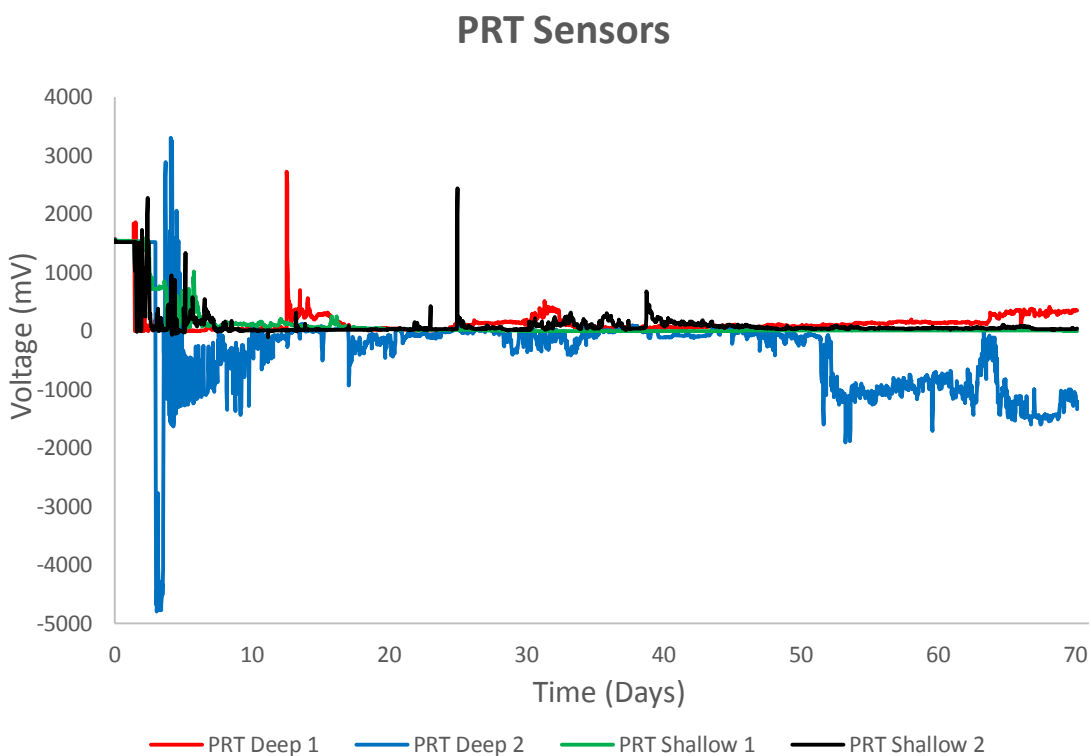


Figure 8-9: PRT sensors data from field trials

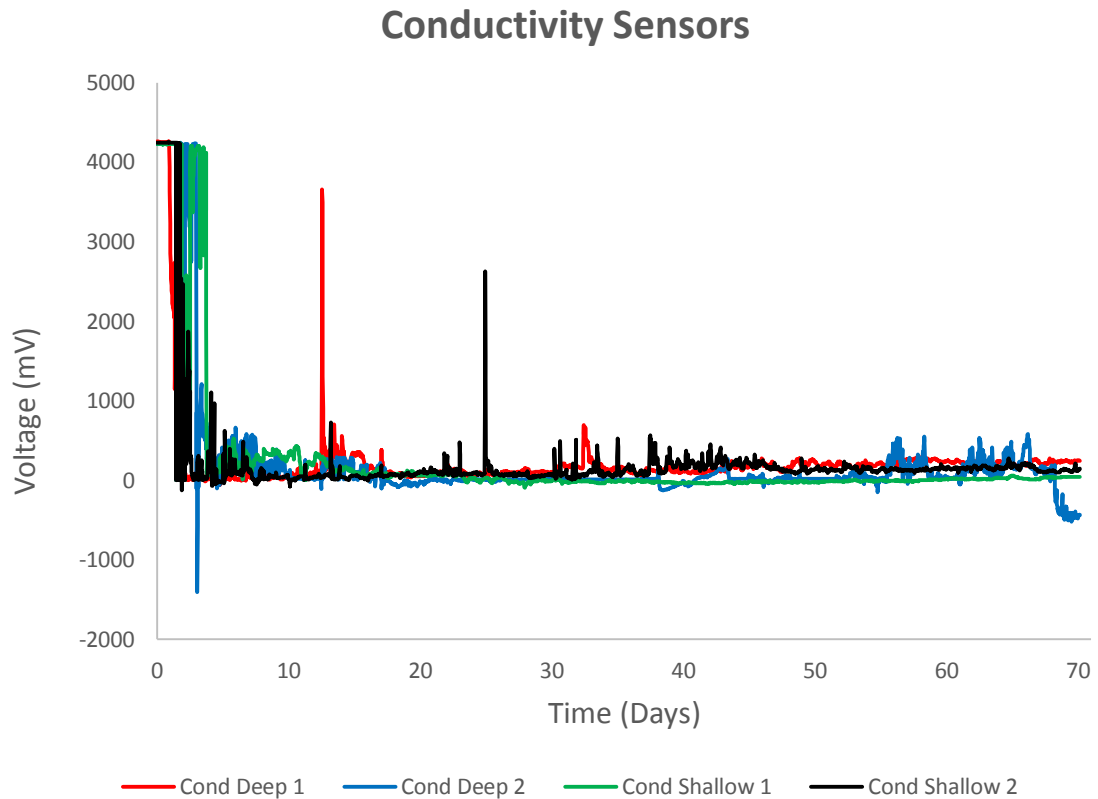


Figure 8-10: Conductivity sensors data from field trials

Looking at the data obtained from the sensors, the reason the battery has run out was obvious. Initially all the sensors were performing in the expected range but after a couple of days, all sensors outputs went down to zero clearly suggesting a short circuit. Digging up the sensors and the boxes with their PCBs from the field, the reason for short circuiting was obvious as shown in Figure 8-11 below.

8. Field Trials



Figure 8-11: Box with PCB after digging it out from the field

Initial field trials have shown that a better waterproofing method is required to protect the PCBs from water. Although the boxes were filled with water, the sensors were found to be in a good condition since they were very well protected from soil due to the foam and the 3D printed holder.

Chapter 9: **Conclusions & Further Work**

9.1 Reference Electrodes

Reference electrodes were one of the most important parts of this research. Existing knowledge from previous experiments was used and further experimentation provided results for further understanding electrodes' operation. It was suspected from previous work that Ag/AgCl paste could have an effect on the performance of the electrodes. After testing several electrodes with different types of Ag/AgCl pastes, it was concluded that Ag/AgCl paste can greatly affect the performance of the electrodes when no KCl polymer matrix was printed on top. Glass PPCFB2 Ag/AgCl paste provided the lowest susceptibility to chloride concentration using a properly cured paste, of approximately -50 mV/decade of [Cl]. It is important to mention that bare silver electrodes provided a susceptibility of approximately -129 mV/decade of [Cl] which tends to suggest that more than one reaction was taking place at the same time. Ideal response for a single reaction is the theoretical Nernstian response of -59 mV/decade of [Cl] at room temperature. Furthermore, electrodes with fired polymer Ag/AgCl paste provided very similar responses to the bare silver electrodes which suggests that most of AgCl was decomposed to Ag and Cl₂ during firing of the paste. Other than the binder, the main difference between different Ag/AgCl pastes was the Ag to AgCl ratio. Pastes with similar Ag to AgCl ratio (PPCFB2 & PPCFC3) provided similar susceptibilities suggesting that this ratio might be the reason for having different susceptibilities from different pastes.

Electrodes without Ag/AgCl layer were investigated in more detail. Looking for the optimum KCl weight percentage in the KCl polymer matrix on the top layer, it was found that as the KCl weight percentage was increased the performance of the electrodes was worse with an optimum point at 20% with a susceptibility of approximately 11 mV/decade of [Cl]. The performance was greatly improved when compared to the same electrodes without the KCl polymer matrix. Further and more detailed work needs to be done on this, to find a more

9. Conclusions & Further Work

precise optimum weight percentage for this type of Ag/AgCl paste because of the very few points investigated. A suggested interval for the KCl percentage would be between 5 and 10 percent between steps.

Adding another layer of KCl polymer matrix on top of the first one was proven to provide the best results obtain from this work. Although different KCl percentages were tested for the first KCl polymer matrix, adding another layer on top improved the performance greatly. The best performance was provided by electrodes with 50% KCl in the first layer and no KCl in the second layer with a susceptibility of approximately 2 mV/decade of [Cl⁻] for the whole range tested (4.35-0.004 M). Electrodes with no KCl in the second layer provided similar susceptibilities but much better responses in terms of lifetime and drift rate. Electrodes with 50% KCl in the first layer and no KCl in the second layer provided the best responses of 30 hours lifetime, 1.92 mV/hour and 0.5 hours of hydration time. It was calculated that on optimum KCl concentration on the first layer of approximately 40% would provide a lifetime of 32 hours, a hydration time of 17 minutes and a drift rate of 1.7 mV/hour. Further work is required in this area as very few experiments were performed to verify the results of the experiments and to provide the required error bars. Test intervals of approximately 5 to 10% of KCl weight percentage would be ideal to provide a sufficient curve to generate a correct correlation between the KCl percentages the electrodes' performance.

These electrodes were further tested in pH buffers of 4, 7 & 10 in a cyclic manner providing satisfactory responses with fluctuations of approximately 7 mV/pH which corresponds to about 0.1 pH units when used with ruthenium oxide ISEs.

A scanning electron microscopy was performed on the cross section of the electrodes with two KCl polymer matrix layers to identify if silver paste was chloridised to AgCl. The results have shown that a very thin

9. Conclusions & Further Work

layer of silver was chloridised to AgCl probably during curing of the KCl polymer matrix since SEM was performed on newly made electrodes.

Electrodes with properly cured polymeric Ag/AgCl paste were calculated to provide an optimum performance at 34% KCl in polymer matrix with a susceptibility of approximately -26 mV/decade of [Cl⁻]. The R² value for this curve was very low, 0.4864 which tends to suggest that fabrication procedure is not very repeatable using the existing equipment. Electrodes with fired polymeric Ag/AgCl paste provided much better results, very similar to the bare silver electrodes but with an optimum KCl concentration of 24% and 2 mV/decade of [Cl⁻] susceptibility.

An optimum KCl percentage was calculated for glass PPCFB2 paste and it is approximately 31% KCl with a susceptibility of -9 mV/decade of [Cl⁻]. The optimum point for glass PPCFC3 paste is 20% KCl concentration with a -30 mV/decade of [Cl⁻].

Electrodes with added Ag in the top KCl polymer matrix were also tested and the main conclusion was that different amounts of Ag in the top layer could affect the absolute potential of the electrodes but not their performance in terms of susceptibility. Adding KCl could affect the performance though and electrodes with 30% KCl provided better responses as predicted by the previously calculated optimum point. After these electrodes were allowed to drift in saturated KCl solution, the electrodes without KCl did not show any significant difference except that most probably Ag has been chloridised by the saturated KCl solution. Furthermore, the only other change observed for the rest of the electrodes is that the forward direction for solution change and the reverse provided very similar result with a much smaller hysteresis than before. Probably the saturated KCl solution affected the Ag in the paste chloridising it as well as either dissolving or absorbing KCl from or to the solution changing the structure of the electrodes to a very similar point. That can explain the smaller differences in the forward and reverse solution direction after the three day drift.

9. Conclusions & Further Work

Testing the binder to powder of Ag/AgCl ratio has provided very useful results. Using a polymer binder in saturated KCl solution for a drift test generates very unstable responses probably because of the ability of the polymer to absorb KCl and then redissolve in the solution. It turns out that glass binder can protect the electrode much better by provide more stable responses. It has been shown that as the ratio of binder to powder decreases, meaning using more powder, the response of the electrodes was more stable and faster for both polymer and glass binders. In 0.04 M KCl solution, both binder types were performing much better but again showing the same relationship between the binder to powder ratio and voltage stability. Furthermore, the absolute potential of the electrodes was not affected by the binder to powder ratio.

Looking into the Ag to AgCl ratio, it turns out that there is dependence on the stability of the electrodes in either 4 M or 0.04 M KCl. Further work needs to be performed to identify how the Ag to AgCl ratio can affect the electrodes' susceptibility to chloride concentration. Further experiments were performed with electrodes having a KCl polymer matrix on top with 5% and 30% KCl and tested for chloride susceptibility. Comparing the glass and polymer electrodes, the glass electrodes show a smaller sensitivity to KCl concentration changes and are more stable in their potential. Therefore, for both solutions glass electrodes perform better than polymer while the most appropriate combination requires further investigation in order to check clearly how the KCl layer affects the performance of the electrodes.

9.1.1 Further work

The most important aspects for reference electrodes that require further research are as follows:

- Test the electrodes for any susceptibilities to other species such as nitrates or phosphates by recording its potential in solutions of varying concentrations.

- Test the electrodes' performance in other chloride solutions such as sodium chloride (NaCl).
- Check if a membrane can be printed to keep the KCl on the electrode for a longer period of time extending its lifetime. A solid state ion conducting material such as Nafion should be tested.
- Define the chloride concentration range that the electrodes can be used as reference electrodes without breaking down.
- Define the hydration time, lifetime, shelf-life and drift rate for the best performing electrodes in KCl solutions as well as other aqueous mediums.
- Test what is the optimum binder to powder and Ag to AgCl ratios in terms of chloride susceptibility.
- Identify the maximum operating pH range for the electrodes.

9.2 pH Ion-Selective-Electrodes

The electrodes' stability in pH buffers was investigated for approximately a month in pH 7 and about two months in pH 4. Both electrodes perform as expected in pH 7 buffer having very stable potential of approximately 245 mV with respect to commercial Ag/AgCl reference electrode. In addition, the stability time of the electrodes is very similar. The glass electrodes reached a constant potential faster than the polymer. In pH 4 buffer solution, the electrodes respond differently which is unexpected. The electrodes with polymer dielectric start at a higher absolute potential and show a potential moving from about 350 to 430 mV. Glassy electrode's potential is initially lower and increases with time but then it drops back to a similar potential as the polymer. It is believed that low pH values in the long term can affect the glass dielectric-ruthenium oxide connection differently than with the polymer and that is why a very different response is observed.

The electrodes presented a very good sensitivity of approximately -58 mV/pH which is in correspondence to the Nernstian theory. Moreover, the electrodes showed no significant signs of hysteresis when cycled

9. Conclusions & Further Work

through various pH buffers in the range of 4-10. It was observed that as the temperature increased the potential of the electrodes in mainly pH 4 was decreasing during the second cycle rather than the first. The sensitivity of the electrodes increases with temperature which is in correspondence with the theory. Furthermore, as the temperature increases the R^2 value decreases indicating a variation of the electrodes' potentials in the same pH buffers in different cycles. This can be caused by the pH buffers changing due to the water evaporating at higher rates at higher temperatures or due to a higher conditioning rate of the electrodes or both. The potential variations are more noticeable in pH 4 buffer and less noticeable as the pH value increases most probably due to the pH changing rates being different for each buffer and the conditioning rate of the electrodes being also different in each buffer

9.2.1 Further work

The required work to complete the research on ruthenium oxide electrodes is as follows:

- Test the electrode for any susceptibilities to other species such as nitrates, phosphates and chlorides by recording its potential in solutions of varying concentrations.
- Check if a glassy ruthenium oxide paste is a valid option and test its performance at elevated temperatures either by finding a commercial glass based ruthenium oxide paste or using a custom made paste.
- Completely characterise the drift rate of the electrodes in various pH buffers.
- Define the electrode's lifetime and shelf life.
- Define the electrode's operating range in pH buffers as well as other acidic solutions (HCl or HNO₃).
- Define the response time of the electrode.

9.3 Humidity & Temperature Sensor

Initial experiments were to investigate the effect of wire length on the performance of the sensor when soldered on a TF substrate. The sensor performed similarly for different wire lengths suggesting no effect of length on sensor's performance. Furthermore, sensors were tested at constant temperature of 25 °C in an environmental chamber, with one and two winding of PTFE membrane and provided very similar results within the specified limits of the manufacturer also suggesting that the performance for both temperature and humidity was not affected by the PTFE membrane. The sensor was also tested in water to check if the PTFE membrane was a valid waterproofing method. Both sensors with one and two windings were proved to be properly waterproofed but the sensor with one winding provided a much faster and linear response than the sensor with two windings.

Six separate sensors were tested without, with one winding and with two windings of PTFE membrane in an environmental chamber with varying humidity to identify if the sensors performed as prescribed by the manufacturer. The results have shown error of approximately $\pm 2\%$ RH which falls within the manufacturer's specifications.

When the sensors were placed in the soil rig and water was poured through, there was a good reading from the sensors reaching approximately 100% RH and maintaining a reading corresponding to room temperature. After some time the sensors have shown an offset with RH reading more than 100% and temperature readings to be totally wrong. In the manufacturer's specifications, it is clearly stated that when the sensors are left in a humidity range above 95% RH for a long period of time might show an offset. It was then realised that since all liquids going through soil will be aqueous solutions the humidity in the soil would always stay at almost 100% RH making the sensors malfunctioning and not suitable for this application.

9. Conclusions & Further Work

Further work is not suggested for this sensor because it was proved that it is not a valid way of measuring the water content of the soil since the humidity in the soil will always be nearly 100% RH and even the temperature sensor would malfunction at that high humidity levels.

9.4 Conductivity Sensor

A conductivity sensor based on the four electrodes method was designed, fabricated and tested. The sensor was designed in such a way to decrease cost, increase reliability, eliminate frequency effects, generate a linear relationship between conductance and conductivity and to be suitable for soil conductivity measurements. The sensor was made of two facing TF substrates with three electrodes on each substrate. This geometry would allow enough space for the soil conductivity measurements to be reliable as a higher surface area was used. Furthermore, it would eliminate any frequency effects on the conductance measured.

After experimenting with gold electrodes with several input square wave currents of magnitudes between 0.2 to 4 mA, it was proven that the sensor has no effect from frequency used on the conductance measured and there was a linear relationship between the input current and the output voltage. The frequency response of the sensor was of the order of 10^{-7} V/Hz which is extremely low.

The distance between the two substrates was also varied and there is also a very linear relationship between the distance and the voltage output of the sensor with an R^2 better than 0.99.

The sensor was also tested using platinum electrodes which provided slightly different results from gold electrodes but that was probably because of the non-pure platinum paste used.

The most important outcome of the experiments performed for this sensor was the relationship between the resistance measured and the

resistivity of the solution. A cell constant expression was derived from curve fitting with an equation of $V = A * \exp\left(-\frac{\rho}{B}\right) + V_0$ with R^2 values higher than 0.999 for both gold and platinum electrodes. For a higher range of conductivities, a linear equation could be fitted showing a constant cell constant as predicted by theory.

9.4.1 Further work

This sensor was developed from the very beginning and was not developed based on existing sensor, therefore a lot of further work is required to fully understand and fully improve the performance of the sensor. The sensor requires further work on the following areas:

- Derive a cell constant expression for a much wider range of resistivities like the ones in the soil.
- Improve cell's geometry and electrodes shapes to improve the sensor's performance. In this attempt the voltage electrodes were surrounded by the current electrodes but it will provide much better results if the voltage electrode surrounded the current electrodes increasing the sensitivity of the sensor. A suggestion would be to print multiple current electrodes on one substrate and the same number of current electrodes on the other substrate, all surrounded and in between them, to print a single voltage electrode. The voltage electrode such acquire a very small surface area and the result should be used for the current electrodes.
- In these experiments on KCl solution was used. More solutions should be tested to check for any interference of other ions.
- The effect of temperature on sensor's performance.
- Using numerical methods, solve the equation generated for the cell constant since it depends on resistivity.
- Simulate the electric field generated by the cell and understand the reasons why it takes that shape.

9. Conclusions & Further Work

- Identify the effect of a highly conductive material getting close to the cell and how and why will the electric field be affected.
- Integrate the sensor on the same substrate as the rest of the sensors.
- Use a microprocessor to automatically detect the range of resistivity to be measured and change the input current levels to a point that the output voltage will fall in the readable range.

9.5 Soil Experiments

9.5.1 Soil pipes Experiments

Initial tests were performed in pH buffers using the existing sensor arrays and an interface on a prototype board to assess the performance of both the sensors and the interface. Dissolved oxygen sensors were performing as expected with a sensitivity of approximately 0.2 V/ppm oxygen. Sensors provided satisfactory performance in both pH buffers 4 and 10. pH sensors in the same experiment were showing a sensitivity of approximately -61 mV/pH which is very close to the Nernstian while the difference was probably due to noise errors. Furthermore, when air was bubbled through the buffers to test the oxygen sensors, pH sensors showed no response suggesting no interference between the two sensors.

Humidity and temperature sensors, SHT21S as explained earlier provided sensible results at the beginning but after a long time in high humidity environment, they broke down for both temperature and humidity measurements. The PRT sensor was performing as expected and was not affected when flushing either water or ascorbic acid through the pipes.

The first set of experiments, inserting the sensor array directly into the pipes, has provided very useful conclusions. The sensors did not have enough time in contact with the flushing solution to be able to sense its chemical properties. Very small changes were observed from the pH

sensor but almost no response was observed by the dissolved oxygen sensors while the PRT sensors were operating normally. A better way of utilising the sensors in the soil needed to be investigated.

The next set of experiments was performed using floral foam with the understanding that the foam would hold the solution around the sensors for a longer period of time and allow them to show proper response. Results were much better than the previous set of experiments for pH sensors showing a much clearer response to the ascorbic acid. Oxygen sensors were not performing as expected and when the sensors were removed from the foam it was discovered that ascorbic acid destroyed the PVC membrane ruining the sensors. PRT sensors were still operating normally. No sensitivity calculations were made since the responses of the sensors were not ideal and a better way of utilising the sensors was still required. From this experiments, it was understood that ascorbic acid, although it was believed to affect the dissolved oxygen concentration and the pH at the same time, had the ability to destroy the oxygen sensors. Therefore, another solution is still required to properly test the sensors in the pipes.

9.5.1.1 Further work

Further work is required in this area to improve the sensors' performance in the soil and fully characterise them in this environment. The main issues that need to be addressed are:

- Use the newly designed and manufactured soil rig to test the arrays.
- Use the new PCB to operate the sensors and also use a better data logger from the custom made used in these experiments. CR1000 would be a good alternative.
- Find a better way of utilising the sensors in the soil. The sensors must be utilised in such a way that they have enough time to respond to the flushing solution and protect them from harmful solutions at the same time.

9. *Conclusions & Further Work*

- Find better flushing solutions to be used to test and characterise the sensors.

9.5.2 **Soil Column for conductivity measurements**

Initial experiments in the soil column for conductivity measurements were performed in conjunction to water content measurements and their relationship was investigated. The conductivity sensor after finding the proper current levels to be used, provided very promising performances which were correlated with the soil water content. Furthermore, from the first experiment after several days, the sensor output voltage from the 30 hour point onwards shows fluctuation on a 24 hour cycle due to day and night time temperature variations experienced by the soil column.

In the second set of experiments with different soil types the results were very promising, not only from the sensor's performance point of view but also on the understanding of how the conductivity of different soil types changes with flushing cycles and from one soil type to the other. For each individual soil type, as the cycle number increased, the resistance measured during flushing was increasing but the trend followed was very similar. It is believed that water flushes away the conductive constituents of the soil, leaving behind a less conductive medium.

Comparing the three different soil types tested it was clear that each soil type provided different trends for the same cycle number. The resistance range for the builder's sand is clearly the highest while the soil mixture has the lowest resistance range. It is believed that this relationship is a result of mechanical property of the soil such as porosity or permeability or perhaps even a chemical property of the soil such as salinity. Looking at the absolute values for resistance obtained as specific water content range, it can also provide information on the packing or structure of the soils in the column. Furthermore, the maximum amount of water level in the column right before the

beginning of drainage might provide an indication of the porosity since the higher the water content the lower the resistance.

9.5.2.1 Further work

This work requires further experimentation in order to provide satisfactory evidence that the pre-mentioned suggestions are valid or not. The areas that need further work are:

- Maintain a constant draining rate in order to provide reliable results on the relationship observed.
- Repeat the experiments with different draining rate to investigate if there is any dependence on the proposed relationship.
- Try the same experiments with more soil types
- Measure further soil properties using external instruments and check how those soil properties correlate to the different water content and resistance relationships.
- Use more sensors in different soil depths to check if there is any difference to the soil properties at different depths and if the relationship of water content and resistance is depth dependent.

9.6 Field Trials

The first attempt for field tests was made. The same techniques used for the soil pipes in the lab were used in the field as well. The sensors were inserted in floral foam and then inserted in the soil at different depths. The sensors were powered by the PCB and the PCB was placed in a waterproof box that was also buried with the sensors. An eight core wire was used to transfer the data from the PCB to the logger which was enclosed in a waterproof box and screwed on an existing pole at the site. The logger was powered by a battery that was charged by existing photovoltaic cells at the site. Results were recorded by the logger at 30 minute time intervals.

9. Conclusions & Further Work

After some time, the battery run out and the sensors were taken out of the soil for inspection. It was found that the waterproof box for the PCB was full of water short circuiting the system and drawing all the power from the battery. After that no data were recorded because the data logger was not powered any more. Looking at the sensor arrays, the floral foam provided a very good protection leaving the sensors in a very good condition that they could probably be used in further experiments. From the obtained data of the data logger, it was clear that at the beginning the sensor arrays were performing in a very similar manner like the ones in soil pipes. After the water got in the PCB box, the sensors' output went down to zero indicating a short circuit in the system.

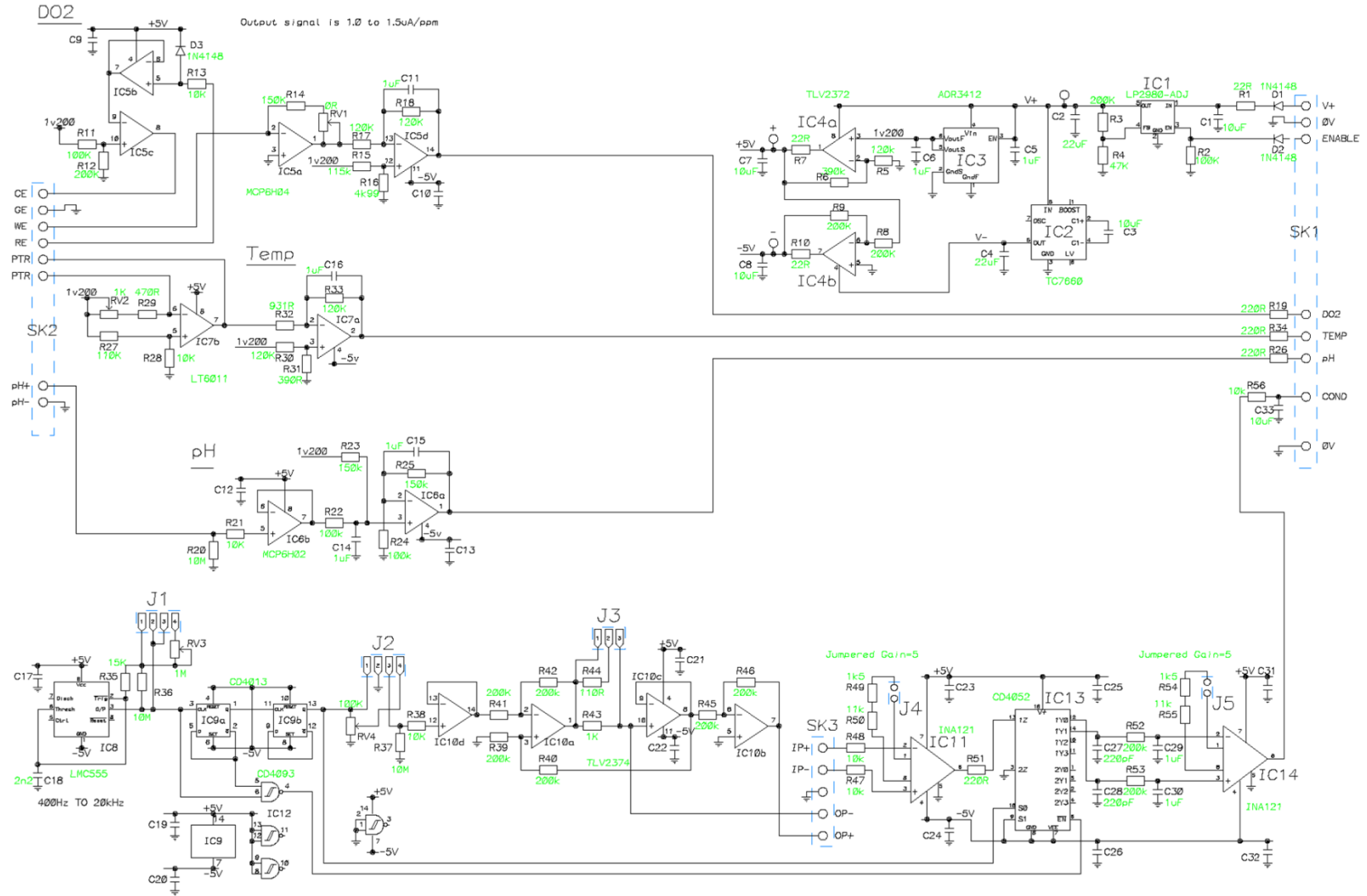
9.6.1 Further work

After the first attempt for field trials and the conclusions drawn by the trials, further experimentation and development is required. The areas that need further experimentation are:

- Better waterproofing method for the PCB box is clearly required.
- Improvements on the PCB tunable aspects would help the calibration procedure and allow a wider operating range for the sensors. Furthermore, a safety switch should be implemented on the PCB in case of any sensor disconnection or short circuiting to prevent the battery.
- It would be a good idea to try and test the sensors in a nearby field rather than at the specific site since it is very far away from the university and no usual access is convenient. After reaching a satisfactory level of deploying techniques then the sensors can be deployed in the field for real field trials.
- Looking at the sensor array in general, the best performing sensors should be integrated on a minimum number of substrates and some freshly made arrays should be tested to compare their performance with the existing arrays.

Appendix

PCB Circuit



List of References

Adamchuk, V., Hummel, J. M. M. & Upadhyaya, S., 2004. On-the-go soil sensors for precision agriculture. *Computers and electronics in agriculture*, Volume 44, pp. 71-91.

Altieri, M., 1994. *Biodiversity and Pest Management in Agroecosystems*. New York: Haworth Press.

Altieri, M. A., 1999. The ecological role of biodiversity in agroecosystems. *Agriculture, Ecosystems & Environment*, Volume 74, pp. 19-31.

Anderson, T.-H., 2003. Microbial eco-physiological indicators to assess soil quality. *Agriculture, Ecosystems and Environment*, Volume 98, pp. 285-293.

Arshad, M. & Martin, S., 2002. Identifying critical limits for soil quality indicators in agro-ecosystems. *Agriculture, Ecosystems and Environment*, Volume 88, pp. 153-160.

Atkinson, J., Cranny, A. & Simonis de Cloke, C., 1998. A low-cost oxygen sensor fabricated as a screen-printed semiconductor device suitable for unheated operation at ambient temperatures. *Sensors and Actuators B: Chemical*, Volume 47, pp. 171-180.

Atkinson, J., Glanc, M., Prakorbjanya, M. & Sophocleous, M., 2013. Thick film screen printed environmental and chemical sensor array reference electrodes suitable for subterranean and subaqueous deployments. *Microelectronics International*, 30(2), pp. 92-98.

Atkinson, J. K., Glanc, M., Boltryk, P. & Sophocleous, M., 2011. An investigation into the effect of fabrication parameter variation on the characteristics of screen-printed thick-film silver/silver chloride reference electrodes. *Microelectronics International*, 28(2), pp. 49-52.

Bibliography

Atkinson, J. K., Siona, R. P. & Turnera, J. D., 1993. A novel accelerometer using thick-film technology. *Sensors and Actuators B*, Volume 37, pp. 348-351.

Bard, A. & Faulkner, L., 2001. *ELECTROCHEMICAL METHODS: Fundamentals and Applications*. 2nd ed. United States of America: John Wiley & Sons.

Beare, M., Cameron, K., Williams, P. & Doscher, C., 1997. *Soil Quality Monitoring for Sustainable Agriculture*. s.l., s.n.

Belford, R., Owen, A. & Kelly, R., 1987. Thick-Film Hybrid pH Sensors. *Sensors and Actuators*, Volume 11, pp. 387-398.

Benton Jones, J. J., 2001. *Laboratory Guide for Conducting Soil Tests and Plant Analysis*. Boca Raton FL: CRC Press.

Bolinder, M. A., Angers, D. A., Gregorich, E. G. & Carter, M. R., 1998. The response of soil quality indicators to conservation management. *Canadian Journal of Soil Science*, pp. 37-45.

Bongiovanni, R. & Lowenberg-Deboer, J., 2004. Precision Agriculture and Sustainability. *Precision Agriculture*, Volume 5, pp. 359-387.

Brett, C. & Brett, A., 1993. *Electrochemistry: Principles, Methods and Applications*. Oxford: Oxford Science Publications.

Brignell, J., Cranny, A. & White, N., 1988. *Sensor applications of thick film technology*. s.l., IEEE Proceedings on Solid-State & Electron Devices.

Burger, J. A. & Kelting, D. L., 1999. Using soil quality indicators to assess forest stand management. *Forest Ecology and Management*, Volume 122, pp. 155-166.

Cambardella, C. & Karlen, D., 1999. Spatial Analysis of Soil Fertility Parameters. *Precision Agriculture*, Volume 1, pp. 5-14.

Cary Institute of Ecosystem Studies, 2015. *Definition of Ecology*. [Online] Available at: <http://www.caryinstitute.org/discover-ecology/definition->

ecology

[Accessed 27 03 2015].

Catteneo, A., Dell'Acqua, R., Forlani, F. & Pirozzi, L., 1980. *Low-cost thick-film pressure sensor*. s.l.:SAE Technical Paper.

Chemnitius, G. & Bilitewski, U., 1996. Development of screen-printed enzyme electrodes for the estimation of fish quality. *Sensors and Actuators B: Chemical*, Volume 32, pp. 107-113.

Cilliers, J. et al., 2001. Electrical resistance tomography using a bi-directional current pulse technique. *Measurement, Science and Technology*, Volume 12, pp. 997-1001.

Cranny, A. et al., 2011. Screen-printed potentiometric Ag/AgCl chloride sensors: Lifetime performance and their use in soil salt measurements. *Sensors and Actuators A: Physical*, Volume 169, pp. 288-294.

Cranny, A. W. J. & Atkinson, J. K., 1998. Thick film silver-silver chloride reference electrodes. *Measurement, Science & Technology*, Volume 9, pp. 1557-1565.

Crescini, D., Ferrari, V., Marioli, D. & Taroni, A., 1993. Triaxial thick-film load cell. *Sensors Mater.*, Volume 5, pp. 45-55.

Davison, W. & Harbinson, T., 1988. Performance Testing of pH Electrodes Suitable for low Ionic Strength Solutions. *Analyst*, Volume 113, pp. 709-713.

Deligianni, H. & Romankiw, L., 1993. In situ surface pH measurement during electrolysis using a rotary pH electrode. *IBM Journal of Research and Development*, 37(2), pp. 85-95.

Desmond, D. et al., 1997. Evaluation of miniaturised solid state reference electrodes on a silicon based component. *Sensors & Actuators B: Chemical*, Volume 44, pp. 389-396.

Bibliography

Dorana, J. W. & Zeiss, M. R., 2000. Soil health and sustainability: managing the biotic component of soil quality. *Applied Soil Ecology*, Volume 15, pp. 3-11.

Doran, J. & Parkin, T., 2011. *Soil Quality: Indicators*. [Online] Available at: <http://soilquality.org/indicators.html> [Accessed 30 03 2015].

Duroux, P. et al., 1991. The ion sensitive field effect transistor (ISFET) pH electrode: a new sensor for long term ambulatory pH monitoring. *GUT*, Volume 32, pp. 240-245.

Dziedzic, A. et al., 1997. Thick-Film resistive temperature sensors. *Measurement Science and Technology*, Volume 8, pp. 78-85.

Ehrenfeld, J., 2003. Effects of Exotic Plant Invasions on Soil Nutrient Cycling Processes. *Ecosystems*, Volume 6, pp. 503-523.

Eine, K., Kjelstrup, S., Nagy, K. & Syrverud, K., 1997. Towards a solid state reference electrode. *Sensors and Actuators B: Chemical*, Volume 44, pp. 381-388.

Fernandes, J. C. B. & Heinke, E. V., 2015. Alternative strategy for manufacturing of all-solid-state reference electrodes for potentiometry. *Journal of Sensors and Sensor Systems*, Volume 4, pp. 53-61.

Fließbach, A., Oberholzer, H.-R., Gunst, L. & Mader, P., 2007. Soil organic matter and biological soil quality indicators after 21 years of organic and conventional farming. *Agriculture, Ecosystems and Environment*, Volume 118, pp. 273-284.

Fog, A. & Buck, R., 1984. Electronic Semiconducting oxides as pH sensors. *Sensors and Actuators*, Volume 5, pp. 137-146.

Galán-Vidal, C. A., Muñoz, J., Domínguez, C. & Alegret, S., 1995. Chemical sensors, biosensors and thick-film technology. *TrAC Trends in Analytical Chemistry*, 15(5), pp. 225-231.

Geirinhas Ramos, H., Ribeiro, A., Komarek, M. & Novotny, M., 2006. *Development and characterization of a conductivity cell for water quality monitoring*. Rio de Janeiro, s.n.

Giller, K. et al., 1997. Agricultural intensification, soil biodiversity and agroecosystem function. *Applied Soil Ecology*, Volume 6, pp. 3-16.

Gil-Sotresa, F., Trasar-Cepeda, C., Leirosa, M. & Seoane, S., 2005. Different approaches to evaluating soil quality using biochemical properties. *Soil Biology & Biochemistry*, Volume 37, pp. 877-887.

Glanc-Gostkiewicz, M., Sophocleous, M., Atkinson, J. & Garcia-Breijo, E., 2013. Performance of miniaturised thick-film solid state pH sensors. *Sensors and Actuators A: Physical*, Volume 202, pp. 2-7.

Glanc, M., Sophocleous, M., Atkinson, J. & Garcia-Breijo, E., 2013. The effect on performance of fabrication parameter variations of thick-film screen printed silver/silver chloride potentiometric reference electrodes. *Sensors and Actuators A: Physical*, Volume 197, pp. 1-8.

Glasspool, W. & Atkinson, J., 1998. A screen-printed amperometric dissolved oxygen sensor utilising an immobilised electrolyte gel and membrane. *Sensors and Actuators B: Chemical*, Volume 48, pp. 308-317.

Gobin, A. et al., 2004. Indicators for pan-European assessment and monitoring of soil erosion by water. *Environmental Science & Policy*, Volume 7, pp. 25-38.

Guth, U. et al., 2009. Solid-state reference electrodes for potentiometric sensors. *Journal of Solid State Electrochemistry*, Volume 13, pp. 27-39.

Ha, J. et al., 2005. A polymeric junction membrane for solid-state reference electrodes. *Analytica Chimica Acta*, Volume 2005, pp. 59-66.

Hanson, B. & Kaita, K., 1997. Response of electromagnetic conductivity meter to soil salinity and soil-water content. *Journal of Irrigation and drainage engineering*, Volume 123, pp. 141-143.

Bibliography

Haskard, M. & Pitt, K., 1997. *Thick-Film Technology and Applications*.
s.l.:Electrochemical Publications.

Herman, R., 2001. An introduction to electrical resistivity in geophysics.
American Journal of Physics, 69(9), pp. 943-952.

Hillel, D., 1992. *Out of the Earth: Civilisation and the Life of the Soil*.
New York: The Free Press.

Högberg, P. & Read, D. J., 2006. Towards a more plant physiological
perspective on soil ecology. *TRENDS in Ecology and Evolution*, 21(10),
pp. 548-554.

Holmes, P. & Loasby, R., 1976. *Handbook of Thick Film Technology*.
s.l.:Electrochemical Publications.

Hrovat, M., Macek, S., Belavic, D. & Zgonik, M., 1990. Thick Film
temperature sensors. *Elektrotehniski Vestnik*, Volume 57, pp. 331-336.

Huang, I.-Y. & Huang, R.-S., 2002. Fabrication and characterisation of a
new planar solid-state reference electrode for ISFET sensors. *Thin Solid
Films*, Volume 406, pp. 255-261.

Idegami, K. et al., 2010. Fabrication and Characterization of Planar
Screen-Printed Ag/AgCl Reference Electrode for Disposable Sensor Strip.
Japanese Journal of Applied Physics, Volume 49, p. 097003.

Imeson, A. & Lavee, H., 1998. Soil erosion and climate change: the
transect approach and the influence of scale. *Geomorphology*, Volume
23, pp. 219-227.

Ineson, P. et al., 1998. Effects of climate change on nitrogen dynamics
in upland soils. 1. A transplant approach. *Global Change Biology*,
Volume 4, pp. 143-152.

Ives, D. & Janz, G., 1961. *Reference Electrodes: Theory and Practice*.
United States of America: Academic Press.

- Kampouris, D., Kadara, R., Jenkinson, N. & Banks, C., 2009. Screen printed electrochemical platforms for pH sensing. *Analytical Methods*, Volume 1, pp. 25-28.
- Karagounis, V., Lun, L. & Liu, C., 1986. A thick-film multiple component cathode three-electrode oxygen sensor. *IEEE Transactions on biomedical engineering*, BME-33(2), pp. 108-112.
- Karlen, D., Eash, N. & Unger, P., 1992. Soil and crop management effects on soil quality indicators. *American Journal of Alternative Agriculture*, 7(1-2), pp. 48-55.
- Keller, J. K., White, J. R., Bridgham, S. D. & Pastor, J., 2004. Climate change effects on carbon and nitrogen mineralization in peatlands through changes in soil quality. *Global Change Biology*, Volume 10, pp. 1053-1064.
- Khang, S. & Fitzgerald, T., 1975. A new probe and circuit for measuring electrolyte conductivity. *Industrial and Engineering Chemistry Fundamentals*, 14(3), pp. 208-213.
- Kirschbaum, M. U., 1995. THE TEMPERATURE DEPENDENCE OF SOIL ORGANIC MATTER DECOMPOSITION, AND THE EFFECT OF GLOBAL WARMING ON SOIL ORGANIC C STORAGE. *Soil Biology & Biochemistry*, 27(6), pp. 753-760.
- Kisiel, A., Marcisz, H., Michalska, A. & Maksymiuk, K., 2005. All-solid-state reference electrodes based on conducting polymers. *The Analyst*, Volume 130, pp. 1655-1662.
- Kisiel, A., Michalska, A., Maksymiuk, K. & Hall, E. A. H., 2008. All-Solid-State Reference Electrodes with Poly(n-butyl acrylate) Based Membranes. *Electroanalysis*, 20(3), pp. 318-323.
- Kizito, F. et al., 2008. Frequency, electrical conductivity and temperature analysis of a low-cost capacitance soil moisture sensor. *Journal of Hydrology*, Volume 352, pp. 367-378.

Bibliography

Koncki, R. & Mascini, M., 1997. Screen-printed ruthenium dioxide electrodes for pH measurements. *Analytica Chimica Acta*, Volume 351, pp. 143-149.

Lam, Y. & Atkinson, J., 2003. Screen-printed transcutaneous oxygen sensor employing polymer electrolytes. *Medical and Biological Engineering and Computing*, Volume 41, pp. 456-463.

Laugere, F. et al., 2003. On-chip contactless four electrode conductivity detection for capillary electrophoresis devices. *Analytical Chemistry*, Volume 75, pp. 306-312.

Lazorchak, J. et al., 2000. *Environmental Monitoring and Assessment Program -Surface Waters: Field Operations and Methods for Measuring the Ecological Condition of Non-Wadeable Rivers and Streams*, Cincinnati OH: U.S. Environmental Protection Agency.

Liao, W. & Chou, T., 2006. Fabrication of a Planar-Form Screen-Printed Solid Electrolyte Modified Ag/AgCl Reference Electrode for Application in a Potentiometric Biosensor. *Analytical Chemistry*, Volume 78, pp. 4219-4223.

Liao, W. & Chou, T., 2008. Development of a Reference Electrode Chip for Application in Ion Sensor Arrays. *Z. Naturforsch*, Volume 63b, pp. 1327-1334.

Lingfang, S. et al., 2009. *Design of electrical conductivity instrument based on pulse-width adjustable bi-directional pulsed voltage*. Los Angeles, IEEE.

Maminska, R., Dybko, A. & Wroblewski, W., 2006. All-solid-state miniaturised planara reference electrodes based on ionic liquids. *Sensors and Actuators B: Chemical*, Volume 115, pp. 552-557.

Martinelli, G. et al., 1999. Screen-printed perovskite-type thick films as gas sensors for environmental monitoring. *Sensors and Actuators B: Chemical*, Volume 55, pp. 99-110.

- Martínez-Máñez, R. et al., 2005. A multisensor in thick-film technology for water quality control. *Sensors and Actuators A: Physical*, Volume 120, pp. 589-595.
- Martínez-Máñez, R. et al., 2004. New potentiometric dissolved oxygen sensors in thickfilm technology. *Sensors and Actuators B: Chemical*, Volume 101, pp. 295-301.
- Marzouk, S., Ufer, S. & Buck, R., 1998. Electrodeposited Iridium Oxide pH electrode for measurement of extracellular myocardial Acidosis during Acute Ischemia. *Analytical Chemistry*, Volume 70, pp. 5054-5061.
- Mayne, P., 2006. *In-Situ Test Calibrations for Evaluating Soil Parameters*. Singapore, Edited by K . K . Phoon , D . W . Hight , S . Leroueil , and T . S . Tan.
- McBratney, A., Whelan, B. & Ancev, T., 2005. Future Directions of Precision Agriculture. *Precision Agriculture*, Volume 6, pp. 7-23.
- McMurray, H. N., Douglas, P. & Abbot, D., 1995. Novel thick-film pH sensors based on ruthenium dioxide-glass composites. *Sensors and Actuators B: Chemical*, Volume 25, pp. 9-15.
- Merrill, S. D. et al., 2013. Comparison of soil quality and productivity at two sites differing in profile structure and topsoil properties. *Agriculture, Ecosystems and Environment*, Volume 179, pp. 53-61.
- Michalska, A., 2012. All-Solid-State Ion Selective and All-Solid-State Reference Electrodes. *Electroanalysis*, 24(6), pp. 1253-1265.
- Michalski, L., Eckersdorf, K., Kucharski, J. & McGhee, J., 2002. *Temperature Measurement*. 2nd Edition ed. s.l.:John Wiley & Sons Ltd.
- Mihell, J. & Atkinson, J., 1998. Planar thick-flim pH electrodes based on ruthenium dioxide hydrate. *Sensors and Actuators B: Chemical*, Volume 48, pp. 505-511.

Bibliography

Mitchell, F. & de Alwis, A., 1989. Electrical conductivity meter for food samples. *Journal of Physics E: Scientific Instrumentation*, Volume 22, pp. 554-556.

Morten, B. et al., 1995. Magneto-resistive thick-film sensor for linear displacements. *Sensors and Actuators A: Physical*, 261(5), pp. 46-47.

Mroz, A. et al., 1998. Disposable reference electrode. *The Analyst*, Volume 123, pp. 1373-1376.

Musa, A. E. et al., 2011. Disposable Miniaturised Screen-Printed pH and Reference Electrodes for Potentiometric Systems. *Electroanalysis*, 23(1), pp. 115-121.

Nabighian, M., 1988. *Electromagnetic Methods Vol.1: Theory (Investigations in Geophysics Series No. 3)*. Oklahoma: Society Of Exploration Geophysicists.

Nolan, M. A., Tan, S. H. & Kounaves, S. P., 1997. Fabrication and Characterization of a Solid State Reference Electrode for Electroanalysis of Natural Waters with Ultramicroelectrodes. *Analytical Chemistry*, Volume 69, pp. 1244-1247.

Nortcliff, S., 2002. Standardisation of soil quality attributes. *Agriculture Ecosystems & Environment*, Volume 88, pp. 161-168.

Norton, M. G. & Reynolds, Q. M., 1985. Thick-film platinum temperature Sensor. *Microelectronics International*, Volume 2, pp. 31-44.

Pang Yew WEE, T., 2014. *The evaluation of thick film soil sensors for monitoring soil properties*, s.l.: MSc Thesis, University of Southampton.

Papendick, R. I. & Parr, J. F., 1992. Soil quality—The key to a sustainable agriculture. *American Journal of Alternative Agriculture*, Volume 7, pp. 2-3.

- Parr, J., Papendick, R., Hornick, S. & Meyer, R., 1992. Soil quality: Attributes and relationship to alternative and sustainable agriculture. *American Journal of Alternative Agriculture*, 7(1-2), pp. 5-11.
- Perry, D., 1994. *Forest Ecosystems*. Baltimore MD: Johns Hopkins University Press.
- Picoux, B. & Le Houedec, D., 2005. Diagnosis and prediction of vibration from railway trains. *Soil Dynamics and Earthquake Engineering*, Volume 25, pp. 905-921.
- Plambeck, J., 1982. *Electroanalytical Chemistry: Basic Principles and Applications*. United States of America: John Wiley & Sons.
- Pletcher, D., 2009. *A first course in electrode processes*. 2nd ed. Cambridge: The Royal Society of Chemistry.
- Prasek, J., Adamek, M. ..., Krivka, J. & Szendiuch, I., 2008. *31st International Spring Seminar on Electronics Technology*. Budapest, IEEE.
- Prudenziati, M., 1991. Thick Film Technology. *Sensors and Actuators A: Physical*, Volume 25-27, pp. 227-234.
- Prudenziati, M. M. B., 1992. The state of the Art in Thick-film Sensors. *Microelectronics Journal*, Volume 23, pp. 133-141.
- Radiometer, A. S., n.d. *Conductivity Theory and Practise Guide*. [Online] Available at: http://www.radiometer-analytical.com/all_resource_centre.asp?code=112 [Accessed 10 04 2015].
- Ramamoorthy, R. & Dutta, P., 2003. Oxygen sensors: Materials, methods designs and applications. *Journal of Materials Science*, Volume 38, pp. 4271-4282.
- Ramos, P., Dias Pereira, J., Geirinhas Ramos, H. & Ribeiro, A., 2008. A four terminal water quality monitoring conductivity sensor. *IEEE transactions on instrumentation and measurement*, 57(3), pp. 577-582.

Bibliography

Reyns, P., Missotten, B., Ramon, H. & De Baerdmecker, J., 2002. A Review of Combine Sensors for Precision Farming. *Precision Agriculture*, Volume 3, pp. 169-182.

Rius-Ruiz, F. X. et al., 2011. Solid-state reference electrodes based on carbon nanotubes and polyacrylate membranes. *Analytical and Bioanalytical Chemistry*, Volume 399, pp. 3613-3622.

Robert, P., 2002. Precision agriculture: a challenge for crop nutrition management. *Plant and Soil*, Volume 247, pp. 143-149.

Schloter, M., Dilly, O. & Muncha, J., 2003. Indicators for evaluating soil quality. *Agriculture, Ecosystems and Environment*, Volume 98, pp. 255-262.

Schoenholtz, S., Van Miegroet, H. & Burger, J., 2000. A review of chemical and physical properties as indicators of forest soil quality: challenges and opportunities. *Forest Ecology and Management*, Volume 138, pp. 335-356.

Scholz, F., 2010. *Electroanalytical Methods: Guide to experiments and Applications*. 2nd, revised and extended ed. Berlin: Springer.

Seelan, S. K., Laguette, S., Casady, G. M. & Seilstad, G. A., 2003. Remote sensing applications for precision agriculture: A learning community approach. *Remote Sensing of Environment*, Volume 88, pp. 157-169.

Shainberg, I. et al., 1989. Use of Gypsum on Soils: A Review. In: *Advances in Soil Science*. s.l.:Springer, pp. 1-111.

Shibusawa, S., 1998. *Precision Farming and Terr-mechanics*. Korea, Fifth ISTVS Asia-Pacific Regional Conference.

Shinwari, M. W. et al., 2010. Microfabricated Reference Electrodes and their Biosensing Applications. *Sensors*, Volume 10, pp. 1679-1715.

Shreiner, R. & Pratt, K., 2004. *Primary Standards and Standard Reference Materials for Electrolytic Conductivity*. Washington: National Institute of Standards and Technology.

Shukla, M., Lal, R. & Ebinger, M., 2006. Determining soil quality indicators by factor analysis. *Soil & Tillage Research*, Volume 87, pp. 194-204.

Sigrimis, N., Hashimoto, Y., Munack, A. & De Baerdemaeker, J., 1999. Prospects in Agricultural Engineering in the Information Age: Technological Developments for the Producer and the Consumer. *CIGR e-journal*.

Simonis, A., Lüth, H., Wang, J. & Schöning, M. J., 2003. Strategies of Miniaturised Reference Electrodes Integrated in a Silicon Based "one chip" pH Sensor. *Sensors*, Volume 3, pp. 330-339.

Simonis, A., Lüth, H., Wang, J. & Schöning, M. J., 2004. New concepts of miniaturised reference electrodes in silicon technology for potentiometric sensor systems. *Sensors and Actuators B: Chemical*, Volume 103, pp. 429-435.

Smith, K. & Mullins, C., 2000. *Soil and Environmental Analysis: Physical Methods, Revised and Expanded*. 2nd ed. New York: Marcel Dekker Inc.

Soleimani, M. et al., 2013. Engine oil acidity detection using solid state ion selective electrodes. *Tribology International*, Volume 65, pp. 48-56.

Sophocleous, M., 2009. *The investigation of Thick-Film Reference Electrodes*, Southampton U.K.: s.n.

Sophocleous, M., Glanc-Gostkiewicz, M., Atkinson, J. K. & Garcia-Breijo, E., 2012. *An experimental analysis of Thick-Film solid-state reference electrodes*. Taipei, IEEE.

Bibliography

Stafford, J. V., 2000. Implementing Precision Agriculture in the 21st Century. *Journal of Agricultural Engineering Research*, Volume 76, pp. 267-275.

Stenberg, B., 1999. Monitoring Soil Quality of Arable Land: Microbiological Indicators. *Acta Agriculturae Scandinavica, Section B — Soil & Plant Science*, Volume 49, pp. 1-24.

Stone, H., Stroock, A. & Ajdari, A., 2004. ENGINEERING FLOWS IN SMALL DEVICES: MICROFLUIDICS TOWARDS A LAB ON A CHIP. *Annual Review of Fluid Mechanics*, Volume 36, pp. 381-411.

Tarr, M., n.d. *Thick Film Technology*. [Online]
Available at: http://www.ami.ac.uk/courses/topics/0255_tft/
[Accessed 30 03 2015].

Theodorakopoulos, D., 2003. Dynamic analysis of a poroelastic half-plane soil medium under moving loads. *Soil Dynamics and Earthquake Engineering*, Volume 23, pp. 521-533.

Theurillat, J.-P. & Guisan, A., 2001. POTENTIAL IMPACT OF CLIMATE CHANGE ON VEGETATION IN THE EUROPEAN ALPS: A REVIEW. *Climatic Change*, Volume 50, pp. 77-109.

Thorp, K. & Tian, L., 2004. A Review on Remote Sensing of Weeds in Agriculture. *Precision Agriculture*, Volume 5, pp. 477-508.

Tymecki, Ł., Zwierkowska, E. & Koncki, R., 2004. Screen-printed reference electrodes for potentiometric measurements. *Analytica Chimica Acta*, Volume 526, pp. 3-11.

Verhoef, A., 2011. *Floodplain Underground Sensors-FUSE*. [Online]
Available at:
<http://www.reading.ac.uk/geographyandenvironmentalscience/Research/ESS/ges-FUSE.aspx>
[Accessed 29 03 2015].

Visser, S. & Parkinson, D., 1992. Soil biological criteria as indicators of soil quality: Soil microorganisms. *American Journal of Alternative Agriculture*, 7(1-2), pp. 33-37.

Vonau, W. & Guth, U., 2006. pH Monitoring: a review. *Journal of Solid State Electrochemistry*, 10(9), pp. 746-752.

Vonau, W., Oelßner, W., Guth, U. & Henze, J., 2010. An all-solid-state reference electrode. *Sensors and Actuators B: Chemical*, Volume 144, pp. 368-373.

Wang, J., 2002. Electrochemical detection for microscale analytical systems: a review. *Talanta*, Volume 56, pp. 223-231.

Wang, M., 2001. Possible adoption of precision agriculture for developing countries at the threshold of the new millennium. *Computers and electronics in agriculture*, Volume 30, pp. 45-50.

Wang, M., Yao, S. & Madou, M., 2002. A long-term stable iridium oxide pH electrode. *Sensors and Actuators B: Chemical*, Volume 81, pp. 313-315.

Wei, Y., Wang, J., Li, D. & Ding, Q., 2010. Design of intelligent Conductivity Meter Based on MSP430F149. *International Federation for Information Processing*, Volume 317, pp. 240-247.

Wellings, S., Bell, J. & Raynor, R., 1985. Use of gypsum resistance blocks for measuring soil water potential in the field. *Institute of Hydrology*.

Whelan, B., McBratney, A. & Boydell, B., 1997. *The Impact of Precision Agriculture*. Moree, UK, Proceedings of the ABARE Outlook Conference 'The Future of Cropping in NW NSW'.

Wittkamp, M. et al., 1997. Silicon thin film sensor for measurement of dissolved oxygen. *Sensors and Actuators B: Chemical*, Volume 43, pp. 40-44.

Bibliography

Yao, S., Wang, M. & Madou, M., 2001. A pH Electrode Based on Melt-Oxidised Iridium Oxide. *Journal of the Electrochemical Society*, Volume 148, pp. H29-H36.

Young, A., 1991. Soil monitoring: a basic task for soil survey organisations. *SOIL USE AND MANAGEMENT*, Volume 7, pp. 126-130.

Zegelin, S., White, I. & Jenkins, D., 1989. Improved field probes for soil water content and electrical conductivity measurement using time domain reflectometry. *Water Resources Research*, 25(11), pp. 2367-2376.

Zen, J. et al., 2002. Photoelectrochemical oxygen sensor using copper-plated screen-printed carbon electrodes. *Analytical Chemistry*, Volume 74, pp. 6126-6130.

Zhang, N., Wang, M. & Wang, N., 2002. Precision agriculture - a worldwide overview. *Computers and electronics in agriculture*, Volume 36, pp. 113-132.

Zheng, R. et al., 2011. A dissolved oxygen sensor based on hot electron induced cathodic electrochemiluminescence at a disposable CdS modified screen-printed carbon electrode. *Sensors and Actuators B: Chemical*, Volume 157, pp. 488-493.